

Title	Combined wave, wind, and current simulation in laboratory basins with floating offshore wind turbines
Authors	Otter, Aldert
Publication date	2022-09-16
Original Citation	Otter, A. 2022. Combined wave, wind, and current simulation in laboratory basins with floating offshore wind turbines. PhD Thesis, University College Cork.
Type of publication	Doctoral thesis
Rights	© 2022, Aldert Otter. - https://creativecommons.org/licenses/by-nc-nd/4.0/
Download date	2024-05-04 15:09:38
Item downloaded from	https://hdl.handle.net/10468/14472



UCC

University College Cork, Ireland
Coláiste na hOllscoile Corcaigh

Ollscoil na hÉireann, Corcaigh
National University of Ireland, Cork



Combined wave, wind, and current simulation
in laboratory basins with Floating Offshore
Wind Turbines

Thesis presented by

Aldert Otter, Bsc, MengSc

<https://orcid.org/0000-0001-9403-4161>

for the degree of

Doctor of Philosophy

University College Cork

School of Engineering

Head of School/Department: Prof. Jorge Oliveira

Supervisor(s): Dr Jimmy Murphy, Dr Cian Desmond, Dr Vikram Pakrashi

2022

Contents:

Declaration of Authorship

Acknowledgments

Abstract

List of abbreviations and acronyms

Nomenclature

List of publications

1. Introduction	1
1.1. Context	1
1.2. Objectives and scope	2
1.3. Outline	3
2. Floating Wind Technology	4
2.1. Overview of Floating Offshore Wind Technology	4
2.2. The INNWIND.EU semisubmersible platform	7
3. Literature Review	9
3.1. Environmental conditions	9
3.1.1. Wind	9
3.1.2. Waves	11
3.1.3. Current	13
3.1.4. Wave-current interactions	13
3.2. Physical modelling	15
3.2.1. Scaling laws	15
3.3. Full physical testing	16
3.3.1. Froude scaled rotor combined with higher than Froude scaled wind velocity	16
3.3.2. Geometrically modified low-Reynolds aerofoils combined with Froude scale wind velocity (performance-scaled)	17
3.4. Hybrid testing	18
3.4.1. Hybrid testing with propeller actuators	19
3.4.2. Hybrid testing with dynamic winch actuators	20
3.4.3. Hybrid testing in wind tunnels	22
3.5. Comparison of test methods: full physical vs hybrid, in laboratory wave basins	23
4. Methodology	28
4.1. Emulation of aerodynamic loads	28
4.1.1. Description of the Multi-Propeller Actuator	28
4.1.2. Open-loop control	30
4.1.3. Closed-loop control	31
4.2. Emulation of current induced loadings	33
4.2.1. Description of the winch actuator	33
4.3. Rigid body dynamics	36
4.4. Description of the scale model of the INNWIND semisubmersible FOWT	36
4.5. Test setup	40

4.6. Test conditions.....	42
4.7. Numerical models.....	43
4.7.1. Ansys AQWA.....	44
4.7.2. FAST.....	44
4.8. Assumptions and simplifications and systemic sources of error and uncertainty.....	45
4.9. Validation metrics.....	46
5. Results.....	50
5.1. Actuation accuracy.....	50
5.1.1. Winch actuator.....	50
5.1.2. MPA.....	50
5.2. Ocean Basin campaign.....	54
5.2.1. Current only.....	54
5.2.2. Wind only.....	55
5.2.3. Waves only.....	57
5.2.4. Waves and current.....	58
5.2.5. Wind and current.....	59
5.2.6. Waves and wind.....	60
5.2.7. Waves, current, and wind.....	61
5.3. Deep Ocean Basin campaign.....	62
5.3.1. Waves only.....	62
5.3.2. Waves and current.....	63
5.4. Wave Current Flume campaign.....	64
5.4.1. Current only.....	64
5.4.2. Current and wind.....	66
5.4.3. Current, wind, and waves.....	67
5.5. Discussion on the results with SIL current.....	69
5.6. Discussion on the results with the MPA and aerodynamics.....	71
6. Conclusion and future recommended work.....	73
6.1. Conclusion.....	73
6.2. Future recommended work.....	74
Bibliography.....	77
Appendix:.....	84
• Paper A, “A review of modelling techniques for floating offshore wind turbines”.....	85
• Paper B, “Emulating aerodynamic forces and moments for hybrid testing of floating wind turbine models”.....	123
• Paper C, “Current simulation with Software in the Loop for floating offshore wind turbines”.....	135
• Paper D, “Combined current and wind simulation for floating offshore wind turbines”.....	149
• MATLAB code for closed-loop control with API XIL protocols and ds1104.....	161
• MATLAB code for open-loop control with Arduino.....	167
• Simulink code (block diagram) for real-time simulation.....	171

Declaration of Authorship

This is to certify that the work I am submitting is my own and has not been submitted for another degree, either at University College Cork or elsewhere. All external references and sources are clearly acknowledged and identified within the contents. I have read and understood the regulations of University College Cork concerning plagiarism and intellectual property.

Signed: _____  _____

Date: _____ 16/09/2022 _____



“Now here, now there, the wild waves sweep,
 Whilst we, betwixt them o'er the deep,
 In shatter'd tempest-beaten bark,
With labouring ropes are onward driven,
 The billows dashing o'er our dark
 Upheaved deck—in tatters riven
Our sails—whose yawning rents between
 The raging sea and sky are seen.”

By Alcaeus



*This work is dedicated to my beautiful wife and our beautiful
daughter: Martha and Gisela.*

*It is my mission in life to do them proud and this work has been a big
part of that mission.*

Acknowledgements

I would like to acknowledge the following amazing people for helping me out a great deal with my work. I would have struggled without them, instead they have made this PhD a very interesting and pleasant experience for me.

To my supervisors Jimmy Murphy, Cian Desmond, and Vikram Pakrashi, for their support and constructive feedback on the papers. A special shoutout to Cian Desmond for always being available and helping me with some of the research questions and for being a good friend, and to Jimmy Murphy for always being understanding and accommodating when I needed it.

To Christian van den Bosch and Tom Walsh who were the technicians in Lir NOTF during my experimental work, for their technical support and for the terrible puns and great banter. Also, to my other colleagues in Lir NOTF, Ian Power, Florent Thiebault, James Kelly, and Milad Zabihi Kooykheily for their help and excellent craic.

To Brian Flannery for trouble shooting my MATLAB code and making it work again.

To Professor Deborah Greaves and Dr Martyn Hann from the University of Plymouth, for their support and suggestions throughout the PhD.

To my PhD buddies Navid, Rahul, Omar, Omer, and Agro who like me have been absorbed into the world of floating wind energy and who are excellent company at conferences.

To my other PhD colleagues and friends Rory, Jess, Nicole, Ross and Liz for the banter and for sharing some of the PhD freakouts, which we apparently all must go through.

To everyone else in the Beaufort Building, and especially Annette O'Sullivan who I may have occasionally driven a bit crazy with my numerous requests for POs.

To my sweet daughter Gisela for the necessary distraction from the number crunching.

To my amazing wife Dr Martha Gosch who has been incredibly supportive throughout my PhD as she is in life outside it.

To my family back in the Netherlands who have always been a great source of inspiration and support to me.

To Ian from the customer service of Schneider Electric who has been instrumental in getting the winch actuator up and running.

And finally, to Science Foundation Ireland for making this PhD possible under the PhD fellowship programme, Grant/Award Number: 17/RC-PhD/3486

Abstract

Testing scale models of Floating Offshore Wind Turbines (FOWT) under realistic offshore conditions at scale in wave basins is challenging. There exists a strong coupling between the turbine aerodynamics and platform hydrodynamics, and working in the two different fluid domains of air and water causes a scaling mismatch between Reynolds- and Froude scaling.

Furthermore, not every test facility with wave basins has the equipment to generate wind and current to simulate combined environmental loadings.

To overcome these challenges a hybrid test method to simulate wind and current was developed for this thesis. Hybrid testing is a combination of real-time numerical modelling and scale model testing. The aerodynamic loads of wind and hydrodynamic loads of currents are calculated in real-time and applied to the FOWT scale model via mechanical actuators.

To emulate aerodynamic loads a Multi-Propeller Actuator (MPA) was developed using off-the-shelf parts from recreational aerial drones on a custom-made frame. By using several propellers with different thrust directions, multiple aerodynamic loads can be emulated simultaneously, and emulating forces rather than viscous loads solves the scaling mismatch.

Aerodynamic loads have been emulated by other researchers with propeller actuators, however, only very few examples of using multiple propellers were found in the literature. The study with the MPA adds to this knowledge gap.

A winch actuator was developed to simulate sea currents. By emulating the drag force of a current on the platform of the FOWT, and approximating wave-current interactions by adjusting wave spectra, currents can reliably be simulated.

No other examples of this method to simulate current were found, representing a clear knowledge gap. The study with the winch actuator fills this gap in the literature.

Both actuators are controlled with a Software-in-the-Loop (SIL) application. This control method uses real-time feedback from a load cell and motion tracking system to update the loads calculation with the real-time numerical simulation for each time-step, improving the accuracy of the simulation. Simulating current with the winch actuator is referred to as SIL current.

Experimental results throughout this body of work have been validated with offline numerical simulations using FAST and AQWA. Two validation metrics, developed for this study, have been applied to the results. Experiments with SIL current have also been validated by repeating the experiments with physical current, referred to as the full physical method, and comparing the results of both methods.

Both actuators were applied to a 1/50 scale model of the INNWIND semisubmersible platform with the NREL 5 MW as the simulated wind turbine.

The results have shown the winch actuator can reliably and accurately emulate the drag force of a current on the FOWT platform and the method to approximate wave-current interactions was found adequate. The results also showed that the MPA can reliably and accurately emulate thrust- and torque loads of the NREL 5 MW turbine.

The SIL current and aerodynamics emulation with the MPA, in combination with physical waves, were found suitable to replicate realistic offshore conditions at scale in the wave basin.

List of publications

Publications Appended to this Thesis

This thesis is presented as a collection of the following four papers included in the Appendix in a text-based manuscript format. The author of this thesis (first author on all four papers) carried out the research work presented in the four publications and the co-authors supervised the work and collaborated in the reviewing process.

- A. Otter, J. Murphy, V. Pakrashi, A. Robertson, C. Desmond, “A review of modeling techniques for floating offshore wind turbines”, *Wind Energy*, 2021;1–27. DOI: 10.1002/we.2701
- A. Otter, J. Murphy, C. Desmond, “Emulating aerodynamic forces and moments for hybrid testing of floating wind turbine models”, *Journal of Physics: Conference Series (Torque 2020)*, **1618** (2020) 032022. DOI:10.1088/1742-6596/1618/3/032022
- A. Otter, B. Flannery, J. Murphy, C. Desmond, “Current simulation with Software in the Loop for floating offshore wind turbines”, *Journal of Physics: Conference Series (Torque 2022)*, **2265** (2022) 042028. DOI:10.1088/1742-6596/2265/4/042028
- A. Otter, C. Desmond, B. Flannery, J. Murphy, “Combined current and wind simulation for floating offshore wind turbines” *Journal of Physics: Conference Series (DeepWind 2022)*, **2362** (2022) 012028. DOI:10.1088/1742-6596/2362/1/012028

List of abbreviations and acronyms

BEM	Boundary Element Method
BEMT	Blade Element Momentum Theory
CAD	Computer Aided Design
COB	Center of Buoyancy
COG	Center of Gravity
DOB	Deep Ocean Basin
DOF	Degree of Freedom
EC	European Commission
ESC	Electronic Speed Controller
FMT	Fraction of Measurements within a user defined Tolerance
FOWT	Floating Offshore Wind Turbine
GM	Metacentric height
GW	Giga Watt
JONSWAP	Joint North Sea Wave Project
LCOE	Levelized Cost of Energy
ME	Morison Equation
MPA	Multi-Propeller Actuator
MW	Mega Watt
NOTF	National Ocean Test Facility
OB	Ocean Basin
ORE	Ocean Renewable Energy
PF	Potential Flow
PI	Proportion Integration
PSD	Power Spectral Density
PWM	Pulse Width Modulation
QTF	Quadratic Transfer Function
RA	Response Amplitude Operator
RE	Relative Error
SIL	Software in the Loop
SWL	Still Water Line
TC	Test Case
TLP	Tension Leg Platform
TSR	Tip Speed Ratio
WCF	Wave Current Flume

Nomenclature

Symbol	Explanation
A	Wetted cross-sectional area in m^2
A_r	Rotor plane area in m^2
A_w	Water plane area in m^2
b	Radiation damping
C	Restoring stiffness in N/m
C_D	Drag coefficient
C_T	Thrust coefficient
C_g	Group velocity in m/s
f	Wave frequency in Hz
f_p	Peak frequency in Hz
F	Fetch length in m
g	Gravitational acceleration in m/s^2
h	Water depth in m
K	Retardation function
k	Wave number
L	Length in m
M	Mass in kg
M_a	Added Mass in kg
M_i	Added inertia in kgm^2
r	Radius in m
t	Time in s
S	Spectral energy in Watt/m^2
U	Current velocity in m/s
u	Velocity of the floating model in m/s
V	Wind speed in m/s
V_D	Volumetric displacement in m^3
V_{in}	Input wind speed in m/s
V_{rel}	Relative wind speed in m/s
ν	Kinematic viscosity m^2/s
x	Distance in m
Z	Height in m
σ	Standard deviation
γ	Peak enhancement factor
λ	Scale ratio
Ω	Angular velocity in rad/s
ω	Wave frequency in rad/s
ρ	Density of sea water in kg/m^3
τ	Time lag in s

Chapter 1

Introduction

This Chapter gives an overview of the objectives and scope of the thesis.

1.1) Context

Offshore Renewable Energy (ORE) is an area of strategic importance and seen as a critical contributor for clean energy production and meeting Europe's carbon emission reduction targets [1]. The European Commission (EC) has proposed to reduce emissions by 55% below 1990 levels, by 2030 [2]. Typically, ORE is referred to as offshore wind-, wave-, and tidal energy. In 2020 the EC set a target of 40 Giga Watt (GW) of electrolysis capacity for green hydrogen from renewable energy sources for 2030. At the same time the EC set a target for offshore wind generation of 60 GW for 2030 [1], which could therefore potentially supply the entire electrolysis capacity for green hydrogen. Currently, total installed offshore wind capacity in European waters is around 25 GW [3], and the total estimated offshore wind resource in Europe is around 4000 GW, of which about 80% is in areas which are suited to floating wind energy [4].

Currently the Levelized Cost of Energy (LCOE) for Floating Offshore Wind Turbine (FOWT) technology - around €130/MWh in 2020 - still exceeds that of its fixed-bottom equivalent - around €80/MWh in 2020 [5]. However, FOWTs are seen as an attractive economic alternative in water deeper than 60m where the costs of fixed-bottom installations may become prohibitive, or in shallower water where seabed geology does not suit fixed-bottom installations [6]. For 2050, cumulative installations of FOWTs are predicted to reach as much as 264 GW globally and LCOE is expected to drop below \$40/MWh [7]. Capacity factors in waters suitable for FOWTs tend to be higher compared to shallow water areas. For example, in 2020 Hywind Scotland (with water depths between 95m and 120m) was found to have an average capacity factor of 57.1% over a twelve month period, compared to capacity factors around 40% for fixed-bottom offshore wind farms in the same period [8], clearly demonstrating a major potential advantage of FOWTs over fixed-bottom offshore wind turbines.

The ORE sector requires the development of floating platforms and devices that must operate and survive in extreme environments and thus require physical model testing as part of their development. Wave basins and flumes can replicate offshore wave conditions but there is a high level of uncertainty associated with methods of combining wave, wind, and current loadings on a floating device in a laboratory setting [9].

An important objective of scale model testing is the validation of numerical models with physical data to minimize risk for the developer, and this is especially valid for floating wind energy, which is a relatively novel technology. At the start of 2022 only three floating wind farms were grid connected and operational globally: Hywind Scotland (30 Megawatt {MW}), Kincardine (50 MW), and WindFloat Atlantic (25 MW). With the absence of publicly available data sets on the behavior of full-scale prototypes of FOWTs in real offshore conditions the reduction of uncertainty and improving the fidelity of scale modelling techniques is essential.

The FOWT is the ideal device for the study of combined wave/wind/current effects at scale. The large surface area of the wind turbine rotor and relatively small floater size gives the FOWT a much stronger coupling between hydrodynamic loads and aerodynamic loads compared to floating wave- and tidal energy converters. Wind-, wave-, and current loads can all lead to significant stresses on the platform, moorings, and turbine components of FOWTs and are therefore considered in the design process. For wave- and tidal technologies the hydrodynamic interactions are more complex while there can be little or no aerodynamic loading. Therefore, for the analysis of combined wave/wind/current effects an FOWT represents a good choice of floating platform.

Floating wind energy is steadily reaching maturity as a technology [10]. Nonetheless, there are still many platform concepts and configurations for FOWTs proposed and under development. Given Europe's large offshore wind resource suitable for FOWTs it is likely that many technology developers will seek to test a scale model of their FOWT design in realistic offshore conditions at scale in a wave basin. However, where test facilities will have wave basins to generate ocean waves at scale, not every test facility has the equipment to generate physical wind and current. Such equipment is bulky and expensive to operate. Furthermore, it is challenging to replicate high quality and realistic wind and current at scale with good repeatability [11], [12].

The focus of this thesis is on combined wave/wind/current testing methods in wave basins and developing a hybrid methodology where the wind and current loadings can be applied dynamically through real-time interaction with a software tool. The aim is to develop better testing methods that reduce uncertainty and ultimately accelerate technologies to commercialization and contribute to the ORE targets set out by the EC.

To simulate wind and current in the wave basin, a Multi-Propeller Actuator (MPA) to emulate wind loads on an FOWT scale model was developed for this thesis of which the novelty factor is that multiple aerodynamic loads can be emulated simultaneously. For the emulation of current loads on the FOWT scale model, a novel winch actuator was developed. There are currently no other examples in the literature of simulating current with this method. Both actuators are controlled with a Software-in-the-Loop (SIL) application.

The physical experiments for this study have been conducted in different wave basins at the Lir National Ocean Test Facility (Lir NOTF), Cork, Ireland.

1.2) Objectives and scope.

There are broadly two methods defined for testing of FOWT scale models in wave basins. The first method is referred to as 'full physical testing', which means all the environmental loads are applied physically. This requires the test facility to have the equipment to generate all the environmental loads, and both platform and wind turbine will need to be built at scale. The second method is referred to as 'hybrid testing'. Hybrid testing is a combination of real-time numerical modelling and physical scale model testing. With the hybrid test method some of the physical loads are replaced by a real-time numerical simulation which calculates the forces of the environmental loads, which are consequently applied to the scale model by mechanical actuators. It still requires the platform of the FOWT to be built at scale, however, it does not require a wind turbine at scale. Instead, the mechanical actuator applies the aerodynamic loads at hub height of the scale model. For currents, the hydrodynamic forces are applied by a different actuator at the height of the Center of Gravity (COG) on the FOWT scale model.

The first objective of this thesis was the development of a hybrid test system to emulate the aerodynamic forces of wind turbines, and the drag force of currents on the submerged parts of floating platforms. The system consists of:

- Two mechanical actuators, one for the aerodynamic forces and another for the hydrodynamic forces.
- A numerical simulation, which consists of two algorithms to calculate the different forces.
- A control strategy for the actuators, with real-time feedback from several sensors to create a closed control-loop.
- A processing unit which runs the numerical simulation and provides communication between the numerical simulation, actuators, and feedback sensors.

A major motivation for the development of the hybrid test system is the absence of equipment to generate physical wind in Lir NOTF. Furthermore, only one basin, the Wave Current Flume (WCF),

has equipment to generate physical current. With the hybrid test system wind- and current loads can be added to physical waves during testing in any of the basins. Other motivations include lower costs, greater control, and lower uncertainty.

The second objective of this thesis was a comparison study between the full physical test method and the hybrid test method. The results of repeated tests with the same environmental conditions, and the same FOWT model, during full physical testing and hybrid testing were compared against each other. The comparison revealed the advantages and disadvantages of both test methods. The following wind turbine and platform were chosen for the FOWT model:

- The NREL 5 MW turbine [13].
- The INNWIND.EU semisubmersible platform [14].

The third, and final, objective of this thesis was the validation of the hybrid test system to demonstrate its proof of concept. Besides the comparison of test results from full physical testing and hybrid testing for current, experimental results are also compared with results from numerical models found with Ansys AQWA and FAST v8, with rigid body dynamics of the model as the quantity of interest. Validation metrics were defined and applied to experimental- and numerical results.

1.3) Outline

Four publications, presenting the main results from this body of work, form the backbone of this thesis. The papers in their original form can be found in the appendix.

Paper A, [15] is an extensive review of the state of the art of both experimental and numerical modelling techniques for FOWTs, which is published in the journal *Wind Energy*. Paper A forms the basis of Chapter 3 in this thesis.

The contents of Paper B, [16] were presented at Torque 2020, and consequently published in the *Journal of Physics*. Paper B forms a significant part of Chapter 4 and Chapter 5 of this thesis and describes the development of a Multi-Propeller Actuator (MPA), essentially a modified aerial drone, which is used for the emulation of aerodynamic forces of a wind turbine. Some experimental results are presented for the MPA emulating aerodynamic loads of the NREL 5 MW turbine. Paper B also describes the definition of two validation metrics which are applied to experimental results throughout this thesis.

The contents of Paper C, [17] were presented at Torque 2022, and consequently published in the *Journal of Physics*. Paper C also forms a significant part of Chapter 4 and Chapter 5 of this thesis and describes the development of the hybrid test system for sea currents, which uses a dynamic winch to emulate the drag force of a current on the FOWT platform. Furthermore, the control strategy for the winch and the MPA are described in this paper, along with the algorithm to calculate the drag force acting on the FOWT platform due to current. Experimental results under combined wave/wind/current test conditions are compared to numerical results under the same conditions.

The contents of Paper D, [18] were presented at DeepWind 2022 and have consequently been accepted for publication in the *Journal of Physics*. Paper D forms a significant part of Chapter 5 of this thesis and describes the comparison between the full physical- and hybrid test methods to apply current loads. Experimental results under combined wave/wind/current loads are presented in this paper, where during all the experiments waves are applied physically, wind loads are applied with the MPA, while current loads are first applied physically and consequently repeated with the dynamic winch actuator.

Chapter 2

Floating Wind Technology

This Chapter gives a brief overview of floating wind technology and a description of the INNWIND semisubmersible platform chosen for the FOWT scale model.

2.1) Overview of Floating Offshore Wind Technology

Floating Offshore Wind Turbines are commonly designated by the type of platform which serves as the floating foundation for the wind turbine.

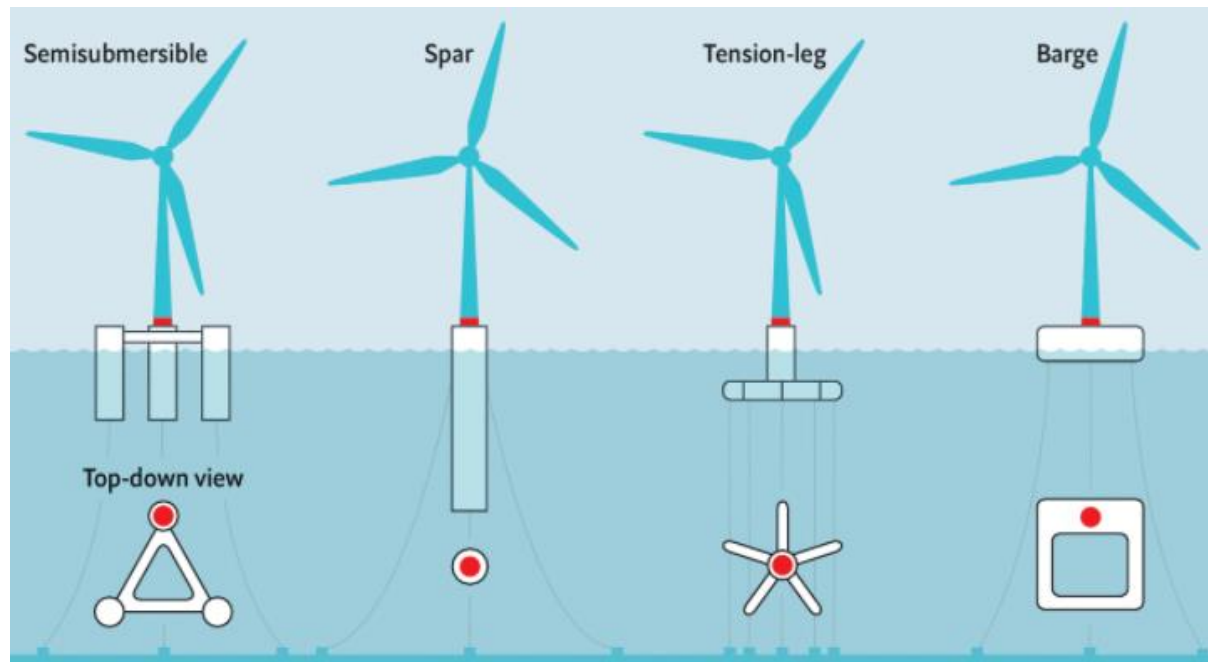


Figure 1. The main types of FOWT foundations. Source: *The Economist* [19]

Most platform designs can be categorized in one of the four main types (Figure 1) of platforms: semisubmersible, spar, Tension Leg Platform (TLP), and barge.

A major challenge for the platform design of FOWTs is its stability. To minimize harmful accelerations on the wind turbine components the platform requires high stability to minimize motions resulting from environmental loads. Furthermore, a stable platform will maximize the efficiency of power production of the wind turbine. However, to keep LCOE as low as possible the challenge is to design a platform that can be manufactured at an industrial scale, with a minimum amount of material, which is relatively easy to install, and complies to the stability requirements.

A different strategy for stability is applied to each of the four types of platforms shown in Figure 1. For detailed descriptions of stability of floating objects the reader is referred to Journee and Massie [20] and Barltrop [21]. In summary, an important measure of a FOWT's static stability is the distance between its COG and its metacenter, GM. The larger GM, the higher its stability. When the metacenter M is below COG, there is negative stability, and the FOWT will capsize when impacted by external forces. Besides a suitably large GM, dynamic stability needs to be sufficient to keep a FOWT stable under the influence of environmental loads. That means restoring forces, from buoyancy or moorings for example, should safely return the FOWT to its equilibrium position after inclination occurs due to impact from waves, wind, current, or other any loads. The restoring stiffness for a free-floating body depends on the length of GM, the location of COG and the Centre of Buoyancy (COB), the buoyancy volume, and shape and size of the waterplane area.

For its stability strategy the spar platform applies a large amount of ballast and a small waterplane area, with a large draft and low COG and high GM for high stability. The spar mainly relies on ballast for stability and less so on its buoyancy and moorings. The spar platform's stability strategy is therefore defined as ballast stabilized. A well-known example of a spar FOWT is Hywind [22].

The stability strategy for each type of platform is illustrated in Figure 2. Each corner of the triangle represents a stability strategy. The blue dots represent the foundation types for FOWTs as indicated. The closer a blue dot is to one of the corners the more its representing FOWT relies on the indicated stability strategy. The closer a blue dot is to the center of the triangle will indicate its representing FOWT is using a mix of the stability strategies.

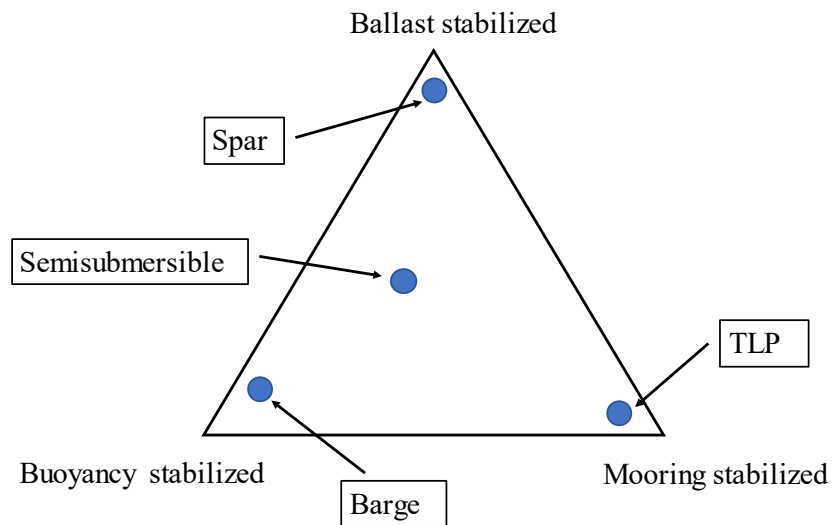


Figure 2. Stability triangle for FOWT platforms.

The TLP relies mainly on its moorings for stability. The TLP's mooring tendons are brought under tension to lower the platform's COG. Like the spar, the TLP has a small waterplane area, but very little ballast. If the mooring tension fails stability will diminish and may lead to capsizing of the TLP platform. The world's first installed FOWT prototype was the Blue H, an 80 kW wind turbine on a TLP platform [23].

In contrast to the spar and TLP, the barge platform relies mainly on its large buoyancy volume for stability and less so on ballast and moorings. The large water plane area of the barge gives it a relatively shallow draft compared to the other concepts, however it also results in higher motion response to environmental loads [21]. The example of a barge platform in Figure 1 has a moonpool to compensate for the large motions; the water within the moonpool has a different natural period than the surrounding structure resulting in damping of the platform motions. A well-known example of a barge FOWT is the 2 MW FLOATGEN demonstrator, which has the IDEOL platform with damping pool as its foundation [24].

The semisubmersible platform uses a combination of these strategies for its stability. The pontoons and columns of the platform provide a large buoyancy volume compared to the spar and TLP. Unlike the barge, the waterplane area of the semisubmersible is small compared to the buoyancy volume and is therefore less affected by environmental loads [21]. The semisubmersible takes a relatively large amount of ballast to lower its COG, and the weight of the moorings also contribute to its stability, though far less so than in the case of the TLP. Hence, the semisubmersible platform is somewhere near

the center on the stability triangle in Figure 2. A well-known example of a semisubmersible FOWT is WindFloat [10].

Most FOWT concepts are designed with either a compliant mooring system, or with a taut mooring system. With a compliant mooring system, such as catenary moorings, the FOWT is relatively free to move in all Degrees of Freedom (DOF) in response to environmental loads. Whereas FOWTs with a taut mooring system, such as tension legs, are constrained in certain DOFs, mainly heave, pitch, and roll. Compliant mooring systems can generally use conventional anchors to keep the FOWT in its intended position. Taut moorings systems on the other hand, require more rigorous methods to anchor the FOWT to the seabed, such as piling or suction anchors.

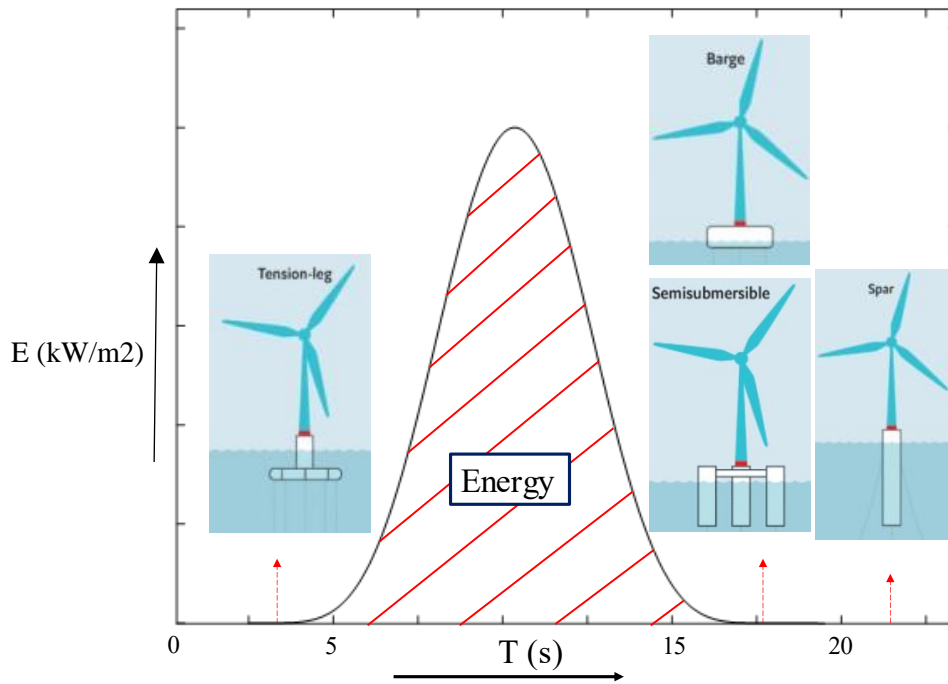


Figure 3. The natural periods of FOWTs are designed to be outside of the range of energetic wave periods in the sea-area where the FOWT will be installed. The X-axis indicates period in seconds and the Y-axis indicates wave energy under the curve.

Mass, buoyancy, geometry, and stability are all parameters that can be used to manipulate the natural, or resonance periods of the platform. Resonance occurs when the natural period of the platform is close to the peak wave period. Therefore, FOWTs are designed to have natural periods of heave, pitch, and roll well away from the peak wave periods of the sea-area where they will be installed (Figure 3) to minimize motions, and therefore accelerations, resulting from wave loads. The natural periods for surge, sway, and yaw of moored FOWTs will generally be longer than naturally occurring wave periods.

The heave natural period, T_h , is found by [25]:

$$T_h = 2\pi \sqrt{\frac{M + M_a}{\rho g A_w}} \quad (1)$$

Where M is the mass of the FOWT, M_a is the added mass, ρ is the density of sea water, g is the gravitational acceleration, and A_w is the waterplane area.

The roll and pitch natural frequencies, $T_{r,p}$, are found by [25]:

$$T_{r,p} = 2\pi \sqrt{\frac{Mr^2 + M_i}{GM \rho g V_D}} \quad (2)$$

Where r is the radius of gyration, M_i is added inertia, GM is the metacentric height, and V_D is the volumetric displacement of the FOWT.

Both equation (1) and (2) clearly show how mass and geometry will influence the natural periods and therefore the overall design of the FOWT.

The type of platform of choice for FOWTs will generally be wind farm specific. Factors which may decide the choice of platform for a specific wind farm site will include met-ocean conditions, geography, nearby ports, and local supply chains.

2.2) The INNWIND.EU semisubmersible platform

The semisubmersible platform design chosen for this body of work was developed for the INNWIND project, an FP7 – EU funded research project. Figure 4 shows the plan- and lateral view of this reference semisubmersible design, which is designed to be made of steel, with dimensions in full scale [14].

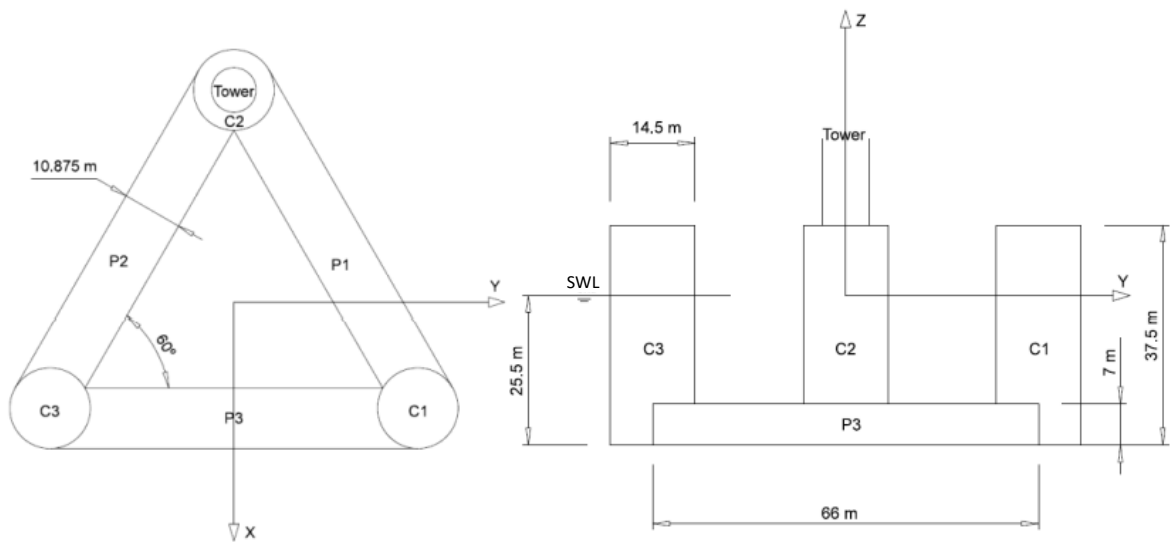


Figure 4. Plan- and lateral view of the INNWIND semisubmersible platform. The origin of the X- and Y coordinates is in COG, with the origin of the Z- coordinate at Still Water Level (SWL).

Simplicity of the design is achieved by connecting the three columns to the triangular pontoon and avoiding any braces between pontoon and columns. The pontoon also acts as a large heave plate. As shown in Figure 4 the tower of the wind turbine is mounted on Column 2. With the turbine mounted away from the center of the platform a full-scale prototype would require an active ballast system to limit roll- and pitch motions. Sea water is used as ballast. The natural periods of the design are all longer than 20 seconds, which is outside the range of energetic wave periods for most wave spectra.

The platform is designed as floating foundation for the DTU 10 MW turbine [26]. For the moorings the designers used a slightly adapted version of the catenary mooring system of the OC4 semisubmersible FOWT [27].

The main characteristics of the platform are shown in Table 1.

Table 1. *Main characteristics of the INNWIND semisubmersible FOWT.*

Distance between columns	66 m
Draft	25.5 m
Freeboard	12 m
Column depth	37.5 m
Column diameter	14.5 m
Pontoon width	10.875 m
Pontoon depth	7 m
Displaced volume	24,907 m ³
Total mass	25,529,675 kg
Center of Gravity	X = 0 m, Y = 0 m, Z = -20.11 m

The semisubmersible platform is a suitable foundation for FOWTs in severe met-ocean conditions due to its high stability and small waterplane area. Along Atlantic coasts in Europe no deep-water ports are available to accommodate spar platforms, with the exception of Norway, yet severe met-ocean conditions are present, as is the case in Ireland. Consequently, the spar buoy, for example, would be a poor choice of foundation type off the coast of Ireland due to its large draft. With that in mind the INNWIND semisubmersible was chosen as the foundation for the scale model of this thesis. The simplicity of this reference platform made the scale model easy to manufacture. Furthermore, its relative shallow draft makes it suitable to use in the shallower wave basins in Lir NOTF as well as in the deep basin, where the harsher met-ocean conditions can be replicated at 1/50 scale.

Chapter 3

Literature review

This Chapter analyses the state-of-the-art of modelling techniques for FOWTs, however, the focus is on experimental techniques. The review of numerical techniques can be found in [15]. In this Chapter techniques which were used for this thesis are reviewed and potential techniques or methods which are currently lacking in the literature were identified through this review. Several experimental techniques for FOWT simulations have been used during this body of work, mostly related to combined wave/wind modelling which are included in this literature review. However, it became apparent from this review that modelling of current with FOWT simulations is mostly neglected in the literature. One of the objectives of this thesis was to fill this gap in the literature. Furthermore, the review only found two examples where propeller actuators were used to simultaneously emulate several aerodynamic loads. The work on the MPA will add to the limited amount of work done on this sort of testing so far. This chapter also gives a brief theoretical overview of the environmental conditions used during numerical simulations and experiments for this body of work and a motivation of why each environmental condition was chosen.

3.1) Environmental conditions

The environmental loads most frequently encountered by FOWTs are those resulting from wind, waves, and current. Other loadings may occur due to ice and earthquakes, for example, however, these will be infrequent in European waters where FOWTs are installed or planned to be installed. Heavy earthquakes could occur in some regions of the Mediterranean Sea. Ice is not uncommon in the Baltic Sea and there are plans for floating wind farms there, however, simulating ice loads or earthquakes falls outside of the scope of this thesis.

Therefore, only wind, waves, and current were considered as the environmental loads for this thesis.

Response of moored FOWTs to wind, waves, and current can include wave-frequency-, low-frequency-, and high-frequency motions. Resonant high-frequency motions, like springing and ringing, can result from higher-order wave loads, mainly on TLPs [25], but are unlikely to occur on semisubmersible FOWTs. However, like any floating object, semisubmersible FOWTs are subjected to first-order wave loads at wave frequencies, and to slow drift, or second-order forces resulting from low frequency wave-, wind-, and current loads.

3.1.1) Wind

Wind is largely the result of uneven heating of Earth's atmosphere by solar radiation due to Earth's tilted axis. This uneven heating causes pressure gradients and as a result air flows from high-pressure areas to low-pressure areas. Other forces influencing airflow in the atmosphere are the Coriolis force, caused by the rotation of the Earth, and friction forces resulting when the motion of an air mass is obstructed by the roughness of Earth's surface [28].

Wind speed varies in time and in height from the surface. For wind energy, the lower part of the atmosphere, often referred to as the atmospheric boundary layer, is of interest. For numerical simulation purposes a 3D profile large enough to envelop the wind turbine is used with room to spare to allow for the motion of the FOWT. Simulation times of up to one hour at full scale have been used for this project to capture aerodynamic loads on the wind turbine and the low-frequency variations which contribute to slow drift loads.

The wind climate in the 3D profile is characterised by mean wind speed, wind direction, wind shear, and a turbulence model, which defines the turbulence intensity, and is based on a frequency spectrum.

TurbSim [29] is used to create a time series of varying wind speeds at hub height of the wind turbine from the Still Water Line (SWL), which is used as input in the aero-elastic simulations with FAST v8.

Mean wind speeds are typically defined at a reference height of $Z = 10\text{m}$ from the surface or SWL. The power law is used to approximate wind speeds at different heights, resulting in a vertical shear profile (Figure 5).

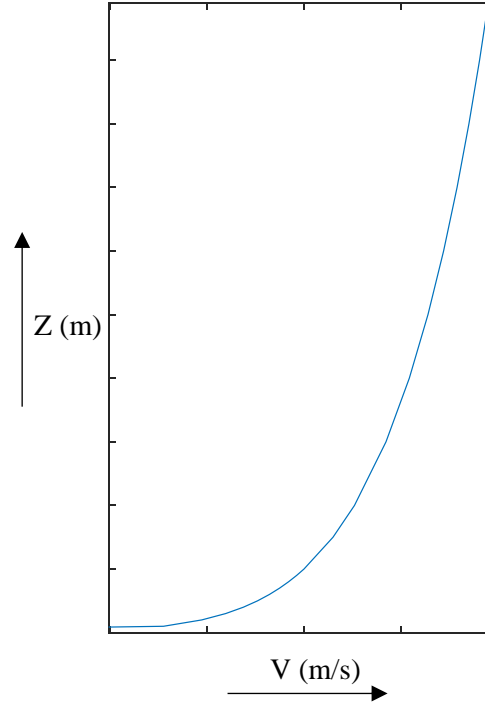


Figure 5. Vertical wind speed profile according to a power law

The power law is defined as [30]:

$$V_{(Z)} = V_{(Z_{10})} \left(\frac{Z}{Z_{10}} \right)^{\alpha} \quad (3)$$

Where V is wind speed, Z is the height in meters from the surface, α is a coefficient for surface roughness. Wind turbulence intensity, TI , is defined as [30]:

$$TI = \frac{\sigma}{V_{(Z)}} \quad (4)$$

Where σ is the standard deviation of the wind speed turbulence, and $V_{(Z)}$ is the wind speed at hub height. The parameters used in TurbSim for the turbulent wind timeseries are defined in Table 2.

Table 2. Parameters used in TurbSim

Mean wind speeds	9 m/s (V1) and 11.4 m/s (V2)
Wind direction	0°
Hub height	90 m
Turbulence intensity factor	0.12
Turbulence model	“smooth”

The turbulence model “smooth” and turbulence intensity = 0.12 have been chosen to reflect wind turbulence over a sea surface with waves.

3.1.2) Waves

Ocean waves are formed by wind blowing over the sea surface (and are therefore indirectly a result of solar radiation). Wave heights and periods will depend on wind strength, the duration the wind is blowing over the sea surface, fetch lengths, and water depths. For brevity, linear wave theory is not reviewed here, however, the reader is referred to e.g. [20], [31]. Instead, the irregular wave spectra used during this project are highlighted. Two JONSWAP spectra have been used during this project, which are described below.

Irregular waves are usually referred to by their wave spectra, which describe the wave elevation of a sea state in the frequency domain, and the wave energy of a sea state as a function of the wave frequency. Some parametric form is used to describe a wave spectrum, for example Pierson Moskowitz, and JONSWAP, both of which are used for wind seas [32]. The Pierson Moskowitz spectrum describes a fully developed wind sea, whereas the JONSWAP spectrum describes a developing sea state. Essentially, the JONSWAP spectrum is a Pierson Moskowitz spectrum multiplied by a peak enhancing factor modifying it for a developing sea state in a fetch limited situation [33].

The Pierson Moskowitz spectrum is defined as [31]:

$$PM = \frac{0.0081g^2}{(2\pi)^4 f^5} \exp\left(-0.74\left[\frac{2\pi Vf}{g}\right]^4\right) \quad (5)$$

Where f is wave frequency. The JONSWAP spectrum is defined as [31]:

$$JS = \frac{\beta g^2}{(2\pi)^4 f^5} \exp\left[-1.25\left(\frac{f}{f_p}\right)^4\right] \gamma^{\exp\left[\frac{\left(\frac{f}{f_p}-1\right)^2}{2\delta^2}\right]} \quad (6)$$

Where:

$$\beta = 0.076 \left[\frac{gF}{V^2}\right]^{-0.22}, \quad f_p = 3.5 \left[\frac{g^2 F}{V^3}\right]^{-0.33}, \quad \text{and } 1 \leq \gamma \leq 7$$

$$\delta = 0.07 \text{ for } f \leq f_p \quad \text{and} \quad \delta = 0.09 \text{ for } f > f_p$$

And where F is the fetch length in meters, γ is a peak enhancing factor, β and δ are coefficients (defined above) and f_p is the peak frequency in Hz. Figure 6 shows a graphical comparison of the Pierson Moskowitz and JONSWAP spectra.

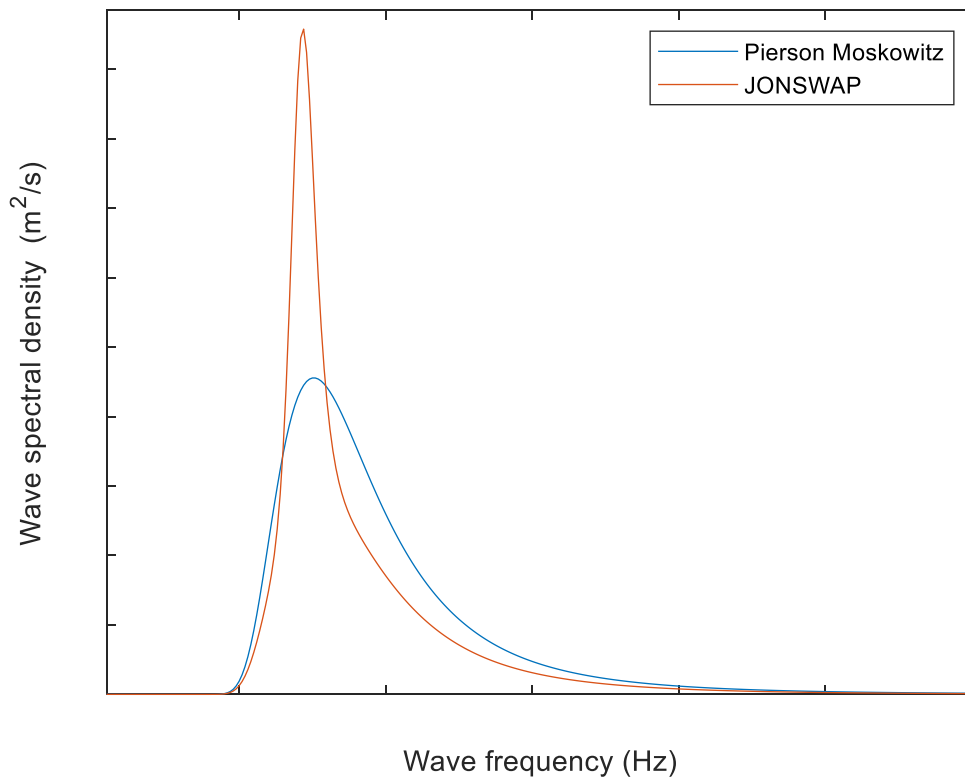


Figure 6. The Pierson Moskowitz spectrum compared to the JONSWAP spectrum

The Pierson Moskowitz spectrum assumes a fully developed sea state which is valid if the wind blows over a large sea area and uninterrupted for several days. The JONSWAP spectrum describes a developing wind sea and was chosen for the simulations and experiments during this project.

The irregular waves used during this project are shown in Table 3.

Table 3. Parameters of JONSWAP spectra used during the project. Wave direction is the same as wind direction.

	H_s	T_p	γ	Direction
JONSWAP 1, Full-scale	5 m	9.5 s	3	0°
JONSWAP 2, Full-Scale	12.5 m	14 s	3	0°
JONSWAP 1, Model-Scale	0.1 m	1.34 s	3	0°
JONSWAP 2, Model-Scale	0.25 m	1.98 s	3	0°

Numerical simulations in this body of work with waves have been conducted at full scale with Ansys AQWA and with FAST v8. Simulation time for the numerical models is one hour. Run times for the scaled experiments with waves is ten minutes, which corresponds to just over one hour at full scale. Both numerical simulations and experiments contain over 100 wave crossings, which in combination with the duration of the tests is sufficient to capture first-order motions and slow drift motions from wave loads [34].

3.1.3) Current

The most common types of sea currents found in areas where FOWTs are installed, or planned are [28]:

- Tidal currents: highly regular cyclical currents generated by tidal forces from the moon and sun.
- Drift currents: wind generated currents due to shear stress between the lower atmosphere and the sea surface. The water particles at the sea surface are dragged along by the wind and the resulting current velocity and direction will depend on the wind velocity and direction.
- Circulating ocean currents: steady, large-scale currents generated by the steady Trade Winds and temperature gradients in the oceans. A well-known example is the Gulfstream.

Hydrodynamic loading from currents is mainly viscous loading, which acts on all submerged parts of the FOWT, including the moorings. The velocity of a sea current varies with the water depth and will be highest near the sea surface, and lowest near the seabed. A similar vertical shear profile exists as for wind, which can be described by a power law like that of equation (3).

The velocity varies in time also, the rate of variation in offshore areas where FOWTs are installed or planned is generally similar to tidally dominated areas. However, for engineering purposes offshore current can be regarded as a steady flow [20].

Peak velocity, and hence maximum viscous loading, is of interest for a FOWT design. Three different, steady velocities have been used during numerical simulations and experiments, which are typical peak velocities in areas where FOWTs are installed or planned. These are shown in Table 4. Durations are the same as for the wind and wave simulations and experiments.

Table 4. Velocities used during numerical simulations and experiments

	Velocity, Model-Scale	Velocity, Full-Scale	Direction
A	0.11 m/s	0.75 m/s	180° to wave direction
B	0.14 m/s	1 m/s	180° to wave direction
C	0.21 m/s	1.5 m/s	180° to wave direction

3.1.4) Wave-current interactions

Wave-current interaction is a well-known phenomenon, which causes the alteration of wave shapes. When the direction of a sea current opposes the incident wave direction, wave lengths will become shorter and wave heights will increase, resulting in steeper waves. The opposite is true when a current follows the incident wave direction: wave lengths become longer and wave heights will decrease, resulting in shallower waves. It is likely that the heave- and pitch response of FOWTs will change due to wave-current interactions and will therefore have to be considered for the simulations and experiments.

When assuming the current as horizontally- and vertically uniform, and using linear wave theory, a reference frame moving at the current velocity can be defined [35] to simplify the analysis. For waves only, and assuming deep water, the wavelength, L , and wave frequency, ω , are defined as:

$$L = \frac{2\pi}{k}, \quad \omega = \sqrt{gk \tanh kh} \quad (7)$$

Where k is the wave number, g is gravity, and h is the water depth. When a current is present the wavelength and wave frequency are defined as:

$$L_1 = \frac{2\pi}{k_1}, \quad \omega_r = \omega \pm k_1 U = \sqrt{gk_1 \tanh k_1 h} \quad (8)$$

Where U is the velocity of the current, and the direction is considered for this thesis as either directly following (+) or directly opposing (-) the wave direction, the subscript 1 denotes the conditions with a current, and ω_r is the wave frequency as measured in the reference frame. For a stationary observer ω

will be the same with or without a current present. The altered wave amplitude, A , in the presence of current [36] is defined as:

$$A_1 = A \sqrt{\left(\frac{C_g}{C_{g1} + U} \right) \left(\frac{1}{1 + U / C_{g1}} \right)} \quad (9)$$

Where C_g is the wave group celerity. Similarly, the spectra of irregular waves are altered by the presence of a current. With an opposing current the spectral energy will increase, and for a following current the spectral energy will decrease. The alteration of wave spectra due to the presence of current is defined [37] as:

$$S_1(\omega) = S(\omega) \frac{4}{\left[1 + \sqrt{1 + (4U\omega/g)} \right]^2 \sqrt{1 + (4U\omega/g)}} \quad (10)$$

Figure 7 shows the theoretical JONSWAP spectra for waves only and waves with opposing current. The opposing current results in a higher peak and increased energy at the higher wave frequencies.

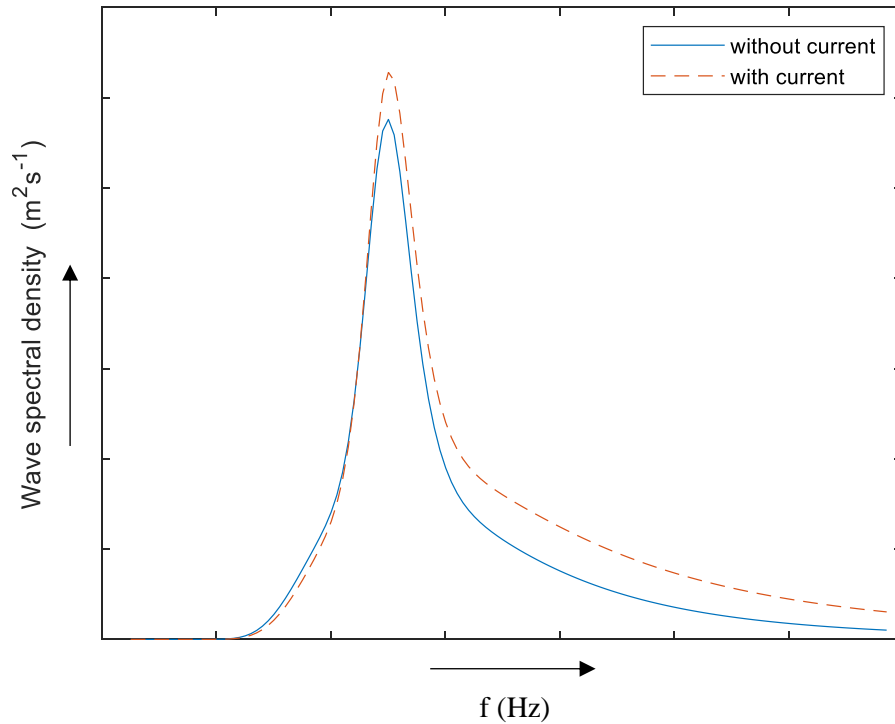


Figure 7. JONSWAP with- and without current opposite of wave direction

By altering wave heights and wave steepness, wave-current interaction will influence the response of the platform, particularly in the heave- and pitch Degree of Freedom (DOF). To simulate wave-current interactions with the SIL experiments, wave shapes as if a current is present will have to be approximated in the basin. It is not possible to change the wave lengths while maintaining the wave period, as this is a limitation of the wave maker. However, it is possible to create steeper- or shallower waves by simply changing the wave heights. For irregular waves, the wave maker is re-programmed to change the wave heights of a wave-only spectrum. This results in a wave spectrum with equivalent spectral energy as if a current is present, by transforming the wave-only spectrum into a spectrum according to equation (10).

3.2) Physical modelling

Comparing numerical results with experimental results obtained in laboratory basins for validation is still considered an essential step in the design process by most designers of FOWTs. As turbine sizes continue to grow, consequently, the platform sizes of FOWTs continue to get larger. To accommodate the increasing dimensions of prototypes at model scale, and reduce the uncertainty of physical modelling, testing techniques of FOWTs in laboratories are evolving. The state-of-the-art of physical modelling techniques is outlined in this section.

3.2.1) Scaling laws

Geometrical, kinematic and dynamic similarity between model scale and full scale is required [38] for the experimental validation of numerical models.

For geometrical similarity this means that all linear dimensions must have the same scale ratio, which is defined as:

$$\lambda = \frac{L_F}{L_M} \quad (11)$$

Where L is physical length, and the subscripts F and M indicate full scale and model scale, respectively. The ratio between inertia and gravity is defined as:

$$\frac{U^2}{gL} \quad (12)$$

Where U is velocity, and g is gravitational acceleration. The dynamic similarity requirement between model scale and full scale then, is defined as:

$$\frac{U_M}{\sqrt{gL_M}} = \frac{U_F}{\sqrt{gL_F}} \quad (13)$$

Which is also known as the Froude number.

The ratio between inertia and viscosity is defined as:

$$\frac{UL}{\nu} \quad (14)$$

Where ν is the kinematic viscosity. The dynamic similarity requirement between model- and full scale is defined as:

$$\frac{U_M L_M}{\nu} = \frac{U_F L_F}{\nu} \quad (15)$$

This is known as the Reynolds number.

As the kinematic viscosity of air will remain the same for prototype and scale model it becomes apparent that for a Froude scaled rotor with geometric similitude, the Reynolds number will be lower at model scale compared to the Reynolds number of the full-scale rotor. Consequently, the lift coefficient of the model scale rotor will be lower, and the drag coefficient will be higher compared to the full-scale rotor. As a result, the aerodynamic performance of the model scale turbine will be affected, causing a misrepresentation of wind load induced motion response of the FOWT. The focus for scaled turbines, however, is on the ability to emulate Froude scaled rotor thrust and torque. The following sections explain how this is achieved.

3.3) Full physical testing

From equations (11) to (15), it becomes apparent that either increasing the velocity of the applied wind or adjusting the turbine rotor geometry at model scale could compensate for the lower Reynolds number. Rotor thrust is the most critical aerodynamic load to impact on motion response of FOWT models. The simplest, and lowest fidelity, method to emulate thrust force is with a mechanical pulley system [39]. This method can only model steady thrust loads but cannot capture aerodynamic damping or the effects of turbine control. A simple method to emulate rotor thrust load with physical wind is using a drag disc instead of a scaled rotor. In combination with a Froude scaled rotating mass, the rotor gyroscopic loads can also be emulated [40]. The drag disc method allows for varied thrust loads but like the pulley system will not be able to capture aerodynamic damping or the effects of turbine control [41].

Increased wind velocity applied to a Froude scaled rotor can overcome the abovementioned limitations of the drag disc and achieve correct rotor thrust. However, maintaining rated rotor speed at higher wind velocities means the Tip Speed Ratio (TSR) cannot be maintained [42]. As a result, rotor torque cannot be modelled correctly, and aerodynamic damping may not be captured correctly. If on the other hand correct TSR is maintained, the Eigen frequencies of the rotor and blade-tower passing frequency (3P frequency) and rotor thrust forces cannot be modelled correctly. Geometrically modified aerofoils to compensate for the low Reynolds number in a Froude scaled wind environment, are better able to emulate aerodynamic loads, and capture damping effects and blade pitch control effects while maintaining TSR. This is generally referred to in the literature as performance scaling of the rotor [43]–[45]. Roughened leading edges on the rotor blades, and slight increases of applied wind velocity, in combination with geometrically altered rotor blades can be applied to fine tune the model thrust forces.

3.3.1 Froude scaled rotor combined with higher than Froude scaled wind velocity

Skaare et al [22] tested a 1/67 scale model of the Hywind FOWT at SINTEF, Norway, in 2005. Their model used a geometrically adjusted rotor with two DC motors along with physically generated wind to control rotational speed of the rotor and blade pitch angle. The experimental results of this campaign were used to validate the integration of the two independent simulation software tools SIMO/RIFLEX (floater) and HAWC2 (turbine) to a coupled simulation tool for FOWTs.

Mortensen et al [46] tested a 1/35 model of a Tension Leg Platform (TLP) with a Froude scaled version of the NREL 5 MW reference turbine [13] and increased wind velocity. The numerical model was validated with the experimental results, which showed that dynamic response of the TLP was predicted correctly.

Bahramiasl et al [47] tested a 1/100 scale model of a TLP FOWT with a Froude-scaled turbine and increased wind velocity at Sharif University, Iran. As the applied wind failed to turn the rotor, an electric motor with variable speed was used to drive the rotor and aid rotation. Increasing the rotational speed of the rotor showed some damping effects caused by the gyroscopic moment. Furthermore, a shift of the peak of the RAO spectra of the platform in heave, surge, pitch and yaw occurred.

Liang Li et al [48] tested a 1/50 scale model of the DeepCwind semisubmersible FOWT with a Froude scaled version of the NREL 5 MW turbine at Shanghai Jiao Tong University, China. Rather than controlling the rotor speed with an electric motor, the rotor was allowed to run freely, and the motor acted as a generator. The mechanical damping by the generator served to slow down the rotor speed and bring TSR closer to the desired rate resulting in improved aerodynamic damping compared to forced rotor speed control with an electric motor.

3.3.2 Geometrically modified low-Reynolds aerofoils combined with Froude scale wind velocity (performance-scaled).

For the University of Maine led DeepCwind consortium, Goupee et al [49], [50] tested 1/50 scaled models of a spar, semisubmersible and TLP platform at MARIN, the Netherlands, to compare the floater responses under similar conditions. Each platform was originally equipped with a geometrically scaled

version of the NREL 5 MW reference turbine.

The DeepCwind team learned that geometrically scaling the rotor (based on a Froude-approach) was not the correct approach for scaled testing of FOWTs. The MARIN reference turbine was redesigned to create a performance-matched scaled model of the NREL 5 MW reference turbine. With this new turbine, the DeepCwind semisubmersible design was retested at MARIN in 2013, and this dataset was used for the validation study conducted in Phase II of the OC5 project.

The performance-matched MARIN reference turbine was also used by De Ridder et al [11] on the GustoMSC Tri-Floater model at MARIN. The results showed that the thrust coefficient of the model turbine was consistent with the thrust coefficient predicted by the CFD models, whereas the power coefficient found in the experiments is lower than the power coefficient predicted by the CFD models. To correctly model floater motions under combined wave/wind loads in laboratory basins a correct thrust coefficient of the model turbine is essential, whereas the influence of the power coefficient is negligible.

Bredmose et al [51] tested a 1/60 scaled version of the DTU 10 MW reference turbine [26] with low-Reynolds aerofoils on the Triple Spar platform, a hybrid spar/semi-submersible platform designed for the INNWIND.EU project, at the Danish Hydraulic Institute (DHI), Denmark. The focus of this campaign was the effect of the blade pitch controller on the response of the platform. Experiments with wind-only loading revealed a clear instability at the natural platform pitch frequency due to aggressive blade pitch control above rated wind speed.

Madsen et al [52] also used the 1/60 scaled low-Reynolds version of the DTU 10 MW turbine on a model of the KIER TLP at DHI, Denmark. They also used three different kinds of controllers for blade pitch and found that use of the land-based controller resulted in high oscillations in blade pitch and increased surge response of the platform.

Koch et al [53] tested a 1/60 scale model of the DeepCwind semisubmersible FOWT with a low-Reynolds version of the DTU 10 MW turbine at Ecole Centrale de Nantes (ECN), France. To compensate for the higher mass of the turbine, ballast was added to lower the centre of gravity of the platform to the same level of the original design with the NREL 5 MW turbine. Free decay tests, wave only tests and wind only tests were performed, and all were found to be in good agreement with the numerical model.

Similarly, Ahn and Shin [54] adapted a 1/90 scale model of the DeepCwind semisubmersible for a low-Reynolds version of the DTU 10 MW turbine at the University of Ulsan, South Korea. Combined wave, wind, and current conditions were modelled, where a steady current load was introduced by a mechanical pulley system. The introduction of current had a damping effect on the surge motion of the platform.

Ward et al [55] developed a model turbine with performance scaled aerofoils, a light-weight Rotor Nacelle Assembly (RNA) and blade pitch control. Although the turbine has a fixed radius, the model turbine can be used for various turbine designs by adding weights to the RNA and varying the thrust load by pitching the blades. The concept was shown numerically to be viable. However, experimental results to validate their claims are not presented in the paper.

Connolly et al [56] tested a 1/50 scale model of the Eolink semisubmersible FOWT with a low-Reynolds version of a 10 MW turbine at L'Institut Français de Recherche pour l'Exploitation de la Mer (IFREMER), France. The Eolink concept uses a pyramid construction to support the RNA with four pillars rather than the traditional single tower, and a single point mooring system for yaw alignment of the platform. Good agreement was found compared with the numerical results of Flexcom for most platform dynamics, however, the experiments showed that pitch response was overestimated by the numerical model.

Zhao et al [57] tested a 1/50 scale model of the WindStar TLP with a low Reynolds version of the NREL 5 MW turbine at Shanghai Jiao Tong University, China. An electro motor was installed on the turbine model to maintain TSR during tests with wind. They found that overall, the model showed relatively

small motion responses, and that wind and current had a damping effect on the surge and pitch response.

3.4) Hybrid testing

Hybrid testing is the alternative to full physical testing of FOWT models. With this method, waves are still generated physically but the aerodynamic loads are replaced by a numerical substructure, i.e., a numerical wind field is introduced in real-time. The Froude/Reynolds mismatch is solved by calculating the aerodynamic loads at full scale and applying them to the physical model at Froude scale via one or several mechanical actuators. The two types of actuators most used in hybrid FOWT wave basin testing so far have been dynamic cable winches and propellers. The simplest, and lowest-fidelity, hybrid method applies a steady load to the actuator to emulate steady thrust load. Aerodynamic damping and turbine control will not be captured by this method. Stochastic wind loads can be emulated by applying a time-series input which tells the actuator to vary the loads. This method will capture aerodynamic damping, however, synchronizing wave elevations and wind loads is challenging. Furthermore, turbine control effects are only emulated as the numerical simulation captures them; it is not possible to emulate turbine control effects that react to the actual motion of the platform with this method. Real-time hybrid testing is a more complex but higher-fidelity method. With this method, physical modelling of the waves is combined with the numerical simulation of wind loads in real-time. The hydrodynamic module of the numerical code is replaced by the input of a motion tracking system, which records the spatial position of the platform for each time-step. According to the motion tracking data, the numerical code then calculates the aerodynamic loads acting on the turbine for the given wind velocity at full scale for each time-step. Finally, the aerodynamic loads are emulated by the actuator(s) at Froude scale and applied to the physical model and the process is repeated for the next time-step. This way, depending on the number of actuators, most aerodynamic effects can be captured (at least those that are captured by the numerical model), and waves and wind are perfectly synchronized. The diagram in Figure 8 shows a FOWT hybrid test setup for a wave basin developed at Centro Nacional de Energías Renovables (CENER), Spain, by Azcona et al [58].

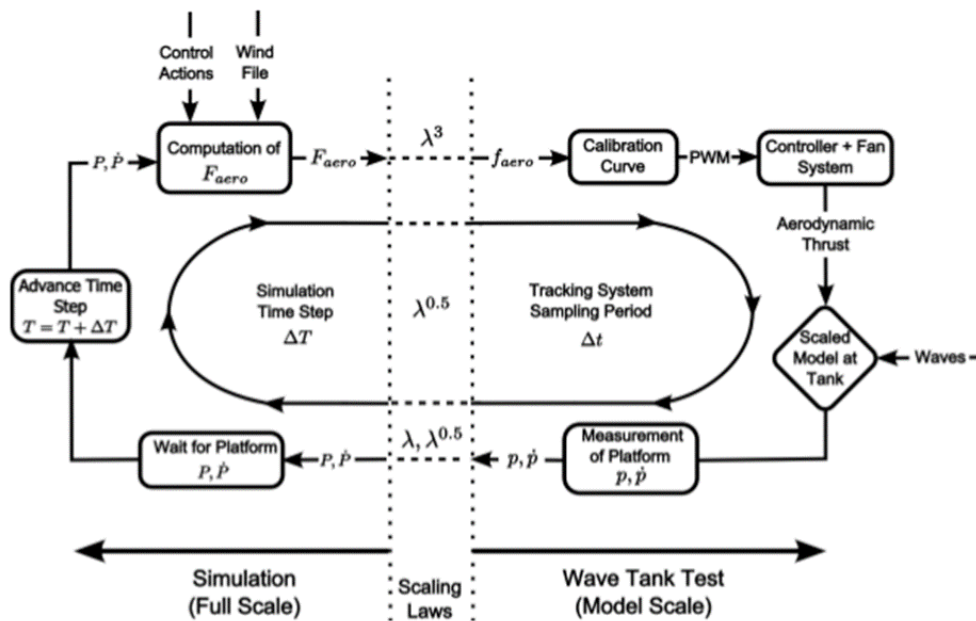


Figure 8. Diagram of the “Software-in-the-Loop” real-time hybrid test setup [58].

3.4.1) Hybrid testing with propeller actuators

Azcona et al [58], from CENER in Spain, were among the first researchers to use a propeller as an actuator for hybrid FOWT modelling. They have named their method Software-In-the-Loop (SIL). This method uses a single ducted propeller at hub height of the model. The diagram in Figure 9 indicates the hardware set-up of the SIL system.

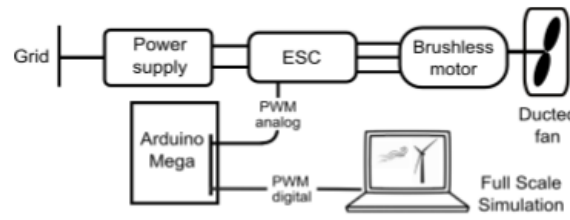


Figure 9. Hardware for the SIL setup [58].

The single propeller of the SIL system only emulates aerodynamic thrust, therefore the focus of their study was on platform pitch and surge response. Azcona et al used the SIL method to test a 1/40 scale model of the Concrete Star Wind Floater semi-submersible platform (Figure 10) at ECN, France. The turbine that was modelled during the experiments was a 6 MW turbine designed by Siemens. Azcona et al found that the platform surge and pitch response were closely matching the numerical models during static wind tests and free decay tests, demonstrating the ability of the SIL method to capture aerodynamic damping.

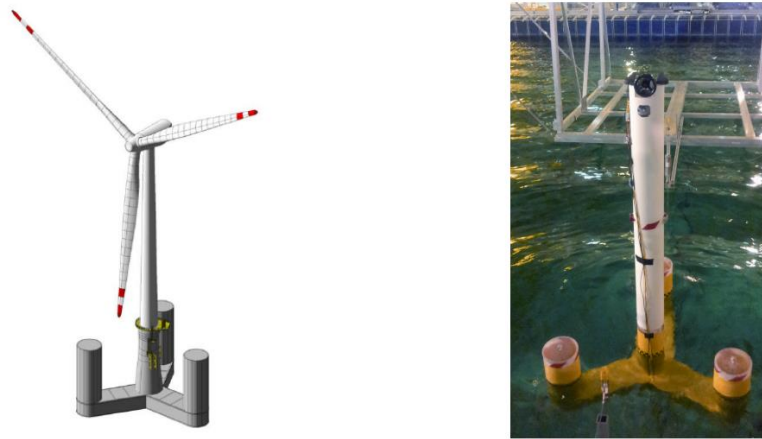


Figure 10. Full-scale CAD visualization (left) and model (right) of the OO-Star semisubmersible with ducted propeller [58].

In a separate campaign, researchers from CENER applied the SIL method to a 1/45 scale model of the DeepCwind semisubmersible platform, also at ECN [59], [60]. Second order hydrodynamics were included in the numerical models. Accuracy between experiments and numerical models had improved compared to the previous test campaign, when the second-order hydrodynamics were included in the numerical model. Best results were achieved for combined irregular wave and turbulent wind cases. In these cases, the aerodynamic excitations of the platform overshadow the second order hydrodynamic excitations for this type of platform.

Wright et al [61], fitted a ducted propeller on a 1/50 and a 1/30 scale model of a hexagonal braced TLP platform at IFREMER, France. Rather than using the SIL method, only steady thrust force was emulated. The aim of this study was to measure the difference in surge response in experiments with- and without spring dampers in the mooring tendons. The results showed that the surge amplitude increased but mooring tension decreased with the spring dampers added to the mooring tendons.

Desmond et al [62] tested a 1/36 scale model of the SCDnezy², a semisubmersible FOWT design with two rotors and a single point mooring system, at Lir National Ocean Test Facility (NOTF), Ireland. Two ducted propellers were used to emulate steady wind loads and two stepper motors driving Froude scaled weights were used to emulate gyroscopic loads. Emulation of rotor thrust loads were found to have a significant impact on uncertainty, whereas the gyroscopic loads had limited impact.

Oguz et al [63], applied the SIL method to a 1/36 scale model of the Iberdrola TLP with the NREL 5 MW reference turbine at the University of Strathclyde, United Kingdom. The model was equipped with a single ducted propeller at hub height emulating aerodynamic thrust of the 5 MW turbine. The

experiments showed that the platform response and tendon tensions were over predicted by the numerical models at the pitch- and surge natural periods.

Andersen [64] fitted a single propeller, using the hybrid method without real-time motion feedback, on a model of a generic semi-submersible model with three main floater columns and heave plates. The aerodynamic thrust loading was modelled using a turbulent wind time series of the DeepCwind semisubmersible FOWT, a comparable platform to the platform used in the experiments. This method is of lower fidelity and accuracy compared to the experiments by Azcona et al and Oguz et al, using the SIL method.

A similar conclusion was found by Matoug et al [65]. Although the focus of their study was the comparison of the DTU 10 MW horizontal-axis wind turbine and the WindQuest 10 MW vertical-axis wind turbine on the same platform, they repeated their testcases, using the hybrid test method, with and without SIL. The experimental results with SIL matched the numerical results better than the test cases without SIL. A 1/42 scale model of the Nautilus semisubmersible FOWT was used for the experiments.

Using a single propeller with the hybrid method means the modelling of aerodynamic loads is limited to thrust load only, and although this is by far the most important excitation mode, other aerodynamic loads such as rotor torque, gyroscopic momentum and 3P tower loading are not captured.

Meseguer and Guanche [66], developed a multi-propeller actuator, which also uses recreational drone technology, with six propellers. Their multi-propeller actuator was used for an experimental test campaign of the TELWIND model FOWT [67] at Instituto Hidraulica Cantabria (IHC), Spain. Only constant wind loads were emulated during the tests.

Researchers from CENER have developed a MPA with four propellers for multi-DOF emulation with SIL [68], which was used on a 1/50 scale model of the DeepCwind semisubmersible FOWT for the Marine Renewable Infrastructure Network for Enhancing Technologies 2 (MaRINET2) project at MARIN [69]. The focus of their studies was on the testing of control strategies with the improved SIL for the NREL 5MW turbine.

Kanner et al [70] applied hybrid testing to a semi-submersible model platform, based on the WindFloat platform, called MIST, at University of California Berkeley, United States of America. Rather than modelling a conventional horizontal-axis turbine, they modelled two vertical-axis turbines on the platform. The tangential force developed by aerofoils on vertical-axis turbines was emulated by two counter-rotating rods in the horizontal plane, each driven by a propeller at one end of the rod. The drive train of the actuators included a gearbox and generator, converting the mechanical power of the rods into actual electrical power. By controlling the generators during the tests, Kanner et al achieved limited yaw orientation of the platform to optimize power production of the turbines.

3.4.2) Hybrid testing with dynamic winch actuators

Researchers from SINTEF, Norway, have performed a series of experiments [71]–[73] using real-time hybrid testing with a 1/30 scale braceless semi-submersible FOWT model [74] and the NREL 5 MW turbine. The researchers from SINTEF have named their method Real-Time Hybrid Model (ReaTHM) testing and use a square frame at hub height of the model connected with the winch cables. A comparison of the experimental results with numerical models is presented by Karimirad et al [75]. An earlier quantification study [76] found the gyroscopic moments and heave response due to aerodynamic forces to be negligible for this type of platform. The SINTEF researchers therefore opted to emulate a limited number of aerodynamic loads. Waves and current, during the experiments were modelled physically. The numerical wind field was generated in TurbSim and the full-scale aerodynamic loads were calculated with AeroDyn.

Thys et al [77] used the ReaTHM test method at SINTEF to test a physical 1/36 scale model of the Nautilus semisubmersible platform with the DTU 10 MW turbine, as part of the LIFES50+ project [78]. An adjusted top frame and cable layout was used for this test campaign, and 3P frequency and first

tower bending frequency were added in addition to the aerodynamic loads emulated on the 5 MW model platform.

Chabaud et al [79], compared the ReaTHM methods used for the test campaigns of the 5 MW and 10 MW model platforms at SINTEF and gave a theoretical overview of the allocation of tension for the actuation cables for the two methods. Where both methods provided similar results in terms of accuracy, the method used for the 10 MW platform provided higher flexibility allowing for a higher number of aerodynamic loads to be included in the tests with the same number of cables and winches. However, the higher flexibility comes at the expense of higher cable tensions and a larger test area as the winches need to be spaced wider apart.

Hall and Goupee [80] used dynamic cable winches for hybrid testing of a 1/50 scale model of the DeepCwind semisubmersible platform, which was also equipped with a geometrically scaled rotor and low Reynolds adjusted blades. They validated the hybrid method by disconnecting the actuator cables and repeating the steady wind case with physical wind generated above the basin, at the University of Maine, United States America. In contrast to the SINTEF test campaigns, Hall and Goupee opted to simplify the test setup by only emulating the aerodynamic thrust in the hybrid tests using two rather than six cable winches. Using a windward and leeward winch cable connected at hub height allows for accurate control of aerodynamic thrust emulation. The results of the hybrid tests and full physical regular wind-wave tests matched closely, validating the hybrid approach. Hall and Goupee found that introducing wind turbulence in the hybrid experiments added a noticeable amount of excitation, accurately reproducing aerodynamic damping found with the numerical models, which was difficult to reproduce with the full physical wind-wave experiments.

Antonutti et al [81] used dynamic cable winches for hybrid testing with SIL of a 1/35 scale model of the Naval Energies semisubmersible FOWT with the Haliade 6 MW turbine at MARIN. Similar to the SINTEF campaigns, Antonutti et al used a cross-shaped metal frame with four front wires and one back wire. This enabled actuation in the surge, pitch and yaw DOFs. For operational and severe sea-states the experimental results were found to match the numerical results closely with combined wave and wind loads.

Some advantages and disadvantages of dynamic cable winches compared to propeller actuators are listed in Table 5.

Table 5. *Advantages, and disadvantages of propeller vs winches.*

	Advantage	Disadvantage
Propellers	<ul style="list-style-type: none"> • Effective simulation of thrust loads • Integrated on the model, small footprint on the test area • Simple control. 	<ul style="list-style-type: none"> • Difficult to effectively simulate aerodynamic moments • Source of high-frequency vibrations and, therefore, systematic uncertainty.
Cable winches	<ul style="list-style-type: none"> • Effective simulation of thrust and aerodynamic moments • Low vibration levels, less systematic uncertainty 	<ul style="list-style-type: none"> • Winches are land-based, large footprint on test area • Control of winches is complex compared to propellers

3.4.3) Hybrid testing in wind tunnels

Another approach to hybrid testing of FOWTs is to use SIL to numerically represent the hydrodynamics of the system, as opposed to the aerodynamics. This approach enables validation of aerodynamic forces in an environment with superior wind quality compared to wind generation over a wave basin, while allowing for examination of these aerodynamic forces under motion typical of a FOWT. This is particularly useful when studying the evolution of turbine wake of FOWTs, and how it may affect

downwind turbines and farm layouts.

Schliffke et al [82] used a simple, 1/500 scale model of the FLOATGEN FOWT in a small wind tunnel at ECN, France to study unsteady aerodynamics and wake development. The model consisted of a porous disc at hub height mounted on a small rig to simulate regular surge motion of the platform. Results showed that the surge motions did not change mean velocities in the wake, however, turbulence intensity in the wake was modified.

Rockel et al [83], [84] performed experiments with two performance scaled, 1/400 scale wind turbine models of a typical horizontal-axis wind turbine with 80 meter rotor diameter in the wind tunnel at Portland State University, United States of America. In the first study the wake of a bottom-fixed model was compared with the wake of a FOWT model that was allowed to oscillate freely in the pitch DOF by mounting the model in a gimbal. In the second study both turbine models were used in tandem in the wind tunnel.

Bayati et al [85]–[87] used a Hardware-in-the-Loop (HIL) setup with a performance scaled, 1/75 scale model of the DTU 10 MW turbine on a 2-DOF rig (Figure 11) to simulate surge and pitch motions of the OC5 semisubmersible FOWT in the wind tunnel of Politecnico di Milano, Italy. Platform kinematics were calculated and applied in real-time. The HIL setup uses load cells, dynamometers, accelerometers, linear variable displacement transducers, and a laser displacement sensor for a position feedback signal to update the numerical simulation of the platform motions for each time-step. The motion feedback combined with increased DOFs allows for a higher-fidelity test setup compared to the abovementioned studies by Schliffke et al and Rockel et al.

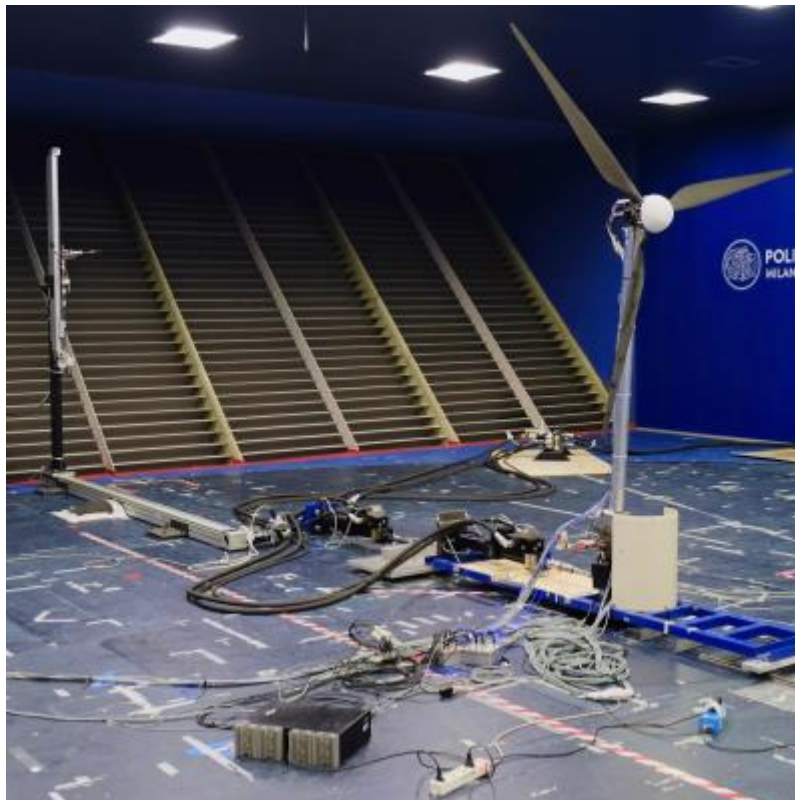


Figure 11. the DTU 10 MW model on the 2-DOF rig in the wind tunnel at Politecnico di Milano [88]

In follow-up studies Bayati et al [89]–[91] used a physical 1/75 scale, performance-scaled model of the DTU 10 MW turbine on a custom-designed 6-DOF robot, named Hexafloat, in the wind tunnel of Politecnico di Milano, Italy, rather than the 2-DOF rig. The platform hydrodynamics emulated by the 6-DOF Hexafloat were based on an ad-hoc model FOWT initially, and on the OO Star semisubmersible FOWT and the Triple Spar FOWT for later tests. The applied wind velocity in the wind tunnel was increased by a factor of 3 to match the Reynolds number at full scale as closely as possible. The higher

DOFs and addition of turbine control equipment allowed Bayati et al to also investigate turbine control routines. The results of the experiments with both the 2-DOF rig and Hexafloat showed close agreement with the wake measurements and platform dynamics found with numerical models.

Thys et al [92] performed scale model hybrid tests for the OO-Star and Nautilus FOWTs with the DTU 10 MW turbine in the wave basin at SINTEF and in the wind tunnel at Politecnico di Milano, Italy, for a comparative study. Wind tunnel experiments of the 1/75 scale model of the DTU 10 MW turbine in combination with the Hexafloat were first performed to validate the aerodynamic model. Next, the validated aerodynamic model was used with a 1/36 scale model of the platform and dynamic winch actuators to emulate wind loads in the wave basin for calibration of the platform and hydrodynamic model.

Arnal et al [93] used a 6-DOF Hexapod with a propeller actuator, rather than the wind tunnel, to simulate the NREL 5 MW turbine with the DeepCwind semisubmersible platform and the Hywind spar platform, and the DTU 10 MW turbine with the Triple Spar platform at ECN, France. They found that, at a scale of 1/30, high frequency aerodynamic loads could be emulated accurately with their system.

3.5) Comparison of test methods: full physical vs hybrid, in laboratory wave basins

In this section the advantages and disadvantages of both full physical testing and hybrid testing are outlined and compared against each other (Figure 12).

Generating physical wind in laboratory basins requires large wind generation installations and large

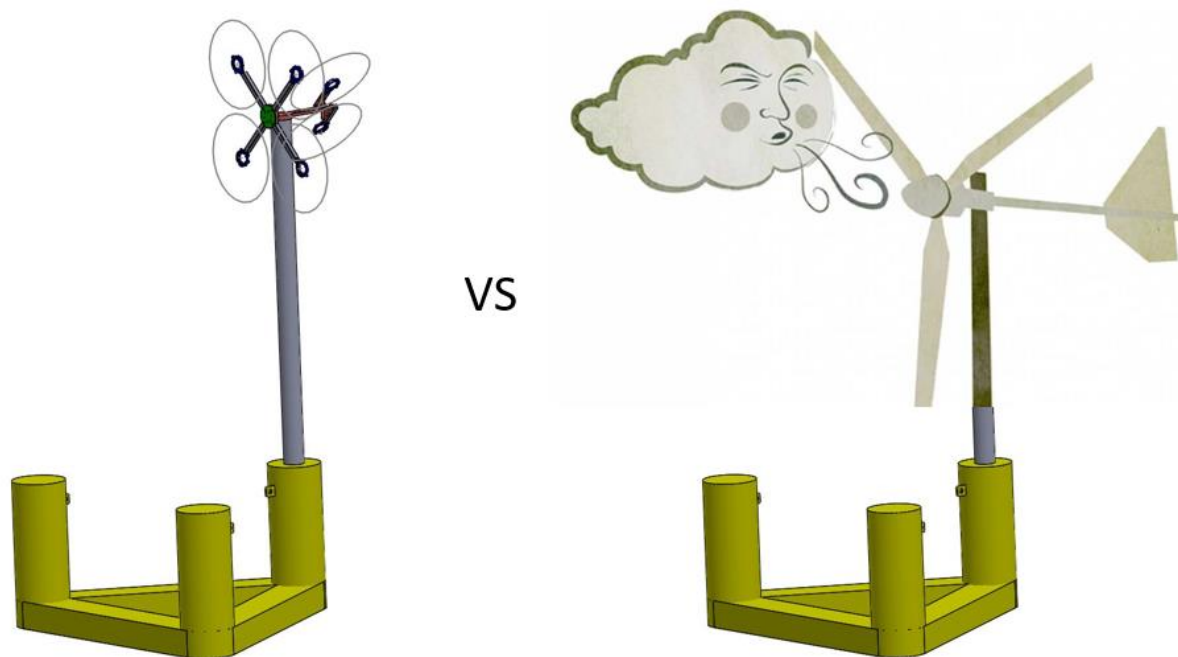


Figure 12. Hybrid testing (left) vs full physical testing (right)

amounts of energy to run said installations, making them expensive to operate. Furthermore, high-quality wind generation and accurate simulation of wind gradients and turbulence in the wind field are difficult to achieve other than in wind tunnels. A typical setup for an above-basin wind generation system consists of a bank of fans arrayed in several rows and columns, pumping the air through ducts with screens, honeycomb mesh, and nozzles over the basin. The screens and honeycomb mesh reduce the turbulence of the outflowing air, and the nozzle directs the flow to an area that can cover the rotor. Stochastic wind can be simulated by varying the revolutions per minute of the fans during tests, and vertical shear can be simulated by controlling each row of fans separately [41]. Accurately measuring and mapping the wind field is important to determine the best location for the model relative to the nozzle. This procedure is described for the MARIN wind setup in de Ridder et al [11] and for DHI in

Madsen et al [52]. They showed that it is difficult to control the boundaries of the wind field and circulation of the airflow once it exits the nozzle. Inconsistencies in the screens and fan motors etc. can be mapped and accounted for during analysis of test results. However, the inability to control the airflow over the basin, unlike in wind tunnels, will decrease the ability of accurate repeatability of the tests, adding uncertainty in the test method.

An advantage of performance-scaled turbines on FOWT models in combination with applied wind generated above the basin is the ability to maintain the correct thrust coefficient and TSR in a Froude-scaled wind environment. This method also captures the effects of rotor gyroscopic moments, rotor torque and aerodynamic damping, and it is possible to implement turbine control. Another advantage is that it is likely that unexpected aerodynamic phenomena and hydrodynamic response, which are not captured with the numerical model, will be captured during the physical experiments. However, the low-Reynolds modifications make it difficult to also model the power coefficient and torque characteristics of the turbine accurately, limiting the scalability of blade pitch control and the ability to capture aerodynamic damping accurately [78], [80]. Other disadvantages are the high costs of developing a modified model turbine, and the requirement of a bespoke scaled model turbine for each different design and scale [41].

Hybrid testing in wave basins has the benefit that it does not require physical wind and current generation in testing facilities that do not have such capabilities. Furthermore, hybrid testing allows for the implementation of wind turbulence, turbine control strategy and aerodynamic damping, and any turbine type can be simulated regardless of the scale, making it far more versatile and cheaper compared to full physical testing.

However, a hybrid test setup is a complex system; fidelity of the test method and accuracy of test results can be influenced by a number of factors such as the force actuation and motion tracking.

The accuracy of wind emulation will depend on the type and number of actuators. However, the mechanical actuators are easier to control than physically generated wind [80]. Careful calibration of the actuators and quantification of actuator inaccuracies provides high experimental repeatability, as was found by Meseguer and Guanche [66] and Bachynski et al [72].

With hybrid FOWT testing, the hydrodynamic module of the aero-hydro-servo-elastic tool used for the numerical substructure is de-coupled, and instead the motion response data of the physical model received from the motion tracking system is used as the hydrodynamic input to calculate the next simulation step, as described in section 3.4. The motion tracking system will therefore require high accuracy of position measurements. Furthermore, it will require a high sampling rate and must be able to operate in a wet environment.

A certain amount of system latency during hybrid testing is unavoidable. Each step in the hybrid testing loop - simulation, actuation, motion tracking and feedback - causes a system delay. An appropriate simulation time-step at scale for hybrid modelling must be determined. Within this time-step the actuator must have sufficient bandwidth to deliver the required load at the right frequency, and the motion tracking sampling rate must be high enough to feed the position data back to the numerical code to calculate the required actuator load for the next time-step. To keep the latency at acceptable levels within each time-step, the actuator will have to emulate the required loads faster than the numerical simulation takes to calculate the loads for each time-step. It becomes apparent then that the computing system will require high processing power.

In the design of the experiments, the appropriate time-step, number of actuators etc. used for hybrid modelling will depend on the parameters of interest to be investigated. Sensitivity studies, e.g. Hall et al [94], [95] and Bachynski et al [76], will give an indication of the required actuation forces and number of actuators, tolerance levels of inaccuracy and latency. A higher number of actuators will increase the fidelity of the hybrid test method, as the three-dimensional wind field can be represented more accurately. However, a higher number of actuators will result in a more complex system and a higher level of uncertainty.

Another disadvantage of hybrid testing compared to full physical testing is that aerodynamic phenomena which are not captured by the numerical model, will not be simulated during the experiments. As a result, the potential hydrodynamic response of the platform to said phenomena may not be captured either. One example is dynamic inflow, this effect cannot be captured effectively by quasi-steady BEMT tools, but the more computationally intensive PF and CFD solvers are capable of capturing this effect. This has implications for hybrid testing of FOWTs. It means that unsteady dynamics might not be captured during hybrid testing when the computationally efficient quasi-steady BEMT tools are used to compute the aerodynamic loads for each time-step. Consequently, the resulting platform motion response and blade pitch control effects from dynamic inflow effects may not be captured either. The BEMT models can be corrected by adding simple dynamic inflow models. However, such improved BEMT tools have not been applied during hybrid tests to date. Furthermore, the actuators used in hybrid test experiments need sufficient bandwidth to replicate any control strategy designed to counter the effects of dynamic inflow. Of course, the same is true for control equipment used during full physical experiments.

A comparative study was performed by Gueydon et al [96] with a 1/50 scale model of a TLP FOWT and the NREL 5 MW turbine at MARIN. Combined wind, wave and current tests were first performed with the full physical method and then repeated with a real-time hybrid method using dynamic cable winches and SIL. Both methods showed comparable results up to 0.55 rad/second. Above this frequency the dynamic cable winches used in these tests were not able to deliver the demanded thrust without a significant delay and Gueydon et al found it problematic to accurately assess the tendon tensions. They concluded that for FOWTs that respond to high frequency, such as TLPs, the use of winches for hybrid testing may not be adequate.

Table 6. *Advantages and disadvantages of the full physical methods and hybrid methods.*

	Advantage	Disadvantage
Full physical modelling	<ul style="list-style-type: none"> Models aerodynamic thrust, torque and gyroscopic moment Captures aerodynamic damping Turbine control can be implemented 	<ul style="list-style-type: none"> Requires expensive and bulky wind generation equipment Difficult to generate high quality laminar steady wind Difficult to generate stochastic wind with good repeatability Requires unique turbine model for each turbine design and scale Rotor often requires the aid of an electric motor to reach correct TSR
Hybrid modelling	<ul style="list-style-type: none"> Depending on number of actuators it is possible to emulate thrust, torque and gyroscopic moment with good repeatability Captures aerodynamic damping Turbine control can be implemented Stochastic wind loads can be implemented without great difficulty Versatile, can be used for any type of turbine or scale Requires less space and considerably cheaper than wind generation system 	<ul style="list-style-type: none"> System latency Multiple actuators required to emulate all aerodynamic loads, adds complexity and uncertainty Phenomena not simulated with the numerical model will not be captured during testing

Both the performance scaled full physical method and the multi-actuator hybrid method can be considered high-fidelity test methods. The level of fidelity is likely somewhat higher for the full physical method, however, as aerodynamic loads which are not captured by the numerical model are still likely to be captured during testing, unlike during hybrid testing. The choice of test method will therefore be a trade-off between budget and fidelity/uncertainty. The advantages and disadvantages of full physical testing and hybrid testing are summarized in Table 6.

The research trends and gaps observed through this review are summarized here:

- As turbine sizes continue to grow, full physical testing of FOWTs at scale will become impractical. Comparative studies between full physical testing and hybrid testing, for the same platform under the same load conditions, are limited, e.g. Hall and Goupee [80] and Gueydon et al [96]. More comparative studies for different kinds of platforms and different types of actuators are desirable to identify the limitations of both methods.
- Studies of unsteady aerodynamics for FOWTs have increased in recent years, both numerically, e.g. Lee and Lee [97] and experimentally, e.g. Belloli et al [91]. However, mention of computationally efficient real-time simulation tools to capture this effect during hybrid testing in wave basins is lacking in the literature.
- The effect of current on platform dynamics, mooring tensions and fatigue life found experimentally is also lacking in the literature. Numerical studies suggest the effects could be significant, therefore further experimental investigation is desirable. There are no examples of hybrid methods to simulate current in the literature.
- The simultaneous emulation of several aerodynamic loads with propeller actuators is also lacking in the literature. Further experimental investigation is desirable.
- As turbine sizes, and consequently, platform sizes continue to grow, structural dynamics of the platform could become more influential on overall FOWT dynamics. However, results of platform structural dynamics during scale model FOWT experiments are also lacking in the literature.

After all this information the reader might ask, “So, what is the best modelling technique or tool FOWT experiments?”

The best choice will generally be case-specific, and the likelihood is that several techniques and tools will be used over the course of the design process. However, recommendations are provided here, which can serve as a guideline for the choice of modelling technique and tool. The first consideration will be the available budget of the designer or researcher; in general, the higher the fidelity of the method, the larger budget requirements will be. Another major consideration is the stage of the design process.

For scale model testing, the consideration will be between choosing either full physical testing or hybrid testing. The recommendations are determined by answering the following set of questions:

1) Does the test facility have equipment to generate the required environmental loads?

- ✓ Yes: Full physical is the preferred method
- ✓ No, or partially: Hybrid is the preferred method

2) Can the investigated phenomena be captured numerically?

- ✓ Yes: Hybrid is the preferred method
- ✓ No: Full physical is the preferred method

3) Is the scale of the model practical to handle for the test facility?

- ✓ Yes: Both methods can be used
- ✓ No: Hybrid is the preferred method

Next, if the choice falls on the hybrid method there are some more distinctions to be considered:

4) Are aerodynamics or hydrodynamics the focus of the investigation?

- ✓ Aerodynamics: Hybrid testing in wind tunnels is the preferred method
- ✓ Hydrodynamics: Hybrid testing in wave basins is the preferred method

5) for wave basin testing, what type of actuator is most suitable?

- ✓ Thrust loading only: A simple, on-board propeller actuator is most suitable
- ✓ Thrust + aerodynamic moments: Dynamic winch actuators are most suitable

The review shows that, despite some technical challenges such as latency, hybrid testing has some clear advantages compared to full-physical testing and has proven to be an effective method to solve the Froude/Reynolds scaling issue for aerodynamic experiments. The lack of equipment to generate physical environmental loads is an important motivation to choose hybrid testing as the experimental test method. The review shows there are very few examples of multiple aerodynamic loads simultaneously simulated with propeller actuators. Hence, a MPA with SIL was developed for aerodynamic loads emulation for this thesis. Modelling of current during FOWT experiments is a clear gap in the literature, hence a winch actuator with SIL for drag force emulation resulting from currents was also developed for this PhD thesis.

Chapter 4

Methodology

This chapter describes the development of the hybrid test systems for wind and current respectively, most of which can be found in [16] and [17]. This chapter also describes the setup of the experiments, setup of the numerical models in FAST and AQWA, the assumptions and simplifications used for the hybrid test system, and the procedure used to validate the system.

4.1) Emulation of aerodynamic loads

The aim for the design of the aerodynamics actuator was to give it the capability to emulate rotor thrust forces of the simulated turbine, as well as rotor torque, aerodynamic yaw and pitch, and preferably also 3P loadings. Bachynski et al [72] and Thys et al [77] achieved results closely matching numerical results with emulating all these aerodynamic loads with dynamic winch actuators. However, the control of the winches is complicated, and the setup of the winches requires a large area over the basin. Whilst the actuator for this project was intended to be used in two test facilities a simpler setup was deemed more appropriate. Instead of using winches, the decision was made to convert an aerial drone into an MPA. Controlling the propellers is relatively easy and several propellers can be combined into a single device making it compact and easy to install compared to a spread of winches.

Two control strategies for the MPA have been used during this body of work: an open-loop strategy with a simple Arduino board as controller, and a closed-loop strategy with a more powerful dSPACE real-time controller. Both strategies will be described in more detail in this chapter.

4.1.1) Description of the Multi-Propeller Actuator

The proposed MPA consists of a custom designed frame with six propellers, which is shown in Figure 13. Much of the technology used for the MPA is borrowed from recreational aerial drones. The Electronic Speed Controllers (ESC), electric motors and propeller blades used for the MPA are all the same parts as used in the DJI S800 aerial drone [98].

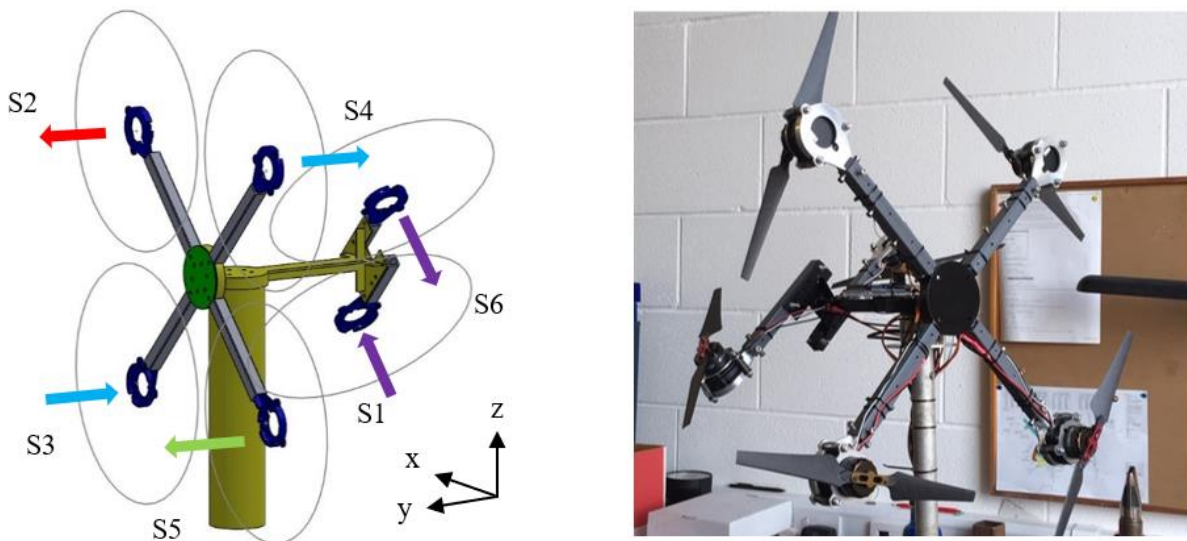


Figure 13. The Multi-Propeller Actuator

The frame of the MPA is made of aluminium and its configuration was chosen to suit the unidirectional thrust of the propellers, while keeping the frame as light as possible. In the configuration shown in Figure 13, propellers S3 & S4 emulate aerodynamic thrust, S1 & S6 emulate rotor torque and S2 & S5 in combination with S3 & S4 can be used to emulate aerodynamic yaw and pitch. The minimum length

of each propeller arm is 200 mm from the centre of the device. If larger moments are required for pitch, yaw or torque the arms can be extended. The arm extending from the tower to the torque propellers S1 & S6 is 235 mm. The torque propellers are kept away from the other propellers to minimize wake interference while all propellers are in operation. When operating, each propeller will generate its own torque and gyroscopic momentum. To ensure that this effect will not influence the test results, the propellers are installed so that each pair (S3 & S4, S2 & S5 and S1 & S6) has a propeller counter-rotating to the other, cancelling out each other's torque and gyroscopic moment. This technique is also used with aerial drones to ensure torque and gyro effects do not interfere with their flying ability. Each propeller has its own ESC controlling the rotational speed of the DC motor. The motors are powered by a 25V DC power supply, which is connected to an AC power source.

An Interface 6A40-50N/5Nm six-axis load cell is mounted between the top of the tower and the MPA to measure forces and moments in the X-Y-Z reference frame. The load cell is positioned at the centre of mass of the rotor-nacelle assembly of the full-scale turbine.

Two types of propeller blades of different size were used to determine the impact of blade size on the accuracy of the MPA. The first type of blade is the original type used on the S800 drone, and the second type is the blade used on the Mavic drone, with blade lengths of 150 mm and 75 mm respectively.

Besides the horizontal mounting as shown in Figure 13, the MPA can also be mounted vertically as shown in Figure 14. In this configuration yaw moments can be emulated more efficiently as the propellers creating the couple are all in the X-Y plane. By using an extra pair of counter-rotating propellers the rotation direction of the couple can be changed swiftly, which is not possible with the horizontal mounting.



Figure 14. *The MPA in the vertical position, no thrust propellers are installed in this example.*

In this configuration it is still possible to emulate thrust force and rotor torque. However, it is no longer possible to emulate aerodynamic pitch and the centre of the torque couple is no longer in the centre of the simulated rotor shaft. The added pair of propellers will also increase the weight of the MPA, which depending on the scale of the model, may exceed the weight of the simulated rotor nacelle assembly.

4.1.2) Open-loop control

To control the propellers with the open-loop strategy, the input signal calculated by the numerical simulation is scaled down and sent by the computer to an Arduino Mega 2560 board. The Arduino board translates the input signal into an analog Pulse Width Modulate (PWM) signal and sends it to the ESCs. The PWM signal range to control the ESCs is 320-545 ms. with minimal increments of 5 ms. MATLAB was used with the Arduino support package to control the Arduino board. The hardware setup is very similar as it is shown in Figure 9.

Offline simulations in FAST v8 of the NREL 5MW turbine were used to generate timeseries of the aerodynamic loads, at full scale, acting at hub height and in the centre of the rotor for thrust, torque and pitch, and in the centre of the tower for yaw. For simplicity the turbine was modelled on a rigid tower and fixed in the reference frame, i.e., no platform or tower motions were considered to ignore any inertia loads from the turbine, resulting in pure aerodynamic thrust. The timeseries are used as the digital input signal in a MATLAB script. The aerodynamic loads for each data point of the timeseries are first scaled down and then translated into a PWM signal. The frequency of the timeseries is adjusted to give a correct time-step of actuation at scale. A detailed calibration of the thrust force each propeller can produce was made for both the S800 and Mavic sets of propeller blades. Each propeller was first calibrated individually, then in pairs and finally with the combined propellers operating simultaneously. The difference in the results between individual, paired and combined calibrations gives an estimation of the wake interference between the propellers. The propellers were operated for 10 seconds, and the measured output was averaged for each PWM step to produce calibration curves. The first two seconds of each record were discarded to exclude the initial vibrations at start-up. The calibration curves are shown in Figure 15.

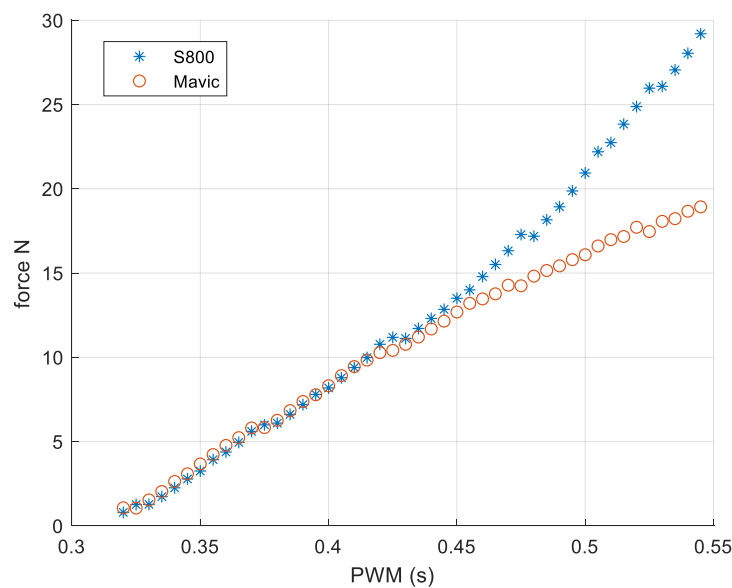


Figure 15. Calibration curves of the propeller blades with PWM as a function of the thrust force

The resulting motion of the model from actuation with the MPA is captured by the Qualisys motion tracking system. However, the real-time data is not used to update the relative wind speed across the turbine rotor, nor will simulated turbine control (blade pitch angle and generator torque) be adjusted accordingly. Figure 16 shows a diagram of the open-loop strategy.

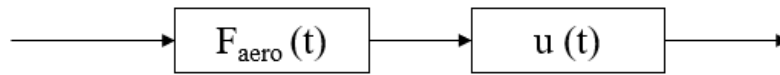


Figure 16. Diagram of the open-loop control strategy for aerodynamic loads

The advantage of this strategy is its simplicity; the whole system can be controlled by a standard laptop with MATLAB and the lightweight Arduino board can be mounted on the MPA keeping the PWM signal cables short while reducing the chance of electro-magnetic interference of the PWM signals. However, the lack of feedback and correction of the loads for each consequent time-step will likely affect the accuracy of the load emulation.

4.1.3) Closed-loop control

For the closed-loop control strategy the Arduino board is replaced by a dSPACE 1104 real-time controller, which is a far more powerful processor than the Arduino. The dSPACE 1104 is linked with MATLAB/Simulink. Rather than a timeseries of the aerodynamic loads generated with offline simulations, the closed-loop control strategy uses an in situ real-time simulation to calculate the loads for emulation at each time-step. The turbulent wind time series generated with TurbSim are used as input for the real-time simulation. As with the open-loop strategy, the loads are calculated at full scale, then scaled down and translated into a PWM signal which is sent to the MPA by the dSPACE 1104. Real-time motion feedback of the scale model from the Qualisys tracking system is used to update the relative wind speed across the wind turbine rotor by combining the input wind speed with the up-scaled surge- and pitch velocity of the scale model. The updated input wind speed is then used to update the load calculation for each consequent time-step. A closed-loop system like this is often referred to as Software-in-the-Loop (SIL), and is similar to the setup described by Azcona et al [58]. Figure 17 shows the diagram of the closed-control loop. The Simulink code is compiled as C+ code, which is used by the software ControlDesk to execute the real-time numerical simulation. A MATLAB plug-in for Qualisys enables the communication between MATLAB and the motion tracking system, and XIL-API protocols are used to communicate in real-time between MATLAB and ControlDesk for the updates of the aerodynamic loads with the motion tracking data.

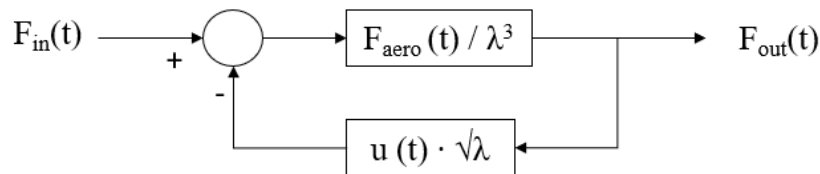


Figure 17. Diagram of the closed-loop control strategy for aerodynamic loads

With the SIL for aerodynamic loads there is no force feedback from the 6-axis load cell, only the motion tracking data is used to update aerodynamic load calculations.

The relative wind speed V_{rel} is defined as:

$$V_{rel} = V_{in} - (u_s + u_p) \sqrt{\lambda} \quad (16)$$

Where V_{in} is the input wind speed from the TurbSim timeseries, u_s and u_p are surge- and pitch velocity respectively of the scale model captured by Qualisys, and λ is the scale ratio of the model.

An algorithm in Simulink uses the relative wind speed to calculate the aerodynamic loads. This algorithm is based on the method described by Matoug et al [65]. Rotor thrust is calculated as a drag force on the entire rotor, rather than with the strip method used in BEMT. Rotor thrust is defined as:

$$T = \frac{1}{2} \rho A_r C_T V_{rel}^2 \quad (17)$$

Where ρ is the density of air, A_r is the swept area of the rotor, and C_T is a thrust coefficient. A lookup table in Simulink is used to select the thrust coefficient for each time step, which is coupled with the Tip Speed Ratio (TSR). The TSR is defined as:

$$TSR = \frac{r\Omega}{V_{rel}} \quad (18)$$

Where r is the radius of the rotor, and Ω is angular velocity of the blade tip. Another lookup table selects rotor torque for each time-step. Rotor torque is coupled with rotor speed and a different lookup table is used to select rotor speed, which is coupled with the relative wind speed. The lookup tables have been derived from offline simulations with FAST for mean wind speeds of 9 m/s and 11.4 m/s, i.e., both turbulent wind timeseries used for the real-time numerical simulations have their own set of lookup tables.

A limited number of thrust coefficients is used with this SIL version. To simulate blade-pitch control of the turbine (that is the control strategy of the simulated turbine, not to be confused with the control strategy for the MPA) correctly would require a separate lookup table for each blade-pitch angle, and a selection method for blade-pitch angle coupled with rotor speed would have to be added to the algorithm in Simulink. However, the lookup tables and additional selection method in the real-time simulations require high processing power from the real-time controller; the addition of each lookup table makes the simulation time slower. If too many lookup tables are added latency could become too high for the real-time simulation. To solve this issue, thrust coefficients and TSR found with the offline simulations in FAST are plotted against each other and a ‘best-fit’ is applied to obtain a single set of thrust coefficients, as shown in Figure 18.

The disadvantage of this method is that the blade-pitch control of the wind turbine will not be simulated accurately and some of the high-frequency thrust fluctuations might therefore not be captured correctly. However, the low-frequency fluctuations will still be captured with this method.

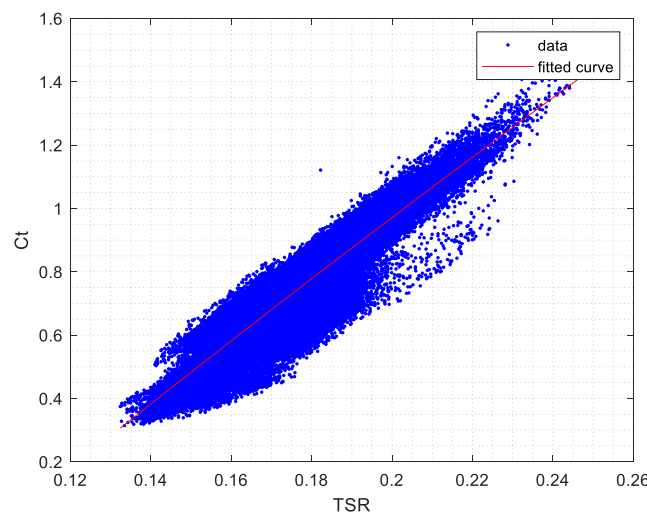


Figure 18. Selection of ‘best-fit’ thrust coefficients from offline aero-elastic simulations

Rotor thrust and rotor torque are the only aerodynamic loads emulated with the closed-loop, or SIL, control strategy. In total five lookup tables are used in the Simulink code for the emulation of aerodynamic loads:

- PWM signal as a function of rotor thrust force
- PWM signal as a function of rotor torque
- Rotor torque as a function of rotor speed
- Rotor speed as a function of relative wind speed
- Thrust coefficient as a function of TSR

Results of experiments with the MPA are described in Chapter 5.

4.2) Emulation of current induced loadings

For the simulation of current during scale model experiments two phenomena will have to be replicated: the drag force of the current on the submerged part of the FOWT platform and the wave-current interactions.

Using one or more submersible propellers mounted on the FOWT platform was considered as a method to emulate the drag force. However, this method was rejected for the following reasons:

- The wake of submerged propellers on the scale model would cause localized wave-current interactions during experiments with waves.
- Any yaw- or pitch motion of the model would effectively change the direction of the simulated current.
- The underwater profile of the model would differ considerably compared to the full-scale model resulting in differences in viscous damping and natural frequencies.
- Installing submerged propellers on the model adds complication.

Instead, a dynamic winch was chosen as actuator to emulate the drag force, which has none of the abovementioned disadvantages. A winch cable is easy to install on the model without significantly changing the underwater profile, there are no localized wave-current interactions, and the pulling direction of the winch does not change with motion of the model therefore the simulated current direction does not change.

4.2.1) Description of the winch actuator

This thesis proposes a novel method to simulate current using a dynamic winch actuator with SIL. This hybrid test method is based on methods to emulate wind loads with dynamic winches and SIL, which has successfully been applied in several test facilities during scaled floating wind experiments, e.g. [72], [80]. To date, this method has not yet been applied for the emulation current loads.

To simulate current, the winch cable is connected to the FOWT model on the downstream side. The tension in the winch cable is altered dynamically to emulate the drag force a current would exert on the platform of the FOWT, depending on the velocity of the current. For floating objects, the relative velocity of the current is found by combining the velocity of the current and the velocity of the floating object. The drag force, F_D , is calculated with the drag term of the Morison equation:

$$F_D = \frac{1}{2} \rho C_D A |U - u| (U - u) \quad (19)$$

Where F_D is the drag force, ρ is the density of water, C_D is a drag coefficient, A is the wetted cross-sectional area of the platform in still water, U is the velocity of the current, and u is the velocity of the platform.

The velocity u of the platform is derived from the displacement of the scale model, which is tracked by the Qualisys system. Velocity u is defined as:

$$u_i = \frac{dx_i}{dt} \quad (20)$$

Where x is the measured displacement in the i^{th} DOF. For the calculation of the drag force only the surge DOF of the scale model is considered to obtain the relative velocity of the current.

The winch actuator consists of a Schneider Electric BCH2 servo motor and a custom-made winch drum. The BCH2 motor is driven by 220V AC, has a maximum torque output of 3.81 Nm, and nominal capacity of 0.4 kW. The maximum rpm of the motor is 5000. The winch motor is operated in torque mode by a Schneider Electric Lexium 28A servo drive, which controls the speed and relative position of the motor shaft. The winch drum is milled from a solid rod of nylon and designed to fit on the motor shaft. The diameter of the winch drum is 40 mm and can fit at least 2 m of winch wire, which is more than sufficient to accommodate the largest surge motions of the scale model. Figure 19 shows a CAD drawing of the winch drum.

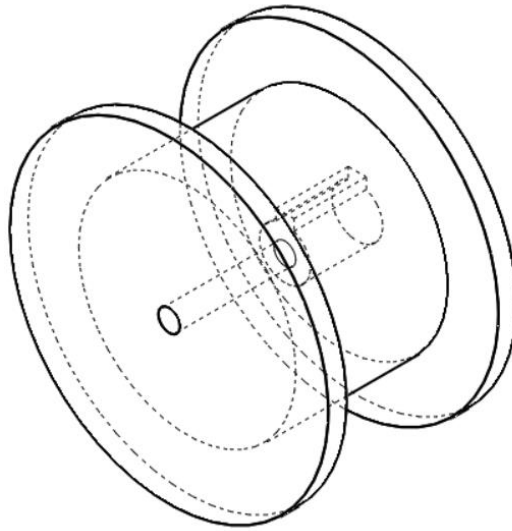


Figure 19. CAD drawing of the custom-made winch drum for the winch actuator

The winch wire of the current emulation system consists of a length of polyester rope with diameter of 3 mm and high axial stiffness. The winch wire is connected, via a pulley system on the instrument bridge, to the turbine column of the platform at $Z = \text{COG}$ in a conventional coordinate system. The connection at $Z = \text{COG}$ was chosen to eliminate additional pitch motions of the platform resulting from actuation with the winch. A spring with stiffness coefficient of 265 N/m is fitted between the platform and the load cell in the winch wire to absorb snap loads. Maximum pulling force of the winch actuator was found to be 56 N.

A similar closed-loop control strategy for SIL is used as described in Section 4.1.3. The dSPACE 1104 real-time controller controls the servo drive. A simple algorithm in Simulink, based on equation (19) and equation (20), calculates the drag force (i.e., demanded tension of the winch wire), at scale, of the current on the platform for each time step. The demanded force/tension from the motor is determined (at each time step) by the real time simulation and this force is maintained by a Proportion Integration (PI) controller using the measured instantaneous force from a load cell in the winch wire. The Qualisys motion tracking system monitors the velocity of the platform. Real-time data from the motion tracking system is used as feedback to update the relative velocity and drag force of the current for each time

step. The winch actuator can be used simultaneously with the MPA for combined wind- and current simulation. The control loop of the system is shown in Figure 20, and the hardware layout in Figure 21.

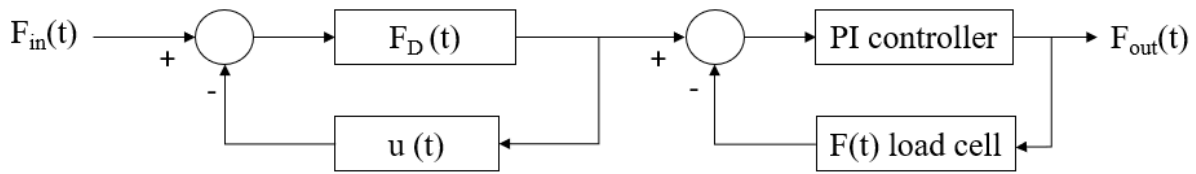


Figure 20. Diagram of the control loop for current induced drag force emulation

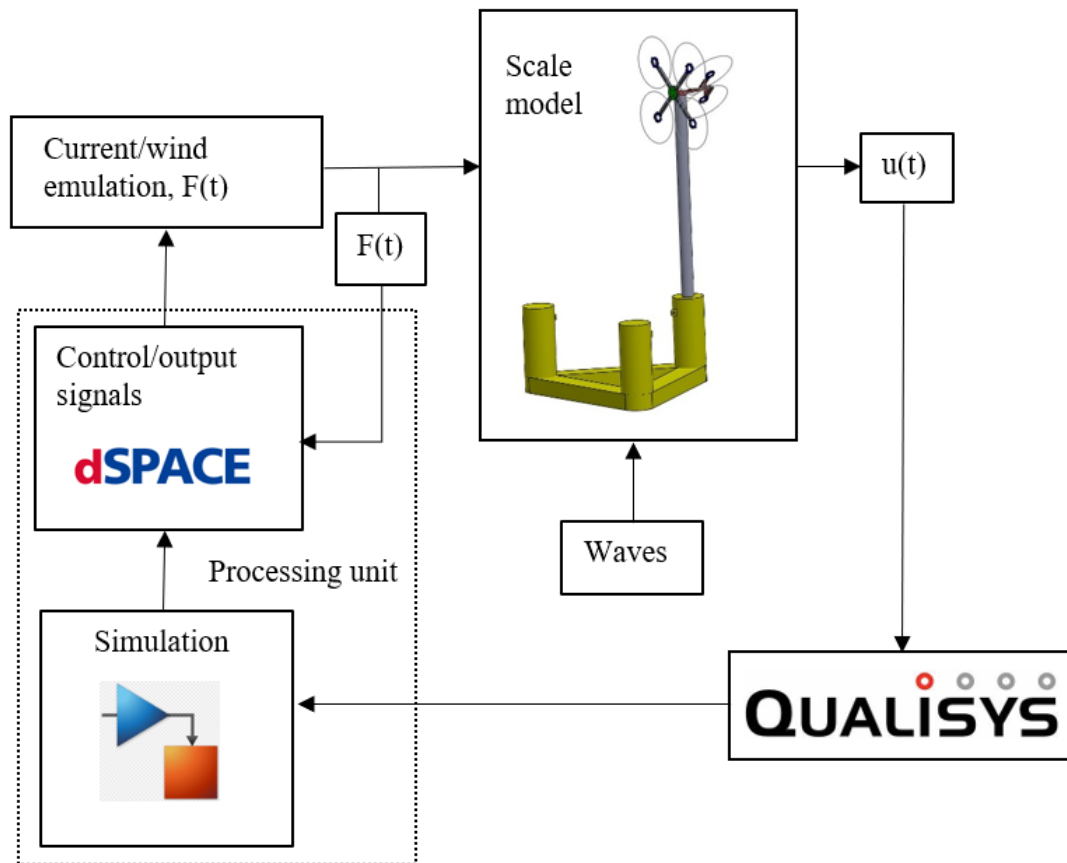


Figure 21. Diagram of the hardware setup for the current- and wind simulation system

Lower simulation- and actuation frequencies are used for the current emulation system, compared to frequencies typically used for SIL applications [80]. For this system the motion tracking- and tension feedback frequency is 32 Hz, the actuation frequency is 25 Hz, and the real-time simulation frequency is 22 Hz, giving a simulation time-step of 0.045 seconds. The reason for these lower frequencies is that the dSPACE 1104 is not powerful enough to control both the MPA and winch actuator simultaneously at typical frequencies.

The P and I values have been determined empirically. By starting at zero and gradually increasing first the P-value and next the I-value until the winch starts oscillating. Next, the P and I values are halved and some tweaking of the values applied for smooth operation of the winch. The P-value found with this method is 0.6, and the I-value is 1.1.

Wave-current interactions during experiments with SIL are simulated with the method described in Section 3.1.3.

4.3) Rigid body dynamics

For this thesis only rigid body dynamics of the response of the FOWT to load emulation and waves were considered; structural dynamics of the blades, tower and platform were not captured during experiments, nor were they evaluated with any of the numerical models.

The experiments have been replicated, at full-scale and in time domain with the offline numerical simulations in AQWA and FAST.

In time domain rigid body dynamics are defined as [99]:

$$(m + a')\ddot{x}_i(t) + \int_{-\infty}^t K(t-\tau)\dot{x}_i(\tau)d\tau + Cx_i(t) = F_{sum}(t) \quad (21)$$

Where m is mass of the body, x_i is motion of the body in the i^{th} DOF, τ is a time lag, and C is the restoring stiffness.

The frequency independent added mass, a' , is defined as:

$$a' = a(\omega) + \frac{1}{\omega} \int_0^{\infty} K(\tau) \sin(\omega\tau) d\tau \quad (22)$$

Where a is added mass, ω is the wave frequency, and K is the retardation function, which is defined as:

$$K(\tau) = \frac{2}{\pi} \int_0^{\infty} b(\omega) \cos(\omega\tau) d\omega \quad (23)$$

Where b is the radiation damping.

The forces, F_{sum} , acting on the body are defined as:

$$F_{sum} = F_{hydro} + F_{aero} + F_{mooring} + F_{inertia} \quad (24)$$

Where

$$F_{hydro} = F_{waves} + F_{current} \quad (25)$$

Wave forces include the inertia-, viscous-, diffraction-, and radiation forces from waves acting on the platform of the FOWT. The current induced force is the viscous force, i.e., drag force, exerted by the current on the FOWT platform.

During the experiments with SIL F_{waves} , $F_{mooring}$, and $F_{inertia}$ are always physically applied. The waves are generated by the wave maker of the basin, mooring forces are the restoring forces from the springs in the mooring lines responding to motion of the model, and inertia forces are provided by the physical mass of the scale model in motion. The aerodynamic forces, F_{aero} are calculated with the in situ real-time numerical simulation according to equation (17) for all experiments with wind and emulated with the MPA. The drag force of the current, $F_{current}$, is either emulated with the winch actuator according to equation (19) or applied physically during the experiments with current.

4.4) Description of the scale model of the INNWIND semisubmersible FOWT

An important motivation to choose this reference platform was its simplicity, making it easy to manufacture at 1/50 scale. Another important motivation was the presence of publicly available test data [100] with this platform from the MaRINET2 round robin test campaign [101]. Originally, this platform was designed as the floating foundation for the DTU 10 MW wind turbine, the combination of this platform with the NREL 5 MW turbine may therefore seem like an unusual one. However, the

focus of this study was the simulation method with the hybrid test system. The combination of turbine and platform is therefore arbitrary. The choice of turbine is discussed further in Section 5.6.

The platform of the 1/50 scale model of the FOWT described in Section 2.2 is constructed from aluminium. The columns and pontoons are made from plates with 4 mm thickness and the covers for the columns are disks of 2 mm thickness. The tower is an aluminium pipe of 4 mm thickness and with an outer diameter of 80 mm along its entire length. The MPA is installed on top of the tower with the horizontal centre line at hub height.

The following scale ratios apply to determine dimensions, weights etc. of the scale model:

- Dimensions: $L_M = L_F / \lambda$
- Mass: $W_M = W_F / \lambda^3$
- Force: $F_M = F_F / \lambda^3$
- Moment: $M_M = M_F / \lambda^4$
- Time: $T_M = T_F / \sqrt{\lambda}$

Where $\lambda = 50$.

As aluminium rather than steel was used to construct the scale model, weight and structural stiffness of the platform and tower are not modelled correctly according to the original design of the INNWIND semisubmersible FOWT. Furthermore, the original design of the INNWIND semisubmersible FOWT is with the DTU 10MW turbine. However, a comparative study between the MPA and a 1/50 physical scale model of the NREL 5MW turbine was originally planned to take place at the Coast Laboratory in Plymouth, which has dictated the use of the 5MW turbine in this study. To accommodate the NREL 5 MW turbine and aluminium platform of the model, the ballast and tower height have been adapted. The number of propellers on the MPA is reduced to four to maintain the same mass envelope of the rotor nacelle assembly of the NREL 5 MW at scale. With the four propellers only rotor thrust, and rotor torque are emulated. Lead ballast is placed in the columns, with a smaller amount in Column 2 compared to Column 1 and 3 to compensate for the weight of the tower and MPA. Figure 22 shows the location of the ballast and connection point for the winch actuator.

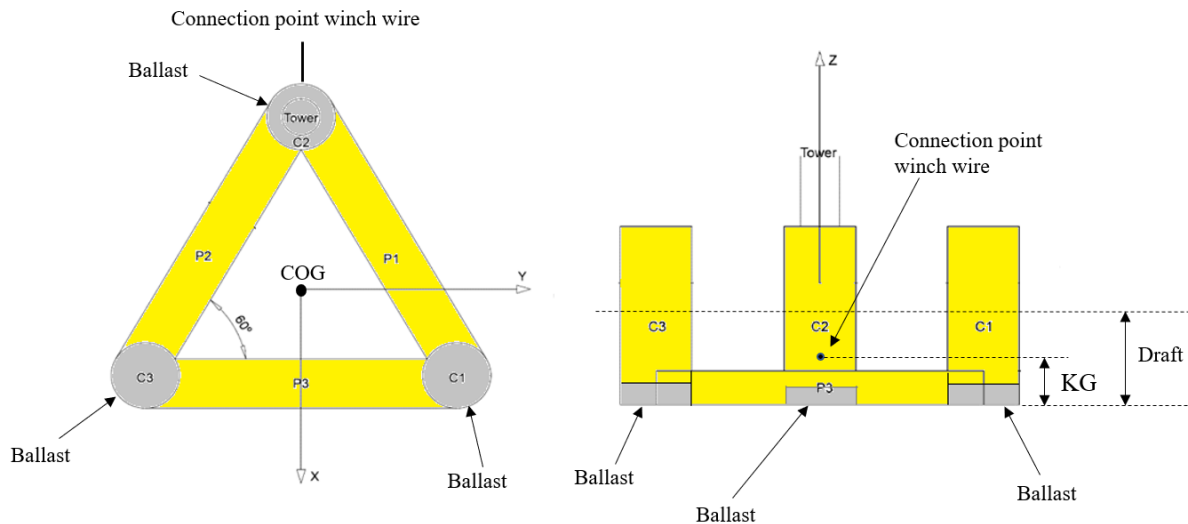


Figure 22. Plan- and lateral view of the scale model

Due to the altered weights total mass, KG (COG in Z-direction), and draft have all changed from the original design. Table 7 shows the main properties of the adapted scale model. The adaptations have been translated, where appropriate, to full-scale for use in the numerical models.

Table 7. *Main properties of the adapted scale model*

	Model Scale	Full Scale
Weight empty platform	54 kg	-
Weight tower	5.7 kg	712,500 kg
Weight MPA	2.8 kg	-
Weight ballast C1 & C3	37.6 kg	-
Weight ballast C2	29.1 kg	-
Total mass	167.3 kg	20,912,500 kg
KG	0.17 m	8.5 m
GM	0.295 m	14.75 m
Draft	0.36 m	17 m (in salt water)
Diameter columns	0.29 m	14.5 m
Depth columns	0.75 m	37.5 m
Width pontoons	0.2175 m	10.875 m
Depth pontoons	0.14 m	7 m
Distance between columns	1.32 m	66 m
Hub height (from SWL)	1.82 m	90 m (in salt water)

Of course, due to the altered mass, moment of inertia and natural periods of the scale model have also changed from the original design. The new moment of inertia has been derived with radius of gyration tests with the model for roll, pitch, and yaw. The natural periods have been calculated and verified with decay tests of the moored scale model in the basin. The new results have also been translated to full scale for use in the numerical models. Table 8 shows the new moments of inertia, and natural periods.

Table 8. *Moments of inertia and natural periods at model scale and full scale.*

	Model Scale	Full Scale
Roll moment of inertia	72.481 kg m ²	22,650,180,300 kg m ²
Pitch “ “	73.413 kg m ²	22,941,478,633 kg m ²
Yaw “ “	88.849 kg m ²	27,765.273,191 kg m ²
T_n Surge	14.9 sec.	105 sec.
T_n Sway	16.1 sec.	113 sec.
T_n Heave	2.8 sec.	19.8 sec.
T_n Roll	2.9 sec.	20.5 sec.
T_n Pitch	2.9 sec.	20.5 sec.
T_n Yaw	10.8 sec.	76 sec.

The Response Amplitude Operators (RAO) of the model have been derived from wave-only tests with an irregular white-noise spectrum. Figure 23 and Figure 24 show the RAOs for the translational- and rotational DOFs respectively.

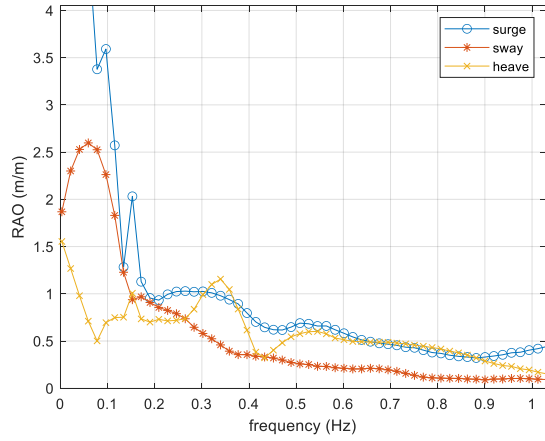


Figure 23. Translational RAOs of the FOWT model.

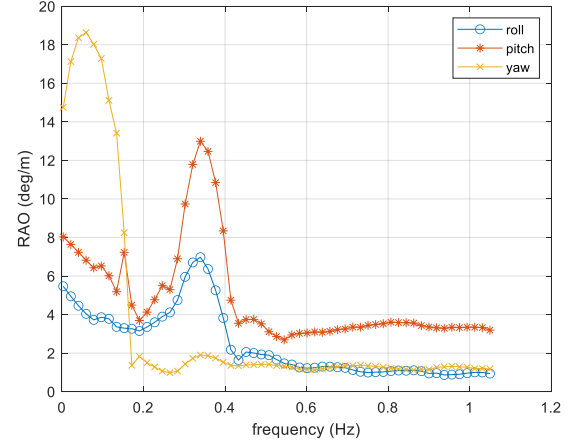


Figure 24. Rotational RAOs of the FOWT model.

The drag coefficient C_D in equation (19) has been empirically derived with resistance tests over a range of velocities in the Wave Current Flume (WCF) in Lir NOTF. During the resistance tests the model was kept stationary in the surge DOF (X-direction of the current flow) while physical current was applied and the force acting on the model in the X-direction was measured. Figure 25 shows the velocity in the X, Y, and Z directions against the percentage of power of the thruster generator, where X is in the longitudinal direction of the flume. The error bars indicate the standard deviation of the measurements. Figure 26 shows the C_D values derived for the velocity range shown in Figure 25.

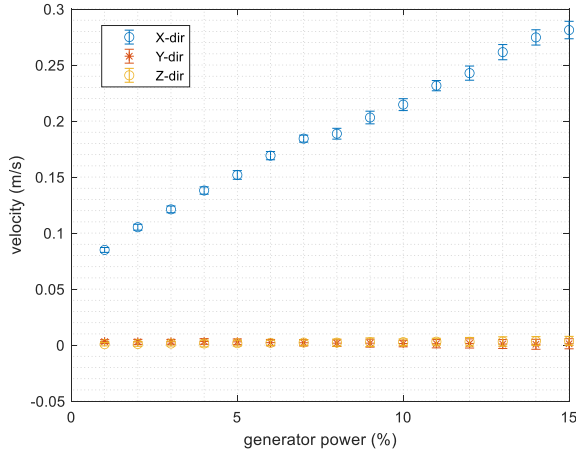


Figure 25. Velocity of the flow in the WCF in X, Y, and Z direction.

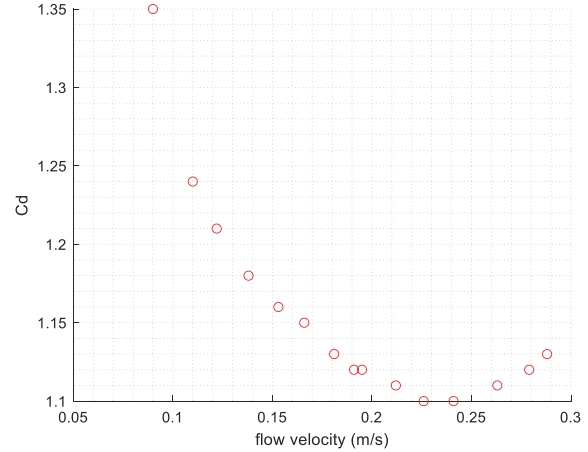


Figure 26. Empirically derived C_D values for the FOWT model.

As with any empirically derived coefficients there is a certain amount of uncertainty associated with the correctness of the RAOs, as well as the drag coefficients. The uncertainty derives from various systemic and facility specific errors which are described in Section 4.8.

Independently from the winch cable, three horizontally mounted mooring cables with springs are attached, above still water level, in a 120-degree spread to the instrument bridge and foot bridge for station-keeping of the model. A plan view of the test setup can be seen in Figure 27. This type of mooring system for scale models is also referred to as a soft mooring system. Although not representative, the horizontal moorings simplify the test set-up and are readily replicated in the

numerical model. The moorings provide the restoring force for the wave loading and simulated wind and current loading. Each mooring line has a spring with stiffness coefficient of 19 N/m, which is equivalent to 47,500 N/m at full scale. Pre-tension of the moorings is set at 10 N, which is equivalent to 1250 kN at full scale. Extension of the springs is linear in the tension region of 10 N and higher. The stiffness coefficient and pre-tension of the scale model have been used at full-scale with the numerical models.

4.5) Test setup

Three separate test campaigns, each in a different wave basin, were conducted in Lir NOTF during this PhD project: in the Ocean Basin (OB), the Wave Current Flume (WCF), and the Deep Ocean Basin (DOB). Information about dimensions and capabilities of each basin can be found in [102]. The dimensions in Figure 27 are skewed, the actual dimensions of the flume are, Length: 28 m, Width: 3 m, Depth: 1.2 m. The FOWT model is located 17 m from the wave maker. A similar setup as in the WCF was used for the test campaigns in the OB and DOB.

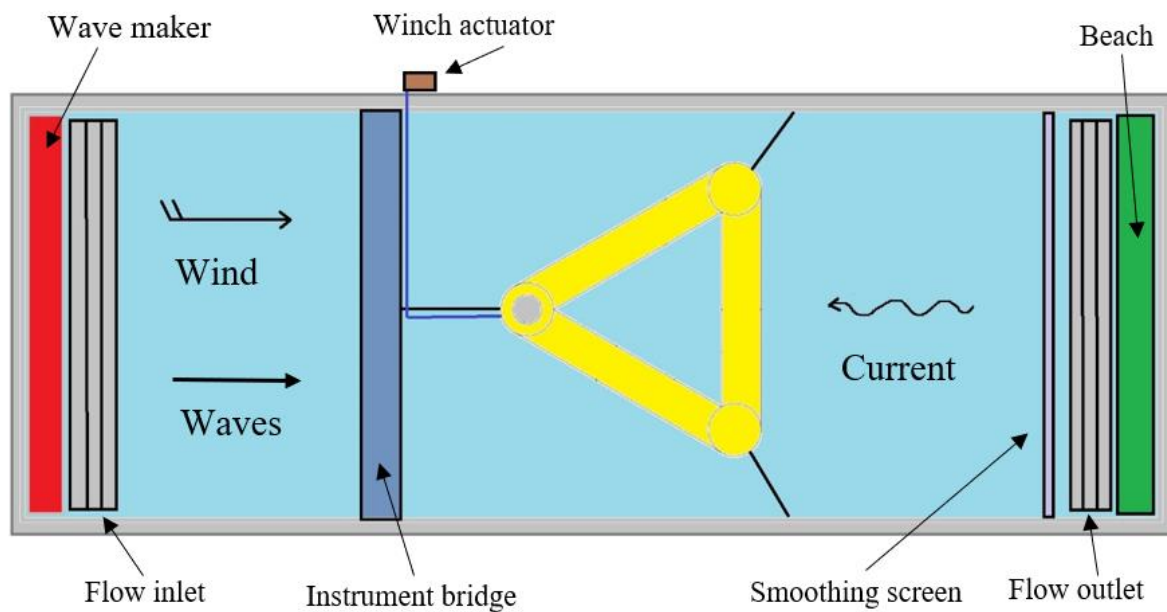


Figure 27. Test setup plan view of the scale model in the WCF

The direction of waves, wind, and current were modelled the same as shown in Figure 27 for the other two basins and with the numerical models. The test campaigns in the OB and DOB were designed to test the simulation methods of wind and current with SIL. Larger waves and longer wave periods were possible in the DOB campaign due to larger water depth of the basin. Figure 28 shows the scale model in the DOB.

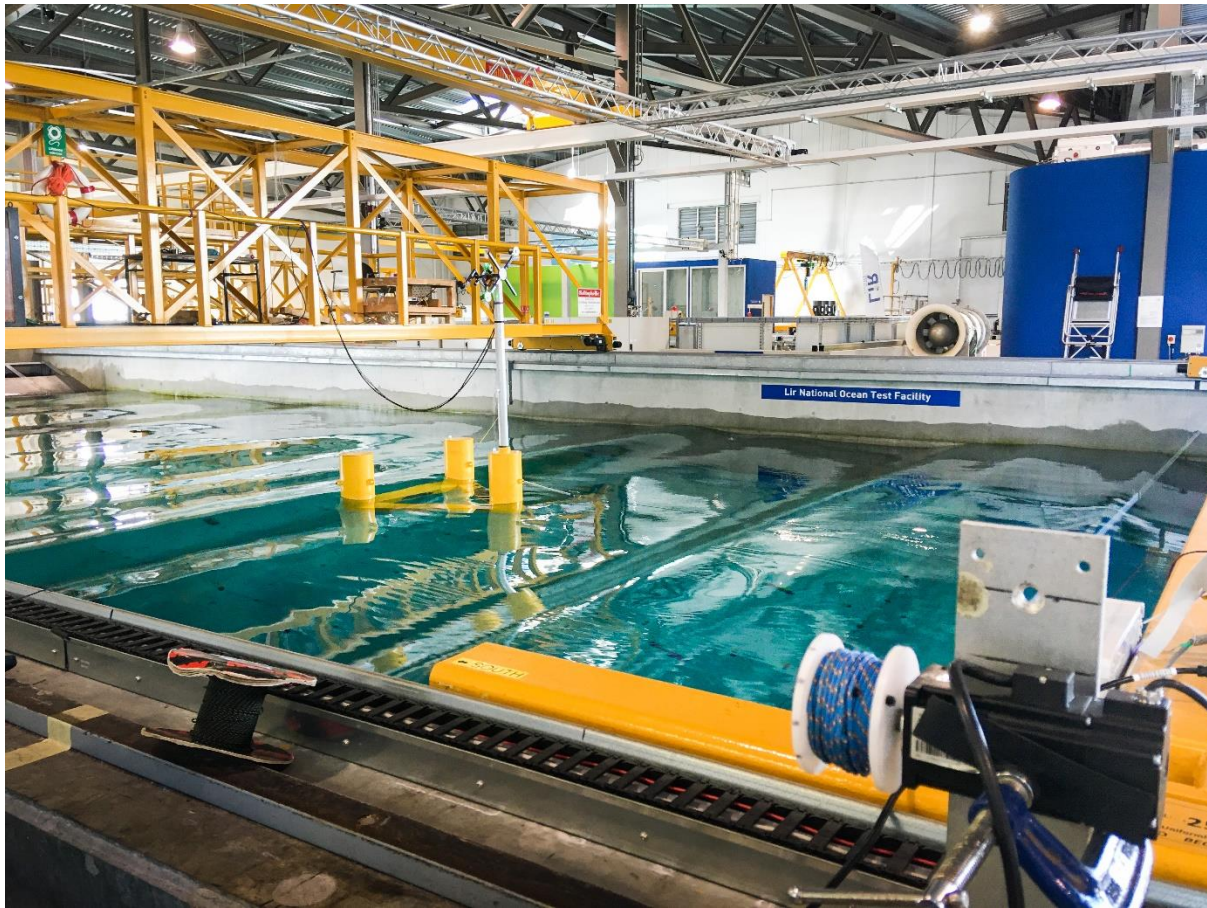


Figure 28. The scale model in the Deep Ocean Basin at Lir NOTF. The winch actuator can be seen in the foreground and the MPA can be seen on top of the tower on the FOWT model. Due to the deeper water depth of the basin bigger waves with longer wave periods can be emulated compared to the Ocean Basin.

The test campaign in the WCF was designed as a comparison study between simulated current with SIL, and physically applied current, i.e., the hybrid test method vs the full physical method. However, even with the ‘full physical’ test method in the WCF the aerodynamic loads were emulated with the MPA using SIL, whereas waves and current were applied physically.

Physical current in the WCF is generated by three thrusters mounted in a circulation gallery under the floor of the flume. The flow inlet is near the wave maker and the outlet is at the opposite end of the flume near the wave absorbing ‘beach’. A smoothing screen with porosity of 44% is mounted vertically in front of the flow outlet and beach. The flow in the WCF can be reversed, however, this renders the smoothing screen ineffective. Therefore, only flow directly opposing the wave direction has been used during experiments. The velocity of the flow was measured on the upstream side of the model at the level of its COG with a Nortek Vectrino acoustic velocimeter, which profiles the water column over a range of 30mm, with a resolution of 1mm.

Figure 29 shows the scale model in the WCF, and Figure 30 shows the layout of the pulley system for the winch actuator in the WCF. Again, the layout of the pulley system was similar for the other basins but longer distances from the winch to the first pulley wheel were applied to keep the model in the centre line of the basin. A longer distance from the instrument bridge to the model was used in the DOB to accommodate the larger wave elevations. The second pulley wheel is submerged to $Z = \text{COG}$ of the scale model. The load cell, which provides tension feedback data for the PI controller, is mounted in the winch wire near the scale model.

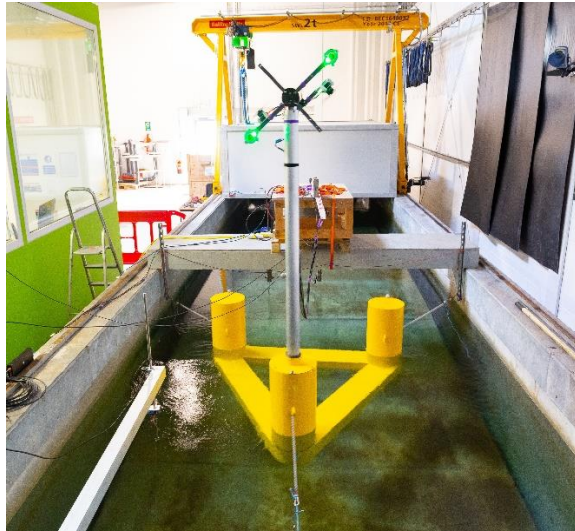


Figure 29. The FOWT model in the WCF at Lir NOTF, with the MPA at the top of the tower. The tower column is downstream of current direction.

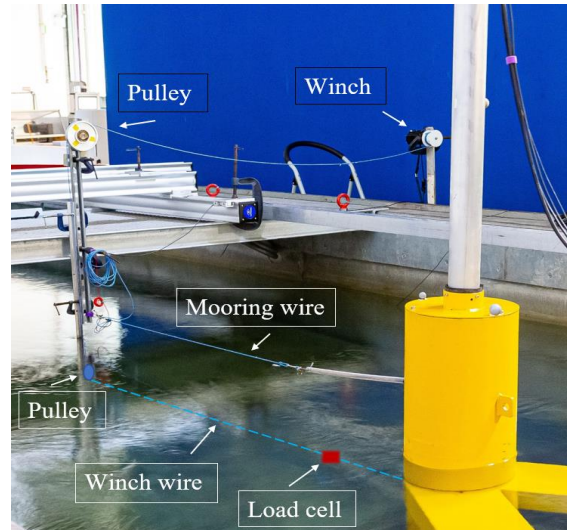


Figure 30. Layout of the winch actuator. The winch is mounted on the basin wall, and the pulley system to the instrument bridge.

The following measuring instruments have been used throughout the project:

Table 9. Measuring instruments used for the test campaigns with the scale model

Measured quantity	Instrument type	Range	Resolution	Frequency
Aerodynamic loads	6-axis load cell	50N, 5 Nm	0.1 N, 0.1 Nm	32 Hz
Position of the model	Qualisys Tracking	Several meters in X, Y, Z directions	1 mm	32 Hz
Tension in winch wire	Futek tension load cell	100 N	0.1 N	32 Hz
Tension in moorings	Futek tension load cell	440 N	0.5 N	32 Hz
Wave elevation	EDL wave gauge	Up to 1 m	1 mm	128 Hz
Flow velocity	Nortek Vectrino	3 m/s	0.01 m/s	32 Hz

4.6) Test conditions

In this section the test conditions for all the experiments and numerical simulations are outlined. The first set of tests is designed to determine how well the actuators are able to emulate the demanded forces and moments. The next sets of tests evaluate the motion response of the FOWT to different combinations of environmental loads and compares experimental results to numerical results. These tests are grouped by the basin in which the experimental campaigns took place. The final set of tests is the comparison study between physical current and simulated current. The conditions for each Test Case (TC) are shown in the following Tables 10 – 13. Table 14 summarizes the environmental loads used for the experiments and numerical simulations.

Table 10. Actuation accuracy

	Actuator	Force/moment	Load type
TC 1	Winch actuator	Tension	Random signal
TC 2	MPA, horizontal	Thrust + torque	V1 & V2
TC 3	MPA, horizontal	Aerodynamic yaw	V2
TC 4	MPA, vertical	Aerodynamic yaw	V2

Table 11. *Ocean Basin campaign*

	Conditions	Load type	DOF	Numerical model
TC 5	Current	A, B	surge	AQWA
TC 6	Wind	V1 & V2	Surge/pitch	FAST
TC 7	Current/wind	B + V2	Surge/pitch	FAST
TC 8	Waves	JONSWAP 1	Surge/pitch/heave	AQWA
TC 9	Waves/current	A, B + JONSWAP 1	Surge/pitch/heave	AQWA
TC 10	Waves/wind	JONSWAP 1 + V2	Surge/pitch/heave	FAST
TC 11	Waves/current/wind	B + JONSWAP 1 + V2	Surge/pitch/heave	FAST

Table 12. *Deep Ocean Basin campaign*

	Conditions	Load type	DOF	Numerical model
TC 12	Waves	JONSWAP 2	Surge/pitch/heave	AQWA
TC 13	Waves/current	A, B, C + JONSWAP 2	Surge/pitch/heave	AQWA

Table 13. *Wave Current Flume campaign*

	Conditions	Current type	Other load types	DOF
TC 14	Current	A, B, C physical	-	Surge
TC 15	Current	A, B, C SIL	-	Surge
TC 16	Current/wind	A, B, C physical	V1	Surge/pitch
TC 17	Current/wind	A, B, C SIL	V1	Surge/pitch
TC 18	Current/wind/waves	A, B, C physical	V1, JONSWAP 1	Surge/pitch/heave
TC 19	Current/wind/waves	A, B, C SIL	V1, JONSWAP 1	Surge/pitch/heave

Table 14. *Summary of environmental loads*

	Model scale	Full scale
Current:		
A	0.11 m/s	0.75 m/s
B	0.14 m/s	1 m/s
C	0.21 m/s	1.5 m/s
Waves:		
JONSWAP1	$T_p = 1.34s$, $H_s = 0.1m$	$T_p = 9.5s$, $H_s = 5m$
JONSWAP2	$T_p = 1.98s$, $H_s = 0.25m$	$T_p = 14s$, $H_s = 12.5m$
Wind:		
V1	-	Turbulent wind around 9 m/s, α : 0.12
V2	-	Turbulent wind around 11.4 m/s, α : 0.12

4.7) Numerical models

As mentioned in section 1.2, numerical simulations of the INNWIND semisubmersible were performed with Ansys AQWA and FAST v8 for validation of the experiments with SIL. Both are considered mid-fidelity engineering tools. The aim of this study is not a comparison between the two numerical codes but proof of concept of the simulation methods for wind and current. AQWA can model wave-current interactions, but it cannot model the turbine aerodynamics. On the other hand, FAST can model turbine aerodynamics, but it cannot model wave-current interactions. Furthermore, hydrodynamic coefficients

of the platform have been generated with AQWA and exported to FAST. The two numerical codes are therefore used to complement each other for this thesis.

4.7.1) Ansys AQWA

AQWA uses a mixed approach of Potential Flow (PF) and the Morison Equation (ME) to solve diffraction, radiation and viscous loads on the platform resulting from waves and current. The hydrodynamic coefficients, such as added mass and Quadratic Transfer Functions (QTF), are determined in the frequency domain with the Boundary Element Method (BEM). This method divides the floating body into panels, and hydrodynamic loads are found by integrating the dynamic pressure over the wetted panels. The submerged geometry is defined as the hydrostatic equilibrium in still water for frequency-domain PF solvers. The QTFs are frequency dependent coefficients to solve for second order wave loads.

Ansys' CAD function was used to generate the 3D body of the platform according to the full-scale design of the INNWIND semisubmersible. The maximum panel size for the mesh was set at 3 m and the defeaturing tolerance at 1.5 m. This resulted in a relatively coarse mesh, which is sufficient for the simple geometry of the platform. Figure 31 shows the mesh of the 3D body in AQWA.

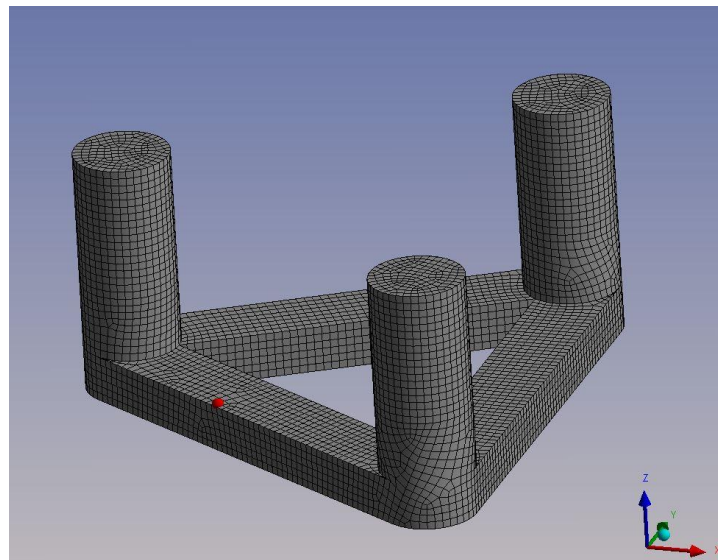


Figure 31. The mesh of the 3D body of the platform in AQWA

To solve the rigid body dynamics in the time domain with AQWA all the parameters found for the scale model as described in Section 4.4 have been added to the numerical model at full-scale. Decay tests with the moored scale model have been replicated at full-scale in time domain simulations with AQWA to calibrate the damping- and stiffness matrices of the platform. The irregular waves and current velocities described in Section 3.1 are used in the time domain simulations. For the cases with current a 'current force coefficient' must be entered for each velocity. The drag coefficients found for the scale model mentioned in section 4.4 have been applied to calculate these current force coefficients. The duration of each simulation is 4000 seconds at full-scale, just over an hour, which corresponds to 10 minutes at model scale.

4.7.2) FAST v8

FAST also uses a combination of PF and ME to solve for diffraction, radiation, and viscous loads. However, as FAST is a time domain only solver, the hydrodynamic coefficients were imported from AQWA. The hydrodynamic coefficients were formatted with the conversion software BEMRosetta [103] to the correct format for FAST.

The same parameters described in section 4.4 have been used in the FAST model to replicate the scale model at full-scale. Rather than using one of the mooring modules in FAST, the mooring stiffness found with the scale model has been integrated in the stiffness- and damping matrices in HydroDyn and calibrated by replicating the decay tests with the scale model at full-scale in FAST.

The length of the tower has been adjusted in AeroDyn to account for the freeboard of the platform while maintaining hub height at 90 m for the NREL 5 MW turbine. The diameter and weight of the tower have also been adjusted to replicate the tower of the scale model. The tower and blade structural DOFs have been disabled in ElastoDyn, whereas generator, drivetrain, and platform DOFs were enabled. Turbine control has been left the same as for the OC4 semisubmersible FOWT in ServoDyn.

4.8) Assumptions, simplifications, and systemic sources of error and uncertainty

To keep the test setup as robust as possible some assumptions and simplifications have been made. Some of the assumptions and simplifications have already been mentioned in earlier sections and will be summarized here, while others will be described in more detail.

The following simplifications have been made:

- No structural dynamics are modelled, only rigid body dynamics are modelled where the entire FOWT is modelled as a single body.
- Only a limited version of turbine control is simulated during SIL experiments. The thrust force is calculated as a drag force with a limited number of thrust coefficients, rather than using BEMT for the real-time simulation. Rotor speed and torque are not calculated with the real-time simulation, instead they are both a function of the relative wind speed in lookup tables derived with offline simulations.
- Open-loop control is used for some of the experiments, meaning there is no feedback or real-time updates of loads due to platform dynamics.
- Current, waves and wind are each only simulated in a single direction.
- Only deep-water waves are applied.

The following assumptions are applied:

- For the emulation of the forces the calculated loads with the numerical simulations are assumed to be correct. The direct comparison between offline simulation and experiment only indicates how well the MPA and winch actuator can replicate the input signal from the real-time simulations and does not give a measure of the ‘accuracy’ of the simulations, that is, how close they are to the expected real-world performance.
- Vortex shedding due to flow around the columns and resulting sway motions of the platform are neglected. Neither AQWA or FAST capture vortex shedding, so only the drag force in surge direction is modelled with both the numerical model and the winch actuator. Lift forces are ignored and only drag forces are modelled.
- The flow of the current is assumed to be steady and uniform. No variation of the flow is modelled and as the soft mooring system is used the vertical velocity profile in the WCF, and numerical models, can be neglected. Only the flow at a depth from the keel of the model up to the surface of the water body is of interest, while the variation in flow over that vertical distance is negligible.
- The wetted surface A in equation (19) is assumed to be a constant, although it changes dynamically during testing as the platform moves in heave and pitch. However, this effect is expected to be small and not have a large influence on the results.
- To eliminate non-representative pitch motion of the model from actuation with the winch, the cable is connected to the turbine column of the model at $Z = \text{Centre of Gravity (COG)}$ in a conventional coordinate system. Although the force centre for current on the wetted area of the

platform shifts during pitch and heave of the platform, any non-representative pitch motion while the platform moves in heave and pitch, is expected to be minimal with the cable connected at $Z = \text{COG}$.

- Dynamic- and kinematic similitude is assumed for experiments with current. As with aerodynamics, Reynolds scaling should be applied to modelling of the flow of current, which would result in different drag coefficients at model scale compared to full-scale. However, for typical semisubmersible platforms in low velocities, such as used for this thesis, the difference between drag coefficients at model scale and full-scale is negligible [104]. Therefore, only Froude scaling is applied to the flow of current.
- Aerodynamic loads are assumed to be distributed uniformly across the turbine rotor and are applied in the centre line at hub height.

The following potential sources of error and uncertainty in the system have been identified:

- Latency is a problem faced by any SIL application; monitoring, feedback and emulation will all have to be fast enough to fit within the real-time simulation time-step. A suitable frequency for each action is required to keep latency to an acceptable level, i.e., to keep the combined time of actuation and control actions for each time step shorter than the simulation time step.
- The level of vibrations generated during operation of the MPA. The level of vibrations depends on the rotation speed and the number of propellers which are used simultaneously. The vibrations caused by the MPA are typically high-frequency in nature and may result in some of the simulated high-frequency loads to become over-shadowed.
- Both the spring in the winch cable and the cable itself are elastic, which helps to prevent damage from large snap loads during testing. However, the spring is likely to cause a phase shift between the demanded signal and measured signal and is also a potential source of hysteresis effects. The PI controller will mitigate the phase shift and hysteresis effects, but its effectiveness depends in part on the accuracy and noise levels of the sensors used for feedback.
- Friction in the pulley system of the winch actuator. Low-friction pulleys were used; however, any amount of friction may increase the surge damping of the platform during the SIL current experiments.
- The accuracy of C_D in equation (19) will have significant influence on the demanded drag force, and hence, also on the accuracy of test cases with current.
- The blockage by the FOWT model across the width of the WCF. With a maximum breadth of 1.6 m, the FOWT model covers just over half the width of the flume and the blockage may influence the response of the model during physical current experiments. However, during SIL experiments with current the boundary layers along the basin walls are ignored.
- Accuracy of AQWA and FAST. Work has been done in the Offshore Code Comparison project [105] to assess the accuracy of FAST and other numerical codes, and a methodology to assess uncertainty of FOWT response during wave basin testing has been developed in [62]. However, the work to assign a specific value to the accuracy of the numerical codes is not part of the scope of this thesis.
- Facility specific errors such as wave reflection in the basin, the accuracy of the wave maker to replicate waves at scale, and accuracy and noise of sensors and their calibration.

The setup of experimental- and numerical methods for this thesis have been discussed. Next, the validation metrics used to monitor the quality of the linkage between experimental- and numerical simulations will be discussed.

4.9) Validation metrics

One of the main objectives of this thesis is to validate the ridged body motion response of the INNWIND semisubmersible FOWT scale model to the emulation of aerodynamic- and hydrodynamic forces with

the MPA and the winch actuator. Validation of response to aerodynamic forces is done by comparing the experiments with the environmental conditions described in section 3.1 to numerical simulations with FAST v8 with the same conditions. Validation of response to hydrodynamic forces, i.e., emulation of the drag force of currents, is two-fold: first the experiments are compared to numerical simulations with Ansys AQWA and FAST v8, second the experiments are repeated with physical current and compared against each other. Validation metrics are applied to all results.

To minimize uncertainty of hybrid testing of FOWT models with the MPA and winch actuator, high accuracy and repeatability at replicating demanded forces and moments are essential. The initial step in the validation process is a qualitative comparison consisting of two parts. The first part graphically compares the measured outputs with the numerical inputs. For the second part Power Spectral Density (PSD) for actuation, and spectral energy for the response of the FOWT model to environmental loads is plotted to compare the difference in energy of the quantity of interest between experiment and simulation. The final step is a quantitative comparison. The following validation metrics are used based on the overview of suitable metrics provided by Holmes [106]:

Relative Error (RE):

$$RE = 1 - \left(\frac{\overline{E}}{S} \right) \quad (26)$$

Fraction of Measurements within a user defined tolerance (FMT):

$$a < \frac{S}{E} \leq b \quad (27)$$

Where E indicates the experiments, S indicates the numerical simulations, a is a lower limit and b is an upper limit. Average values are indicated with an overbar. With a perfect performance RE would be zero, i.e., with a perfect match the error is zero percent. As the difference between experiment and numerical simulation increases, the number for RE becomes larger. Therefore, small numbers for RE indicate good performance of the actuators, whereas large numbers for RE indicate poor performance. With a perfect performance FMT would be 1, with $a = b = 1$, i.e., the closer the numbers are to 1 for FMT with the tolerance as close to 1 as possible, the better the results. The PSD (for actuation) or spectral energy (for motion response) of each time series is used to calculate RE, whereas the measured- and numerical values of experiments and numerical simulations are used directly to calculate FMT. Either power density or energy density can be used to calculate RE, however, energy density was chosen for the response of the model to environmental loads because the energy spectra tend to be graphically clearer than the power spectra in most cases.

The direct comparison between simulation and experiment only indicates how well the MPA or winch actuator can replicate the input signal from the numerical simulations and does not give a measure of the ‘accuracy’ of the system, that is, how close the laboratory experiments are to the expected real-world performance. As a performance indicator for the MPA and winch actuator, direct comparison is an interesting metric from an engineering perspective to assist with the set up and calibration of multi degree of freedom actuation devices. However, it does not take the accuracy of the numerical codes into account. In this thesis, loads calculated with offline simulations by FAST for the MPA are assumed to be ‘correct’ and the ability of the MPA to emulate these loads with the open-loop control is assessed. Similarly, loads calculated with the real-time simulations for the MPA and the winch actuator during SIL experiments with closed-loop control are assumed to be ‘correct’. A generalized approach is used with RE and FMT for the validation of the MPA and winch actuator. These validation metrics take different sources of error and uncertainty into account and represent bias and scatter of the data.

With FMT, a user defined tolerance can be introduced by setting the limits of a and b . This is a clear benefit of FMT over RE as it allows the user to focus analysis on non-trivial or unknown sources of error in the system.

The method described above is applied to validate the ability of the actuators to accurately emulate the calculated loads and to validate the motion response of the scale model to the emulated loads compared with the numerical models. For the comparison study of applied physical current vs simulated current with SIL a slightly different approach is used. The relative difference between experiments with physical current and SIL current is determined for each test case. The relative difference is found by applying the validation metric RE, which is adapted for the comparison study. Each test case is repeated three times and those repeated measurements are combined into an average record. This is done for all the experiments with physical current and SIL current. The spectral energy of platform surge, heave, pitch, and mooring tensions of the combined average of the test cases with physical current are compared against the equivalent test cases with SIL current to determine RE, which for the comparison study is defined as:

$$RE = 1 - \left(\frac{\overline{E_p}}{\overline{E_s}} \right) \quad (28)$$

Where E_p is the spectral energy of the records with physical current, E_s is the spectral energy of the records with SIL current, and the overbar indicates the average records. Again, a perfect match between the physical- and SIL records would give an RE of zero. For the comparison study FMT is not a very useful metric as the comparison is between two sets of experiments and most of the systemic errors and uncertainty apply to both sets. Therefore, only RE is applied. Table 15 summarizes how the validation metrics are determined and used.

Table 15. Summary of the validation metrics.

	Quantity	Result for perfect performance	Remarks
RE, actuation only	Power Spectral Density	0	Direct comparison. The smaller the number, the smaller the difference between experiment and numerical simulation, the better the result.
RE, for response to environmental loads	Energy Spectral Density	0	As above
RE, for response to physical loads vs SIL loads	Energy Spectral Density	0	The smaller the difference between the experiments, the better the result.
FMT	Measured data for experiments, and resulting data from numerical simulations	1, with $a = b = 1$	With a user-defined tolerance to allow for errors and uncertainty. Numbers close to 1 with a narrow tolerance close to 1 indicate good results.

The validation metrics used provide a quantitative assessment of the performance of the actuators and simulation methods. For RE the closer the result is to zero the better the performance. For FMT the closer the result is to 1, with the tolerance as close to 1 as possible, the better the performance.

Chapter 5

Results

This Chapter describes the results of numerical modelling and experiments with the hybrid test system and the FOWT scale model and provides a discussion on the results. The bulk of these results can be found in [16], [17], and [18].

5.1) Actuation accuracy

In this Section the accuracy of actuation by the MPA and winch actuator is described.

5.1.1) Winch actuator

To demonstrate the capabilities of the winch actuator, first a sinusoidal tension signal is emulated with the scale model in still water. For TC1 the PI controller received instantaneous tension feedback, however, no motion tracking feedback was used. This test case is therefore regarded as emulating without SIL. The results are shown in Figure 32, and a comparison of the PSD for demanded and measured tension in Figure 33.

The measured signal is in close agreement with the demanded signal. Furthermore, repeatability is excellent, with a correlation coefficient between the measurements of 0.994.

For the SIL experiments the winch actuator only emulates the drag force resulting from steady current velocities, rather than varying current velocities.

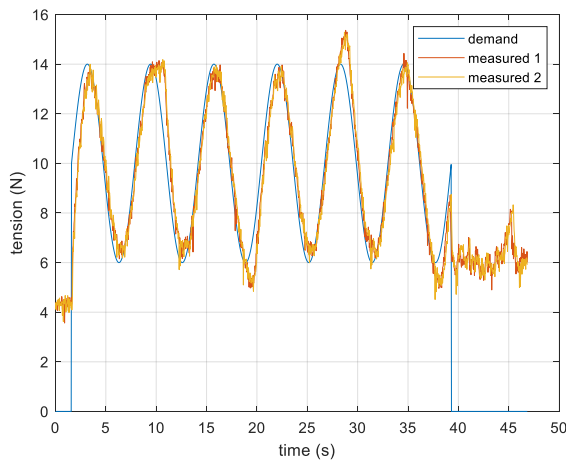


Figure 32. Actuation with the winch

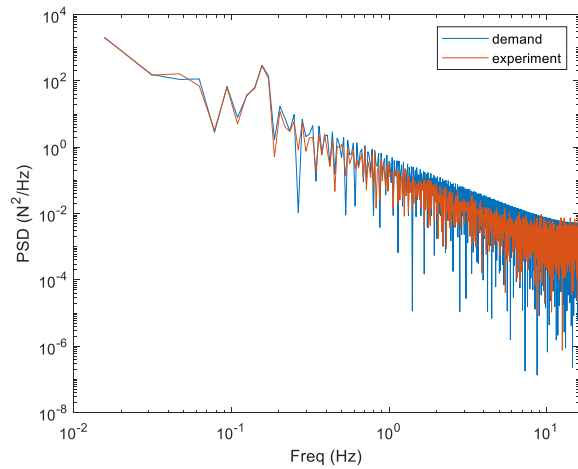


Figure 33. PSD of actuation with the winch

The validation metrics for TC 1 are shown in Table 16.

Table 16. Validation metrics for actuation.

	RE	FMT, $a=0.85$, $b=1.15$
Tension signal	0.013	0.95

5.1.2) MPA

Maximum delivered thrust per propeller is 15 N and 9 N with the S800 and Mavic blades respectively (blade lengths of 150 mm and 75 mm respectively). To demonstrate the capabilities of the MPA a time

series of steady loads is emulated with the aluminium tower fixed to the instrument bridge, i.e., the tower is fixed in all DOFs. The results are shown in Figure 34, which indicates that the MPA generates a considerable amount of high-frequency vibration noise during operation.

The rates of change for thrust and moment by the propellers were derived from the calibration data. High rates of change are achieved with both S800 blades and Mavic blades. Thrust changes at a rate of 65 N/s and 50 N/s with the S800 and Mavic blades respectively, and moment changes at a rate of 7.5 Nm/s and 5 Nm/s respectively.

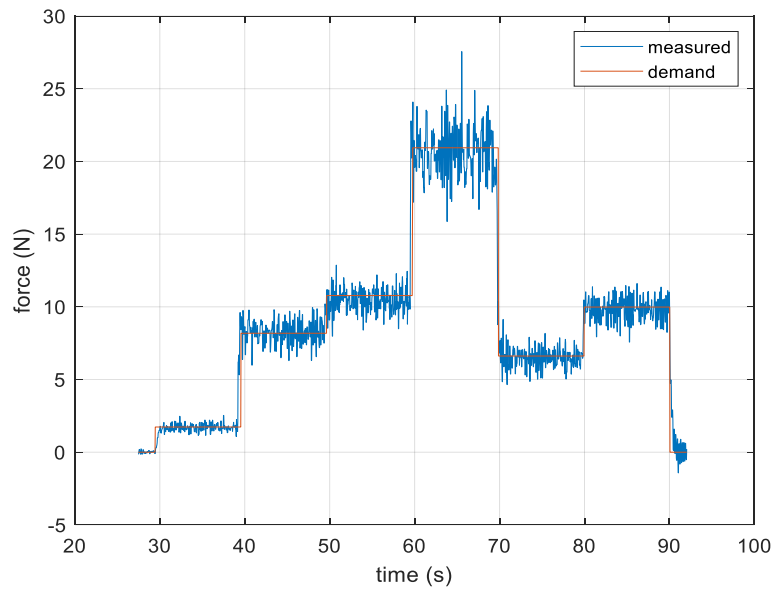


Figure 34. Timeseries of steady loads with the two thrust propellers S3 and S4 with the S800 blades.

Rotor thrust and torque curves of the NREL 5 MW turbine were replicated by emulating thrust and torque at steady wind speeds found with FAST simulations at 1:37 scale. The propellers were operated for 15 s at each wind speed and measured forces and moments were averaged. The results are shown in Figure 35 and Figure 36, where the error bars indicate the standard deviation of the measurements.

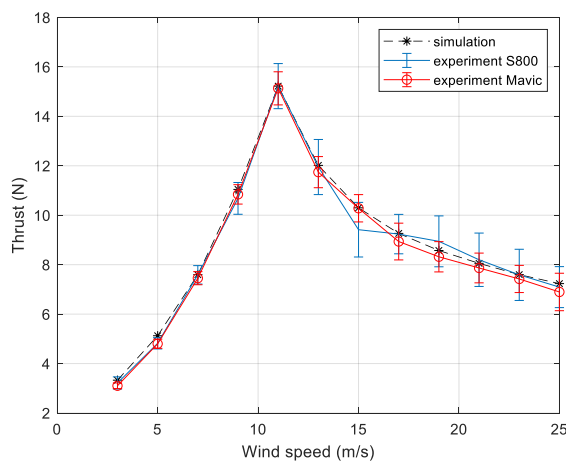


Figure 35. Thrust curve, NREL 5 MW turbine. Thrust values are shown at model scale with corresponding wind speeds at full-scale.

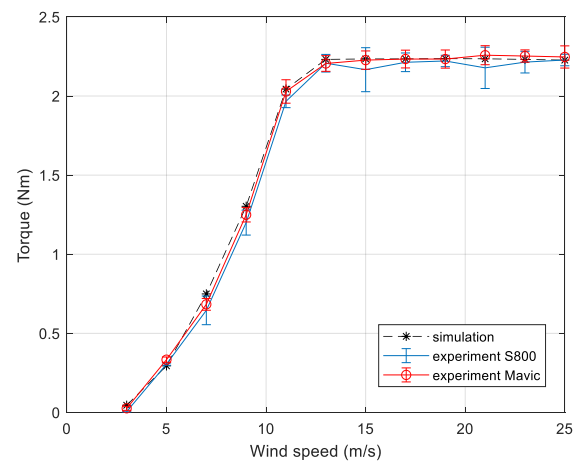


Figure 36. Torque curve, NREL 5 MW turbine. Torque values are shown at model scale with corresponding wind speeds at full-scale

Next, for TC2 a timeseries of 350 seconds of turbulent wind around rated wind speed from offline simulations with FAST is emulated with the MPA at 1:37 scale, using open-loop control. Figure 37 and Figure 38 show the results for emulating rotor thrust and torque with the Mavic blades. All values are shown at scale. A low-pass filter was applied to the measured data to filter out the high frequency noise. All frequencies higher than 12 Hz were filtered out to allow the capture of all the relevant frequencies, including the 3P-frequency (approximately 10 Hz at scale) and low-frequency thrust variations.

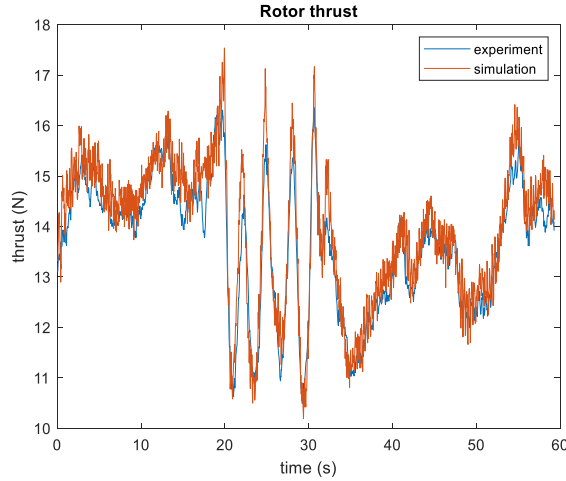


Figure 37. Emulated rotor thrust with Mavic blades.

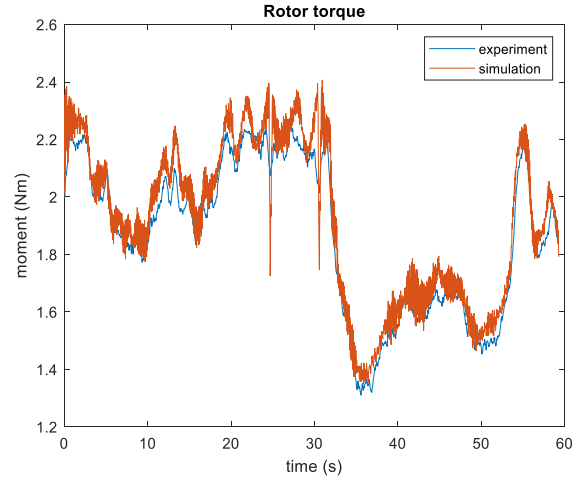


Figure 38. Emulated rotor torque with Mavic blades.

TC2 was repeated with closed-loop control at scale 1/50 and the Mavic blades, and turbulent wind speeds around 9 m/s (below rated) and 11.4 m/s (rated) at full-scale. The duration of the real-time simulations was 10 minutes. The tower was also fixed for these tests.

Figure 39 and Figure 40 show the thrust PSD for the open-loop and closed-loop control respectively.

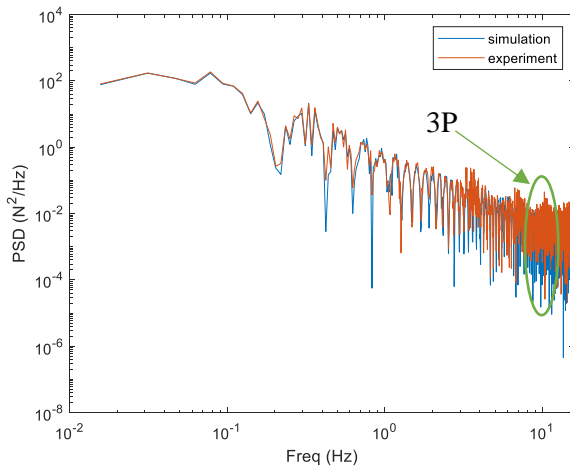


Figure 39. Thrust PSD with open-loop control, with Mavic blades and V2

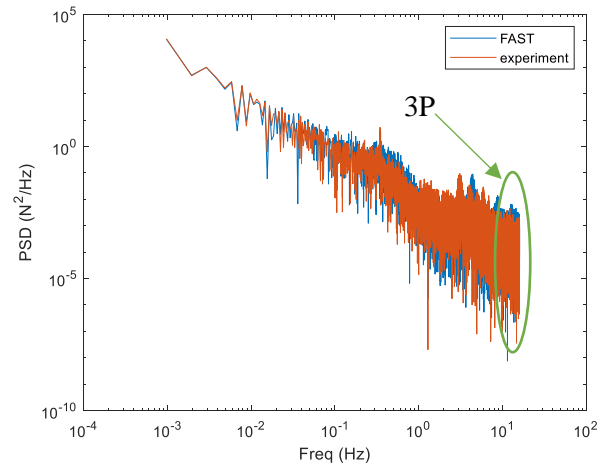


Figure 40. Thrust PSD with closed-loop control, with Mavic blades and V2

Low-frequency fluctuations are captured with both control strategies. However, Figure 40 shows the closed-loop control strategy struggles to capture some of the high frequency fluctuations accurately such as 3P frequency, as was expected. On the other hand, with open-loop control the high frequency loads are captured more accurately as is shown in Figure 39.

For TC3 the MPA was used in the horizontal configuration to emulate aerodynamic yaw, or gyroscopic moment, with open-loop control. The scale for TC3 was 1:37 and a time series of 350 seconds for yaw moment resulting from steady wind at rated speed at full-scale was used as input. Poor results compared to thrust and torque were achieved for TC3, which is discussed in Section 5.6. The emulated yaw moment is shown in Figure 41. A clear time lag is visible, and the experimental curve is far from the smooth curve like that of the simulation. The PSD is shown in Figure 42. The propeller pairs S2 & S4 and S3 & S5 acting intermittently at high rotational speeds were exciting a natural frequency of the MPA, with significant vibrations as a result and causing a noticeable displacement of the propeller arms. A slight delay in the start-up of the propellers from zero rpm to the initial spin could explain the time lag.

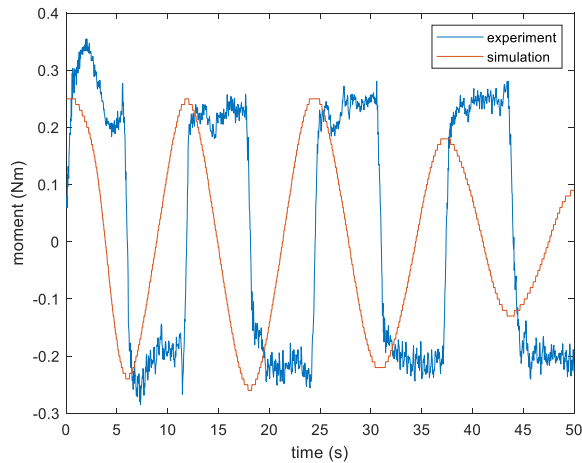


Figure 41. Emulated yaw moment, TC3

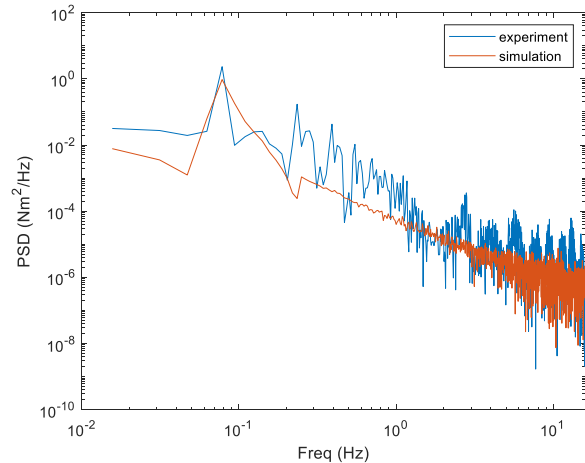


Figure 42. PSD of emulated yaw moment, TC3

For TC4 the MPA was used in the vertical configuration as shown in Figure 14, again to emulate aerodynamic yaw. A 350 second timeseries of turbulent wind around rated speed at full-scale was used for TC4. The scale of the emulated yaw moment was 1:37 and again the Mavic blades were used for this test. The emulated yaw moment and PSD are shown in Figure 43 and Figure 44 respectively.

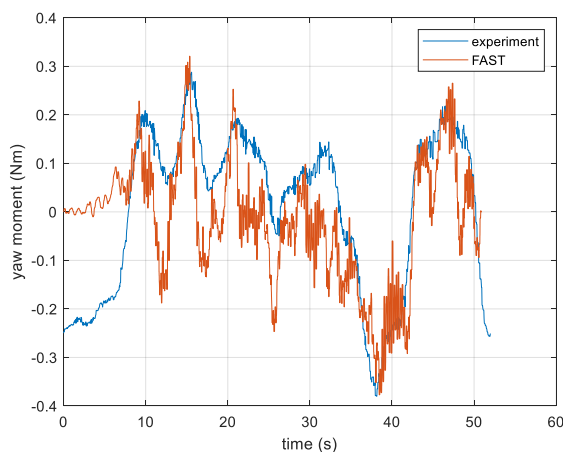


Figure 43. Emulated yaw moment, TC4

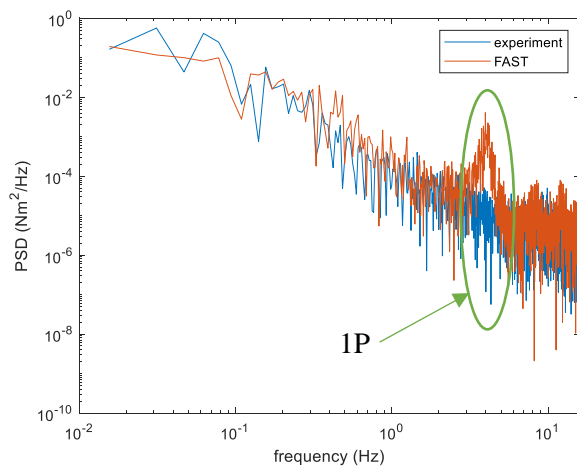


Figure 44. PSD of emulated yaw moment, TC4

The results show there is no time lag for the low frequency fluctuations between the experiments and offline numerical simulations, in contrast to TC3. However, Figure 44 shows there is significant

difference in the amplitudes and the higher frequency fluctuations are not captured accurately, which is also evident in Figure 45. In this configuration the MPA is unable to effectively capture either the 1P-frequency (around 3 Hz) or the 3P-frequency (around 10 Hz). This is discussed further in Section 5.6.

The validation metrics for TC 2 – TC 4 are shown in Table 17. Clearly, the metrics are most favourable with the Mavic blades on the MPA when emulating rotor thrust and rotor torque. Slightly more favourable values for RE are achieved with closed-loop control compared to open-loop control for thrust and torque at rated wind speed, despite the inability of capturing the high frequency loads accurately with closed-loop control. However, this inability is reflected in FMT, which is more favourable for open-loop control. Poor metrics are achieved for the emulation of aerodynamic yaw, regardless of the configuration of the MPA.

Table 17. Validation metrics for TC2 – TC4

	Load	S800 blades	Mavic blades	Control	Wind speed	Scale	RE	FMT
TC2	Thrust	√	×	Open-loop	11.4 m/s	1:37	0.06	0.61 ($a=0.9, b=1.05$)
TC2	Torque	√	×	Open-loop	11.4 m/s	1:37	0.06	0.74 ($a=0.9, b=1.05$)
TC2	Thrust	×	√	Open-loop	11.4 m/s	1:37	0.03	0.97 ($a=0.9, b=1.05$)
TC2	Torque	×	√	Open-loop	11.4 m/s	1:37	0.04	0.98 ($a=0.9, b=1.05$)
TC2	Thrust	×	√	Closed-loop	9 m/s	1:50	0.04	0.89 ($a=0.8, b=1.15$)
TC2	Torque	×	√	Closed-loop	9 m/s	1:50	0.04	0.96 ($a=0.8, b=1.15$)
TC2	Thrust	×	√	Closed-loop	11.4 m/s	1:50	0.02	0.95 ($a=0.8, b=1.15$)
TC2	Torque	×	√	Closed-loop	11.4 m/s	1:50	0.02	0.92 ($a=0.8, b=1.15$)
TC3	Yaw	×	√	Open-loop	11.4 m/s	1:37	0.55	0.27 ($a=0.5, b=2$)
TC4	Yaw	×	√	Open-loop	11.4 m/s	1:37	0.33	0.34 ($a=0.5, b=2$)

Due to the more favourable results with the Mavic propeller blades, only the Mavic blades have been used with the MPA for all the experiments of TC6 – TC19, results for which are presented in Sections 5.2.2 – 5.4.3.

5.2) Ocean Basin Campaign

5.2.1) Current only

The results for TC5 are shown in Figure 45 and Figure 46, for the response in the surge DOF of the scale model to drag force emulation with- and without SIL respectively of the experiments and simulations with AQWA. Current velocities of 0.11 m/s and 0.14 m/s are simulated, which correspond to 0.75 m/s and 1 m/s respectively at full scale. Results are shown at model scale. Greater agreement of results is achieved with SIL. Without SIL, larger- and more oscillations occur before the system settles, and after settling, the surge excursions are smaller than with SIL. A PID controller should be able to damp out oscillations in the no-SIL situation and settle the system quicker. However, the Derivative component requires a clean feedback signal. The tension feedback signal was found to be very noisy, up to 5N without filtering, which was reduced to 0.5N after shielding of all the signal cables. However, adding numerical filters in Simulink, resulted in a broken saw-tooth signal with maximum amplitudes of 2.5N at best. Instead, a PI controller was opted for the current simulation system, which is able to handle the unfiltered noisy signal of 0.5N. Figures 45 and 46 also show there is a slight phase shift between experimental and numerical signals. The numerical signal lags the experimental signal, where the opposite is expected due to the spring in the winch wire. The validation metrics for TC5 are shown in Table 18.

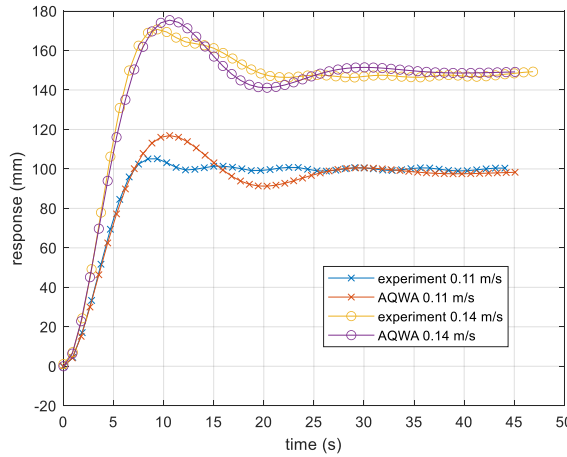


Figure 45. Experiments vs AQWA, surge response to current simulation with SIL.

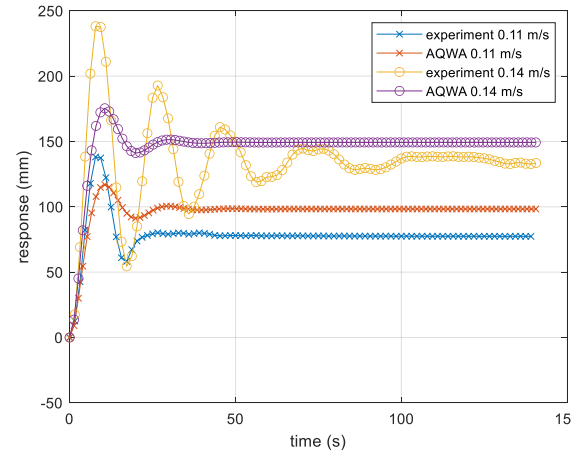


Figure 46. Experiments vs AQWA, surge response to current simulation without SIL.

Table 18. Validation metrics for TC5

	RE	FMT
With SIL, 0.11 m/s	0.02	0.96 ($a = 0.85$, $b = 1.15$)
With SIL, 0.14 m/s	0.02	0.99 ($a = 0.85$, $b = 1.15$)
Without SIL, 0.11 m/s	0.18	0.05 ($a = 0.85$, $b = 1.15$)
Without SIL, 0.14 m/s	0.08	0.62 ($a = 0.85$, $b = 1.15$)

5.2.2) Wind only

The motion and the energy spectrum for the surge DOF of the scale model with turbulent wind around 9 m/s at full-scale (V1) and closed-loop control are shown in Figure 47 and Figure 48 respectively. Motion and energy spectrum for the pitch DOF under the same conditions are shown in Figure 49 and Figure 50. Results from the experiments and offline FAST simulations are all shown at model scale.

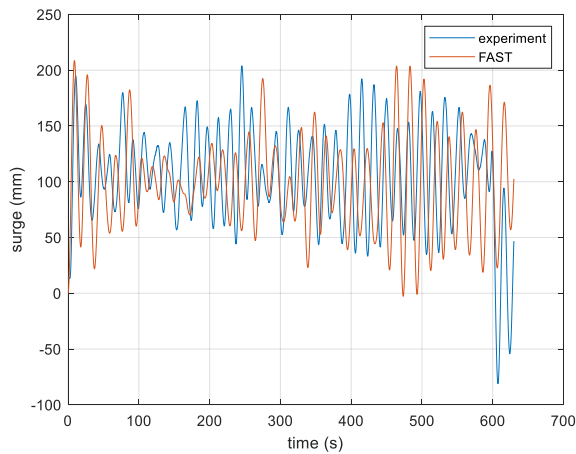


Figure 47. Surge motion of the FOWT model with closed-loop control and wind speed V1

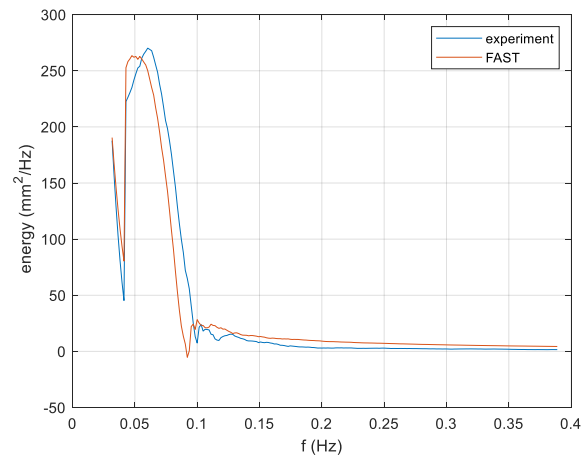


Figure 48. Energy spectrum of surge with closed-loop control and wind speed V1

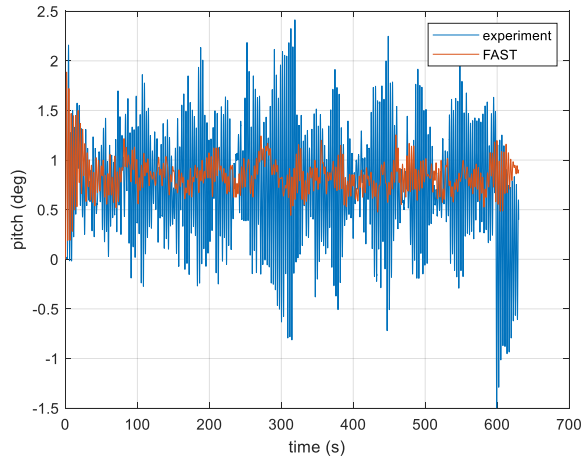


Figure 49. Pitch motion of the FOWT model with closed-loop control and wind speed V1

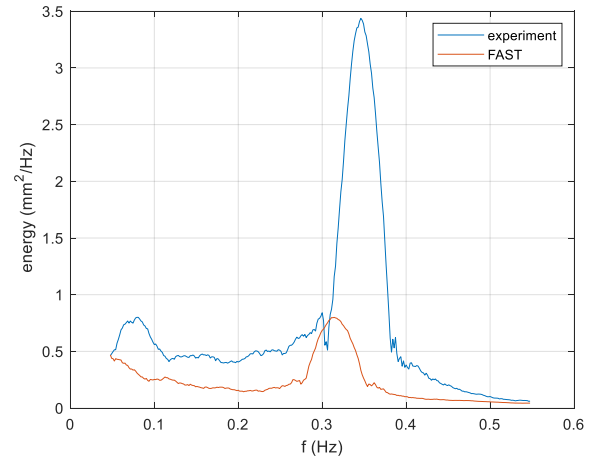


Figure 50. Energy spectrum of pitch with closed-loop control and wind speed V1

Although the experimental surge motion does not follow the same pattern as the surge motion from the FAST simulation, spectral energy of the experiments compared to the numerical simulations is similar, which is reflected in the RE validation metrics. FMT is slightly less favourable. Pitch motion on the other hand, is significantly under-predicted by FAST compared to the experiments and experimental energy is substantially higher than that of the FAST simulations, giving poor RE and FMT metrics. A possible explanation is discussed in section 5.6.

For the experiments with turbulent wind around 11.4 m/s (V2) the RE validation metrics for surge are similar compared to turbulent wind around 9 m/s (V1), with slightly more favourable FMT metrics. However, RE validation metrics for pitch with turbulent wind around 11.4 m/s are considerably more favourable compared to wind around 9 m/s. Rotor thrust around 11.4 m/s wind is steadier compared with wind around 9 m/s with fewer large fluctuations. Around rated- and higher wind speeds the blade pitch control of the turbine is active to maintain rotor speed around 12 rpm, whereas at below rated wind speeds only generator torque control is active and rotor speeds tend to fluctuate more.

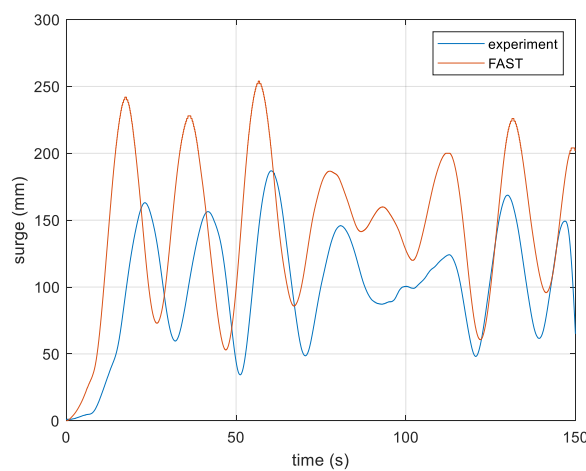


Figure 51. Surge motion of the model with open-loop control and wind speed V2

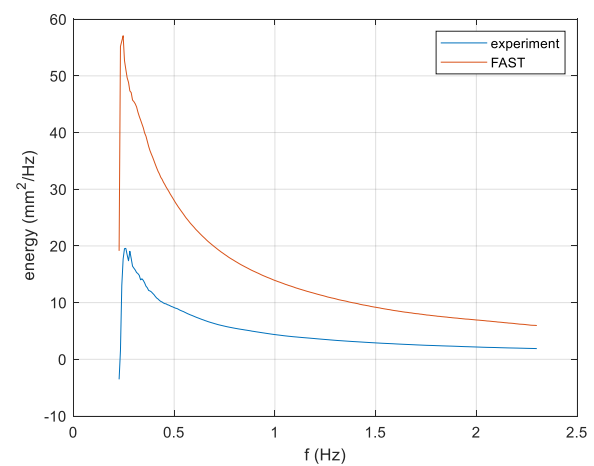


Figure 52. Energy spectrum of surge with open-loop control and wind speed V2

As a result, the amplitudes of surge and pitch of the FOWT with wind only loads are smaller around 11.4 m/s wind compared to 9 m/s wind, resulting in more favourable metrics. The validation metrics for the wind only test cases are shown in Table 19. With open-loop control the pattern for surge motion of the FOWT model is followed better compared to closed-loop control, however, amplitudes are lower with experiments compared to offline FAST simulations resulting in significant difference in spectral energy, as shown in Figure 51 and Figure 52. This is reflected in the validation metrics. Similar results were achieved for pitch of the scale model with open-loop control.

Table 19. Validation metrics for TC6

	DOF	RE	FMT
V1, closed-loop	Surge	0.01	0.71 ($a = 0.5, b = 2$)
V1, closed-loop	Pitch	0.77	0.66 ($a = 0.5, b = 2$)
V2, closed-loop	Surge	0.03	0.87 ($a = 0.15, b = 4.55$)
V2, closed-loop	Pitch	0.03	0.84 ($a = 0.15, b = 4.55$)
V2, open-loop	Surge	0.39	0.75 ($a = 0.5, b = 2$)
V2, open-loop	Pitch	0.33	0.83 ($a = 0.5, b = 2$)

5.2.3) Waves only

The heave- and pitch spectral energy of the FOWT model for TC8, experiments compared to numerical simulations in AQWA, are shown in Figure 53 and Figure 54 respectively. Both figures clearly show a shift of the peak around wave energy between the experiments and numerical simulations. A second peak around the natural frequency of the FOWT model also clearly shows for both heave and pitch for the experiments. The peaks around the natural frequencies are not captured by AQWA as these frequencies fall outside of the input wave frequency range in AQWA. As a result, there is a significant difference in spectral energy for heave and pitch, which is reflected in the validation metrics. The validation metrics are shown in Table 20.

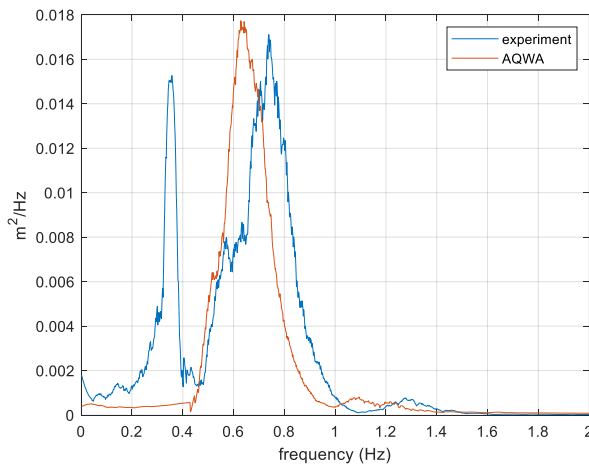


Figure 53. Spectral energy for heave DOF in waves only

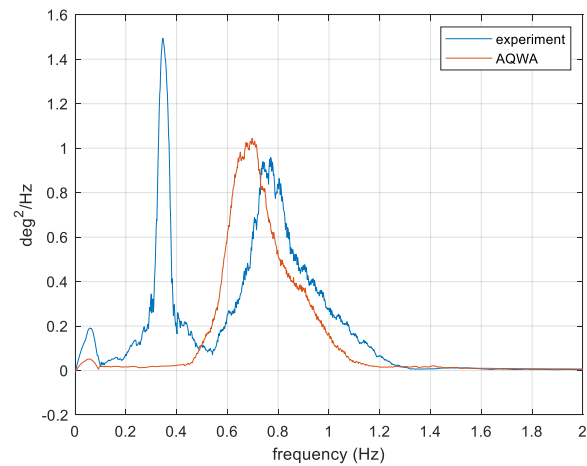


Figure 54. Spectral energy for pitch DOF in waves only

For the surge DOF of the FOWT model with waves only there is significant under-prediction of the amplitudes from wave excitation by AQWA, again resulting in significant difference in spectral energy.

Table 20. Validation metrics for TC8

	Waves	RE	FMT
Surge	JONSWAP 1	1.20	0.38 ($a = 0.15$, $b = 4.55$)
Heave	JONSWAP 1	0.36	0.34 ($a = 0.15$, $b = 4.55$)
Pitch	JONSWAP 1	0.36	0.36 ($a = 0.15$, $b = 4.55$)

5.2.4) Waves and current

Similar to TC8, the energy spectra of heave and pitch of the FOWT model for TC9 show a shift in the peak around wave frequencies and an extra peak around the natural frequencies for the experiments under combined wave and current loading, as shown in Figure 55 and Figure 56. Again, this results in significant differences in spectral energy between experimental results and numerical results. However, when the spectral energy of the wave-only and wave-current cases around wave frequencies are compared experimentally and numerically respectively, it shows there is similar difference between them. Further discussion on these results can be found in Section 5.5.

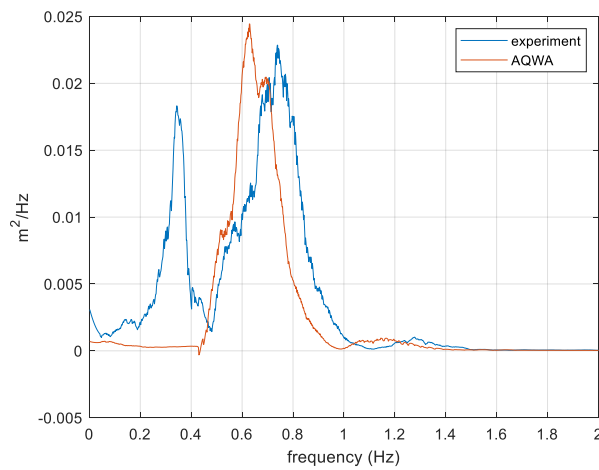
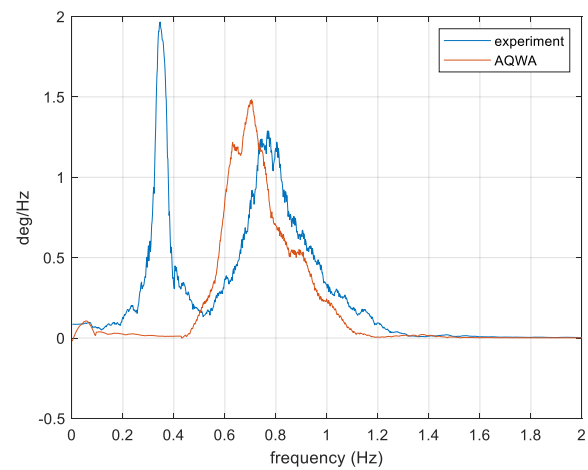
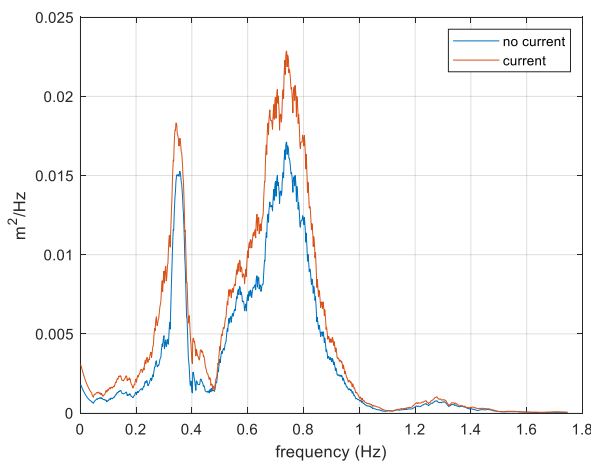
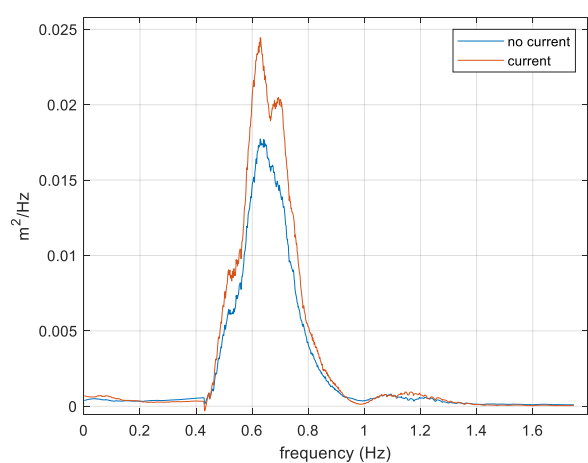
**Figure 55.** Spectral energy of heave DOF for waves and current, experiment vs AQWA, TC9**Figure 56.** Spectral energy of pitch DOF for waves and current, experiment vs AQWA, TC9**Figure 57.** Spectral energy of experimental heave DOF, TC8 vs TC9**Figure 58.** Spectral energy of numerical heave DOF, TC8 vs TC9

Figure 57 and Figure 58 show the difference of spectral energy between wave-only and wave-current cases for the experiments and for the numerical simulations respectively. The difference in heave spectral energy between wave-only and wave-current cases for the experiments is 37%, and for the numerical simulations it is 34%. This gives some confidence that wave-current interactions are simulated correctly with the current simulation system. Similar results were found for the pitch DOF. The conditions for the test cases shown in Figure 55 – 58 are with JONSWAP1 and current B. Although there is still some under-prediction of the wave excited surge amplitudes by AQWA compared to the experiments for TC9, the difference is considerably smaller compared to surge for TC8. As a result, the validation metrics are more favourable as is shown in Table 21.

Table 21. Validation metrics for TC9

	Waves	Current	RE	FMT
Surge	JONSWAP1	A	0.04	0.92 ($a = 0.15, b = 4.55$)
Heave	JONSWAP1	A	0.46	0.34 ($a = 0.15, b = 4.55$)
Pitch	JONSWAP1	A	0.44	0.35 ($a = 0.15, b = 4.55$)
Surge	JONSWAP1	B	0.06	0.92 ($a = 0.15, b = 4.55$)
Heave	JONSWAP1	B	0.46	0.35 ($a = 0.15, b = 4.55$)
Pitch	JONSWAP1	B	0.40	0.34 ($a = 0.15, b = 4.55$)

5.2.5) Wind and current

A comparison of the experimental cases of TC7 shows there is some damping of pitch motions due to current during wind/current cases compared to wind-only cases. Furthermore, there is a significant reduction of wind induced surge motions, and an increase of surge stiffness with the addition of current in wind/current cases compared to wind-only cases, as is shown in Figure 59 and Figure 60 where the larger wind induced surge motions for wind-only show as a peak around 0.06 Hz and the damped surge motions for wind-current as a smaller peak around 0.15 Hz (as an exception to the rule PSD compared clearer graphically than energy density for this case, which is why PSD is shown here). Of course, in real ocean conditions wind and current without waves would be a rare combination.

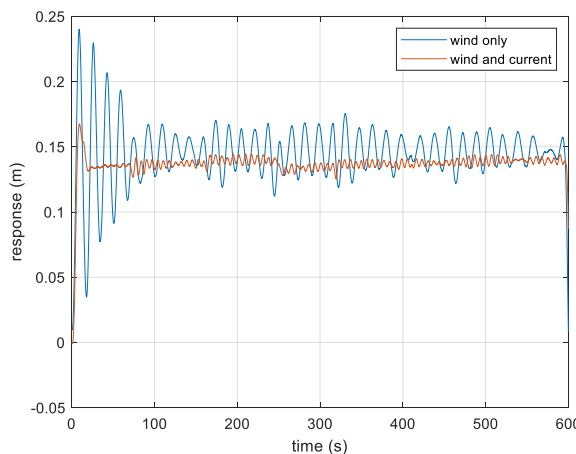


Figure 59. Surge response, experimental results of TC6 vs TC7

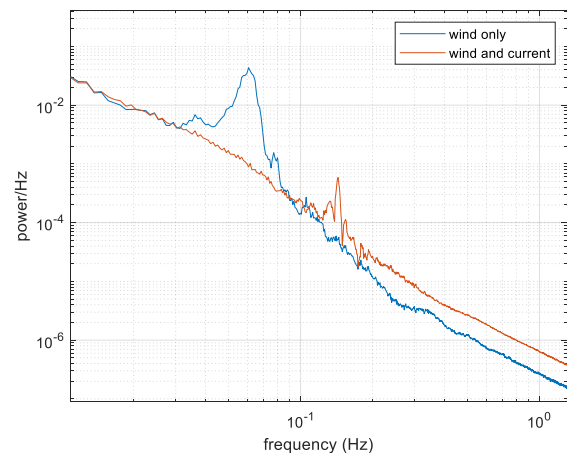


Figure 60. Surge PSD, experimental results of TC6 vs TC7

The surge damping due to current found with the experiments is not captured by FAST, as is shown in Figure 61. After the initial surge excursion, the wind induced surge oscillations are over-predicted by FAST compared to the experimental surge oscillations. The difference in spectral energy due to this over-prediction can be seen in Figure 62.

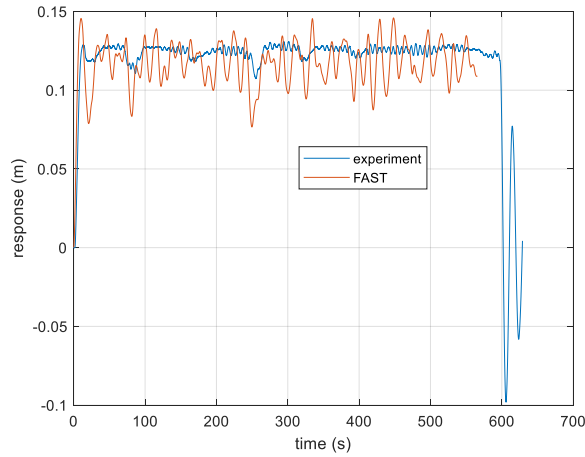


Figure 61. Surge motion of the FOWT model, TC7

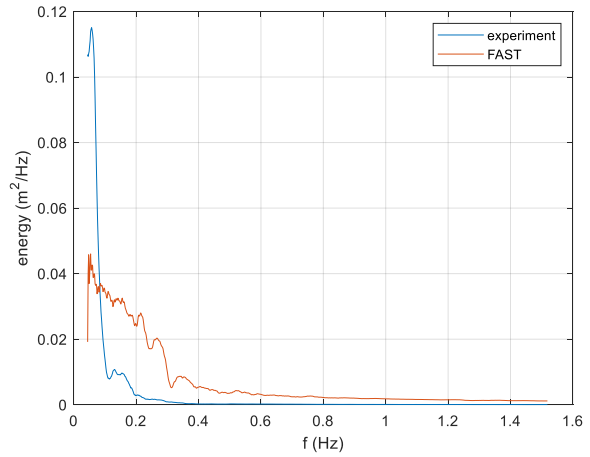


Figure 62. Spectral energy for the surge DOF of the FOWT model, TC7

The validation metrics for TC7 of the FOWT model's DOFs found with experiments compared to FAST simulations are shown in Table 22.

Table 22. Validation metrics for TC7

	DOF	Current	RE	FMT
V2, Closed-loop	Surge	B	0.12	0.87 ($a = 0.15, b = 4.55$)
V2, Closed-loop	Pitch	B	0.06	0.85 ($a = 0.15, b = 4.55$)

5.2.6) Waves and wind

A comparison of experimental cases of TC10 show that there is a small amount of damping of the heave motions of the platform due to wind during wave/wind cases compared to wave-only cases, whereas the addition of wind causes a significant increase of pitch motion of the platform around the natural frequencies of the FOWT model. Figure 63 and Figure 64 show the experimental spectral energy of the heave- and pitch DOFs of the FOWT model respectively for wave-only cases compared to wave-wind cases.

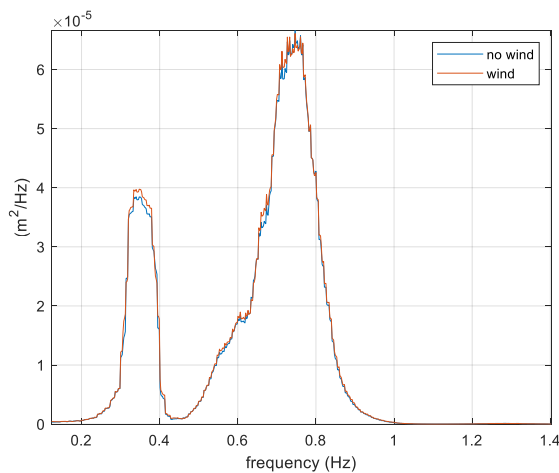


Figure 63. Heave spectral energy, experimental results TC8 and TC10

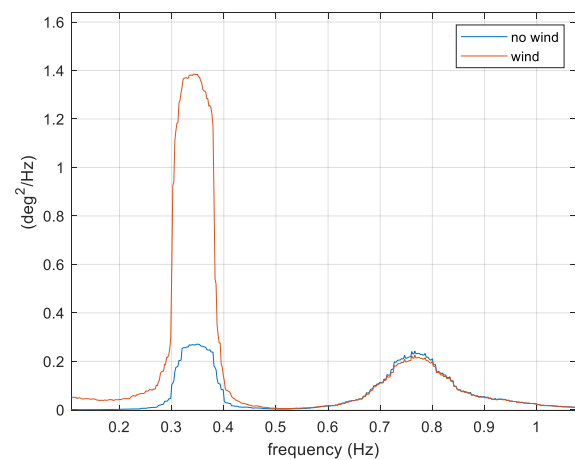


Figure 64. Pitch spectral energy, experimental results TC8 and TC10

The validation metrics for TC10 of the FOWT model DOFs found with experiments compared to FAST simulations are shown in Table 23. All DOFs are significantly overpredicted by FAST compared to experimental results for TC10.

Table 23. Validation metrics for TC10

	Waves	Wind	RE	FMT
Surge	JONSWAP1	V2	0.45	$0.77 (a = 0.5, b = 2)$
Heave	JONSWAP1	V2	0.43	$0.20 (a = 0.5, b = 2)$
Pitch	JONSWAP1	V2	0.10	$0.49 (a = 0.5, b = 2)$

5.2.7) Waves, current, and wind

Figure 65 and Figure 66 show the surge motion of the FOWT model and surge spectral energy for TC11 respectively of the experiments compared to FAST simulations. Both figures clearly show FAST is over-predicting surge motion around the wave frequencies. The initial excursion in the surge DOF by the FOWT model closely matches between experiments and FAST simulations, with the average distance of the experiments at 0.12 m and the corresponding distance of the FAST simulations at 0.11 m.

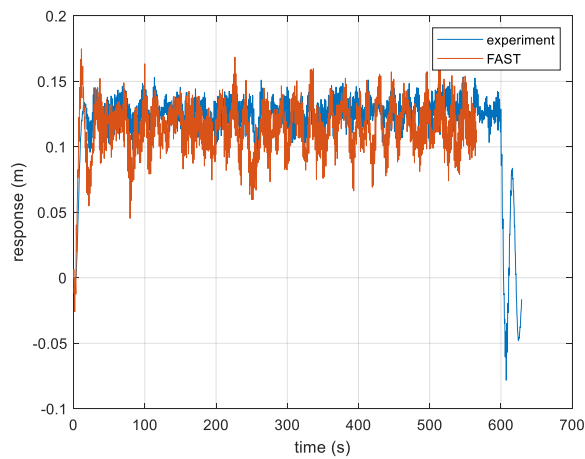


Figure 65. Surge motion of the FOWT model with waves, current, and wind

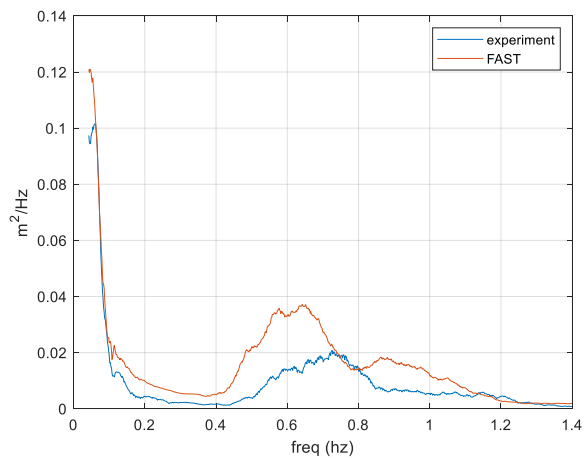


Figure 66. Spectral energy for surge DOF of the FOWT model with waves, current, and wind

The validation metrics for TC11 of the FOWT model surge DOF found with experiments compared to FAST simulations are shown in Table 24. Only the metrics for the surge DOF are given for this test case; FAST does not capture wave-current interactions which will impact the results of heave- and pitch motions, whereas surge motions are not likely to be affected much by wave-current interactions.

Table 24. Validation metrics for TC11.

	Waves	Current	Wind	RE	FMT
Surge	JONSWAP1	B	V2	0.18	$0.86 (a = 0.15, b = 4.55)$

When comparing the experiments of wave/wind cases of TC10 to the experiments of wave/wind/current cases of TC11, there is still some damping of wave/wind induced surge motions with the addition of current, however, surge stiffness remains the same and is dominated by wave excitation.

Figure 67 and Figure 68 show the theoretical- and measured spectra of the irregular waves which were used during the Ocean Basin test campaign. Both figures clearly show a higher peak and increased energy at the higher wave frequencies for the spectra with opposing currents at 0.11 m/s and 0.14 m/s. The difference in spectral energy between theory and measurement is 11.4% for the wave-only cases, 9.9% for waves and current = 0.11 m/s, and 5.8% for waves and current = 0.14 m/s.

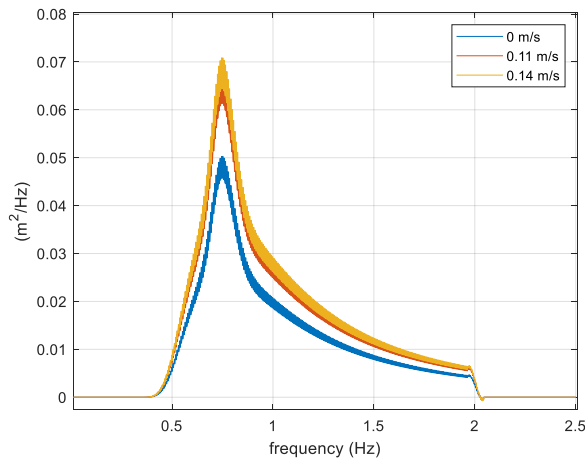


Figure 67. Theoretical wave spectra for wave-only and wave-current test cases.

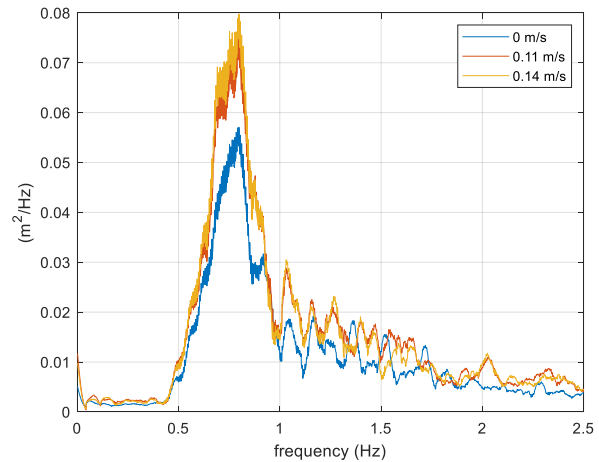


Figure 68. Measured wave spectra for wave-only and wave-current test cases.

5.3) Deep Ocean Basin campaign

To determine the performance of the winch-actuator in more energetic waves compared to the waves used for the OB campaign, a series of experiments was conducted in the DOB. Due to the larger water depth in the DOB compared to the OB (3m. compared to 1m.) larger waves with longer wave periods could be used and still be considered ‘deep-water’ waves.

5.3.1) Waves only

For the DOB campaign the frequency range of the irregular waves in AQWA was widened to include wave frequencies around the natural frequencies of the FOWT model to ensure the motion energy of these frequencies is also captured by the numerical simulations. This was achieved by using the measured wave timeseries of the experiments at full-scale as input in AQWA.

However, despite the widened wave frequency range AQWA significantly under-predicts the motion and energy of all DOFs of the FOWT model compared to the experiments under the conditions of TC12. Figure 69 and Figure 70 show the surge motion and spectral energy respectively of the FOWT model for the experiments compared to AQWA simulations.

The under-prediction by AQWA in larger waves and longer wave periods is reflected in the validation metrics, which are shown in Table 25.

Table 25. Validation metrics for TC12

	Waves	RE	FMT
Surge	JONSWAP 2	1.33	0.47 ($a = 0.15$, $b = 4.55$)
Heave	JONSWAP 2	2.14	0.34 ($a = 0.15$, $b = 4.55$)
Pitch	JONSWAP 2	2.87	0.32 ($a = 0.15$, $b = 4.55$)

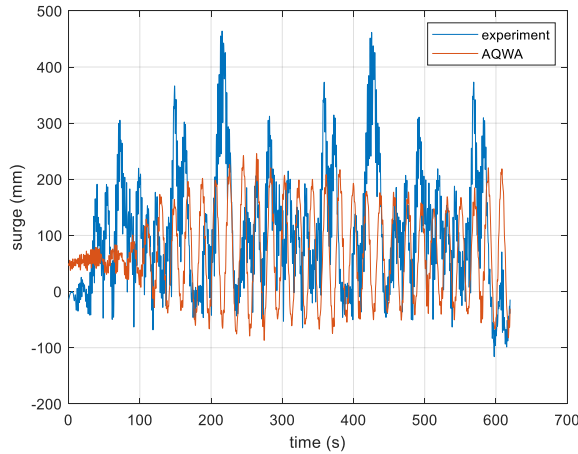


Figure 69. Surge motion of the FOWT model in surge DOF for TC12

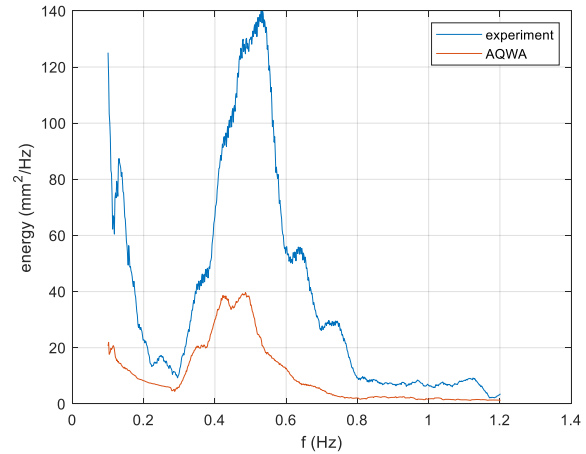


Figure 70. Spectral energy of the FOWT model in surge DOF for TC12

5.3.2) Waves and current

With the addition of current there is still significant under-prediction by AQWA of the motion and energy of all DOFs of the FOWT model compared to the experiments. This under-prediction remains significant as the current velocity increases, which becomes apparent with the validation metrics shown in Table 26. Figure 71 and Figure 72 show the spectral energy of the heave- and pitch DOF respectively of the FOWT model with waves and current velocity C . Both figures show that some energy around the natural frequencies is captured in AQWA and the peak frequency for heave is the same for experiments and AQWA simulations. However, both figures also clearly show the under-prediction by AQWA.

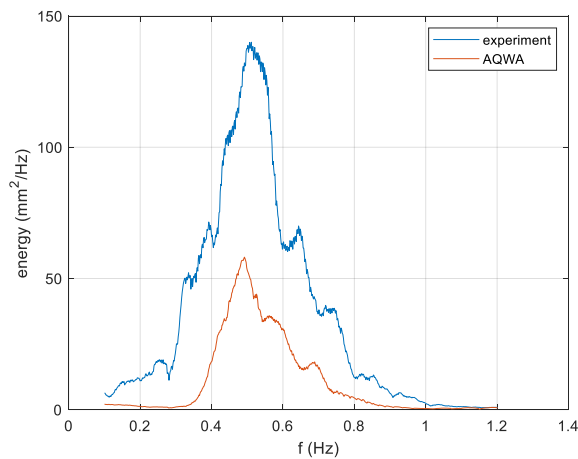


Figure 71. Spectral energy of the FOWT model in heave DOF for TC13

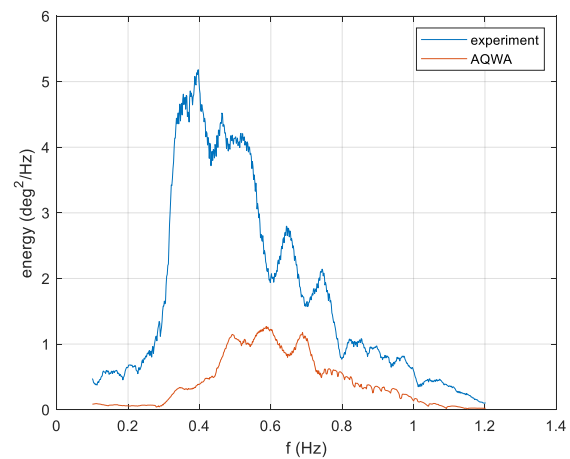
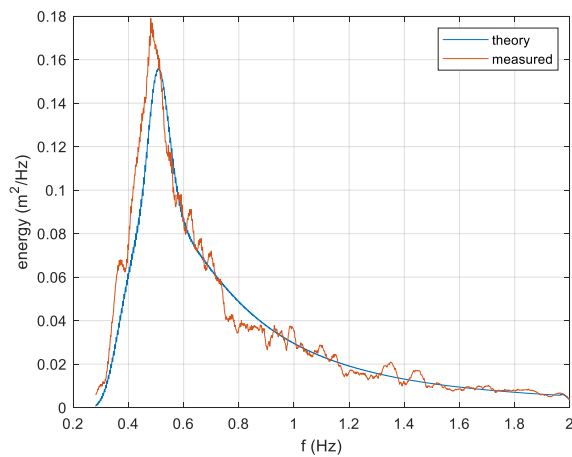
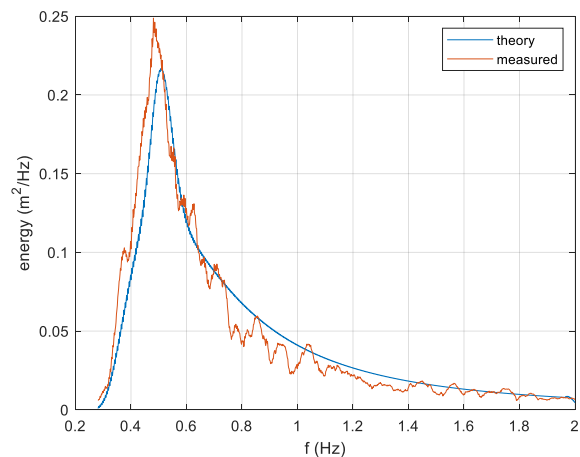


Figure 72. Spectral energy of the FOWT model in pitch DOF for TC13

Table 26. Validation metrics for TC13

	Waves	Current	RE	FMT
Surge	JONSWAP2	A	1.33	0.58 ($a = 0.15$, $b = 4.55$)
Heave	JONSWAP2	A	2.14	0.32 ($a = 0.15$, $b = 4.55$)
Pitch	JONSWAP2	A	2.97	0.32 ($a = 0.15$, $b = 4.55$)
Surge	JONSWAP2	B	1.05	0.72 ($a = 0.15$, $b = 4.55$)
Heave	JONSWAP2	B	2.05	0.32 ($a = 0.15$, $b = 4.55$)
Pitch	JONSWAP2	B	2.74	0.30 ($a = 0.15$, $b = 4.55$)
Surge	JONSWAP2	C	0.85	0.95 ($a = 0.15$, $b = 4.55$)
Heave	JONSWAP2	C	2.20	0.35 ($a = 0.15$, $b = 4.55$)
Pitch	JONSWAP2	C	2.94	0.32 ($a = 0.15$, $b = 4.55$)

Figure 73 and Figure 74 show the theoretical wave spectra compared to the measured wave spectra for wave only cases and waves with 0.21 m/s current respectively as an example of irregular waves used during the Deep Ocean Basin test campaign. Table 27 shows the difference between theoretical and measured spectral energy for all the test cases used during the Deep Ocean Basin test campaign.

**Figure 73.** Theoretical and measured spectra JONSWAP2, waves only**Figure 76.** Theoretical and measured spectra JONSWAP2 with current C**Table 27.** difference in spectral energy between theoretical- and measured wave spectra for the Deep Ocean Basin test campaign.

Environmental condition	Difference in spectral energy
JONSWAP2	5%
JONSWAP2 + A	4%
JONSWAP2 + B	2%
JONSWAP2 + C	1%

5.4) Wave Current Flume campaign

5.4.1) Current only

The test campaign in the WCF was conducted as a comparison study between physically applied current and emulated current with the SIL application, which is referred to as SIL current.

For the current-only cases the model is pulled against a fixed barrier upstream of the model before recording starts. While current is running the model is released and the surge motion of the model is allowed to decay and eventually settle at some distance from the start position.

Figure 75 shows the plotted surge motion with physical current (TC14) and SIL current (TC15) with current C. Although the decay oscillations are larger with physical current, the model settles at roughly the same surge distance with physical current and SIL current. Similar patterns were achieved with current A and current B. The period of the oscillations is slightly longer with SIL current; 1.03 times longer compared to physical current. The smaller oscillations show there is some surge damping of the model by the pulley system with SIL current, resulting in a slightly larger natural period of the surge DOF. Figure 75 also shows there are some small random oscillations after settling with physical current. These are caused by vortex shedding around the columns of the model. Vortex shedding is not simulated with SIL current.

Figure 76 shows the demanded tension and the measured tension in the winch wire for current C with SIL current. While the model is held at the start position the measured tension is around 11 N and demanded tension is 0 N. As the model is not moving, no tension is demanded. However, when the model is released and starts moving, demanded tension follows the same pattern as measured tension. Again, a small phase shift between demanded- and measured tension caused by the spring in the winch wire is apparent. When RE is applied to compare measured- vs demanded winch tension with SIL current an average value of 0.015 is found for the current-only test cases.

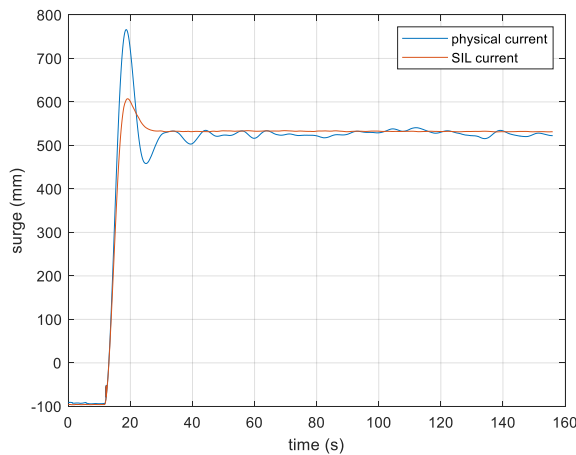


Figure 75. Surge motion of the FOWT model for TC 3 with physical- and SIL current.

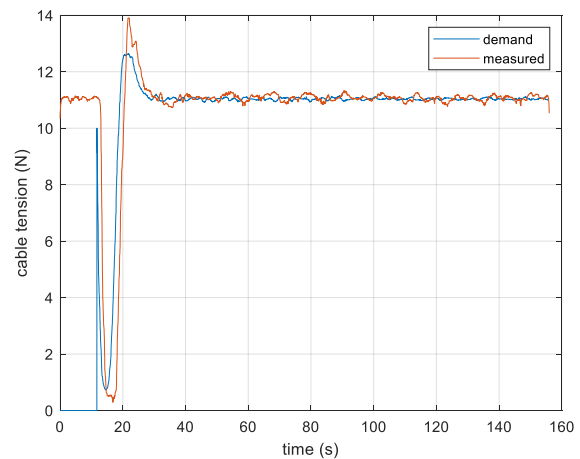


Figure 76. Demanded and measured tension in the winch wire for TC 3 with SIL current.

Figure 77 and Figure 78 show there is a large difference in sway motion of the FOWT model for the current-only cases with current C, indicating that SIL current does not capture vortex shedding. The difference in spectral energy for the sway DOF shown in Figure 78 is 39% larger for physical current compared to SIL current. In fact, the sway motion with SIL current is likely caused by a slight offset in the sway DOF at the start of the tests resulting in small decaying sway oscillations after release of the model. Without this offset the sway motion would likely be significantly smaller with SIL current. On the other hand, the sway oscillations are significantly larger with physical current compared to SIL current, and non-linear, as is typical with vortex shedding.

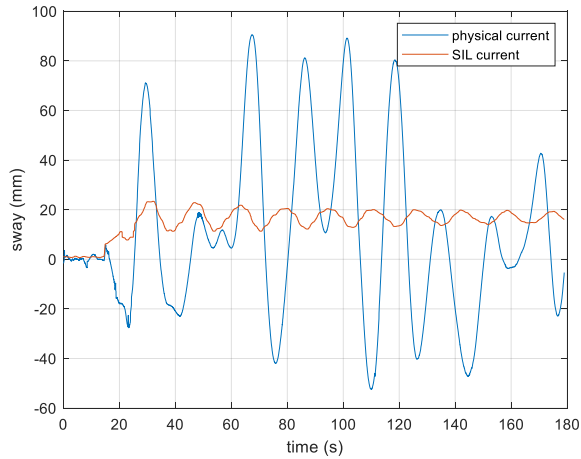


Figure 77. Sway motion of the FOWT model, TC14 vs TC15 with current C

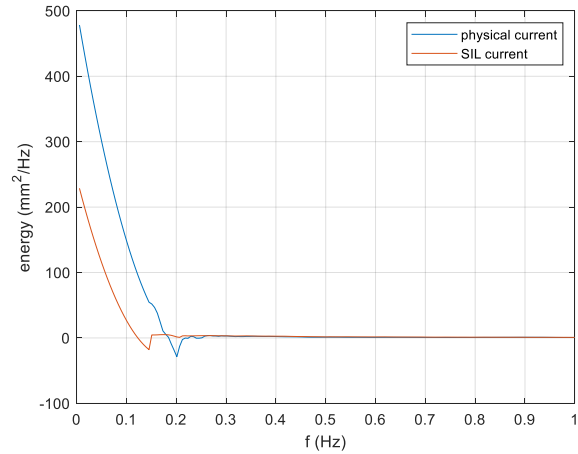


Figure 78. Spectral energy for the sway DOF of the FOWT model, TC14 vs TC15 with current C

Table 28 shows the validation metrics of the surge DOF of the FOWT model for the current-only test cases. There is little or no heave- and pitch motion during the current-only tests. The difference in mooring tensions between TC14 and TC15 is an important indicator whether the drag force on the FOWT platform is applied correctly with SIL current and are therefore included in the validation metrics. The average of the two upstream moorings is used to calculate RE for the mooring tensions.

Table 28. RE for current-only cases

Current	Surge	Mooring tension
Current A	0.020	0.017
Current B	0.023	0.016
Current C	0.004	0.017

5.4.2) Current and wind

For TC 16 and TC17 current is applied before recording and the start position of the model is the settled surged distance with current. Then, wind loads are applied with the MPA. During the current/wind tests there is only noticeable surge- and pitch motion of the FOWT model. Surge amplitudes are slightly larger with physical current for each test; however, pitch amplitudes are significantly larger around the natural frequency of the FOWT model with SIL current. Figure 79 and Figure 80 show the surge- and pitch spectral energy respectively with wind V1 and current A.

Validation metrics are shown in Table 29 for all the current/wind test cases.

Table 29. RE for current/wind test cases.

Current	Wind	Surge	Pitch	Mooring tension
Current A	V1	0.013	0.431	0.026
Current B	V1	0.156	0.142	0.068
Current C	V1	0.087	0.117	0.040

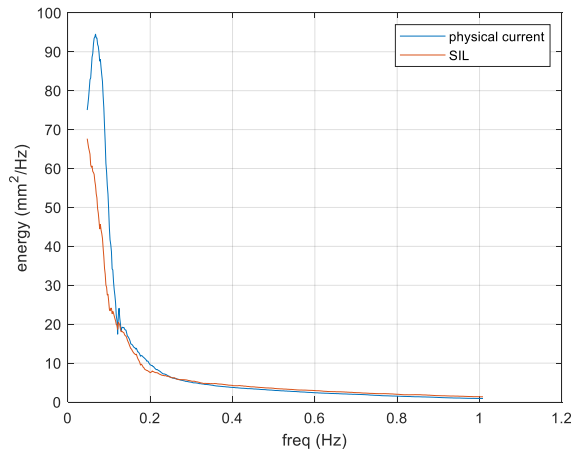


Figure 79. Spectral energy of the FOWT model in surge DOF with current A and wind V1

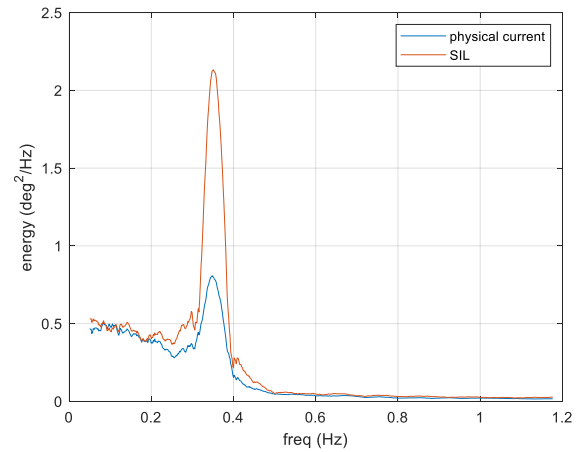


Figure 80. Spectral energy of the FOWT model in pitch DOF with current A and wind V1

5.4.3) Current, wind, and waves

For TC 18 and TC19 current is also applied before recording and the start position of the model is the settled surge distance with current. Then, wind loads are applied with the MPA, and the wave maker is started. During the WCF campaign the FOWT model was moored at 17 m from the wave maker, therefore the waves took several seconds to reach the model. To make sure current, wind and waves are all acting on the model, data from each experiment for TC 18 and TC19 between $t = 20$ seconds and $t = 600$ seconds were used for the calculation of RE. The validation metrics for the current/wind/wave cases are shown in Table 30. Figure 81 and Figure 82 show the surge- and heave spectral energy of the FOWT model under combined loads respectively. The figures show there is higher energy around the wave frequencies for surge with physical current, whereas for heave there is higher energy mainly around the natural frequency of the FOWT model with SIL current.

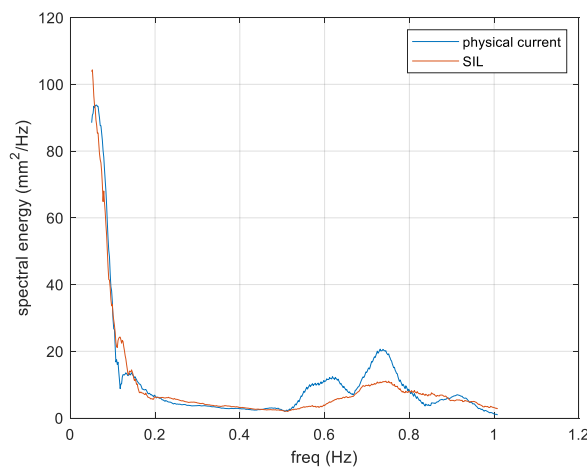


Figure 81. Spectral energy of the FOWT model in surge DOF with current A, wind V1, and JONSWAP1

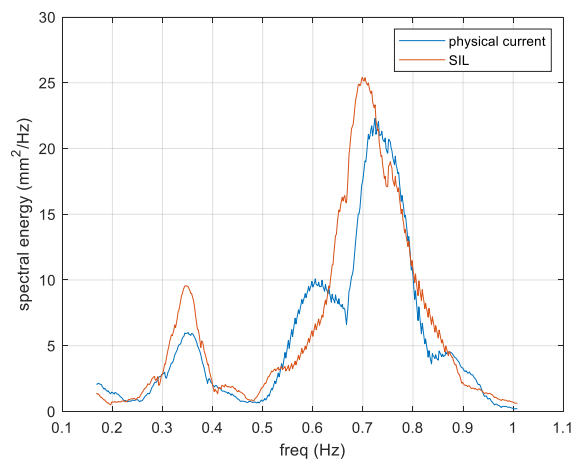


Figure 82. Spectral energy of the FOWT model in heave DOF with current A, wind V1, and JONSWAP1

Figure 83 and Figure 84 show the tension of the upstream moorings and spectral energy of said moorings respectively. The maximum amplitudes are slightly larger with SIL current, however, there is little difference in spectral energy between the two methods.

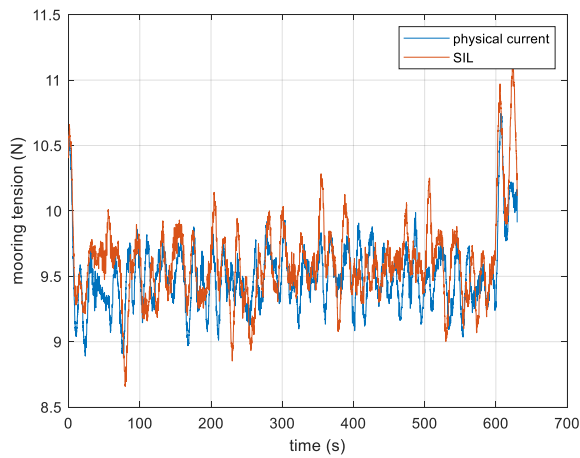


Figure 83. Upstream mooring tension with current A, wind V1, and JONSWAP1

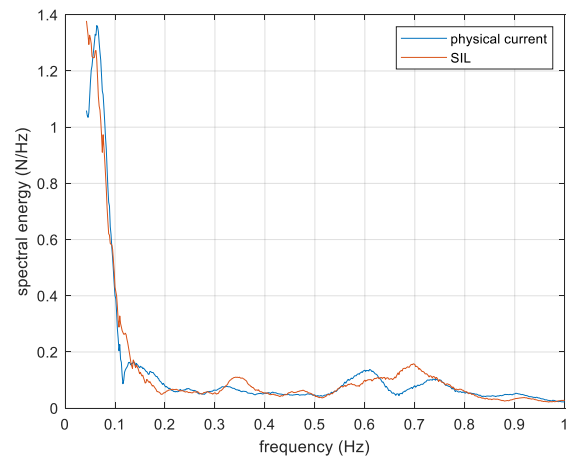


Figure 84. Spectral energy of upstream mooring tension with current A, wind V1, and JONSWAP1

Table 30. RE for current/wind/wave test cases

Current	Wind	Waves	Surge	Heave	Pitch	Mooring tension
Current A	V1	JONSWAP1	0.044	0.149	0.189	0.027
Current B	V1	JONSWAP1	0.080	0.101	0.162	0.027
Current C	V1	JONSWAP1	0.100	0.080	0.072	0.026

To check the validity of the simulated wave-current interaction, the measured spectra of waves with physical current were compared against measured spectra with SIL current. Initial results showed the energy of the spectra with SIL current was 15% less on average compared to spectra with physical current. A correction coefficient of 1.13 was added to equation (15) to increase spectral energy. Figure 85 shows the difference with- and without correction of the theoretical spectra.

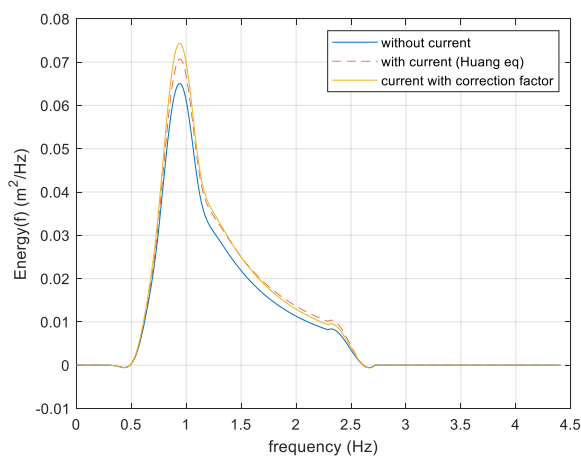


Figure 85. Theoretical wave spectra with- and without current.

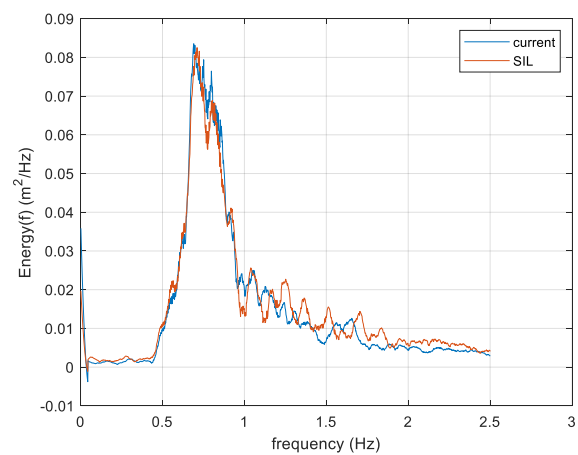


Figure 86. Measured spectra with physical current vs SIL current with current C

After applying the correction coefficient, the difference in spectral energy between waves with physical current and waves with SIL current was 3% on average. Figure 86 shows the measured spectra with current C for physical current and SIL current.

5.5) Discussion on the results with SIL current

The WCF campaign clearly showed that the response of the model with SIL current compares well to response of the model with physical current for all test conditions, with RE staying below 0.2 for most cases.

However, where the experimental results have been validated with results from numerical simulations poor validation metrics were achieved in some cases. For example, in the most severe sea states used during this body of work, during the DOB campaign, the motion response of the FOWT model is consistently underpredicted by AQWA compared to the experiments. During the OB campaign poor validation metrics were achieved for most cases in the heave- and pitch DOFs. The natural frequencies of the scale model in the heave- and pitch DOF, around 0.35 Hz, are excited during the experiments, possibly due to 2nd order effects, which aren't captured by the numerical models. The RAOs of the scale model are significantly larger around 0.35 Hz for heave and pitch compared to the original design of the INNWIND platform, meaning even small 2nd order loads will result in large responses in these DOFs. As these 2nd order loads aren't captured by the numerical models, they have a detrimental effect on the validation metrics.

Similarly, wave/wind cases during the OB campaign achieved poor validation metrics of the experiments compared to FAST. As the number of environmental loads is increased, the level of uncertainty increases, and accuracy drops. Particularly the addition of waves has a detrimental effect on the validation metrics for heave and pitch of the platform. This can be explained, again, by the additional resonance frequency of the platform in heave and pitch which is not captured by the numerical model. The poor comparison between numerical- and experimental results is also reflected by the RAOs of model. The RAOs found empirically for the scale model in Section 4.4 do not compare very well to the full-scale RAOs found with the numerical simulations in AQWA.

On the other hand, results and validation metrics show that emulating the current induced drag force with the winch actuator achieves validation metrics with an acceptable degree of accuracy for the surge DOF compared to numerical simulations for most cases of the OB campaign.

Clearly, fidelity of the validation metrics is dependent on the accuracy of the numerical model. Where RE is a direct comparison between experiments and numerical models, FMT is more ambiguous. The tolerance in FMT allows the user to estimate errors and uncertainty, and the level of confidence in the numerical model. However, this metric should be used cautiously; a number close to 1 may be achieved but depending on how wide the tolerance is the result may still be unfavourable. Therefore, both the RE and FMT metrics should be used to complement each other, RE for the direct comparison and FMT for uncertainty estimation. If both metrics are favourable, there is high confidence in the accuracy of the results.

The rather poor validation metrics for many of the OB- and DOB campaign experiments compared to numerical models, and the mostly excellent validation metrics for physical current experiments compared to SIL current experiments, would suggest poor accuracy of the numerical models in AQWA and FAST rather than under-performance of the SIL current.

As was shown in Figure 32 and Figure 75, a phase shift between demanded tension signal and measured tension signal exists due to the presence of a spring in the winch wire. The PI controller mitigates the phase shift, and although it is not able to eliminate it entirely, the phase shift is kept acceptably small. Protecting the winch from snap loads by keeping the spring in the wire was deemed more important than eliminating the phase shift.

Figure 45 and 46 showed that there is a lag in surge between the experimental signals and numerical signals for the current-only cases of the OB campaign. Unexpectedly, the numerical results are lagging the experimental results. It is possible that, despite the phase shift between demanded tension and measured tension caused by the spring, the PI controller is controlling the winch too aggressively, resulting in higher surge stiffness of the model during experiments. However, the current-only cases of the WCF campaign showed a phase shift between the surge signals of physical current and SIL current, with the SIL current signal lagging the physical current signal. The phase shift between physical current and SIL current is as expected.

Promising results were achieved for platform surge with SIL current for all test cases during the WCF campaign, the large blockage ratio of the model in the flume does not affect results, with $RE \leq 0.15$ for all cases. This suggests that the values of C_D in equation (19) are correct.

Repeatability was found to be good with SIL current, although it reduced when all three environmental loads were combined. Repeatability is less favourable with physical current. As an example, the Pearson correlation coefficient, i.e., how close do all the repeated experiments match each other, for surge response of the FOWT model for the repeated experiments of TC14 & TC15, and TC18 & TC19 is given in Table 31, where the first experiment is the reference.

Table 31. Pearson Correlation Coefficient of surge response for TC14 & TC15, and TC18 & TC19.

	Experiment 1	Experiment 2	Experiment 3
TC14, physical current	1	0.9963	0.9940
TC15, SIL current	1	1	0.9999
TC18, physical current	1	0.8968	0.6487
TC19, SIL current	1	0.9848	0.8610

An important reason to simulate current with FOWT experiments is to examine the effect on mooring tensions, which may influence fatigue life and structural integrity of the platform. Although they have not been evaluated for the OB or DOB campaign, good results were achieved for mooring tensions during the WCF campaign; RE is lower than 0.07 for all test conditions, i.e., there is less than 7% difference in tension on average on the moorings between SIL current and physical current for all the simulations of the WCF campaign.

Another important reason for current simulation is the alteration of wave shapes due to wave-current interaction and the effect this may have on platform heave and pitch, and hence on accelerations acting on the turbine. Heave- and pitch RE remains below 0.2 for all test cases with waves of the WCF campaign. This suggests that the method to simulate wave-current interactions with the adjusted wave spectra is adequate. The exception is pitch motion with wind and current of 0.11 m/s (TC17), with $RE = 0.431$. The pitch natural frequency of the FOWT model is around 0.35 Hz and for all test cases with wind the spectral energy of pitch is higher around this frequency with SIL current compared to physical current, possibly due to the moment created by the connection of the winch cable and the centre of thrust of the MPA during SIL current experiments.

The comparison of experimental results from the OB campaign has shown there is some damping of surge motions of the FOWT model during wind/current cases compared to wind-only cases, which is not captured by FAST. There is also some damping of surge motion during wave/wind/current cases compared to wave/wind cases due to current. Of course, the direction of the current was opposite to the direction of the waves for all cases during this project. It is likely, therefore, that if the current direction is following the wave direction there will be increased surge motions of the FOWT model. This has implications for the unsteady aerodynamics of FOWTs. It means the dynamic inflow will change with the addition of current to environmental loads, regardless of the direction of the current, unless it is

perpendicular to wave- and wind direction in which case interactions will be minimal. Either way, it is another reason why current should not be neglected during FOWT simulations and experiments.

Eventually, the SIL current method will be used with catenary- or truncated moorings on FOWT models rather than the soft mooring system used for this study. The soft mooring system was used to keep the SIL current method as robust and simple as possible. It allows the current to be assumed as uniform and ignores the vertical shear profile of the water column and hydrodynamic loading on the moorings. With catenary- or truncated moorings fixed to the bottom of the basin, shear profile and hydrodynamic loading of current can no longer be ignored and will have to be accounted for in the real-time numerical simulation. The hydrodynamic loading on the moorings of currents is likely small compared to the loading on the platform. However, with increased (simulated) water depth and current velocity the hydrodynamic loading on the moorings will likely increase and with it the response of the platform. If the contribution of the hydrodynamic loading on the moorings is significant, it will need to be added to the loading on the platform found with equation (19) during the real-time simulation.

A limitation of SIL current is that vortex shedding is not captured. Regardless, the results show that SIL current can reliably emulate current loads on the FOWT model in combination with wind and waves. The advantage of this method is that it can be used in any wave basin without the need for bulky and expensive equipment to generate physical current for a range of test conditions. Furthermore, creating a realistic boundary layer with low turbulent flow, while also limiting wave reflection in the basin when applying physical current, is challenging. These challenges can be eliminated by using SIL current.

5.6) Discussion on the results with the MPA and aerodynamics

As with SIL current, the results for simulating wind loads are a miscellany of poor and good results. The validation process showed that the MPA is a suitable actuator to emulate aerodynamic thrust- and torque loads. The rates of change of the propellers are high enough for the MPA to emulate the aerodynamic loads within the required frequency range at model scale.

However, the device underperforms when emulating yaw moments in either the horizontal- or vertical configuration of the MPA. Rotor torque is a moment which always acts in the same rotational direction. Although rotor torque is an irregular load, it is relatively straightforward to replicate with the MPA. In contrast, aerodynamic yaw is a moment of which the rotation changes direction in cycles, while simultaneously being irregular, making it challenging to replicate with the MPA. The excessive high-frequency vibrations when the propellers operate at high rotational speeds exacerbate the problems, made worse when the propeller pairs are operated intermittently to change the direction of the moment acting in the yaw DOF. There is marginal improvement with the MPA in the vertical configuration in terms of time lag. The counter-rotating propellers are better able to keep pace with the low-frequency fluctuations, although it is still unable to replicate the amplitudes of aerodynamic yaw accurately. Figure 43 and Figure 44 also show that the MPA in the vertical configuration is not able to accurately capture the high-frequency loads, where even the influence of the 1P frequency on aerodynamic yaw cannot be replicated accurately. Again, the high-frequency vibrations of the device are suspected to have a large influence on these results.

Structural stiffness of the device and vibration damping of the propellers will have to be improved to reduce the vibrations. However, the stiffness will be a trade-off between weight and strength; increasing the stiffness will increase the weight of the device, meaning the mass envelope could be exceeded on models with small scales. Some attempts at increasing stiffness and vibration damping have been made during this project, however, these have not resulted in any improvement. Another potential improvement of the device would be the use of bi-directional propellers rather than two pairs of counter-rotating propellers. That would reduce the weight of the MPA, however, the efficiency of the propeller blades is not equal in both directions, creating an imbalance. Bi-directional propellers have not been used during this body work.

To calculate the validation metric RE for actuation with the MPA, PSD was chosen, rather than using the measured and numerical values directly for equations (26). The high frequency vibrations generated by the MPA are likely to have limited effect on the motion response of the platform of the FOWT model it will be used on. The high frequencies form only a small part of the total spectral energy of the actuator outputs and some of the high frequency signal can be attributed to sensor noise. Therefore, using PSD will give a better representation of how the platform reacts to the MPA and is considered more appropriate to calculate the validation metrics for actuation. Energy density rather than power density was used to calculate RE of the response of the model to actuation with the MPA. For the calculation of RE, it does not make much of a difference, however, the graphic comparison of the energy spectra tends to be clearer than the power spectra for the response of the FOWT model. For the calculation of FMT measured and numerical values are used directly for equation (27), rather than spectral energy.

The number of aerodynamic loads to be emulated simultaneously will depend on the type of FOWT model and its sensitivity to each load. The aim of the design of the MPA was to emulate as many loads as possible and so make it suitable for any type of FOWT model. However, for hybrid testing of TLP models, with their strong structural coupling between tower and moorings, the MPA in its current configuration is most likely not the best type of actuator. Semisubmersible FOWTs in contrast, are not as sensitive to tower/mooring coupling, nor is platform response to aerodynamic yaw very high. For example, with the INNWIND semisubmersible FOWT model the maximum yaw amplitude in response to the actuation of TC4 was 13 degrees with a 16 s period at scale. Such slow rotations and relatively small amplitudes are unlikely to cause harmful accelerations on the nacelle or cause problems for yaw control, nor would they be likely to cause harmful tensions in the moorings.

In its current configuration a lot of effort is expended by the MPA to cause only small yaw responses of the platform, and this at poor accuracy. However, when tower structural dynamics are a quantity of interest during testing, accurate emulation of aerodynamic yaw and pitch are important. Clearly, the MPA is not a suitable actuator for such loadings. Instead, a system with multiple winch actuators such as is used by SINTEF [77] would be better suited.

On the other hand, good results for emulation of rotor thrust and torque have been achieved with the MPA, therefore, if only platform response is of interest a simpler actuator like the MPA would be better suited. It is important, however, to investigate the sensitivity of the FOWT to aerodynamic loads numerically prior to each testing campaign to decide on the suitability of the actuator.

Of course, a thorough sensitivity study requires accurate numerical models, and as the results from the OB- and DOB campaigns have shown the numerical models used for this thesis are lacking in accuracy. Unfortunately, there was no opportunity for a comparison study of the MPA with a full physical scale model of the NREL 5 MW, which could have provided an additional validation of the accuracy of response of the platform to aerodynamic loads with the MPA. A future comparison study of the MPA with a physical wind turbine scale model is desirable.

A comparison study between a scale model turbine and the MPA was planned to be conducted at the Coast Laboratory at the University of Plymouth. The presence of a 1/50 scale model of the NREL 5 MW turbine at the Coast Laboratory was the main motivation to choose this turbine as it means there was no need to manufacture a new model of a turbine. It did, however, dictate the scale of the platform, which also needed to be 1/50. Unfortunately, the planned comparison study could not go ahead due to technical issues with the wind generator at the Coast Laboratory.

The numerical model of the NREL 5 MW turbine on FOWTs in FAST has been extensively validated, both experimentally and with other numerical codes, e.g. [49], [107]. Therefore, the confidence in the accuracy of the emulation of rotor thrust and torque loads with the MPA is high. For any of the numerical modelling of the FOWT model with FAST this means it is most likely the hydrodynamic model of the platform that is inaccurate rather than the aerodynamic model. The DOB campaign showed

the hydrodynamic model in AQWA also lacks the required accuracy. As the hydrodynamic coefficients found with AQWA are imported into FAST, it is likely that the inaccuracy has spilled over into FAST from AQWA. For example, pitch motion of the model for the wind-only test case is significantly underpredicted by FAST compared to the experimental results. Again, this is most likely due to an inaccurate numerical hydrodynamic model of the platform rather than any inaccuracies of the aerodynamic model.

As the results of wind-only cases of the OB campaign showed, using the MPA with closed-loop control strategy as opposed to open-loop control, achieved the best results for RE of platform response. The experimental spectral energy of the response of the FOWT model to actuation with the MPA is comparable to the spectral energy found with the FAST simulations. This is valid for the surge DOF for most cases, but only for some cases with the pitch DOF. On the other hand, the results for FMT with the closed-loop control strategy are rather poor. Although amplitudes and frequencies of the response of the FOWT model are similar to the numerical simulations, they do not follow the same pattern, as can be seen in Figure 48, for example.

With the open-loop control strategy for the MPA the results for RE are also rather poor and slightly more favourable for FMT for the wind-only cases. Although the pattern of surge- and pitch response of the FOWT model is followed better than with closed-loop control, the amplitudes are significantly smaller. As there is no real-time feedback with the open-loop control, there is no adaptation to the environmental conditions.

To improve the accuracy of actuation with the MPA, the algorithm in Simulink for closed-loop control could be linked with OpenFAST through the XIL API protocols. Rather than calculating rotor thrust with equation (17) and the look-up tables for thrust coefficients, OpenFAST would calculate the rotor thrust and torque in real-time. This method would also use feedback from the motion-tracking system, and translate rotor thrust and torque into control signals for the MPA. The advantage of this method would be the accurate replication of the simulated turbine control in real-time, and therefore rotor thrust and torque emulation with higher accuracy compared to the method that is currently used to control the MPA.

Another approach that could be used to improve MPA accuracy is to build the turbine controller in Simulink in combination with equation (17) to calculate rotor thrust. An advantage of this method, besides improved accuracy, is that it would be relatively easy to adjust wind turbine control and experiment with different turbine control strategies. However, for best accuracy this method will need look-up tables with the full set of thrust coefficients for each blade pitch angle. Furthermore, the Simulink algorithm will be significantly more extensive compared to the Simulink algorithm that is currently used to control the MPA. That means a more powerful real-time controller with higher processing power than the ds1104 would be required.

Structurally, the MPA could be improved by using carbon fibre for the frame. Its lower weight compared to aluminium, yet high stiffness makes it a suitable material to improve the structural stiffness of the MPA.

Chapter 6

Conclusion and future recommended work

This chapter provides the main conclusions of this work and some recommendations for future work.

6.1) Conclusion

In the drive for realistic offshore test-conditions in laboratory wave basins, hybrid simulation methods to simulate wind- and current loads have been developed for this thesis. Due to its strong coupling between aerodynamics and hydrodynamics the FOWT was regarded as the ideal candidate to test these simulation methods in the laboratory. A 1/50 scale model of the INNWIND semisubmersible FOWT with the NREL 5 MW turbine were used for all the experimental work during this body of work.

To simulate the aerodynamic loads acting on the wind turbine of the FOWT an MPA with six propellers was developed. To simulate the hydrodynamic loads of sea currents on the platform of the FOWT a system with a dynamic winch actuator was developed. Two validation metrics, RE and FMT, were also developed for this thesis. A perfect performance of the actuators would result in $RE = 0$, and $FMT = 1$, with $a = b = 1$.

The main findings of this thesis are:

- The MPA has shown it can accurately emulate rotor thrust and rotor torque of the NREL 5 MW turbine at scale, this was one of the main findings in [16]. Only small differences between the validation metrics were found when operating the MPA with open-loop control or closed-loop control for the actuation only test cases.
- For other aerodynamic loads than rotor thrust, or rotor torque the MPA was not able to emulate accurately, regardless of the configuration of the MPA. This was another finding in [16]. Using the propellers at high rotational speeds results in high-frequency vibrations on the MPA. This effect is exaggerated when several propellers are operated simultaneously, and even more so when pairs of propellers are operated intermittently. Not only has this resulted in poor performance compared to thrust and torque when attempting to emulate aerodynamic yaw, potentially it also masks any high-frequency aerodynamic loads which are being emulated.
- If thrust and torque are the only aerodynamic loads required for emulation, then simple on-board propeller actuators such as the MPA are suitable for FOWT scale model testing in wave basins. However, if aerodynamic pitch and yaw are also required a more complex test setup with several winch actuators is the more suitable option. This was an important finding in the literature review of [15].
- The winch actuator is not required to emulate anything as complex as the aerodynamic loads. It showed it can accurately emulate the drag force of current on the FOWT platform, as was found in [17], and [18]. The demanded tension in the winch wire compared closely to the measured tension of the winch wire for the actuation-only test case.
- For the wind-only cases close matching results were achieved for the surge DOF of the model with closed-loop control of the MPA, whereas for the pitch DOF the results were matching less closely in some cases. With open-loop control the RE metrics for response of the model are less favourable compared to closed-loop control.
- Close matching results were achieved for surge response of the current-only cases, both with SIL current compared to the numerical models as was found in [17], as well as SIL current

compared to physical current as was found in [18]. In general, the validation metrics for the response of the FOWT model become less favourable, compared to current only, as more environmental loads, and therefore more errors, are introduced to the tests.

- Fidelity of the validation metrics is dependent on the accuracy of the numerical model. Confidence in the numerical model of the NREL 5 MW wind turbine is high, meaning most of the less favourable validation metrics are likely due to an inaccurate hydrodynamic model of the FOWT platform in AQWA and FAST.
- Close matching results were found with the comparison study in the WCF, where SIL current was compared to physical current. A significant gap in the literature is filled with this finding in [18]. The effect of current loading is mostly neglected with scale model tests of FOWTs. With SIL current a reliable method is now available to study these effects on the behaviour of FOWTs.
- Mooring tensions have only been evaluated during the WCF campaign, which was discussed in [18]. The average of the two upstream moorings was compared between the experiments with physical current and SIL current. Mooring tensions matched closely for all test cases of the comparison study.
- The mostly close matching results for the heave- and pitch DOFs during the WCF campaign also show that the method to simulate wave-current interactions with the SIL current tests is adequate, another finding of [18]. To simulate wave-current interactions wave spectra were converted to have the equivalent amount of energy as if a current is present.

Validating numerical models of FOWT designs with results from scaled experiments is common practice. Results throughout this body of work have only confirmed that this is good practice; fidelity of numerical models is not at a level where scaled experiments can be skipped as part of the design process. And, while hybrid test methods are more versatile and cheaper than full physical test methods, the comparison study of physical current vs SIL current has shown that the full physical method is a useful tool to validate hybrid test methods and should therefore not be dismissed as a modelling tool for FOWTs.

Overall, the results throughout this body of work have shown that the MPA can reliably emulate rotor thrust and rotor torque of a wind turbine and the winch actuator can reliably emulate the hydrodynamic loads of a current on the FOWT platform. The resulting motion response of the scale model FOWT to the emulation of said aerodynamic- and hydrodynamic loads have shown an acceptable degree of accuracy. As such, both systems can contribute to creating realistic offshore conditions at scale in laboratory wave basins.

6.2) Future recommended work

The findings in this thesis have highlighted some areas for improvement of SIL current and the MPA, which are mentioned here. Suggestions to improve the SIL current system include:

- Expanding the PI controller for the winch tension into a PID controller.
- Expanding the control algorithm to dynamically alter the wetted cross-section of the platform, A , in equation (19) during testing.
- Expansion of the test setup with two or more winches, so that current can be simulated in more than one direction. In addition, an Artificial Neural Network, trained by offline CFD

simulations, could be used to approximate vortex shedding effects during the experiments if the system has at least three winches.

- Inclusion of the hydrodynamic loading on moorings in the algorithm for the drag force from currents in the real-time numerical simulation.

Suggestions to improve the accuracy of actuation with the MPA includes:

- Either using FAST as the real-time numerical simulation or expanding the existing algorithm to better simulate wind turbine control.
- Improve the structure of the frame for the MPA.

Bibliography:

- [1] European Commission, “Offshore wind and ocean energy.” https://energy.ec.europa.eu/topics/renewable-energy/offshore-wind-and-ocean-energy_en (accessed Aug. 29, 2022).
- [2] European Commission, “2030 Climate Target Plan.” https://ec.europa.eu/clima/eu-action/european-green-deal/2030-climate-target-plan_en (accessed Feb. 24, 2022).
- [3] Wind Europe, “Offshore wind energy | WindEurope.” <https://windeurope.org/policy/topics/offshore-wind-energy/> (accessed Aug. 29, 2022).
- [4] Carbon Trust, “Floating Offshore Wind: Market and Technology Review,” 2015.
- [5] Wind Energy Ireland, “Revolution, A vision for Irish floating wind energy,” 2021. Accessed: Mar. 01, 2022. [Online]. Available: <https://windenergyireland.com/images/files/revolution-final-report-july-2021-revised.pdf>.
- [6] Wind Europe, “Floating offshore wind energy, a policy blueprint for Europe,” 2017.
- [7] Offshorewind.biz, “Floating Wind LCOE to Drop Below USD 40/MWh by 2050, Installed Capacity to Reach 264 GW | Offshore Wind.” <https://www.offshorewind.biz/2022/02/17/floating-wind-lcoe-to-drop-below-usd-40-mwh-by-2050-installed-capacity-to-reach-264-gw/> (accessed Mar. 01, 2022).
- [8] Offshorewind.biz, “World’s First Floating Wind Farm Best Performer in UK | Offshore Wind.” <https://www.offshorewind.biz/2021/03/23/worlds-first-floating-wind-farm-best-performer-in-uk/> (accessed Mar. 01, 2022).
- [9] International Towing Tank Conference, “Guide to the Expression of Uncertainty in Experimental Hydrodynamics, 7.5-02-01-01,” 2014.
- [10] C. Cermelli, C. Leroux, S. Diaz Dominguez, and A. Peiffer, “Experimental measurements of WindFloat 1 prototype responses and comparison with numerical model,” in *Proceedings of the ASME 2018 37th International Conference on Ocean, Offshore and Arctic Engineering OMAE2018*, 2018, no. OMAE2018-77057, pp. 1–10.
- [11] E.-J. de Ridder, W. Otto, G.-J. Zondervan, F. Huijs, and G. Vaz, “Development of a Scaled-Down Floating Wind Turbine for Offshore Basin Testing,” *Proc. ASME 2014 33rd Int. Conf. Ocean. Offshore Arct. Eng.*, pp. 1–11, 2014.
- [12] A. Robinson, D. Ingram, I. Bryden, and T. Bruce, “The effect of inlet design on the flow within a combined waves and current flumes, test tank and basins,” *Coast. Eng.*, vol. 95, pp. 117–129, Jan. 2015, doi: 10.1016/J.COASTALENG.2014.10.004.
- [13] J. M. Jonkman, S. Butterfield, W. Musial, and G. Scott, “Definition of a 5-MW reference wind turbine for offshore system development,” 2009. doi: 10.1115/1.4038580.
- [14] F. Sandner *et al.*, “INNWind.EU Deliverable D4.3.3 - Innovative Concepts for Floating Structures,” 2015.
- [15] A. Otter, J. Murphy, V. Pakrashi, A. Robertson, and C. Desmond, “A review of modelling techniques for floating offshore wind turbines,” *Wind Energy*, 2021, doi: 10.1002/we.2701.
- [16] A. Otter, J. Murphy, and C. J. Desmond, “Emulating aerodynamic forces and moments for hybrid testing of floating wind turbine models,” in *Journal of Physics: Conference Series*, 2020, doi: 10.1088/1742-6596/1618/3/032022.
- [17] A. Otter, B. Flannery, J. Murphy, and C. Desmond, “Current simulation with Software in the Loop for floating offshore wind turbines,” *J. Phys. Conf. Ser.*, vol. 2265, no. 4, p. 042028,

- May 2022, doi: 10.1088/1742-6596/2265/4/042028.
- [18] A. Otter, C. J. Desmond, B. Flannery, and J. Murphy, “Combined current and wind simulation for floating offshore wind turbines,” *Accept. J. Phys. Conf. Ser.*, 2022.
 - [19] The Economist, “Floating wind turbines could rise to great heights | The Economist,” 2021. <https://www.economist.com/science-and-technology/2021/07/21/floating-wind-turbines-could-rise-to-great-heights> (accessed Sep. 01, 2022).
 - [20] J. Journee and W. Massie, *Offshore hydromechanics*. Delft University of Technology, 2001.
 - [21] N. D. P. Barltrop, *Floating Structures: A Guide For Design And Analysis Vol 1*. Ledbury: Oilfield Publications Limited, 1988.
 - [22] B. Skaare, F. G. Nielsen, and T. D. Hanson, “Integrated dynamic analysis of floating offshore wind turbines,” *Eur. Wind Energy Conf. Exhib. 2006, EWEC 2006*, vol. 3, no. January 2016, pp. 1834–1842, 2006.
 - [23] Blue H Engineering, “Historical development.” <http://www.bluehengineering.com/historical-development.html> (accessed Mar. 02, 2022).
 - [24] F. Borisade, T. Choisnet, and P. W. Cheng, “Design study and full scale MBS-CFD simulation of the IDEOL floating offshore wind turbine foundation,” *J. Phys. Conf. Ser.*, vol. 753, no. 9, p. 092002, Sep. 2016, doi: 10.1088/1742-6596/753/9/092002.
 - [25] O. M. Faltinsen, *Sea loads on ships and offshore structures*. Cambridge University Press, 1990.
 - [26] M. H. Christian Bak, Frederik Zahle, Robert Bitsche, Taeseong Kim, Anders Yde, Lars C. Henriksen, Anand Natarajan, “DTU Wind Energy Report-I-0092,” 2013.
 - [27] A. Robertson *et al.*, “Definition of the Semisubmersible Floating System for Phase II of OC4,” 2014. Accessed: Apr. 07, 2022. [Online]. Available: www.nrel.gov/publications.
 - [28] C. van der Ham, C. Korevaar, W. Moens, and P. Stijman, *Meteorologie & Oceanografie voor de zeevaart*, 1998th ed. Haarlem, The Netherlands: Uitgeverij Holandia BV, 1983.
 - [29] N. D. Kelley and B. J. Jonkman, “Overview of the TurbSim Stochastic Inflow Turbulence Simulator: Version 1.21 (Revised February 1, 2007),” 2007. Accessed: Apr. 15, 2022. [Online]. Available: <http://www.osti.gov/bridge>.
 - [30] J. F. Manwell, J. G. McGowan, and A. L. Rogers, *Wind Energy Explained. Theory, Design and Application*. John Wiley & Sons Ltd. Chichester, United Kingdom, 2009.
 - [31] US Army Corps of Engineers, *Coastal Engineering Manual - Part 2*, EM 1110-2-. 2002.
 - [32] DNV-GL, “Coupled analysis of floating wind turbines - Recommended Practice, DNVGL-RP-0286.” 2019.
 - [33] Hasselmann *et al.*, “Measurements of wind-wave growth and swell decay during the Joint North Sea Wave Project (JONSWAP),” Hamburg, 1973.
 - [34] International Towing Tank Conference, “Recommended Procedures and Guidelines - Seakeeping Experiments, 7.5-02-07-02.1,” 2017.
 - [35] T. S. Hedges, “Some effects of currents on wave spectra,” in *1st Indian Conference on Ocean Engineering*, IIT Madras, 1981.
 - [36] S. Draycott *et al.*, “Re-creation of site-specific multi-directional waves with non-collinear current,” *Ocean Eng.*, vol. 152, pp. 391–403, Mar. 2018, doi: 10.1016/J.OCEANENG.2017.10.047.

- [37] N. E. Huang, D. T. Chen, C.-C. Tung, and J. R. Smith, "Interactions between Steady Non-Uniform Currents and Gravity Waves with Applications for Current Measurements," *J. Phys. Oceanogr.*, vol. 2, no. 4, pp. 420–431, 1972, doi: 10.1175/1520-0485(1972)002<0420:ibswuc>2.0.co;2.
- [38] S. Steen, *Experimental methods in marine hydrodynamics: statistical analysis*, no. August. Faculty of Engineering Science and Technology, NTNU Trondheim, 2014.
- [39] G. R. Tomasicchio *et al.*, "Experimental modelling of the dynamic behaviour of a spar buoy wind turbine," *Renew. Energy*, vol. 127, pp. 412–432, 2018, doi: 10.1016/j.renene.2018.04.061.
- [40] D. Roddier, C. Cermelli, A. Aubault, and A. Weinstein, "WindFloat: A floating foundation for offshore wind turbines," *J. Renew. Sustain. Energy*, vol. 2, no. 3, pp. 1–35, 2010, doi: 10.1063/1.3435339.
- [41] C. Wright, C. Desmond, and K. Lynch, "MARINET Report on Physical Modelling Methods for Floating Wind Turbines," 2015.
- [42] H. R. Martin, R. W. Kimball, A. M. Viselli, and A. J. Goupee, "Methodology for wind/wave basin testing of floating offshore wind turbines," *J. Offshore Mech. Arct. Eng.*, vol. 136, no. 2, pp. 1–9, 2014, doi: 10.1115/1.4025030.
- [43] A. Pegalajar-Jurado *et al.*, "Experimental and numerical study of a 10MW TLP wind turbine in waves and wind," *J. Phys. Conf. Ser.*, vol. 753, no. 9, p. 092007, Sep. 2016, doi: 10.1088/1742-6596/753/9/092007.
- [44] I. Bayati, M. Belloli, L. Bernini, R. Mikkelsen, and A. Zasso, "On the aero-elastic design of the DTU 10MW wind turbine blade for the LIFES50+ wind tunnel scale model," *J. Phys. Conf. Ser.*, vol. 753, no. 2, 2016, doi: 10.1088/1742-6596/753/2/022028.
- [45] M. Fowler, R. Kimball, D. A. T. Iii, and A. Goupee, "Wave basin model tests of floating offshore wind turbines," *Proc. ASME 32nd Int. Conf. Ocean. Offshore Arct. Eng.*, pp. 1–11, 2013, doi: 10.1115/OMAE2013-10122.
- [46] S. M. Mortensen, K. Laugesen, J. K. Jensen, K. Jessen, and M. Soltani, "Experimental Verification of the Hydro-Elastic Model of a Scaled Floating Offshore Wind Turbine," *2018 IEEE Conf. Control Technol. Appl. CCTA 2018*, pp. 1623–1630, 2018, doi: 10.1109/CCTA.2018.8511565.
- [47] S. Bahramiasl, M. Abbaspour, and M. Karimirad, "Experimental study on gyroscopic effect of rotating rotor and wind heading angle on floating wind turbine responses," *Int. J. Environ. Sci. Technol.*, vol. 15, no. 12, pp. 2531–2544, 2018, doi: 10.1007/s13762-017-1519-4.
- [48] L. Li, Y. Gao, Z. Hu, Z. Yuan, S. Day, and H. Li, "Model test research of a semisubmersible floating wind turbine with an improved deficient thrust force correction approach," *Renew. Energy*, vol. 119, pp. 95–105, 2018, doi: 10.1016/j.renene.2017.12.019.
- [49] A. N. Robertson *et al.*, "Summary of conclusions and recommendations drawn from the deepwind scaled floating offshore wind system test campaign," in *Proceedings of the International Conference on Offshore Mechanics and Arctic Engineering - OMAE*, 2013, doi: 10.1115/OMAE2013-10817.
- [50] A. J. Goupee, B. J. Koo, R. W. Kimball, K. F. Lambrakos, and H. J. Dagher, "Experimental comparison of three floating wind turbine concepts," *J. Offshore Mech. Arct. Eng.*, vol. 136, no. 2, pp. 1–9, 2014, doi: 10.1115/1.4025804.
- [51] H. Bredmose *et al.*, "The Triple Spar campaign: Model tests of a 10MW floating wind turbine with waves, wind and pitch control," *Energy Procedia*, vol. 137, pp. 58–76, 2017, doi: 10.1016/j.egypro.2017.10.334.

- [52] F. J. Madsen *et al.*, “Experimental analysis of the scaled DTU10MW TLP floating wind turbine with different control strategies,” *Renew. Energy*, vol. 155, pp. 330–346, 2020, doi: 10.1016/j.renene.2020.03.145.
- [53] F. Borisade, C. Koch, F. Lemmer, P. W. Cheng, F. Campagnolo, and D. Matha, “Validation of innwind.Eu scaled model tests of a semisubmersible floating wind turbine,” *Int. J. Offshore Polar Eng.*, vol. 28, no. 1, pp. 54–64, 2018, doi: 10.17736/ijope.2018.fv04.
- [54] H. Ahn and H. Shin, “Experimental and Numerical Analysis of a 10 MW Floating Offshore Wind Turbine in Regular Waves,” *Energies*, vol. 13, no. 2608, pp. 1–17, 2020, doi: 10.3390/en13102608.
- [55] J. C. Ward, M. J. Fowler, A. M. Viselli, A. J. Goupee, and H. J. Dagher, “Design and validation of a multi-scale model floating offshore test wind turbine,” *ASME 2018 1st Int. Offshore Wind Tech. Conf. IOWTC 2018*, pp. 1–10, 2018, doi: 10.1115/IOWTC2018-1084.
- [56] A. Connolly, M. Guyot, M. Le Boulluec, L. Hery, and A. O’Connor, “Fully coupled aero-hydro-structural simulation of new floating wind turbine concept,” in *Proceedings of the ASME 2018 1st International Offshore Wind Technical Conference IOWTC2018*, 2018, vol. IOWTC2018-, pp. 1–11.
- [57] Y. sheng Zhao, X. he She, Y. ping He, J. min Yang, T. Peng, and Y. feng Kou, “Experimental Study on New Multi-Column Tension-Leg-Type Floating Wind Turbine,” *China Ocean Eng.*, vol. 32, no. 2, pp. 123–131, 2018, doi: 10.1007/s13344-018-0014-0.
- [58] J. Azcona *et al.*, “Aerodynamic thrust modelling in wave tank tests of offshore floating wind turbines using a ducted fan,” *J. Phys. Conf. Ser.*, vol. 524, no. 1, 2014, doi: 10.1088/1742-6596/524/1/012089.
- [59] J. Azcona, F. Bouchotrouch, and F. Vittori, “Low-frequency dynamics of a floating wind turbine in wave tank–scaled experiments with SiL hybrid method,” *Wind Energy*, vol. 22, no. 10, pp. 1402–1413, 2019, doi: 10.1002/we.2377.
- [60] F. Vittori, F. Lemmer, F. Bouchotrouch, and J. Azcona, “Hybrid scaled testing of a 5 MW floating wind turbine using the SIL method compared with numerical models,” in *Proceedings of the ASME 2018 37th International Conference on Ocean, Offshore and Arctic Engineering OMAE2018*, 2018, pp. 1–8.
- [61] C. Wright, K. O’Sullivan, J. Murphy, and V. Pakrashi, “Experimental comparison of dynamic responses of a tension moored floating wind turbine platform with and without spring dampers,” *J. Phys. Conf. Ser.*, vol. 628, no. 1, 2015, doi: 10.1088/1742-6596/628/1/012056.
- [62] C. J. Desmond, J. C. Hinrichs, and J. Murphy, “Uncertainty in the Physical Testing of Floating Wind Energy Platforms’ Accuracy versus Precision,” *Energies*, vol. 12, no. 3, pp. 1–14, 2019, doi: 10.3390/en12030435.
- [63] E. Oguz *et al.*, “Experimental and numerical analysis of a TLP floating offshore wind turbine,” *Ocean Eng.*, vol. 147, pp. 591–605, 2018, doi: 10.1016/j.oceaneng.2017.10.052.
- [64] M. T. Andersen, “Floating Foundations for Offshore Wind Turbines,” Aalborg University, 2016.
- [65] C. Matoug, B. Augier, B. Paillard, G. Maurice, C. Sicot, and S. Barre, “An hybrid approach for the comparison of VAWT and HAWT performances for floating offshore wind turbines,” in *Journal of Physics: Conference Series*, 2020, doi: 10.1088/1742-6596/1618/3/032026.
- [66] A. Meseguer and R. Guanche, “Wind turbine aerodynamics scale-modeling for floating offshore wind platform testing,” *J. Wind Eng. Ind. Aerodyn.*, vol. 186, no. November 2018, pp. 49–57, 2019, doi: 10.1016/j.jweia.2018.12.021.

- [67] J. A. Armesto, A. Jurado, R. Guanche, B. Counago, J. Urbano, and J. Serna, "Telwind. Numerical analysis of a floating wind turbine supported by a two bodies platform," *Proc. Int. Conf. Offshore Mech. Arct. Eng. - OMAE*, vol. 10, no. June, 2018, doi: 10.1115/OMAE2018-77587.
- [68] O. Pires *et al.*, "Inclusion of rotor moments in scaled wave tank test of a floating wind turbine using SiL hybrid method," in *Journal of Physics: Conference Series*, 2020, doi: 10.1088/1742-6596/1618/3/032048.
- [69] A. Fontanella *et al.*, "A hardware-in-the-loop wave-basin scale model experiment for the validation of control strategies for floating offshore wind turbines," *J. Phys. Conf. Ser.*, no. 1618 032038, pp. 1–10, 2020.
- [70] S. Kanner, R. W. Yeung, and E. Koukina, "Hybrid testing of model-scale floating wind turbines using autonomous actuation and control," *Ocean. 2016 MTS/IEEE Monterey, OCE 2016*, pp. 1–6, 2016, doi: 10.1109/OCEANS.2016.7760997.
- [71] T. Sauder, V. Chabaud, M. Thys, E. E. Bachynski, and L. O. Sæther, "Real-time hybrid model testing of a braceless semi-submersible wind turbine. Part 1: the hybrid approach," in *Proceedings of the ASME 2016 35th International Conference on Ocean, Offshore and Arctic Engineering OMAE2016*, 2016, pp. 1–13.
- [72] E. E. Bachynski, T. Sauder, M. Thys, V. Chabaud, and L. O. Sæther, "Real-time hybrid model testing of a braceless semisubmersible wind turbine. Part 2: experimental results," in *Proceedings of the ASME 2016 35th International Conference on Ocean, Offshore and Arctic Engineering OMAE2016 June*, 2016, no. OMAE2016-54437, pp. 1–12.
- [73] P. A. Berthelsen, E. E. Bachynski, M. Karimirad, and M. Thys, "Real-time hybrid model tests of a braceless semisubmersible wind turbine. Part 3: calibration of a numerical model," in *Proceedings of the ASME 2016 35th International Conference on Ocean, Offshore and Arctic Engineering OMAE2016*, 2016, no. OMAE2016-54640, pp. 1–13.
- [74] C. Luan, Z. Gao, and T. Moan, "Design and Analysis of a Braceless Steel 5 MW Semi-Submersible Wind Turbine," in *Proceedings of the 35th International Conference on Ocean and Arctic Engineering OMAE 2016*, 2016, pp. 1–12.
- [75] M. Karimirad, E. E. Bachynski, P. A. Berthelsen, and H. Ormberg, "Comparison of real-time hybrid model testing of a braceless semisubmersible wind turbine and numerical simulations," in *Proceedings of the ASME 2017 36th International Conference on Ocean, Offshore and Arctic Engineering OMAE2017 June*, 2017, pp. 1–10.
- [76] E. E. Bachynski, V. Chabaud, and T. Sauder, *Real-time hybrid model testing of floating wind turbines: Sensitivity to limited actuation*, vol. 80, no. 1876. Elsevier B.V., 2015.
- [77] M. Thys, V. Chabaud, L. O. Sæther, Ø. B. Magnussen, L. Eliassen, and T. Sauder, "Real-time hybrid model testing of a semisubmersible 10MW floating wind turbine and advances in the test method," in *Proceedings of the ASME 2018 1st International Offshore Wind Technical Conference IOWTC2018*, 2018, no. Iowtc2018-10 81, pp. 1–11.
- [78] F. J. Madsen, F. Lemmer, K. Müller, A. Pegalajar-Jurado, R. Faerron-Guzman, and H. Bredmose, "LIFES50+ D4.6 Model validation against experiments and map of model accuracy across load cases," 2018.
- [79] V. Chabaud, L. Eliassen, M. Thys, and T. Sauder, "Multiple-degree-of-freedom actuation of rotor loads in model testing of floating wind turbines using cable-driven parallel robots," *J. Phys. Conf. Ser.*, vol. 1104, no. 1, 2018, doi: 10.1088/1742-6596/1104/1/012021.
- [80] M. Hall and A. J. Goupee, "Validation of a hybrid modeling approach to floating wind turbine basin testing," *Wind Energy*, vol. 21, no. 6, pp. 391–408, 2018, doi: 10.1002/we.2168.

- [81] R. Antonutti, J.-C. Poirier, and S. Gueydon, "Coupled Testing of Floating Wind Turbines in Waves and Wind Using Winches and Software-in-the-Loop," in *Offshore Technology Conference 2020, Houston, Texas, USA*, 2020, doi: 10.4043/30555-ms.
- [82] B. Schliffke, S. Aubrun, and B. Conan, "Wind Tunnel Study of a 'floating' Wind Turbine's Wake in an Atmospheric Boundary Layer with Imposed Characteristic Surge Motion," in *Journal of Physics: Conference Series*, 2020, doi: 10.1088/1742-6596/1618/6/062015.
- [83] S. Rockel, E. Camp, J. Schmidt, J. Peinke, R. B. Cal, and M. Hölling, "Experimental study on influence of pitch motion on the wake of a floating wind turbine model," *Energies*, 2014, doi: 10.3390/en7041954.
- [84] S. Rockel, J. Peinke, M. Hölling, and R. B. Cal, "Wake to wake interaction of floating wind turbine models in free pitch motion: An eddy viscosity and mixing length approach," *Renew. Energy*, 2016, doi: 10.1016/j.renene.2015.07.012.
- [85] I. Bayati, M. Belloli, L. Bernini, and A. Zasso, "Wind Tunnel Wake Measurements of Floating Offshore Wind Turbines," in *Energy Procedia*, 2017, doi: 10.1016/j.egypro.2017.10.375.
- [86] I. Bayati, M. Belloli, and A. Facchinetti, "Wind tunnel 2-DOF hybrid/HIL tests on the OC5 floating offshore wind turbine," in *Proceedings of the International Conference on Offshore Mechanics and Arctic Engineering - OMAE*, 2017, doi: 10.1115/OMAE2017-61763.
- [87] S. Ambrosini, I. Bayati, A. Facchinetti, and M. Belloli, "Methodological and technical aspects of a two-degrees-of-freedom hardware-in-the-loop setup for wind tunnel tests of floating systems," *J. Dyn. Syst. Meas. Control. Trans. ASME*, 2020, doi: 10.1115/1.4046155.
- [88] A. Fontanella, I. Bayati, R. Mikkelsen, M. Belloli, and A. Zasso, "UNAFLOW: A holistic wind tunnel experiment about the aerodynamic response of floating wind turbines under imposed surge motion," *Wind Energy Sci.*, vol. 6, no. 5, pp. 1169–1190, Sep. 2021, doi: 10.5194/WES-6-1169-2021.
- [89] I. Bayati, M. Belloli, D. Ferrari, F. Fossati, and H. Giberti, "Design of a 6-DoF robotic platform for wind tunnel tests of floating wind turbines," in *Energy Procedia*, 2014, doi: 10.1016/j.egypro.2014.07.240.
- [90] I. Bayati, A. Facchinetti, A. Fontanella, H. Giberti, and M. Belloli, "A wind tunnel/HIL setup for integrated tests of Floating Offshore Wind Turbines," *J. Phys. Conf. Ser.*, vol. 1037, no. 5, 2018, doi: 10.1088/1742-6596/1037/5/052025.
- [91] M. Belloli *et al.*, "A hybrid methodology for wind tunnel testing of floating offshore wind turbines," *Ocean Eng.*, vol. 210, no. May, 2020, doi: 10.1016/j.oceaneng.2020.107592.
- [92] M. Thys, A. Fontanella, F. Taruffi, M. Belloli, and P. A. Berthelsen, "Hybrid model tests for floating offshore wind turbines," in *ASME 2019 2nd International Offshore Wind Technical Conference, IOWTC 2019*, 2019, doi: 10.1115/IOWTC2019-7575.
- [93] V. Arnal, F. Bonnefoy, J. C. Gilloteaux, and S. Aubrun, "Hybrid model testing of floating wind turbines: Test bench for system identification and performance assessment," in *Proceedings of the International Conference on Offshore Mechanics and Arctic Engineering - OMAE*, 2019, doi: 10.1115/OMAE2019-96374.
- [94] M. Hall, J. Moreno, and K. Thiagarajan, "PERFORMANCE SPECIFICATIONS FOR REAL-TIME HYBRID TESTING OF 1:50-SCALE FLOATING WIND TURBINE MODELS," in *Proceedings of the ASME 2014 33rd International Conference on Ocean, Offshore and Arctic Engineering OMAE2014*, 2014, pp. 1–9.
- [95] M. Hall, A. Goupee, and J. Jonkman, "Development of performance specifications for hybrid modeling of floating wind turbines in wave basin tests," *J. Ocean Eng. Mar. Energy*, vol. 4, no. 1, pp. 1–23, 2018, doi: 10.1007/s40722-017-0089-3.

- [96] S. Gueydon, R. Lindeboom, W. van Kampen, and E.-J. de Ridder, "COMPARISON OF TWO WIND TURBINE LOADING EMULATION TECHNIQUES BASED ON TESTS OF A TLP-FOWT IN COMBINED WIND, WAVES AND CURRENT," in *Proceedings of the ASME 2018 1st International Offshore Wind Technical Conference IOWTC2018*, 2018, pp. 1–11.
- [97] H. Lee and D. J. Lee, "Effects of platform motions on aerodynamic performance and unsteady wake evolution of a floating offshore wind turbine," *Renew. Energy*, 2019, doi: 10.1016/j.renene.2019.04.134.
- [98] DJI, "Spreading Wings S800." https://www.dji.com/ie/spreading-wings-s800?site=brandsite&from=insite_search (accessed Apr. 19, 2022).
- [99] W. E. Cummins, "The impulse response function and ship motions," in *Symposium on Ship Theory at the Institut für Schiffbau der Universität Hamburg, 25-27 January 1962*, 1962.
- [100] S. Gueydon *et al.*, "Round Robin Laboratory Testing of a Scaled 10 MW Floating Horizontal Axis Wind Turbine," *J. Mar. Sci. Eng. 2021, Vol. 9, Page 988*, vol. 9, no. 9, p. 988, Sep. 2021, doi: 10.3390/JMSE9090988.
- [101] F. M. Judge *et al.*, "MaRINET2, Deliverable 2.5: Round robin findings and recommendations," 2021. doi: 10.13140/RG.2.2.32278.88648.
- [102] Lir NOTF, "Wave Basins – Lir." <http://www.lir-notf.com/wavebasins/> (accessed May 01, 2022).
- [103] Inaki Zabala *et al.*, "BEMRosetta: An open-source hydrodynamic coefficients converter and viewer integrated with Nemoh and FOAMM," in *Proceedings of the 14th European Wave and Tidal Energy Conference 5-9th Sept 2021, Plymouth, UK*, 2021, doi: ISSN 2309-1983.
- [104] S. K. Chakrabarti, "Physical Modelling of Offshore Structures," in *Handbook of Offshore Engineering*, 2005th ed., vol. 1, Elsevier, 2005, pp. 1001–1054.
- [105] A. Robertson, E. E. Bachynski, S. Gueydon, F. Wendt, and P. Schünemann, "Total experimental uncertainty in hydrodynamic testing of a semisubmersible wind turbine, considering numerical propagation of systematic uncertainty," *Ocean Eng.*, vol. 195, no. November 2018, p. 106605, 2020, doi: 10.1016/j.oceaneng.2019.106605.
- [106] H. A. Holmes, "Quality assurance of wind energy assessment models WAUDIT Guidance Report – WP6 Deliverable D24," 2011.
- [107] A. N. Robertson *et al.*, "OC5 Project Phase II: Validation of Global Loads of the DeepCwind Floating Semisubmersible Wind Turbine," *Energy Procedia*, vol. 137, pp. 38–57, 2017, doi: 10.1016/j.egypro.2017.10.333.

Appendix

Paper A

A review of modelling techniques for Floating Offshore Wind Turbines

Published in

Wind Energy, Wiley, 2021, DOI: 10.1002/we.2701

Authors:

A. Otter¹, J. Murphy¹, V. Pakrashi², A. Robertson³, C. Desmond⁴

¹ Marine and Renewable Energy Ireland, University College Cork, P43 C573, Ireland

² Dynamical Systems and Risk Laboratory, Marine and Renewable Energy Ireland, UCD Energy Institute, UCD Centre for Mechanics, University College Dublin, D04 V1W8, Ireland

³ National Renewable Energy Laboratory, Golden CO, 80401, USA

⁴ Gavin and Doherty Geosolutions Ltd, Dublin 14, D14 X627, Ireland

Abstract

Modelling Floating Offshore Wind Turbines (FOWT) is challenging due to the strong coupling between the aerodynamics of the turbine and the hydrodynamics of the floating platform. Physical testing at scale is faced with the additional challenge of the scaling mismatch between Froude number and Reynolds number due to working in the two fluid domains, air and water. In the drive for cost-reduction of floating wind energy, designers may be seeking to move towards high-fidelity numerical modelling as a substitute for physical testing. However, the numerical engineering tools typically used for FOWT modelling are considered as mid-fidelity to low-fidelity tools, and currently lack the level of accuracy required to do so. Furthermore, there is a lack of operational FOWT data available for further development and validation. High-fidelity tools, such as CFD, have greater accuracy but are cumbersome tools and still require validation. Physical scale model testing therefore continues to play an essential role in the development of FOWTs both as a source of validation data for numerical models and as an important development step along the path to commercialization of all platform concepts.

The aim of this paper is to provide an overview of both numerical modelling and physical FOWT scale model testing approaches and to provide guidance on the selection of the most appropriate approach (or combination of approaches). The current state-of-the-art will be discussed along with current research trends and areas for further investigation.

Introduction

Floating wind energy is an emerging industry. Currently just three floating farms, Hywind Scotland (30 megawatts [MW]), Kincardine (50 MW) and Windfloat Atlantic (25 MW), are connected to the grid, and several other floating farms are in the construction and planning stages. Whilst the industry is advancing at pace, the costs associated with floating wind are still significantly higher than for fixed offshore wind energy. However, significant price reductions are expected over the period 2021-2028, which could make floating economically competitive with the current price of fixed wind [104].

To achieve these cost reductions, and for floating wind energy to establish itself as a reliable technology, high-fidelity design and modelling software are essential. Modelling of Floating Offshore Wind Turbines (FOWT) is challenging due to the strong coupling between the aerodynamics of the turbine and the hydrodynamics of the floating platform. A variety of numerical and physical modelling approaches are currently in use, both independently and using a cross validation approach to de-risk the commercial development of concepts through the Technology Readiness Levels (TRL) [105].

This paper informs the reader about the state-of-the-art of FOWT modelling, both numerically and experimentally, and attempts to aid in the decision of which methods and tools are most suitable for the design or research the reader may wish to perform. The paper builds on reviews of physical modelling approaches by Robertson et al [45], Muller et al [106], Stewart and Muskulus [107], and Gueydon et al [108], and numerical modelling approaches by Cordle et al [109] and Joao Cruz et al [110].

The first part of this paper reviews the numerical methods and the leading software available for FOWT modelling. The second part reviews the methods employed to date in experimental campaigns of FOWT models, and the different methods to overcome the scaling mismatch caused by working in the two fluid domains, air and water. The focus of this paper will be on the modelling techniques required for the design stages up to TRL 4 (technology validated in a laboratory). The emphasis will therefore be on numerical and physical approaches used at an early concept-development stage and will not consider high-fidelity or component level analysis at the final design stages in detail.

Finally, in the third part gaps in the state-of-the-art are identified and recommendations for guidelines for the combined use of physical and numerical approaches in the FOWT development process are suggested.

Numerical modelling

A broad range of numerical techniques and software packages are available for the initial stages of the design process of a FOWT prototype. Some overarching aspects and contemporary directions are considered in this section. Traditionally, a numerical model of a new design is developed, and then validated using model-scale laboratory tests [111], [112]. However, in the drive for cost reduction of FOWT technology designers may be looking to use high-fidelity numerical tools in an effort to reduce reliance on costly and time-consuming physical tests, and also to reduce the uncertainty that simpler numerical models contain. On the other hand, when considering lifetime operations and maintenance aspects [113], control [114], or end of life decision-making [115], [116], lower-fidelity models can be of significance. The competing needs and relevance of high-fidelity and low-fidelity models exist in a wide range of TRLs [117].

Computational methods

For numerical modelling purposes the FOWT can be divided into roughly three categories (Figure 1): structural dynamics, hydrodynamics, and aerodynamics. Scaling aspects [106], [108] of each of these categories and their requirements can differ significantly, and change based on the context of their uses, including control [118]. In this paper, turbine control will not be reviewed as a separate category since it requires an in-depth review of its own. The choice of numerical modelling method will generally be a trade-off between accuracy and/or fidelity, and computational efficiency with respect to the phenomena of interest and their acceptable performance levels. Accuracy is defined here as the deviation of simulated estimates from measured physical responses and is often presented as a statistical summary or in the form of metrics for direct comparison. On the other hand, fidelity describes the level of simplification of the underlying physics or phenomena of interest by the numerical model [119], [120], providing a level of confidence that said accuracy is indeed achieved during simulations. Computational efficiency is often reported as the amount of time required for a simulation to complete using standard computing equipment but estimates of the complexity of the problem in terms of floating-point operators are becoming more visible in the dynamical systems literature.

Overall, numerical models may be classified into three levels: low-, mid- and high-fidelity, where increasing fidelity leads to a higher demand on computational resources, reducing computational efficiency. The choice of fidelity level is a function of the objective of the simulation and the level at which such analysis and its accuracy is required. Typically, low-fidelity models are used during the initial stage of FOWT design for sizing analysis and optimization. Mid-fidelity models, or engineering-level tools, are used after the initial design stage for loads analysis of FOWTs to examine operational and extreme conditions. High-fidelity models are typically used during the final design stages for detailed investigations, especially to accurately obtain stresses on the structure. A multi-fidelity approach may also be used where elements of each fidelity-level model is used in the different stages of design. As an example, higher-fidelity tools may be used to tune lower-fidelity ones, or as checks for certain high-impact design conditions.

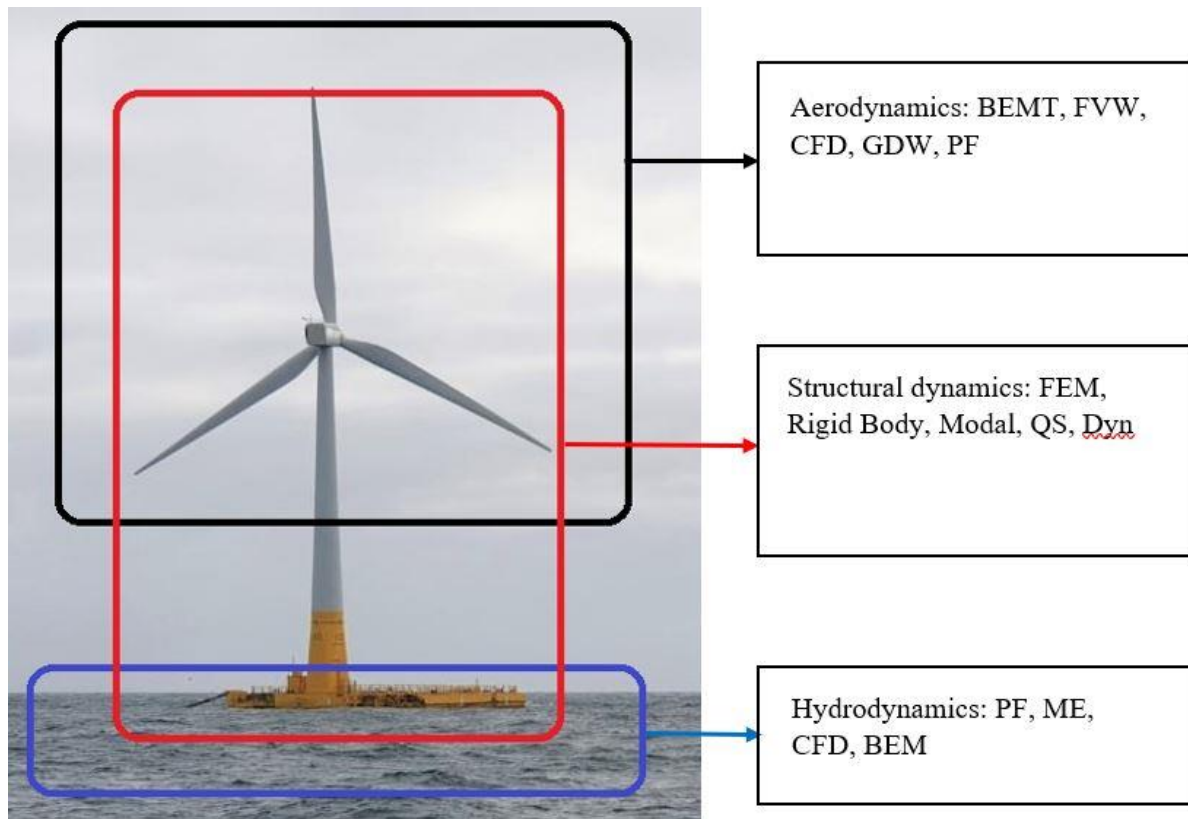


Figure 1. Numerical structure of the FOWT (Photo: FLOATGEN, by A. Otter). Abbreviations are defined in Table 1.

Table 1. Explanation of abbreviations of computational methods in Figure 1.

Acronym:	Category:	Fidelity:
BEM: Boundary Element Method	Hydrodynamic	Mid
BEMT: Blade Element Momentum Theory	Aerodynamic	Mid
CFD: Computational Fluid Dynamics	Aero-/hydrodynamic	High
Dyn: Dynamic method	Structural	Mid
FEM: Finite Element Method	Structural	High
FVW: Free Vortex Wake method	Aerodynamic	Mid
GDW: Generalized Dynamic Wake method	Aerodynamic	Mid
ME: Morison Equation	Hydrodynamic	Mid
PF: Potential Flow	Aero-/hydrodynamic	Mid
QS: Quasi-Static method	Structural	Low

For brevity, the various computational methods will not be described in detail in this paper, as most can be found in standard texts. Instead, examples of numerical studies where low-, mid-, and high-fidelity approaches were used will be reviewed for the structure, hydrodynamic and aerodynamic categories. A detailed overview of computational methods relating to FOWT modelling can be found in Joao Cruz et al [110].

Software for FOWT modelling.

There are several open-source and commercial numerical software packages for FOWT modelling. Some of the popular software packages are listed in the following sections.

Low-fidelity

For the early design stages, simple low-fidelity frequency-domain models can be used to simulate linear dynamics of the FOWT. Although no commercial standalone frequency-domain solvers seem to be available for FOWTs, there are a number of examples developed in-house, e.g. Hegseth and Bachynski [121], Karimi et al [122] and Pegalajar-Jurado et al [123].

Mid-fidelity

Mid-fidelity software, often referred to as engineering tools, are used for global dynamics analysis, both in linear and nonlinear loads. The most popular engineering tools are listed below.

- FAST [124] is an open-source software developed as a research tool by the National Renewable Energy Laboratory (NREL) in the United States. Recently, it was re-named OpenFAST, with the idea of having a more community-driven development of the tool. OpenFAST is made up of several modules able to solve the coupled nonlinear aero-hydro-servo-elastic-mooring dynamics of FOWTs in time-domain only. The linearization of the underlying nonlinear system equations for OpenFAST is described in Jonkman et al [125].
- HAWC2 [126], developed by the Technical University of Denmark (DTU), is an aero-elastic time-domain solver, which also includes a hydrodynamic model for FOWT modelling.
- SIMA [127], developed by Selskapet for INdustriell og TEknisk Forskning ved Norges tekniske hoegskole (SINTEF), comprises the hydrodynamic- and mooring modules SIMO and RIFLEX. Initially it was developed for floating platforms in the oil & gas industry but now can also be used for FOWT modelling.
- Bladed [128], developed by Det Norske Veritas (DNV), is an aero-elastic code which can be coupled with SINTEF's SIMA workbench for FOWT modelling.
- SIMPACK [129], is a general multi body simulation tool with a dedicated wind simulator, which has an elastic module and interfaces with HydroDyn, AeroDyn (both FAST modules) and Bladed for coupled simulations of FOWTs.
- Both Orcaflex [130] and Flexcom [131], hydrodynamic solvers for floating objects developed by Orcina and Woods Group respectively, can be coupled with FAST for a full time-domain FOWT analysis. Both these numerical codes were originally developed for the offshore oil & gas industry to model moorings, riser pipes etc.

Most of the engineering tools mentioned above require input from frequency-domain PF solvers, such as WAMIT, AQWA and Nemoh, for hydrodynamic coefficients to solve the radiation/diffraction problems.

The underlying numerical methods for the three main elements of FOWT design are detailed in Table 2 for the engineering tools discussed in this section.

Table 2. Engineering tools used for FOWT modelling.

Software	Hydrodynamics	Aerodynamics	Structure
FAST	PF + ME	BEMT + GDW/FVW	RB + Modal /FEM +Dyn/QS
HAWC2	PF + ME	BEMT + GDW	FEM + Dyn
SIMA	PF + ME	BEMT	FEM + Dyn
Bladed	With SIMA	BEMT + GDW	Modal
SIMPACK	With HydroDyn	AeroDyn/AeroModule	FEM

Orcaflex	PF + ME	With FAST	RB + FEM + Dyn
Flexcom	PF + ME	With FAST	RB + FEM + Dyn

Several studies have been conducted to compare engineering tools against each other, e.g. Ormberg and Bachiynski [132], which compared the aerodynamic results obtained by RIFLEX with those obtained by AeroDyn, and found comparable results.

However, the most comprehensive benchmark study to date is the Offshore Code (OC) Comparison Collaboration project. Most of the engineering tools mentioned in this section have been featured in the OC projects and were used by the participants to simulate the dynamic behaviour of a spar FOWT design similar to Hywind in the OC3 [109] and OC4 projects, and the DeepCwind semisubmersible FOWT in the OC4, OC5 and OC6 projects [103], [133], [134]. Some important findings include:

- Similar results for the semisubmersible were found with potential flow and Morison-only solvers within the wave-frequency region, pitch variations were slightly higher with the latter
- Significant difference in viscous drag loads is achieved with calculating the Morison drag terms for each member compared to approximation with a global drag matrix
- Mean and slow drift caused by wave excitation varies significantly between the numerical codes when nonlinear hydrodynamics are included
- Heave response is improved when dynamic pressure on heave plates is included in the Morison-only approach
- There is significant difference for moorings with the Dynamic method compared to the Quasi-Static method, particularly in frequencies above the linear wave range
- Response Amplitude Operators (RAO) are a good way of comparing the dynamic response of FOWTs between the different numerical codes, both with and without wind loads.

Comparison between the engineering tools will only highlight their differences but cannot determine the accuracy of the simulations. To validate the numerical results [103], the simulations of the DeepCwind semisubmersible were compared to experimental results measured in a test campaign at Maritime Research Institute Netherlands (MARIN) [135]. Some important findings from this study include:

- Ultimate and fatigue loads were underpredicted compared to the experiments in varying degrees by all the numerical codes.
- The largest underpredictions were found at the low-frequency responses in pitch and surge due to inaccuracies in the nonlinear difference-frequency loads; codes that used second order hydrodynamics achieved the closest result, but still underpredicted loads.
- Differences in aerodynamics were masked by the differences in hydrodynamic loads; without an uncertainty assessment the researchers found it difficult to accurately quantify the differences in the results between experimental and numerical simulations.
- Some nonlinear loads could have been caused by the cables for the loadcells on the model, for example.

In a separate campaign Robertson et al [101], [136] attempted to quantify the experimental uncertainty in order to get a reliable assessment of the accuracy of the numerical codes. For these tests a model of the DeepCwind semisubmersible was used, but only hydrodynamics were considered because that was the significant source of load under-prediction. Random uncertainty, i.e., the differences in conditions across repeated tests, was negligible compared to the systematic uncertainty, i.e., unknown bias in the waves and physical properties of the scaled model. Of course, these results are facility-specific (MARIN), however repeatability was found to be excellent. The differences between experiments and numerical models were found to be larger than the uncertainties in the experiments. The level of under-

prediction of loads (around 20%) falls within the uncertainty assumptions for the FOWT design process, but improved accuracy will enable further design optimization to lower cost. In the next phase of the OC6 project, Robertson et al [134] investigated why the engineering tools all underpredict the response of the DeepCwind semisubmersible at the natural surge- and pitch frequencies due to nonlinear hydrodynamic loads. Engineering tools were found to be missing some of the important physics needed to accurately predict the nonlinear, low-frequency loads. In comparison, high-fidelity CFD tools should be able to accurately predict the surge and pitch loads with high accuracy. Current efforts in the OC6 project are underway to validate the CFD tools using the same dataset and improve the engineering tools based on CFD results.

High-fidelity

High-fidelity software is used for detailed investigations of local flow phenomena and stress hot spots in the structure, for example, as well as for increased accuracy, especially for extreme conditions. Although, no high-fidelity method software programmes have been developed specifically for FOWTs, there are nonetheless a number of both open-source and commercial software packages available for general engineering purposes that can also be used for FOWT design. Some of the popular software packages are listed in Table 3.

Table 3. High-fidelity software which can be used for FOWT modelling.

Software	Computational method
OpenFOAM	CFD
Star CCM+	CFD
Ansys	CFD + FEM
Autodesk	FEM
Abaqus	FEM + CFD

Frequency-domain vs time-domain

Irrespective of the software of in-house developed codes, the question of time- versus frequency-domain simulations often needs to be considered. Linear frequency-domain simulations would typically fall in the low-fidelity category, due to the simple approximations of the underlying physics used in such models, and are used in the initial design stages. For example, Hegseth and Bachynski [121] developed a frequency-domain modelling approach and applied it to two types of spar FOWTs. Here, the platform was rigid, and the tower was a slender flexible beam. For long-term fatigue response, and short-term extreme response, the difference in results varied up to 30% as compared to the nonlinear time-domain models. On the other hand, for long-term effects and global-load assessments, especially from mid- to high-fidelity models, one needs to run computationally intensive time-domain analyses. Extensive time-domain simulations, though computationally expensive, tend to provide the most detailed estimates of the responses due to the coupled nature between the aerodynamics, hydrodynamics, structural dynamics, and control actions. Typically, the numerical results in the form of dynamic motions and loads are compared against experimental measurements using an error metric [137]. Such metrics are valuable for comparison and repeatability of different experiments, as well as investigating the performances of various experimental models at different scales, TRLs and repeated experiments, or experiments in different wave basins.

Structural dynamics

The progression from lower- to higher-fidelity of the structural model of a FOWT is based on the type, range, detail and complexity of the responses it can capture successfully. In its simplest form, a low-fidelity model captures rigid-body motions [138], [139] overall, or of its constituent rigid-body elements, and can be relevant for examining global stability, but are not appropriate for representing

deformation responses. They are, however, particularly helpful for concept level, rapid and early designs or assessments of such structures. One can also sometimes choose to model parts of the system rigidly and others with flexibility.

Mid-fidelity models are typically defined through elements (e.g. beams, cables, and joints) with linear and nonlinear properties [140], [141]. They have been used to examine aerodynamic stability [142], [143], and estimate dynamic response related to deformation [144] and physical characteristics [111]. These models are often described via a set of differential equations and lend themselves to non-dimensional forms, enabling validation via scaled model tests. Such models can also, with numerical implementation, include additional aspects like damage via reduction of stiffness from chemical/physical processes (e.g. corrosion) [145] and marine growth [137]. These mid-fidelity models are also relevant for establishing or assessing safety in terms of fatigue and ultimate limit states (ULS) through analyses set out by standardised documents, e.g. IEC [146] and DNV [147]. Early in the design process, a static analysis is used to assess loads, an overview of which may be obtained from Baltrop [17] and Journee and Massie [16]. At later stages, time-domain simulations are required to properly assess fatigue and extreme loads across a variety of operational, extreme, and fault/start-up conditions.

Another common approach in structural dynamics is to use a modal approach, where certain flexible degrees of freedom are represented by their modes and mode shapes. This approach can be used for modelling the blades and tower in FAST, for example. At the highest level, FEM [148]–[150] is commonly used to represent one or all aspects of the design, including the platform, tower, blades and mooring lines. Many times, a mixture of fidelities is used for different components of the system depending on the purpose of the analysis and the relative flexibility of the different components. FEM models are associated with a large number of Degrees of Freedom (DOF), and to increase computational efficiency, dimension reduction is often attempted [151]. For linear analyses or linear approximations of these structures, a modal superposition approach often provides a good response estimate of a structure with state space models [110], [152]. However, the success of such modal superposition driven dynamic models is related to careful choice of system parameters, assumptions about the physics of the systems and loading excitation. Deviations in reality from such assumptions will thus quickly lead to significantly higher errors, since the response information is represented by only a number of finite, generalised modal coordinates.

Reduced DOFs are also possible for certain cases by computing rigid body kinematics of various structural components and then combining them with pre-computed elastic properties to obtain deformation estimates [138]. The BEM [110] is another method that is often used in this regard, often with low-order meshing [153], which is suitable for understanding the interaction between fluids and rigid structures [154]. Recently, there has also been an emergence of using Finite Volume Method (FVM) [155], [156] for significantly deformable structures [157], in a Simo-Reissner format [150].

Nonlinear dynamic characteristics of mooring lines and power cables [158], and additional impacts on them over the lifetime [159], are relevant and are part of a particularly active field of research, including interconnections and additional components like buoyancy elements and effect of ballasting. While traditional QS models, computed in terms of equivalence of relevant parameters of interest in each time-step, are used to assess mooring dynamics for computational ease [160]–[162], they tend to underpredict the restoring force and is more noticeable for extreme sea states. they are also less useful for platforms that use catenary moorings and have natural frequencies close to peak wave frequencies. Dynamic analyses do not have these challenges and despite a higher computational demand, are becoming a natural choice since they match experimental results better [163]. Computational efficiency in such approaches, including those in frequency-domain [164] are also being investigated.

Overall, the evolution of structural modelling has been in terms of allowing for complexity and detail to capture the widest range of phenomena, physical responses and stochastic aspects for various spatial and temporal scales through a range of discretization processes. Over time, the strong focus on

computational ease has diminished in terms of its importance with the current expansion of capabilities in computing and the ease with which large scale computing facilities can be engaged for such analyses.

Hydrodynamics

Numerical modelling methods for hydrodynamic problems have been mainly developed for the maritime [16] and offshore oil & gas industries [17] but can equally be applied to floaters and platforms of FOWTs [165]. The Potential Flow method, the Morison Equation, or a combination of the two, are used for the computation of first- and second-order wave excitations. These mid-fidelity methods generally deliver the required accuracy at reasonable computational efficiency but can have problems with complex geometries where the disruption of flow between members is not adequately addressed.

The PF method [16] is used to solve diffraction/radiation loads. Limitations of PF include viscous effects being ignored, and the oscillation amplitudes are assumed to be small compared to the cross-sectional area of the floating body [21]. Numerical tools based on PF theory use BEM. This method divides the floating body into panels, and hydrodynamic loads are found by integrating the dynamic pressure over the wetted panels. The submerged geometry is defined as the hydrostatic equilibrium in still water for frequency-domain PF solvers. Most time-domain-only PF solvers need to import a set of hydrodynamic coefficients pre-processed with a frequency-domain PF solver to define the panels of the submerged geometry of the platform.

The Morison Equation is generally used for structures consisting of slender cylindrical members. It models inertial loads, and unlike PF, viscous loads, and can therefore be used to simulate structures in waves and currents. It is an empirical equation, originally developed by Morison et al [166] for fixed, infinitely long cylindrical offshore structures, but can also be used for FOWTs. A limitation of the Morison equation is that it ignores the alteration of the incident wave field by the floating body.

A mixed modelling approach of combining PF methods with ME is used when either method on its own will be unable to capture certain hydrodynamic effects, and is regarded as a computationally efficient alternative for CFD modelling [52]. This hybrid method could be useful for FOWT platforms consisting of large columns and slender braces, or for viscous drag effects resulting from severe sea states.

Complex flow problems are solved with high-fidelity CFD [167] models. CFD solvers are based on the Navier Stokes equation and are generally used to solve specific nonlinear problems such as slamming loads due to extreme wave events and complex flow patterns such as vortex shedding around heave plates. CFD models are also used to tune model parameters for lower-fidelity models [168], [169] numerically rather than with decay tests from physical experiments.

Making direct comparisons between CFD models and PF + ME models [169]–[171] is non-trivial. The accuracy of the models will depend on a number of factors such as: the load cases being investigated; whether steady state equations or transient equations are used for the CFD model; whether the hydrodynamic coefficients used are tuned; mesh characteristics and the competence of the user; and ensuring a converged solution for the CFD model. There are many components to the PF + ME solution that are needed for an accurate solution in some cases. Most significant is the calculation of the second-order PF solution, rather than just first-order. Other key components are wave stretching, which means that the wave forces are calculated above the water free surface, and the correct viscous damping in the model, especially if second-order PF loads are included.

Other alternatives, besides the PF + ME methods, to CFD are being investigated e.g. Chan et al [172] and Office of Energy Efficiency & Renewable Energy WETO. [173].

Aerodynamics

The most challenging aspect regarding aerodynamics for FOWTs is the variation in relative wind velocity due to motions of the platform, both for horizontal axis turbines [93], [174]–[176], and vertical

axis turbines [177]. This effect is referred to as dynamic inflow, or unsteady dynamics, and may cause an overshoot of rotor thrust loading, also referred to as negative damping. The efficient, mid-fidelity, quasi-steady BEMT models [26] were found to be incapable of capturing dynamic inflow effectively [178]. BEMT combines momentum theory and blade element theory and divides the turbine blades into smaller elements or strips. The aerodynamic properties for each element are calculated individually and the properties for the entire rotor are solved by integrating the values of each element. The quasi-steady BEMT models assume instant equilibrium of turbine wake. Some studies, e.g. Henriksen et al [179], Chen and Agarwal [180], and Ferreira et al [181], suggest that by adding a simple dynamic inflow model, BEMT models can effectively capture dynamic inflow effects, while maintaining computational efficiency.

Higher-fidelity models using PF and CFD based methods [182]–[184] are able to capture the effects of dynamic inflow, however, at the expense of lower efficiency. The UNsteady Aerodynamics for Floating Wind (UNAFLOW) project [185], [186] studied the ability of numerical tools to capture unsteady aerodynamics of FOWTs in detail. In the OC6 Phase III project [187], the UNAFLOW dataset will be used for in-depth comparison of the modelling approaches for aerodynamics of large motion. Other alternatives to study dynamic inflow, for example using machine learning [188], are also being investigated.

Recently, modelling tools have been incorporating a mid-fidelity approach for aerodynamic modelling, the FVW method [189]–[191]. With increasing turbine rotor sizes, there is a greater need to accurately capture aerodynamic effects due to large blade deflections. The FVW method satisfies this need with a level of fidelity and computational efficiency between that of BEMT and CFD methods. The FVW method is a more detailed modelling method of the wake, which affects the aerodynamic loading on the rotor, and uses Lagrangian discretization of vorticity. FVW is introduced to the latest version of OpenFAST [192] and other industry tools.

Mitigating the effects of dynamic inflow is an important task of the turbine controller in addition to optimizing power production. Several studies, e.g. Lackner [193], Yu et al [194], Savenije and Peeringa [195], Fontanella et al [65], and Jonkman [196] on turbine control for FOWTs can be found in the literature.

Another important consideration is the evolution of turbine wake [197]–[199] and the effects that it may have on FOWT dynamics, on downwind turbines, and on FOWT farm layout.

As mentioned before, the choice of which type of numerical method to use across the design stages is largely a trade-off between the available monetary budget and time budget on the one hand, and the level of uncertainty and accuracy of the numerical model that are acceptable on the other hand. Other considerations may be what sort of load cases are to be investigated, what type of FOWT is being modelled, and what phase one is in for the design cycle – preliminary/early stages or detailed investigations/final stage.

Physical modelling

Comparing numerical results with experimental results obtained in laboratory basins for validation is still considered an essential step in the design process by most designers of FOWTs. As turbine sizes continue to grow, consequently, the platform sizes of FOWTs continue to get larger. To accommodate the increasing dimensions of prototypes at model scale, and reduce the uncertainty of physical modelling, testing techniques of FOWTs in laboratories are evolving. The state-of-the-art of physical modelling techniques is outlined in this section.

Scaling laws

Geometrical, kinematic and dynamic similarity between model scale and full scale is required [34] for the experimental validation of numerical models.

For geometrical similarity this means that all linear dimensions must have the same scale ratio, which is defined as:

$$\lambda = L_F / L_M \quad (1)$$

The subscripts F and M indicate full scale and model scale, respectively. The ratio between inertia and gravity is defined as:

$$U^2 / g L \quad (2)$$

where U is velocity, g is gravitational acceleration and L is physical length. The dynamic similarity requirement between model scale and full scale then, is defined as:

$$U_M / (g L_M)^{1/2} = U_F / (g L_F)^{1/2} \quad (3)$$

which is also known as the Froude number.

The ratio between inertia and viscosity is defined as:

$$UL / \nu \quad (4)$$

where ν is the kinematic viscosity. The dynamic similarity requirement between model- and full scale is defined as:

$$U_M L_M / \nu = U_F L_F / \nu \quad (5)$$

This is known as the Reynolds number.

As the kinematic viscosity of air will remain the same for prototype and scale model it becomes apparent that for a Froude scaled rotor with geometric similitude, the Reynolds number will be lower at model scale compared to the Reynolds number of the full-scale rotor. Consequently, the lift coefficient of the model scale rotor will be lower, and the drag coefficient will be higher compared to the full-scale rotor. As a result, the aerodynamic performance of the model scale turbine will be affected, causing a misrepresentation of wind load induced motion response of the FOWT. The focus for scaled turbines, however, is on the ability to emulate Froude scaled rotor thrust and torque. The following sections explain how this is achieved.

Full physical testing

From equations (1) to (5), it becomes apparent that either increasing the velocity of the applied wind or adjusting the turbine rotor geometry at model scale could compensate for the lower Reynolds number. Rotor thrust is the most critical aerodynamic load to impact on motion response of FOWT models. The simplest, and lowest fidelity, method to emulate thrust force is with a mechanical pulley system [35]. This method can only model steady thrust loads but cannot capture aerodynamic damping or the effects of turbine control. A simple method to emulate rotor thrust load with physical wind is using a drag disc instead of a scaled rotor. In combination with a Froude scaled rotating mass, the rotor gyroscopic loads can also be emulated [36]. The drag disc method (Figure 2) allows for varied thrust loads but like the pulley system will not be able to capture aerodynamic damping or the effects of turbine control [37].

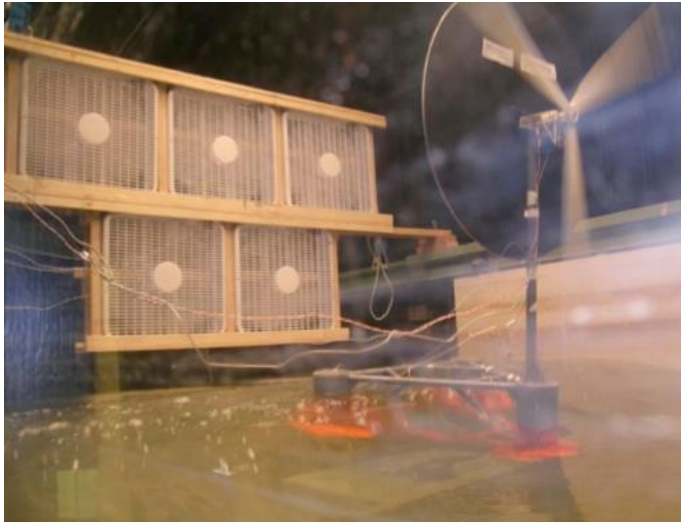


Figure 2. WindFloat model with drag disc and rotating mass [36].

Increased wind velocity applied to a Froude scaled rotor can overcome the abovementioned limitations of the drag disc and achieve correct rotor thrust. However, maintaining rated rotor speed at higher wind velocities means the Tip Speed Ratio (TSR) cannot be maintained [38]. As a result, rotor torque cannot be modelled correctly, and aerodynamic damping may not be captured correctly. If on the other hand correct TSR is maintained, the Eigen frequencies of the rotor and blade-tower passing frequency (3P frequency) and rotor thrust forces cannot be modelled correctly. Geometrically modified aerofoils to compensate for the low Reynolds number in a Froude scaled wind environment, are better able to emulate aerodynamic loads, and capture damping effects and blade pitch control effects while maintaining TSR. This is generally referred to in the literature as performance scaling of the rotor [39]–[41]. Roughened leading edges on the rotor blades, and slight increases of applied wind velocity, in combination with geometrically altered rotor blades can be applied to fine tune the model thrust forces.

Froude scaled rotor combined with higher than Froude scale wind velocity.

Skaare et al [18] tested a 1/67 scale model of the Hywind FOWT (Figure 3) at SINTEF, Norway, in 2005. Their model used a geometrically adjusted rotor with two DC motors along with physically generated wind to control rotational speed of the rotor and blade pitch angle. The experimental results of this campaign were used to validate the integration of the two independent simulation software tools SIMO/RIFLEX (floater) and HAWC2 (turbine) to a coupled simulation tool for FOWTs.

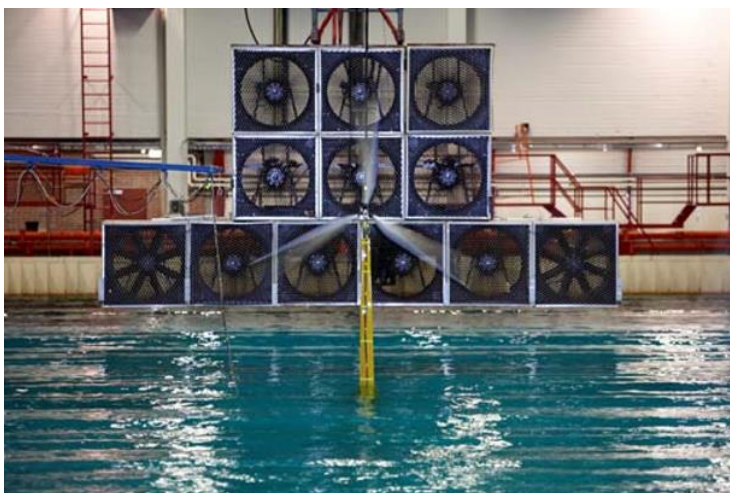


Figure 3. The Hywind model at SINTEF [18].

Mortensen et al [42] tested a 1/35 model of a Tension Leg Platform (TLP) with a Froude scaled version of the NREL 5 MW reference turbine [13] and increased wind velocity. The numerical model was validated with the experimental results, which showed that dynamic response of the TLP was predicted correctly.

Bahramiasl et al [43] tested a 1/100 scale model of a TLP FOWT with a Froude-scaled turbine and increased wind velocity at Sharif University, Iran. As the applied wind failed to turn the rotor, an electric motor with variable speed was used to drive the rotor and aid rotation. Increasing the rotational speed of the rotor showed some damping effects caused by the gyroscopic moment. Furthermore, a shift of the peak of the RAO spectra of the platform in heave, surge, pitch and yaw occurred.

Liang Li et al [44] tested a 1/50 scale model of the DeepCwind semisubmersible FOWT with a Froude scaled version of the NREL 5 MW turbine at Shanghai Jiao Tong University, China. Rather than controlling the rotor speed with an electric motor, the rotor was allowed to run freely, and the motor acted as a generator. The mechanical damping by the generator served to slow down the rotor speed and bring TSR closer to the desired rate resulting in improved aerodynamic damping compared to forced rotor speed control with an electric motor.

Geometrically modified low-Reynolds aerofoils combined with Froude scale wind velocity (performance-scaled).

For the University of Maine led DeepCwind consortium, Goupee et al [45], [46] tested 1/50 scaled models of a spar, semisubmersible and TLP platform at MARIN, the Netherlands, to compare the floater responses under similar conditions. Each platform was originally equipped with a geometrically scaled version of the NREL 5 MW reference turbine.

The DeepCwind team learned that geometrically scaling the rotor (based on a Froude-approach) was not the correct approach for scaled testing of FOWTs. The MARIN reference turbine was redesigned to create a performance-matched scaled model of the NREL 5 MW reference turbine. With this new turbine, the DeepCwind semisubmersible design was retested at MARIN in 2013, and this dataset was used for the validation study conducted in Phase II of the OC5 project.

The performance-matched MARIN reference turbine was also used by De Ridder et al [11] on the GustoMSC Tri-Floater model at MARIN. The results showed that the thrust coefficient of the model turbine was consistent with the thrust coefficient predicted by the CFD models, whereas the power coefficient found in the experiments is lower than the power coefficient predicted by the CFD models. To correctly model floater motions under combined wave/wind loads in laboratory basins a correct thrust coefficient of the model turbine is essential, whereas the influence of the power coefficient is negligible.

Bredmose et al [47] tested a 1/60 scaled version of the DTU 10 MW reference turbine [22] with low-Reynolds aerofoils on the Triple Spar platform (Figure 4), a hybrid spar/semi-submersible platform designed for the INNWIND.EU project, at the Danish Hydraulic Institute (DHI), Denmark. The focus of this campaign was the effect of the blade pitch controller on the response of the platform. Experiments with wind-only loading revealed a clear instability at the natural platform pitch frequency due to aggressive blade pitch control above rated wind speed.



Figure 4. The Triple Spar model, left the visualization at scale and right the model in the basin at DHI [47].

Madsen et al [48] also used the 1/60 scaled low-Reynolds version of the DTU 10 MW turbine on a model of the KIER TLP at DHI, Denmark. They also used three different kinds of controllers for blade pitch and found that use of the land-based controller resulted in high oscillations in blade pitch and increased surge response of the platform.

Koch et al [49] tested a 1/60 scale model of the DeepCwind semisubmersible FOWT with a low-Reynolds version of the DTU 10 MW turbine at Ecole Centrale de Nantes (ECN), France. To compensate for the higher mass of the turbine, ballast was added to lower the centre of gravity of the platform to the same level of the original design with the NREL 5 MW turbine. Free decay tests, wave only tests and wind only tests were performed, and all were found to be in good agreement with the numerical model.

Similarly, Ahn and Shin [50] adapted a 1/90 scale model of the DeepCwind semisubmersible for a low-Reynolds version of the DTU 10 MW turbine at the University of Ulsan, South Korea. Combined wave, wind, and current conditions were modelled, where a steady current load was introduced by a mechanical pulley system. The introduction of current had a damping effect on the surge motion of the platform.

Ward et al [51] developed a model turbine with performance scaled aerofoils, a light-weight Rotor Nacelle Assembly (RNA) and blade pitch control. Although the turbine has a fixed radius, the model turbine can be used for various turbine designs by adding weights to the RNA and varying the thrust load by pitching the blades. The concept was shown numerically to be viable. However, experimental results to validate their claims are not presented in the paper.

Connolly et al [52] tested a 1/50 scale model of the Eolink semisubmersible FOWT (Figure 5) with a low-Reynolds version of a 10 MW turbine at L'Institut Français de Recherche pour l'Exploitation de la Mer (IFREMER), France. The Eolink concept uses a pyramid construction to support the RNA with four pillars rather than the traditional single tower, and a single point mooring system for yaw alignment of the platform. Good agreement was found compared with the numerical results of Flexcom for most platform dynamics, however, the experiments showed that pitch response was overestimated by the numerical model.



Figure 5. The Eolink model at ECN [52].

Zhao et al [53] tested a 1/50 scale model of the WindStar TLP with a low Reynolds version of the NREL 5 MW turbine at Shanghai Jiao Tong University, China. An electro motor was installed on the turbine model to maintain TSR during tests with wind. They found that overall, the model showed relatively small motion responses, and that wind and current had a damping effect on the surge and pitch response.

Hybrid testing

Hybrid testing is the alternative to full physical testing of FOWT models. With this method, waves are still generated physically but the aerodynamic loads are replaced by a numerical substructure. The Froude/Reynolds mismatch is solved by calculating the aerodynamic loads at full scale and applying them to the physical model at Froude scale via one or several mechanical actuators. The two types of actuators most used in hybrid FOWT wave basin testing so far have been dynamic cable winches and propellers. The simplest, and lowest-fidelity, hybrid method applies a steady load to the actuator to emulate steady thrust load. Aerodynamic damping and turbine control will not be captured by this method. Stochastic wind loads can be emulated by applying a time-series input which tells the actuator to vary the loads. This method will capture aerodynamic damping, however, synchronizing wave elevations and wind loads is challenging. Furthermore, turbine control effects are only emulated as the numerical simulation captures them; it is not possible to emulate turbine control effects that react to the actual motion of the platform with this method. Real-time hybrid testing is a more complex but higher-fidelity method. With this method, physical modelling of the waves is combined with the numerical simulation of wind loads in real-time. The hydrodynamic module of the numerical code is replaced by the input of a motion tracking system, which records the spatial position of the platform for each time-step. According to the motion tracking data, the numerical code then calculates the aerodynamic loads acting on the turbine for the given wind velocity at full scale for each time-step. Finally, the aerodynamic loads are emulated by the actuator(s) at Froude scale and applied to the physical model and the process is repeated for the next time-step. This way, depending on the number of actuators, most aerodynamic effects can be captured (at least those that are captured by the numerical model), and waves and wind are perfectly synchronized. The diagram in Figure 6 shows a FOWT hybrid test setup for a wave basin developed at Centro Nacional de Energías Renovables (CENER), Spain, by Azcona et al [54].

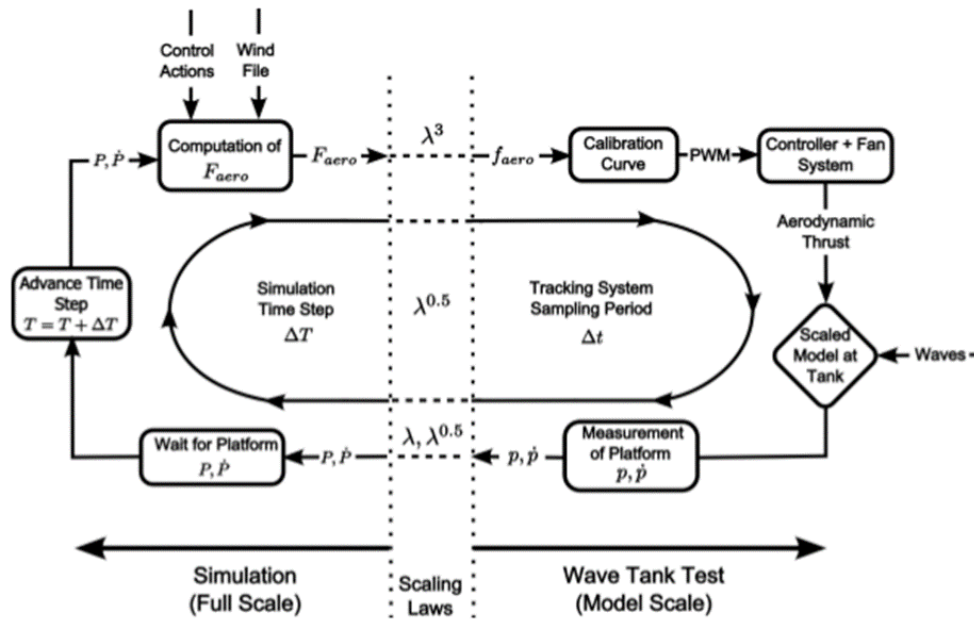


Figure 6. Diagram of the “Software-in-the-Loop” real-time hybrid test setup [54].

Hybrid testing with propeller actuators

Azcona et al [54], from CENER in Spain, were among the first researchers to use a propeller as an actuator for hybrid FOWT modelling. They have named their method Software-In-the-Loop (SIL). This method uses a single ducted propeller at hub height of the model. The diagram in Figure 7 indicates the hardware set-up of the SIL system.

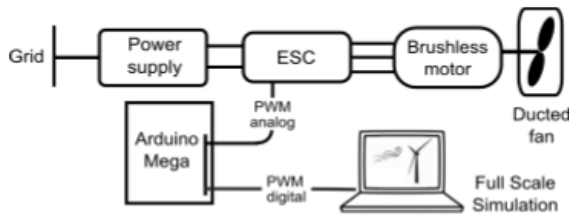


Figure 7. Hardware for the SIL setup [54].

The single propeller of the SIL system only emulates aerodynamic thrust, therefore the focus of their study was on platform pitch and surge response. Azcona et al used the SIL method to test a 1/40 scale model of the Concrete Star Wind Floater semi-submersible platform (Figure 8) at ECN, France. The turbine that was modelled during the experiments was a 6 MW turbine designed by Siemens. Azcona et al found that the platform surge and pitch response were closely matching the numerical models during static wind tests and free decay tests, demonstrating the ability of the SIL method to capture aerodynamic damping.

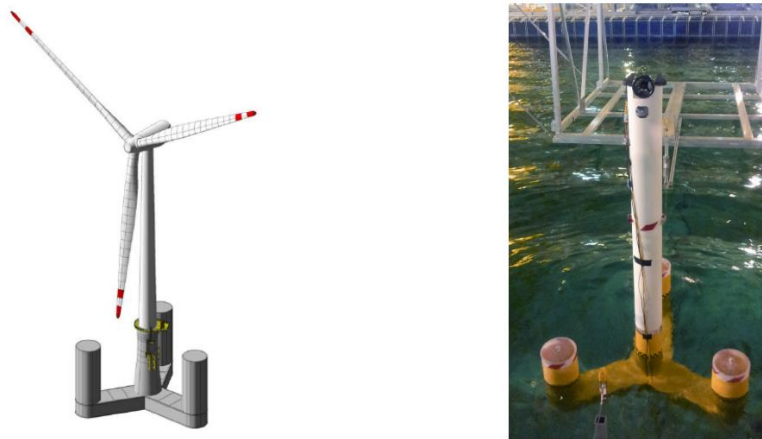


Figure 8. Full-scale CAD visualization (left) and model (right) of the OO-Star semisubmersible with ducted propeller [54].

In a separate campaign, researchers from CENER applied the SIL method to a 1/45 scale model of the DeepCwind semisubmersible platform, also at ECN [55], [56]. Second order hydrodynamics were included in the numerical models. Accuracy between experiments and numerical models had improved compared to the previous test campaign, when the second-order hydrodynamics were included in the numerical model. Best results were achieved for combined irregular wave and turbulent wind cases. In these cases, the aerodynamic excitations of the platform overshadow the second order hydrodynamic excitations for this type of platform.

Wright et al [57], fitted a ducted propeller on a 1/50 and a 1/30 scale model of a hexagonal braced TLP platform at IFREMER, France. Rather than using the SIL method, only steady thrust force was emulated. The aim of this study was to measure the difference in surge response in experiments with- and without spring dampers in the mooring tendons. The results showed that the surge amplitude increased but mooring tension decreased with the spring dampers added to the mooring tendons.

Desmond et al [58] tested a 1/36 scale model of the SCDnezy² (Figure 9), a semisubmersible FOWT design with two rotors and a single point mooring system, at Lir National Ocean Test Facility (NOTF), Ireland. Two ducted propellers were used to emulate steady wind loads and two stepper motors driving Froude scaled weights were used to emulate gyroscopic loads. Emulation of rotor thrust loads were found to have a significant impact on uncertainty, whereas the gyroscopic loads had limited impact.

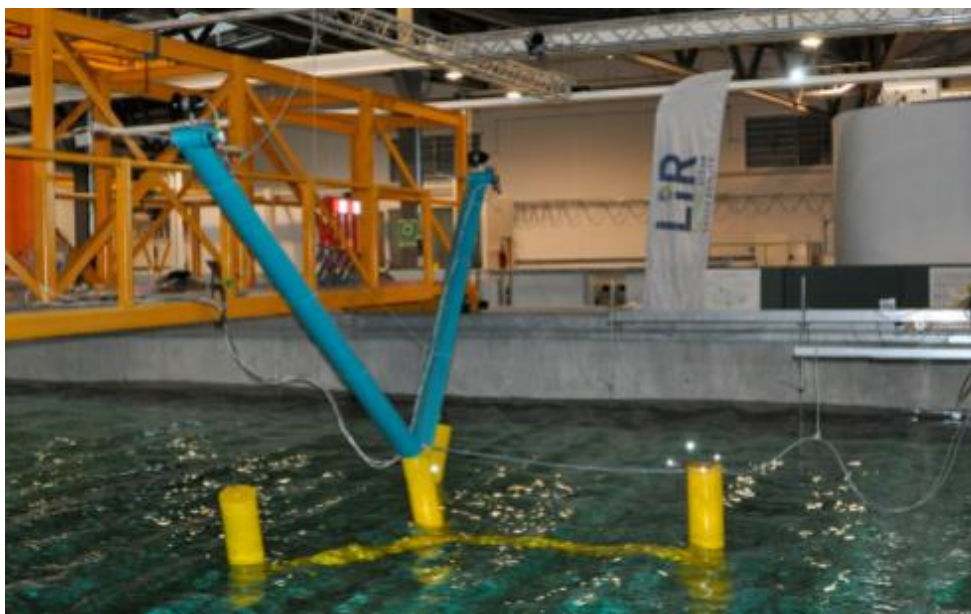


Figure 9. The SCDnezy² model in the basin at Lir NOTF [58].

Oguz et al [59], applied the SIL method to a 1/36 scale model of the Iberdrola TLP with the NREL 5 MW reference turbine at the University of Strathclyde, United Kingdom. The model was equipped with a single ducted propeller at hub height emulating aerodynamic thrust of the 5 MW turbine. The experiments showed that the platform response and tendon tensions were over predicted by the numerical models at the pitch- and surge natural periods.

Andersen [60] fitted a single propeller, using the hybrid method without real-time motion feedback, on a model of a generic semi-submersible model with three main floater columns and heave plates. The aerodynamic thrust loading was modelled using a turbulent wind time series of the DeepCwind semisubmersible FOWT, a comparable platform to the platform used in the experiments. This method is of lower fidelity and accuracy compared to the experiments by Azcona et al and Oguz et al, using the SIL method.

A similar conclusion was found by Matoug et al [61]. Although the focus of their study was the comparison of the DTU 10 MW horizontal-axis wind turbine and the WindQuest 10 MW vertical-axis wind turbine on the same platform, they repeated their testcases, using the hybrid test method, with and without SIL. The experimental results with SIL matched the numerical results better than the test cases without SIL. A 1/42 scale model of the Nautilus semisubmersible FOWT was used for the experiments.

Using a single propeller with the hybrid method means the modelling of aerodynamic loads is limited to thrust load only, and although this is by far the most important excitation mode, other aerodynamic loads such as rotor torque, gyroscopic momentum and 3P tower loading are not captured.

Otter et al [200] developed a multi-propeller actuator with six aerial drone propellers to emulate aerodynamic loads in multiple DOFs simultaneously (Figure 10). The device performs well for thrust and torque, however, it underperforms for aerodynamic pitch and yaw.

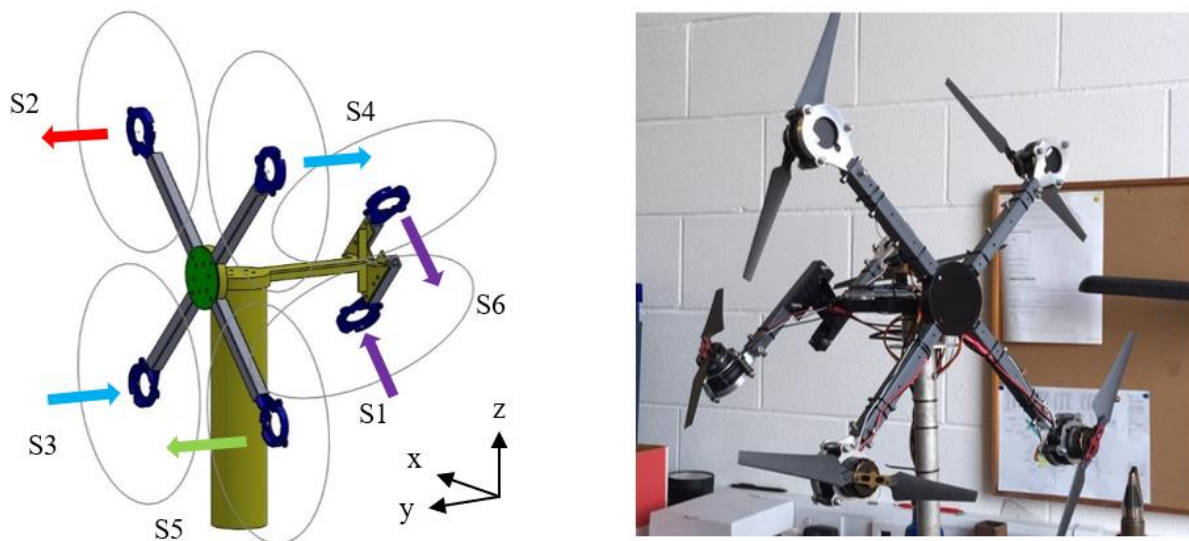


Figure 10. Multi-Propeller Actuator, the arrows indicate the thrust direction of the propellers [200].

Meseguer and Guanche [62], developed a similar device, which also uses recreational drone technology, with six propellers. Their multi-propeller actuator was used for an experimental test campaign of the TELWIND model FOWT [63] at Instituto Hidraulica Cantabria (IHC), Spain. Only constant wind loads were emulated during the tests.

Recently, researchers from CENER have developed a multi-propeller actuator with four propellers for multi-DOF emulation with SIL [64], which was used on a 1/50 scale model of the DeepCwind semisubmersible FOWT for the Marine Renewable Infrastructure Network for Enhancing Technologies 2 (MaRINET2) project at MARIN [65]. The focus of their studies was on the testing of control strategies with the improved SIL for the NREL 5MW turbine.

Kanner et al [66] applied hybrid testing to a semi-submersible model platform, based on the WindFloat

platform, called MIST, at University of California Berkeley, United States of America. Rather than modelling a conventional horizontal-axis turbine, they modelled two vertical-axis turbines on the platform. The tangential force developed by aerofoils on vertical-axis turbines was emulated by two counter-rotating rods in the horizontal plane, each driven by a propeller at one end of the rod. The drive train of the actuators included a gearbox and generator, converting the mechanical power of the rods into actual electrical power. By controlling the generators during the tests, Kanner et al achieved limited yaw orientation of the platform to optimize power production of the turbines.

Hybrid testing with dynamic cable winch actuators.

Researchers from SINTEF, Norway, have performed a series of experiments [67]–[69] using real-time hybrid testing with a 1/30 scale braceless semi-submersible FOWT model [70] and the NREL 5 MW turbine. The researchers from SINTEF have named their method Real-Time Hybrid Model (ReaTHM) testing and use a square frame at hub height of the model connected with the winch cables. A comparison of the experimental results with numerical models is presented by Karimirad et al [71]. Figure 11 shows the model with the top frame. The arrows indicate the direction of actuation of each dynamic cable winch. An earlier quantification study [72] found the gyroscopic moments and heave response due to aerodynamic forces to be negligible for this type of platform. The SINTEF researchers therefore opted to emulate a limited number of aerodynamic loads. Waves and current, during the experiments were modelled physically. The numerical wind field was generated in TurbSim and the full-scale aerodynamic loads were calculated with AeroDyn.

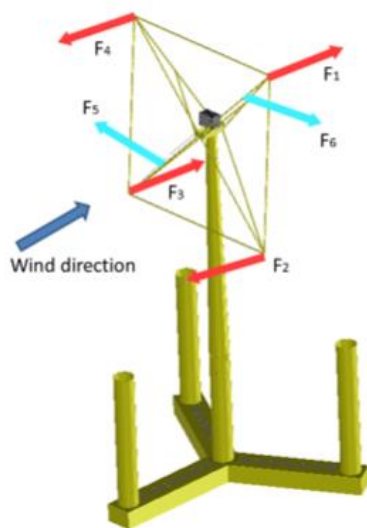


Figure 11. The semisubmersible model with top frame for the ReaTHM setup [67].

Thys et al [73] used the ReaTHM test method at SINTEF to test a physical 1/36 scale model of the Nautilus semisubmersible platform with the DTU 10 MW turbine, as part of the LIFES50+ project [74]. An adjusted top frame and cable layout was used for this test campaign, and 3P frequency and first tower bending frequency were added in addition to the aerodynamic loads emulated on the 5 MW model platform.

Chabaud et al [75], compared the ReaTHM methods used for the test campaigns of the 5 MW and 10 MW model platforms at SINTEF and gave a theoretical overview of the allocation of tension for the actuation cables for the two methods. Where both methods provided similar results in terms of accuracy, the method used for the 10 MW platform provided higher flexibility allowing for a higher number of aerodynamic loads to be included in the tests with the same number of cables and winches. However, the higher flexibility comes at the expense of higher cable tensions and a larger test area as the winches need to be spaced wider apart.

Hall and Goupee [76] used dynamic cable winches for hybrid testing of a 1/50 scale model of the DeepCwind semisubmersible platform, which was also equipped with a geometrically scaled rotor and

low Reynolds adjusted blades. They validated the hybrid method by disconnecting the actuator cables and repeating the steady wind case with physical wind generated above the basin, at the University of Maine, United States America. In contrast to the SINTEF test campaigns, Hall and Goupee opted to simplify the test setup by only emulating the aerodynamic thrust in the hybrid tests using two rather than six cable winches. Using a windward and leeward winch cable connected at hub height allows for accurate control of aerodynamic thrust emulation. The results of the hybrid tests and full physical regular wind-wave tests matched closely, validating the hybrid approach. Hall and Goupee found that introducing wind turbulence in the hybrid experiments added a noticeable amount of excitation, accurately reproducing aerodynamic damping found with the numerical models, which was difficult to reproduce with the full physical wind-wave experiments.

Antonutti et al [77] used dynamic cable winches for hybrid testing with SIL of a 1/35 scale model of the Naval Energies semisubmersible FOWT with the Haliade 6 MW turbine at MARIN. Similar to the SINTEF campaigns, Antonutti et al used a cross-shaped metal frame with four front wires and one back wire. This enabled actuation in the surge, pitch and yaw DOFs. For operational and severe sea-states the experimental results were found to match the numerical results closely with combined wave and wind loads.

Some advantages and disadvantages of dynamic cable winches compared to propeller actuators are listed in Table 4.

Table 4. Advantages, and disadvantages of propeller vs winches.

	Advantage	Disadvantage
Propellers	<ul style="list-style-type: none"> • Effective simulation of thrust loads • Integrated on the model, small footprint on the test area • Simple control. 	<ul style="list-style-type: none"> • Difficult to effectively simulate aerodynamic moments • Source of high-frequency vibrations and, therefore, systematic uncertainty.
Cable winches	<ul style="list-style-type: none"> • Effective simulation of thrust and aerodynamic moments • Low vibration levels, less systematic uncertainty 	<ul style="list-style-type: none"> • Winches are land-based, large footprint on test area • Control of winches is complex compared to propellers

Hybrid testing in wind tunnels.

Another approach to hybrid testing of FOWTs is to use SIL to numerically represent the hydrodynamics of the system, as opposed to the aerodynamics. This approach enables validation of aerodynamic forces in an environment with superior wind quality compared to wind generation over a wave basin, while allowing for examination of these aerodynamic forces under motion typical of a FOWT. This is particularly useful when studying the evolution of turbine wake of FOWTs, and how it may affect downwind turbines and farm layouts.

Schliffke et al [78] used a simple, 1/500 scale model of the FLOATGEN FOWT in a small wind tunnel at ECN, France to study unsteady aerodynamics and wake development. The model consisted of a porous disc at hub height mounted on a small rig to simulate regular surge motion of the platform. Results showed that the surge motions did not change mean velocities in the wake, however, turbulence intensity in the wake was modified.

Rockel et al [79], [80] performed experiments with two performance scaled, 1/400 scale wind turbine models of a typical horizontal-axis wind turbine with 80 meter rotor diameter in the wind tunnel at Portland State University, United States of America. In the first study the wake of a bottom-fixed model was compared with the wake of a FOWT model that was allowed to oscillate freely in the pitch DOF by mounting the model in a gimbal. In the second study both turbine models were used in tandem in the wind tunnel.

Bayati et al [81]–[83] used a Hardware-in-the-Loop (HIL) setup with a performance scaled, 1/75 scale model of the DTU 10 MW turbine on a 2-DOF rig to simulate surge and pitch motions of the OC5 semisubmersible FOWT in the wind tunnel of Politecnico di Milano, Italy. Platform kinematics were calculated and applied in real-time. The HIL setup uses load cells, dynamometers, accelerometers, linear variable displacement transducers, and a laser displacement sensor for a position feedback signal to update the numerical simulation of the platform motions for each time-step. The motion feedback combined with increased DOFs allows for a higher-fidelity test setup compared to the abovementioned studies by Schliffke et al and Rockel et al.

In follow-up studies Bayati et al [85]–[87] used a physical 1/75 scale, performance-scaled model of the DTU 10 MW turbine on a custom-designed 6-DOF robot, named Hexafloat, in the wind tunnel of Politecnico di Milano, Italy, rather than the 2-DOF rig. The platform hydrodynamics emulated by the 6-DOF Hexafloat were based on an ad-hoc model FOWT initially, and on the OO Star semisubmersible FOWT and the Triple Spar FOWT for later tests. The applied wind velocity in the wind tunnel was increased by a factor of 3 to match the Reynolds number at full scale as closely as possible. The higher DOFs and addition of turbine control equipment allowed Bayati et al to also investigate turbine control routines. The results of the experiments with both the 2-DOF rig and Hexafloat showed close agreement with the wake measurements and platform dynamics found with numerical models.

Thys et al [88] performed scale model hybrid tests for the OO-Star and Nautilus FOWTs with the DTU 10 MW turbine in the wave basin at SINTEF and in the wind tunnel at Politecnico di Milano, Italy, for a comparative study. Wind tunnel experiments of the 1/75 scale model of the DTU 10 MW turbine in combination with the Hexafloat were first performed to validate the aerodynamic model. Next, the validated aerodynamic model was used with a 1/36 scale model of the platform and dynamic winch actuators to emulate wind loads in the wave basin for calibration of the platform and hydrodynamic model.

Arnal et al [89] used a 6-DOF Hexapod with a propeller actuator, rather than the wind tunnel, to simulate the NREL 5 MW turbine with the DeepCwind semisubmersible platform and the Hywind spar platform, and the DTU 10 MW turbine with the Triple Spar platform at ECN, France. They found that, at a scale of 1/30, high frequency aerodynamic loads could be emulated accurately with their system.

Comparison of test methods: full physical vs hybrid, in laboratory wave basins

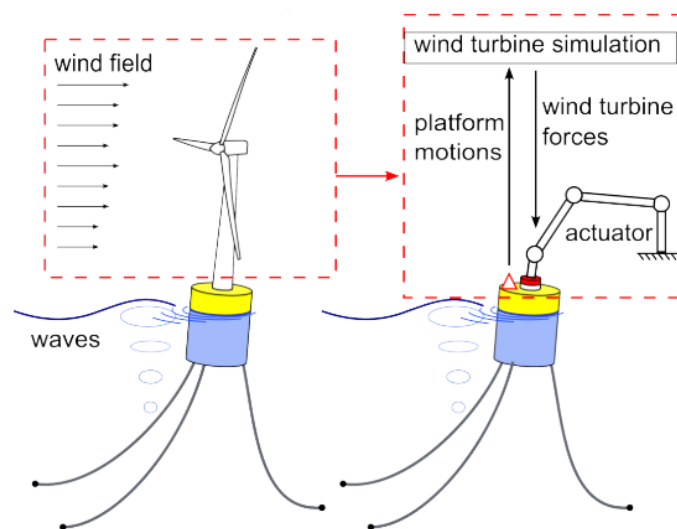


Figure 12. Full physical testing (left) vs hybrid testing (right) [90].

Generating physical wind in laboratory basins requires large wind generation installations and large amounts of energy to run said installations, making them expensive to operate. Furthermore, high-quality wind generation and accurate simulation of wind gradients and turbulence in the wind field are difficult to achieve other than in wind tunnels. A typical setup for an above-basin wind generation system consists of a bank of fans arrayed in several rows and columns, pumping the air through ducts

with screens, honeycomb mesh, and nozzles over the basin. The screens and honeycomb mesh reduce the turbulence of the outflowing air, and the nozzle directs the flow to an area that can cover the rotor. Stochastic wind can be simulated by varying the revolutions per minute of the fans during tests, and vertical shear can be simulated by controlling each row of fans separately [37]. Accurately measuring and mapping the wind field is important to determine the best location for the model relative to the nozzle. This procedure is described for the MARIN wind setup in de Ridder et al [11] and for DHI in Madsen et al [48]. They showed that it is difficult to control the boundaries of the wind field and circulation of the airflow once it exits the nozzle. Inconsistencies in the screens and fan motors etc. can be mapped and accounted for during analysis of test results. However, the inability to control the airflow over the basin, unlike in wind tunnels, will decrease the ability of accurate repeatability of the tests, adding uncertainty in the test method.

An advantage of performance-scaled turbines on FOWT models in combination with applied wind generated above the basin is the ability to maintain the correct thrust coefficient and TSR in a Froude-scaled wind environment. This method also captures the effects of rotor gyroscopic moments, rotor torque and aerodynamic damping, and it is possible to implement turbine control. Another advantage is that it is likely that unexpected aerodynamic phenomena and hydrodynamic response, which are not captured with the numerical model, will be captured during the physical experiments. However, the low-Reynolds modifications make it difficult to also model the power coefficient and torque characteristics of the turbine accurately, limiting the scalability of blade pitch control and the ability to capture aerodynamic damping accurately [74], [76]. Other disadvantages are the high costs of developing a modified model turbine, and the requirement of a bespoke scaled model turbine for each different design and scale [37].

Hybrid testing in wave basins has the benefit that it does not require physical wind and current generation in testing facilities that do not have such capabilities. Furthermore, hybrid testing allows for the implementation of wind turbulence, turbine control strategy and aerodynamic damping, and any turbine type can be simulated regardless of the scale, making it far more versatile and cheaper compared to full physical testing.

However, a hybrid test setup is a complex system; fidelity of the test method and accuracy of test results can be influenced by a number of factors such as the force actuation and motion tracking.

The accuracy of wind emulation will depend on the type and number of actuators. However, the mechanical actuators are easier to control than physically generated wind [76]. Careful calibration of the actuators and quantification of actuator inaccuracies provides high experimental repeatability, as was found by Meseguer and Guanche [62] and Bachynski et al [68].

With hybrid FOWT testing, the hydrodynamic module of the aero-hydro-servo-elastic tool used for the numerical substructure is de-coupled, and instead the motion response data of the physical model received from the motion tracking system is used as the hydrodynamic input to calculate the next simulation step, as described in section 3.3. The motion tracking system will therefore require high accuracy of position measurements. Furthermore, it will require a high sampling rate and must be able to operate in a wet environment.

A certain amount of system latency during hybrid testing is unavoidable. Each step in the hybrid testing loop – simulation, actuation, motion tracking and feedback – causes a system delay. An appropriate simulation time-step at scale for hybrid modelling must be determined. Within this time-step the actuator must have sufficient bandwidth to deliver the required load at the right frequency, and the motion tracking sampling rate must be high enough to feed the position data back to the numerical code to calculate the required actuator load for the next time-step. To keep the latency at acceptable levels within each time-step, the actuator will have to emulate the required loads faster than the numerical simulation takes to calculate the loads for each time-step. It becomes apparent then that the computing system will require high processing power.

In the design of the experiments, the appropriate time-step, number of actuators etc. used for hybrid modelling will depend on the modes of interest to be investigated. Sensitivity studies, e.g. Hall et al

[90], [91] and Bachynski et al [72], will give an indication of the required actuation forces and number of actuators, tolerance levels of inaccuracy and latency. A higher number of actuators will increase the fidelity of the hybrid test method, as the three-dimensional wind field can be represented more accurately. However, a higher number of actuators will result in a more complex system and a higher level of uncertainty.

Another disadvantage of hybrid testing compared to full physical testing is that aerodynamic phenomena which are not captured by the numerical model, will not be simulated during the experiments. As a result, the potential hydrodynamic response of the platform to said phenomena may not be captured either. One example is dynamic inflow, this effect cannot be captured effectively by quasi-steady BEMT tools, but the more computationally intensive PF and CFD solvers are capable of capturing this effect. This has implications for hybrid testing of FOWTs. It means that unsteady dynamics might not be captured during hybrid testing when the computationally efficient quasi-steady BEMT tools are used to compute the aerodynamic loads for each time-step. Consequently, the resulting platform motion response and blade pitch control effects from dynamic inflow effects may not be captured either. As mentioned in section 2.5, BEMT models can be corrected by adding simple dynamic inflow models. However, such improved BEMT tools have not been applied during hybrid tests to date. Furthermore, the actuators used in hybrid test experiments need sufficient bandwidth to replicate any control strategy designed to counter the effects of dynamic inflow. Of course, the same is true for control equipment used during full physical experiments.

A comparative study was performed by Gueydon et al [92] with a 1/50 scale model of a TLP FOWT and the NREL 5 MW turbine at MARIN. Combined wind, wave and current tests were first performed with the full physical method and then repeated with a real-time hybrid method using dynamic cable winches and SIL. Both methods showed comparable results up to 0.55 rad/second. Above this frequency the dynamic cable winches used in these tests were not able to deliver demanded thrust without a significant delay and Gueydon et al found it problematic to accurately assess the tendon tensions. They concluded that for FOWTs that respond to high frequency, such as TLPs, the use of winches for hybrid testing may not be adequate.

Table 5. Advantages and disadvantages of the full physical methods and hybrid methods.

	Advantage	Disadvantage
Full physical modelling	<ul style="list-style-type: none"> • Models aerodynamic thrust, torque and gyroscopic moment • Captures aerodynamic damping • Turbine control can be implemented 	<ul style="list-style-type: none"> • Requires expensive and bulky wind generation equipment • Difficult to generate high quality laminar steady wind • Difficult to generate stochastic wind with good repeatability • Requires unique turbine model for each turbine design and scale • Rotor often requires the aid of an electric motor to reach correct TSR
Hybrid modelling	<ul style="list-style-type: none"> • Depending on number of actuators it is possible to emulate thrust, torque and gyroscopic moment with good repeatability • Captures aerodynamic damping • Turbine control can be implemented • Stochastic wind loads can be implemented without great difficulty • Versatile, can be used for any type of turbine or scale • Requires less space and considerably cheaper than wind generation system 	<ul style="list-style-type: none"> • System latency • Multiple actuators required to emulate all aerodynamic loads, adds complexity and uncertainty • Phenomena not simulated with the numerical model will not be captured during testing

Both the performance scaled full physical method and the multi-actuator hybrid method can be considered high-fidelity test methods. The level of fidelity is likely somewhat higher for the full physical method, however, as aerodynamic loads which are not captured by the numerical model are still likely to be captured during testing, unlike during hybrid testing. The choice of test method will therefore be a trade-off between budget and fidelity/uncertainty. The advantages and disadvantages of full physical testing and hybrid testing are summarized in table 5.

Discussion

The state-of-the-art of numerical and experimental modelling approaches available for the design of FOWTs cover every aspect of aero/hydro/servo/elastic modelling. However, there are still inconsistencies in accuracy between the different numerical codes, as shown in the OC5 project and studies by Roberston et al [103], [133]. Additionally, a level of uncertainty in experimental methods is unavoidable [87], [101], [136], [200]. The applicability of an approach will be case dependent. The configuration of the FOWT design and the goal of the analysis will dictate fidelity and type of modelling approach that is warranted. The design process for a FOWT is a multi-step process. Eventually, a detailed loads analysis is needed at the component (member) level. However, typically, the global analysis is used with simpler models, and then, a detailed analysis focuses on a few load cases and perhaps a few points in the structure.

In the continuing drive for reduction of Levelized Cost of Energy (LCOE) of FOWT technology, platform designers may seek to replace some of the physical test stages in the design-to-prototype process with high-fidelity numerical modelling. The authors would caution against such an approach. Numerical modelling tools show some limitations in accurately modelling the physics of floating wind designs for some conditions and configurations (as discussed in the IEA Wind Task 30 – OC projects [103], [134]), and there is also a lack of sufficient measurements to validate their capabilities in realistic ocean conditions. The limited deployment of full-scale FOWTs to date has resulted in only a few publicly available data sets, e.g. Cermelli et al [10], ORE Catapult [201], of dynamic response and fatigue life. The continued upscaling of turbine sizes is another factor in the drive for LCOE reduction. However, turbines of that size, and the impact of environmental loads on their components [202], have not been tried and tested yet. High-fidelity tools, such as CFD tools, have greater accuracy but are cumbersome tools and still require validation. Therefore, the authors believe that the traditional approach, of combining numerical modelling with scale model testing, is still the preferred approach for FOWT engineering.

As Gueydon et al [108] highlighted, improved accuracy of numerical tools and concise quantification of uncertainty for experimental tools can be achieved if “hydrodynamic testing facilities engage with more critical comparisons of results obtained from all available FOWT testing techniques”, and validation of both numerical and experimental tools would also benefit from the inclusion of test data from full-scale prototypes in real ocean-conditions. However, it should be considered that whilst full-scale turbines continue to get larger, the full physical test method will become increasingly impractical. As rotor diameters continue to grow, either the flow field of wind generators over wave basins will have to get larger too, or researchers will have to work with ever-smaller scales, which will exacerbate the scaling difficulties and increase the significance of sensor uncertainty. The authors are of the opinion that hybrid testing will become the preferred experimental method for FOWT modelling as bulky and expensive wind generation equipment is not needed, nor is it necessary to construct a physical model of the turbine rotor for each new test campaign in wave basins. Instead, the actuator emulates the wind loads, which a) it can do cheaper, and b) it can do for any turbine at a wide range of scales, making hybrid testing more versatile and more practical than the full physical method. The same could be said for hybrid tests in wind tunnels. Although the turbine is a physical model in this case, hydrodynamic loads are emulated by the actuator and any type of platform at any scale can easily be simulated.

To improve the fidelity and accuracy, identifying the limitations and quantifying the uncertainty of hybrid systems will therefore be essential. Comparative studies such as Hall and Goupee [76] and Gueydon et al [92], for a wide variety of platform types and load emulation systems are strongly recommended. Testing the same platform with the full physical method and the hybrid method, at a scale that is practical for the test facility involved, will help to identify the limitations of both systems.

Unsteady aerodynamics can be pronounced for FOWTs due to platform motions and large blade deflections, particularly with large rotor diameters. Sensitivity studies could reveal whether the effects of unsteady aerodynamics are noticeable and determine whether the effects should be emulated during hybrid testing. For example, Lupton et al [203] found that the effect of blade deflections on platform response is limited. This might suggest that blade deflections could be ignored during hybrid testing if platform dynamics are the quantity of interest. However, if for example structural dynamics of the tower are a quantity of interest, the effect of blade deflections should be included in the hybrid tests. The question then is whether the real-time simulation software used during hybrid testing can capture this effect, and whether the actuator is able to emulate it. The majority of the experimental campaigns mentioned in section 3.3.1, 3.3.2 and 3.3.3 used FAST as the real-time simulation software during hybrid testing, FAST is a CPU-efficient tool, i.e., simulation time is fast enough to keep latency at an acceptable level for each time-step, and therefore a suitable real-time engineering tool for hybrid testing. AeroDyn, FAST's aerodynamic module, uses a combination of BEMT and GDW to model dynamic inflow. However, with the introduction of the FVW based module cOnvecting LAgrangian Filaments (OLAF), the of capture dynamic inflow and unsteady dynamics, and computational efficiency during hybrid testing may be improved. However, this has not yet been tested in practice. Tentative steps, e.g. Chen et al [204] are being taken to replace the real-time simulation tool with an Artificial Neural Network (ANN) to predict wind loads. The use of ANN has the potential to improve computational efficiency during hybrid testing.

Furthermore, the majority of FOWT test campaigns focus on combined wave and wind loads. Although several studies found in the literature mention the addition of a current during testing there is little mention of the resulting effects of current. However, some numerical studies, e.g. Chen and Basu [205], suggest there is significant impact of current on mooring tensions and fatigue loads. Therefore, further experimental investigation of the effects of current on the dynamic response and fatigue life of FOWTs is recommended.

Finally, the structural dynamics of FOWTs are generally investigated numerically and several examples can be found in the literature where the tower elasticity is modelled physically. However, the elasticity of the platform is generally not considered for physical experiments. Scaling effects will mean the physical modelling of platform elasticity is challenging and, in most cases, modelling the platform as a rigid body will give acceptable results for FOWT dynamics. However, as turbine sizes continue to get larger, platform sizes will follow a similar trend. As a result, platform structural dynamics could become more influential and should not be ignored during experimental modelling.

The research trends and gaps observed through this review are summarized here.

- As turbine sizes continue to grow, full physical testing of FOWTs at scale will become impractical. Comparative studies between full physical testing and hybrid testing, for the same platform under the same load conditions, are limited, e.g. Hall and Goupee [76] and Gueydon et al [92]. More comparative studies for different kinds of platforms and different types of actuators are desirable to identify the limitations of both methods.
- Studies of unsteady aerodynamics for FOWTs have increased in recent years, both numerically, e.g. Lee and Lee [93] and experimentally, e.g. Belloli et al [87]. However, mention of computationally efficient real-time simulation tools to capture this effect during hybrid testing in wave basins is lacking in the literature.
- The effect of current on platform dynamics, mooring tensions and fatigue life found experimentally is also lacking in the literature. Numerical studies suggest the effects could be significant, therefore further experimental investigation is desirable.
- As turbine sizes, and consequently, platform sizes continue to grow, structural dynamics of the platform could become more influential on overall FOWT dynamics. However, results of platform structural dynamics during scale model FOWT experiments are also lacking in the literature.
- The use of both numerical and experimental tools is generally good practice for the validation of any design, but in the case of FOWT modelling is essential. The confidence in numerical models only is not yet at an acceptable level due to the inaccuracy of the engineering tools and

the limited availability of FOWT prototype data in real ocean conditions with which numerical models could be validated.

- There is, however, an ongoing drive to improve fidelity and computational efficiency, particularly of engineering tools, e.g. Lemmer et al [138].

After all this information the reader might ask, “So, what is the best modelling technique or tool to design a FOWT?”

The best choice will generally be case-specific, and the likelihood is that several techniques and tools will be used over the course of the design process. However, recommendations are provided here, which can serve as a guideline for the choice of modelling technique and tool. The first consideration will be the available budget of the designer or researcher; in general, the higher the fidelity of the method, the larger budget requirements will be. This is valid for both numerical and experimental methods. Another major consideration is the stage of the design process. For numerical modelling the standard practice is as follows:

- ✓ Low-fidelity tools are used at the early design stages and for sizing purposes. Typically, linear frequency-domain models with high computational efficiency and fast simulation times are used. A few examples are mentioned in section 2.2.1.
- ✓ Mid-fidelity tools, referred to as ‘engineering tools’, are used at the more advanced stages for global dynamics analysis of the FOWT design under operational and extreme conditions. Typically, these tools use nonlinear time-domain models. Accuracy of these tools will generally be higher compared to the low-fidelity models, yet efficiency is lower. Some popular choices of engineering tools are summarized in Table 2.
- ✓ High-fidelity tools are used at the final stages of the design and for detailed investigations. These tools use complex nonlinear time-domain models, and their accuracy is considered higher than that of the low- and mid-fidelity tools. However, computational efficiency is low for these tools. Some popular examples are mentioned in Table 3.

For scale model testing, the consideration will be between choosing either full physical testing or hybrid testing. The recommendations are determined by answering the following set of questions:

1) Does the test facility have equipment to generate the required environmental loads?

- ✓ Yes: Full physical is the preferred method
- ✓ No, or partially: Hybrid is the preferred method

2) Can the investigated phenomena be captured numerically?

- ✓ Yes: Hybrid is the preferred method
- ✓ No: Full physical is the preferred method

3) Is the scale of the model practical to handle for the test facility?

- ✓ Yes: Both methods can be used
- ✓ No: Hybrid is the preferred method

Next, if the choice falls on the hybrid method there are some more distinctions to be considered:

4) Are aerodynamics or hydrodynamics the focus of the investigation?

- ✓ Aerodynamics: Hybrid testing in wind tunnels is the preferred method
- ✓ Hydrodynamics: Hybrid testing in wave basins is the preferred method

5) for wave basin testing, what type of actuator is most suitable?

- ✓ Thrust loading only: A simple, on-board propeller actuator is most suitable
- ✓ Thrust + aerodynamic moments: Dynamic winch actuators are most suitable

Conclusion

This paper gives an overview of the modelling methods for FOWTs. The first part reviews numerical modelling methods and software. The choice of computational method and software will generally be a trade-off between accuracy and computational efficiency. A computational method is considered efficient if it is able to complete a simulation within a timeframe that is acceptable for the user's purpose using standard computing equipment. Low-fidelity and computationally efficient methods, such as linear frequency-domain solvers, are used at the initial design stages of FOWTs for sizing purposes. Mid-fidelity methods are used for global dynamics analysis of FOWTs. Long time-domain simulations of FOWT dynamics are performed with engineering tools, coupled hydro-aero-servo-elastic solvers using computationally efficient methods such as PF and BEMT. Code-to-code comparisons and uncertainty assessments have shown that, despite representing the state-of-the-art, accuracy of the majority of numerical engineering tools needs improving. In particular for the prediction of low-frequency loads and motion response in the surge and pitch DOFs of FOWTs. High-fidelity methods are used at the final design stages and for detailed analysis. Specific load cases, such as slamming events due to non-linear waves, are best modelled with high-fidelity methods such as CFD. The main disadvantage of high-fidelity software is their low computational efficiency. High-fidelity software is also used for the tuning of hydrodynamic coefficients used with mid-fidelity engineering tools.

The second part gives an overview of physical test methods, which are used to validate and calibrate the numerical models. Physical test methods can be classified in two categories: full physical testing and hybrid testing. A review is given of experimental campaigns for both methods, and the advantages and disadvantages of both experimental methods are outlined. The choice of experimental method is a consideration between test facility, budget, and uncertainty associated with the respective test methods. The full physical method with performance scaled turbines can model all aspects and phenomena of the FOWT, such as aerodynamic damping, for example. It also has the potential to identify unexpected aerodynamic phenomena which are not captured by the numerical model, but may have an effect on overall dynamics of the FOWT. For example, dynamic inflow is not effectively captured by quasi-steady BEMT. However, the full physical method is expensive and requires a dedicated physical model for each turbine design. The hybrid test method is cheaper and more versatile than the full physical method. It does not require bulky wind generation equipment and any type of turbine at a range of scales can be simulated with the same actuator when used in wave basins. With hybrid tests in wind tunnels, it is the hydrodynamic loading which is emulated and any type of platform at any scale can be simulated without the need for a dedicated scale model platform.

The final part identifies trends and gaps in current FOWT related research, such as a desire for more comparative studies between the full physical and hybrid test methods, and the improvement of the accuracy of numerical engineering tools. Recommendations on which modelling method or tool to use, both numerically and experimentally, are provided in the discussion in section 4.

Several factors, such as the accuracy of numerical tools, limited availability of prototype data in real ocean conditions, and the continued upscaling of turbine sizes, contribute to the fact that the traditional modelling approach of numerical modelling validated by physical scale model testing remains essential for FOWT designs.

References

- [1] DNV-GL. Floating wind: the power to commercialize n.d. <https://www.dnv.com/focus-areas/floating-offshore-wind/commercialize-floating-wind-report.html> (accessed March 5, 2021).
- [2] Horizon 2020. Technology readiness levels (TRL). 2014.
- [3] Robertson AN, Jonkman JM, Goupee AJ, Coulling AJ, Prowell I, Browning J, et al. Summary of conclusions and recommendations drawn from the deepwind scaled floating offshore wind system test campaign. Proc. Int. Conf. Offshore Mech. Arct. Eng. - OMAE, 2013. <https://doi.org/10.1115/OMAE2013-10817>.

- [4] Muller K, Sandner F, Bredmose H, Azcona J, Manjock A, Pereira R. Improved tank test procedures for scaled floating offshore wind turbines. *Int Wind Eng Conf (IWECC 2014)* 2014;1–12.
- [5] Stewart G, Muskulus M. A Review and Comparison of Floating Offshore Wind Turbine Model Experiments. *Energy Procedia* 2016;94:227–31. <https://doi.org/10.1016/j.egypro.2016.09.228>.
- [6] Gueydon S, Bayati I, de Ridder EJ. Discussion of solutions for basin model tests of FOWTs in combined waves and wind. *Ocean Eng* 2020;209:107288. <https://doi.org/10.1016/j.oceaneng.2020.107288>.
- [7] Cordle A, Jonkman J. State of the art in floating wind turbine design tools. *Proc Int Offshore Polar Eng Conf* 2011:367–74.
- [8] Joao Cruz MA. *Floating Offshore Wind Energy: The Next Generation of Wind Energy*. Springer International Publishing Switzerland; 2016. <https://doi.org/DOI.10.1007/978-3-319-29398-1>.
- [9] Jaksic V, O'Shea R, Cahill P, Murphy J, Mandic DP, Pakrashi V. Dynamic response signatures of a scaled model platform for floating wind turbines in an ocean wave basin. *Philos Trans R Soc A Math Phys Eng Sci* 2015. <https://doi.org/10.1098/rsta.2014.0078>.
- [10] Jaksic V, Wright CS, Murphy J, Afeef C, Ali SF, Mandic DP, et al. Dynamic response mitigation of floating wind turbine platforms using tuned liquid column dampers. *Philos Trans R Soc A Math Phys Eng Sci* 2015. <https://doi.org/10.1098/rsta.2014.0079>.
- [11] Nielsen JS, Sørensen JD. Methods for risk-based planning of O&M of wind turbines. *Energies* 2014. <https://doi.org/10.3390/en7106645>.
- [12] Arrigan J, Pakrashi V, Basu B, Nagarajaiah S. Control of flapwise vibrations in wind turbine blades using semi-active tuned mass dampers. *Struct Control Heal Monit* 2011. <https://doi.org/10.1002/stc.404>.
- [13] Velarde J, Mankar A, Kramhøft C, Sørensen JD. Probabilistic calibration of fatigue safety factors for offshore wind turbine concrete structures. *Eng Struct* 2020. <https://doi.org/10.1016/j.engstruct.2020.111090>.
- [14] Rocher B, Schoefs F, François M, Salou A, Caouissin AL. A two-scale probabilistic time-dependent fatigue model for offshore steel wind turbines. *Int J Fatigue* 2020. <https://doi.org/10.1016/j.ijfatigue.2020.105620>.
- [15] Bhattacharya S, Lombardi D, Amani S, Aleem M, Prakhya G, Adhikari S, et al. Physical modelling of offshore wind turbine foundations for trl (Technology readiness level) studies. *J Mar Sci Eng* 2021. <https://doi.org/10.3390/jmse9060589>.
- [16] O'Donnell D, Murphy J, Desmond CJ, Jaksic V, Pakrashi V. Tuned Liquid Column Damper based Reduction of Dynamic Responses of Scaled Offshore Platforms in Different Ocean Wave Basins. *J Phys Conf Ser* 2017;842. <https://doi.org/10.1088/1742-6596/842/1/012043>.
- [17] Agarwal P, Manuel L. Simulation of offshore wind turbine response for long-term extreme load prediction. *Eng Struct* 2009. <https://doi.org/10.1016/j.engstruct.2009.04.002>.
- [18] Larsen JW, Iwankiewicz R, Nielsen SRK. Nonlinear stochastic stability analysis of wind turbine wings by Monte Carlo simulations. *Probabilistic Eng Mech* 2007. <https://doi.org/10.1016/j.probengmech.2006.11.002>.
- [19] Hegseth JM, Bachynski EE. A semi-analytical frequency domain model for efficient design evaluation of spar floating wind turbines. *Mar Struct* 2019. <https://doi.org/10.1016/j.marstruc.2018.10.015>.

- [20] Karimi M, Hall M, Buckham B, Crawford C. A multi-objective design optimization approach for floating offshore wind turbine support structures. *J Ocean Eng Mar Energy* 2017. <https://doi.org/10.1007/s40722-016-0072-4>.
- [21] Pegalajar-Jurado A, Borg M, Bredmose H. An efficient frequency-domain model for quick load analysis of floating offshore wind turbines. *Wind Energy Sci* 2018. <https://doi.org/10.5194/wes-3-693-2018>.
- [22] NREL. FAST n.d. <https://www.nrel.gov/wind/nwtc/fast.html> (accessed November 2, 2021).
- [23] Jonkman JM, Wright AD, Hayman GJ, Robertson AN. Full-system linearization for floating offshore wind turbines in OpenFAST. *ASME 2018 1st Int. Offshore Wind Tech. Conf. IOWTC 2018*, 2018. <https://doi.org/10.1115/IOWTC2018-1025>.
- [24] DTU. HAWC2 n.d. www.hawc2.dk (accessed April 28, 2020).
- [25] MARINTEK. SIMA. 2016 n.d. www.windbench.net/models-offshore/sima (accessed April 28, 2020).
- [26] DNV. Bladed n.d. <https://www.dnv.com/services/wind-turbine-design-software-bladed-3775> (accessed November 3, 2021).
- [27] Dassault Systems. SIMPACK Multibody System Simulation Software n.d. <https://www.3ds.com/products-services/simulia/products/simpack/product-modules/wind-modules/> (accessed June 16, 2021).
- [28] Orcina. Orcaflex n.d. <https://www.orcina.com/webhelp/OrcaFlex/Default.htm> (accessed April 28, 2020).
- [29] Wood Group. Flexcom n.d. <https://www.woodplc.com/capabilities/digital-and-technology/software,-applications-and-analytics/flexcom> (accessed April 28, 2020).
- [30] Ormberg H, Bachynski EE. Global analysis of floating wind turbines: Code development, model sensitivity and benchmark study. *Proc Int Offshore Polar Eng Conf 2012*;4:366–73.
- [31] Robertson A, Jonkman J, Vorpahl F, Popko W, Qvist J, Frøyd L, et al. Offshore code comparison collaboration continuation within IEA wind task 30: Phase II results regarding a floating semisubmersible wind system. *Proc Int Conf Offshore Mech Arct Eng - OMAE 2014*;9B. <https://doi.org/10.1115/OMAE2014-24040>.
- [32] Robertson AN, Wendt F, Jonkman JM, Popko W, Dagher H, Gueydon S, et al. OC5 Project Phase II: Validation of Global Loads of the DeepCwind Floating Semisubmersible Wind Turbine. *Energy Procedia* 2017;137:38–57. <https://doi.org/10.1016/j.egypro.2017.10.333>.
- [33] Robertson AN, Gueydon S, Bachynski E, Wang L, Jonkman J, Alarcón D, et al. OC6 Phase I: Investigating the underprediction of low-frequency hydrodynamic loads and responses of a floating wind turbine. *J. Phys. Conf. Ser.*, 2020. <https://doi.org/10.1088/1742-6596/1618/3/032033>.
- [34] Goupee AJ, Kimball RW, Helder J, Fowler MJ, de Ridder E-J. Additional wave/wind basin testing of the DeepCwind semisubmersible with a performance matched wind turbine. *Proc. ASME 2014 33rd Int. Conf. Ocean. Offshore Arct. Eng. OMAE2014*, 2014, p. 1–10.
- [35] Robertson AN, Bachynski EE, Gueydon S, Wendt F, Schünemann P, Jonkman J. Assessment of experimental uncertainty for a floating wind semisubmersible under hydrodynamic loading. *Proc Int Conf Offshore Mech Arct Eng - OMAE 2018*;10. <https://doi.org/10.1115/OMAE2018-77703>.
- [36] Robertson A, Bachynski EE, Gueydon S, Wendt F, Schünemann P. Total experimental uncertainty in hydrodynamic testing of a semisubmersible wind turbine, considering numerical propagation of systematic uncertainty. *Ocean Eng* 2020;195:106605.

- <https://doi.org/10.1016/j.oceaneng.2019.106605>.
- [37] Campos A, Molins C, Trubat P, Alarcón D. A 3D FEM model for floating wind turbines support structures. *Energy Procedia*, 2017. <https://doi.org/10.1016/j.egypro.2017.10.344>.
- [38] Lemmer F, Yu W, Luhmann B, Schlipf D, Cheng PW. Multibody modeling for concept-level floating offshore wind turbine design. *Multibody Syst Dyn* 2020. <https://doi.org/10.1007/s11044-020-09729-x>.
- [39] Tran TT, Kim DH. The platform pitching motion of floating offshore wind turbine: A preliminary unsteady aerodynamic analysis. *J Wind Eng Ind Aerodyn* 2015. <https://doi.org/10.1016/j.jweia.2015.03.009>.
- [40] Rega G. Nonlinear vibrations of suspended cables - Part I: Modeling and analysis. *Appl Mech Rev* 2004. <https://doi.org/10.1115/1.1777224>.
- [41] Rega G. Nonlinear vibrations of suspended cables - Part II: Deterministic phenomena. *Appl Mech Rev* 2004. <https://doi.org/10.1115/1.1777225>.
- [42] Bir G, Jonkman J. Aeroelastic instabilities of large offshore and onshore wind turbines. *J. Phys. Conf. Ser.*, 2007. <https://doi.org/10.1088/1742-6596/75/1/012069>.
- [43] Larsen JW, Nielsen SRK. Nonlinear parametric instability of wind turbine wings. *J Sound Vib* 2007. <https://doi.org/10.1016/j.jsv.2006.06.055>.
- [44] Larsen JW, Nielsen SRK. Non-linear dynamics of wind turbine wings. *Int J Non Linear Mech* 2006. <https://doi.org/10.1016/j.ijnonlinmec.2006.01.003>.
- [45] Sun C. Mitigation of offshore wind turbine responses under wind and wave loading: Considering soil effects and damage. *Struct Control Heal Monit* 2018. <https://doi.org/10.1002/stc.2117>.
- [46] IEC 61400-3, International Electro technical Committee IEC 61400-3: Wind Turbines part 3: Design Requirements for Offshore Wind Turbines. 2009.
- [47] DNV-GL. DNVGL-ST-0119 Floating wind turbine structures 2018:162.
- [48] Barltrop NDP. *Floating Structures: A Guide For Design And Analysis Vol 1*. Ledbury: Oilfield Publications Limited; 1988.
- [49] Journee J, Massie W. *Offshore hydromechanics*. Delft University of Technology; 2001.
- [50] Bathe KJ. *Finite Element Procedures*. 1996.
- [51] Cook RD, Malkus DS, Plesha ME, Witt RJ. *Concepts and applications of Finite Element analysis*. 4th ed. John Wiley and sons; 2002.
- [52] Meier C, Popp A, Wall WA. Geometrically Exact Finite Element Formulations for Slender Beams: Kirchhoff–Love Theory Versus Simo–Reissner Theory. *Arch Comput Methods Eng* 2019. <https://doi.org/10.1007/s11831-017-9232-5>.
- [53] Craig RR, Bampton MCC. Coupling of substructures for dynamic analyses. *AIAA J* 1968. <https://doi.org/10.2514/3.4741>.
- [54] Oh S, Ishii K, Iijima K, Suzuki H. Implementation of potential flow hydrodynamics to time-domain analysis of flexible platforms of floating offshore wind turbines. *J. Phys. Conf. Ser.*, 2019. <https://doi.org/10.1088/1742-6596/1356/1/012041>.
- [55] Suzuki H, Shiohara H, Schnepf A, Houtani H, Carmo LHS, Hirabayashi S, et al. Wave and wind responses of a very-light fowt with guy-wired-supported tower: Numerical and experimental studies. *J Mar Sci Eng* 2020. <https://doi.org/10.3390/jmse8110841>.

- [56] Cheng AHD, Cheng DT. Heritage and early history of the boundary element method. *Eng Anal Bound Elem* 2005. <https://doi.org/10.1016/j.enganabound.2004.12.001>.
- [57] Eymard R, Gallouët T, Herbin R. Finite volume methods. *Handb Numer Anal* 2000. [https://doi.org/10.1016/S1570-8659\(00\)07005-8](https://doi.org/10.1016/S1570-8659(00)07005-8).
- [58] Cardiff P, Demirdžić I. Thirty Years of the Finite Volume Method for Solid Mechanics. *Arch Comput Methods Eng* 2021. <https://doi.org/10.1007/s11831-020-09523-0>.
- [59] Feyrer K. Wire Ropes Under Bending and Tensile Stresses. *Wire Ropes*, 2007. https://doi.org/10.1007/978-3-540-33831-4_3.
- [60] Xu S, Wang S, Guedes Soares C. Review of mooring design for floating wave energy converters. *Renew Sustain Energy Rev* 2019. <https://doi.org/10.1016/j.rser.2019.05.027>.
- [61] Yang SH, Ringsberg JW, Johnson E, Hu Z. Biofouling on mooring lines and power cables used in wave energy converter systems—Analysis of fatigue life and energy performance. *Appl Ocean Res* 2017. <https://doi.org/10.1016/j.apor.2017.04.002>.
- [62] Azcona J, Palacio D, Munduate X, Gonzalez L, Nygaard TA. Impact of mooring lines dynamics on the fatigue and ultimate loads of three offshore floating wind turbines computed with IEC 61400-3 guideline. *Wind Energy* 2017;20:797–813:1–20. <https://doi.org/10.1002/we.2064>.
- [63] Hall M, Buckham B, Crawford C. Evaluating the importance of mooring line model fidelity in floating offshore wind turbine simulations. *Wind Energy* 2014;17:1835–18:1–20. <https://doi.org/10.1002/we.1669>.
- [64] Jonkman JM. Dynamics Modeling and Loads Analysis of an Offshore Floating Wind Turbine. 2007.
- [65] Ishihara T, Zhang S. Prediction of dynamic response of semi-submersible floating offshore wind turbine using augmented Morison's equation with frequency dependent hydrodynamic coefficients. *Renew Energy* 2019. <https://doi.org/10.1016/j.renene.2018.08.042>.
- [66] Chen L, Basu B, Nielsen SRK. Nonlinear periodic response analysis of mooring cables using harmonic balance method. *J Sound Vib* 2019. <https://doi.org/10.1016/j.jsv.2018.09.027>.
- [67] Benitz MA, Lackner MA, Schmidt DP. Hydrodynamics of offshore structures with specific focus on wind energy applications. *Renew Sustain Energy Rev* 2015. <https://doi.org/10.1016/j.rser.2015.01.021>.
- [68] Faltinsen OM. Sea loads on ships and offshore structures. 1990. <https://doi.org/9780521458702>.
- [69] Morison JR, Johnson JW, Schaaf SA. The Force Exerted by Surface Waves on Piles. *J Pet Technol* 1950;2:149–54. <https://doi.org/10.2118/950149-g>.
- [70] Connolly A, Guyot M, Boulluec M Le, Hery L, O'Connor A. Fully coupled aero-hydro-structural simulation of new floating wind turbine concept. *Proc. ASME 2018 1st Int. Offshore Wind Tech. Conf. IOWTC2018*, vol. IOWTC2018-, 2018, p. 1–11.
- [71] Wendt JF, Anderson JD, Degroote J, Degrez G, Dick E, Grundmann R, et al. Computational fluid dynamics: An introduction. 2009. <https://doi.org/10.1007/978-3-540-85056-4>.
- [72] Zhang D, Paterson EG. A study of wave forces on an offshore platform by direct CFD and Morison equation. *E3S Web Conf.*, 2015. <https://doi.org/10.1051/e3sconf/20150504002>.
- [73] Benitz MA, Schmidt DP, Lackner MA, Stewart GM, Jonkman J, Robertson A. Comparison of hydrodynamic load predictions between reduced order engineering models and computational fluid dynamics for the OC4-deepcwind semi-submersible. *Proc. Int. Conf. Offshore Mech.*

- Arct. Eng. - OMAE, 2014. <https://doi.org/10.1115/OMAE2014-23985>.
- [74] Benitz MA, Schmidt DP, Lackner MA, Stewart GM, Jonkman J, Robertson A. Validation of hydrodynamic load models using CFD for the OC4-deepcwind semisubmersible. Proc. Int. Conf. Offshore Mech. Arct. Eng. - OMAE, 2015. <https://doi.org/10.1115/OMAE2015-41045>.
- [75] Zhou Y, Xiao Q, Liu Y, Incecik A, Peyrard C, Li S, et al. Numerical modelling of dynamic responses of a floating offshore wind turbine subject to focused waves. Energies 2019. <https://doi.org/10.3390/en12183482>.
- [76] Chan GKY, Sclavounos PD, Jonkman J, Hayman G. Computation of nonlinear hydrodynamic loads on floating wind turbines using fluid-impulse theory. Proc. Int. Conf. Offshore Mech. Arct. Eng. - OMAE, 2015. <https://doi.org/10.1115/OMAE2015-41053>.
- [77] Office of Energy Efficiency & Renewable Energy WETO. Floating and fixed-bottom structures can benefit from further design optimization 2018. <https://www.energy.gov/eere/wind/articles/iea-research-study-extended-improve-accuracy-offshore-wind-systems-design-tools> (accessed March 19, 2021).
- [78] Liu Y, Xiao Q, Incecik A, Wan DC. Investigation of the effects of platform motion on the aerodynamics of a floating offshore wind turbine. J Hydrodyn 2016. [https://doi.org/10.1016/S1001-6058\(16\)60611-X](https://doi.org/10.1016/S1001-6058(16)60611-X).
- [79] Sebastian T, Lackner MA. Characterization of the unsteady aerodynamics of offshore floating wind turbines. Wind Energy 2013. <https://doi.org/10.1002/we.545>.
- [80] Wen B, Zhang Q, Wei S, Tian X, Dong X, Peng Z. Comparisons between the typical wind shear and the wind shear induced by platform pitch motion for an offshore floating wind turbine. Proc. Int. Conf. Offshore Mech. Arct. Eng. - OMAE, 2018. <https://doi.org/10.1115/OMAE2018-77797>.
- [81] Lee H, Lee DJ. Effects of platform motions on aerodynamic performance and unsteady wake evolution of a floating offshore wind turbine. Renew Energy 2019. <https://doi.org/10.1016/j.renene.2019.04.134>.
- [82] Tavernier D De, Ferreira C. The need for dynamic inflow models for vertical axis wind turbines. J. Phys. Conf. Ser., 2019. <https://doi.org/10.1088/1742-6596/1356/1/012036>.
- [83] Manwell JF, McGowan JG, Rogers AL. Wind Energy Explained. Theory, Design and Application. John Wiley & Sons Ltd. Chichester, United Kingdom; 2009. <https://doi.org/10.1002/9781119994367>.
- [84] Matha D, Fischer SV, Hauptmann S, Cheng PW, Bekiropoulos D, Lutz T, et al. Variations in ultimate load predictions for floating offshore wind turbine extreme pitching motions applying different aerodynamic methodologies. Twenty-third Int. Offshore Polar Eng. Conf. 30 June-5 July, Anchorage, Alaska, International Society of Offshore and Polar Engineers; 2013.
- [85] Henriksen LC, Hansen MH, Poulsen NK. A simplified dynamic inflow model and its effect on the performance of free mean wind speed estimation. Wind Energy 2013;16:1213–24. <https://doi.org/10.1002/WE.1548/FORMAT/PDF/OEBPS/PAGES/1.PAGE.XHTML>.
- [86] Chen X, Agarwal RK. Inclusion of a simple dynamic inflow model in the blade element momentum theory for wind turbine application. 32nd AIAA Appl Aerodyn Conf 2014. <https://doi.org/10.2514/6.2014-2849>.
- [87] Ferreira C, Yu W, Sala A, Vire A. Dynamic inflow model for a Floating Horizontal Axis Wind Turbine in surge motion. Wind Energy Sci Discuss 2021:1–22. <https://doi.org/10.5194/WES-2021-34>.
- [88] Liu Y, Xiao Q, Incecik A, Peyrard C. Aeroelastic analysis of a floating offshore wind turbine

- in platform-induced surge motion using a fully coupled CFD-MBD method. *Wind Energy* 2019. <https://doi.org/10.1002/we.2265>.
- [89] Dunbar AJ, Craven BA, Paterson EG. Development and validation of a tightly coupled CFD/6-DOF solver for simulating floating offshore wind turbine platforms. *Ocean Eng* 2015. <https://doi.org/10.1016/j.oceaneng.2015.08.066>.
- [90] Wu CHK, Nguyen VT. Aerodynamic simulations of offshore floating wind turbine in platform-induced pitching motion. *Wind Energy* 2017. <https://doi.org/10.1002/we.2066>.
- [91] Bayati I, Belloli M, Bernini L, Boldrin DM, Boorsma K, Caboni M, et al. UNAFLOW project: UNsteady Aerodynamics of FLOating Wind turbines. *J. Phys. Conf. Ser.*, 2018. <https://doi.org/10.1088/1742-6596/1037/7/072037>.
- [92] Fontanella A, Bayati I, Mikkelsen R, Belloli M, Zasso A. UNAFLOW: A holistic wind tunnel experiment about the aerodynamic response of floating wind turbines under imposed surge motion. *Wind Energy Sci* 2021;6:1169–90. <https://doi.org/10.5194/WES-6-1169-2021>.
- [93] IEA Wind Task 30 n.d. <https://iea-wind.org/task30/> (accessed August 9, 2021).
- [94] Vijayakumar G, Yellapantula S, Branlard E, Ananthan S. Enhancement of Unsteady and 3D Aerodynamics Models using Machine Learning. *J. Phys. Conf. Ser.*, 2020. <https://doi.org/10.1088/1742-6596/1452/1/012065>.
- [95] Sebastian T, Lackner MA. Development of a free vortex wake method code for offshore floating wind turbines. *Renew Energy* 2012. <https://doi.org/10.1016/j.renene.2012.03.033>.
- [96] Jeon M, Lee S, Lee S. Unsteady aerodynamics of offshore floating wind turbines in platform pitching motion using vortex lattice method. *Renew Energy* 2014. <https://doi.org/10.1016/j.renene.2013.09.009>.
- [97] Ramos-García N, Kontos S, Pegalajar-Jurado A, Horcas SG, Bredmose H. Investigation of the floating IEA Wind 15 MW RWT using vortex methods Part I: Flow regimes and wake recovery. *Wind Energy* 2021. <https://doi.org/10.1002/WE.2682>.
- [98] Shaler K, Branlard E, Platt A, Jonkman J. Preliminary Introduction of a Free Vortex Wake Method into OpenFAST. *J. Phys. Conf. Ser.*, 2020. <https://doi.org/10.1088/1742-6596/1452/1/012064>.
- [99] Lackner MA. An investigation of variable power collective pitch control for load mitigation of floating offshore wind turbines. *Wind Energy* 2013. <https://doi.org/10.1002/we.1500>.
- [100] Yu W, Lemmer F, Schlipf D, Cheng PW, Visser B, Links H, et al. Evaluation of control methods for floating offshore wind turbines. *J. Phys. Conf. Ser.*, 2018. <https://doi.org/10.1088/1742-6596/1104/1/012033>.
- [101] Savenije F, Peeringa J. Control development for floating wind. *J. Phys. Conf. Ser.*, 2014. <https://doi.org/10.1088/1742-6596/524/1/012090>.
- [102] Fontanella A, Liu Y, Azcona J, Pires O, Bayati I, Gueydon S, et al. A hardware-in-the-loop wave-basin scale model experiment for the validation of control strategies for floating offshore wind turbines. *J Phys Conf Ser* 2020:1–10.
- [103] Jonkman JM. Influence of control on the pitch damping of a floating wind turbine. 46th AIAA Aerosp. Sci. Meet. Exhib., 2008. <https://doi.org/10.2514/6.2008-1306>.
- [104] Kadum H, Rockel S, Viggiano B, Dib T, Hölling M, Chevillard L, et al. Assessing intermittency characteristics via cumulant analysis of floating wind turbines wakes. *J Renew Sustain Energy* 2021. <https://doi.org/10.1063/5.0022699>.
- [105] Kheirabadi AC, Nagamune R. A low-fidelity dynamic wind farm model for simulating time-

- varying wind conditions and floating platform motion. *Ocean Eng* 2021. <https://doi.org/10.1016/j.oceaneng.2021.109313>.
- [106] Sebastian T, Lackner M. Analysis of the induction and wake evolution of an offshore floating wind turbine. *Energies* 2012. <https://doi.org/10.3390/en5040968>.
- [107] Steen S. Experimental methods in marine hydrodynamics: statistical analysis. Faculty of Engineering Science and Technology, NTNU Trondheim; 2014.
- [108] Tomasicchio GR, D'Alessandro F, Avossa AM, Riefole L, Musci E, Ricciardelli F, et al. Experimental modelling of the dynamic behaviour of a spar buoy wind turbine. *Renew Energy* 2018;127:412–32. <https://doi.org/10.1016/j.renene.2018.04.061>.
- [109] Roddier D, Cermelli C, Aubault A, Weinstein A. WindFloat: A floating foundation for offshore wind turbines. *J Renew Sustain Energy* 2010;2:1–35. <https://doi.org/10.1063/1.3435339>.
- [110] Wright C, Desmond C, Lynch K. MARINET Report on Physical Modelling Methods for Floating Wind Turbines. 2015.
- [111] Martin HR, Kimball RW, Viselli AM, Goupee AJ. Methodology for wind/wave basin testing of floating offshore wind turbines. *J Offshore Mech Arct Eng* 2014;136:1–9. <https://doi.org/10.1115/1.4025030>.
- [112] Pegalajar-Jurado A, Hansen AM, Laugesen R, Mikkelsen RF, Borg M, Kim T, et al. Experimental and numerical study of a 10MW TLP wind turbine in waves and wind. *J Phys Conf Ser* 2016;753:092007. <https://doi.org/10.1088/1742-6596/753/9/092007>.
- [113] Bayati I, Belloli M, Bernini L, Mikkelsen R, Zasso A. On the aero-elastic design of the DTU 10MW wind turbine blade for the LIFES50+ wind tunnel scale model. *J Phys Conf Ser* 2016;753. <https://doi.org/10.1088/1742-6596/753/2/022028>.
- [114] Fowler M, Kimball R, Iii DAT, Goupee A. Wave basin model tests of floating offshore wind turbines. *Proc ASME 32nd Int Conf Ocean Offshore Arct Eng* 2013:1–11. <https://doi.org/10.1115/OMAE2013-10122>.
- [115] Skaare B, Nielsen FG, Hanson TD. Integrated dynamic analysis of floating offshore wind turbines. *Eur Wind Energy Conf Exhib* 2006, EWEC 2006 2006;3:1834–42.
- [116] Mortensen SM, Laugesen K, Jensen JK, Jessen K, Soltani M. Experimental Verification of the Hydro-Elastic Model of a Scaled Floating Offshore Wind Turbine. 2018 IEEE Conf Control Technol Appl CCTA 2018 2018:1623–30. <https://doi.org/10.1109/CCTA.2018.8511565>.
- [117] Jonkman JM, Butterfield S, Musial W, Scott G. Definition of a 5-MW reference wind turbine for offshore system development. 2009. <https://doi.org/10.1115/1.4038580>.
- [118] Bahramiasl S, Abbaspour M, Karimirad M. Experimental study on gyroscopic effect of rotating rotor and wind heading angle on floating wind turbine responses. *Int J Environ Sci Technol* 2018;15:2531–44. <https://doi.org/10.1007/s13762-017-1519-4>.
- [119] Li L, Gao Y, Hu Z, Yuan Z, Day S, Li H. Model test research of a semisubmersible floating wind turbine with an improved deficient thrust force correction approach. *Renew Energy* 2018;119:95–105. <https://doi.org/10.1016/j.renene.2017.12.019>.
- [120] Goupee AJ, Koo BJ, Kimball RW, Lambrakos KF, Dagher HJ. Experimental comparison of three floating wind turbine concepts. *J Offshore Mech Arct Eng* 2014;136:1–9. <https://doi.org/10.1115/1.4025804>.
- [121] de Ridder E-J, Otto W, Zondervan G-J, Huijs F, Vaz G. Development of a Scaled-Down Floating Wind Turbine for Offshore Basin Testing. *Proc ASME 2014 33rd Int Conf Ocean Offshore Arct Eng* 2014:1–11.

- [122] Bredmose H, Lemmer F, Borg M, Pegalajar-Jurado A, Mikkelsen RF, Larsen TS, et al. The Triple Spar campaign: Model tests of a 10MW floating wind turbine with waves, wind and pitch control. *Energy Procedia* 2017;137:58–76. <https://doi.org/10.1016/j.egypro.2017.10.334>.
- [123] Christian Bak, Frederik Zahle, Robert Bitsche, Taeseong Kim, Anders Yde, Lars C. Henriksen, Anand Natarajan MH. DTU Wind Energy Report-I-0092 2013.
- [124] Madsen FJ, Nielsen TRL, Kim T, Bredmose H, Pegalajar-Jurado A, Mikkelsen RF, et al. Experimental analysis of the scaled DTU10MW TLP floating wind turbine with different control strategies. *Renew Energy* 2020;155:330–46. <https://doi.org/10.1016/j.renene.2020.03.145>.
- [125] Borisade F, Koch C, Lemmer F, Cheng PW, Campagnolo F, Matha D. Validation of innwind.Eu scaled model tests of a semisubmersible floating wind turbine. *Int J Offshore Polar Eng* 2018;28:54–64. <https://doi.org/10.17736/ijope.2018.fv04>.
- [126] Ahn H, Shin H. Experimental and Numerical Analysis of a 10 MW Floating Offshore Wind Turbine in Regular Waves. *Energies* 2020;13:1–17. <https://doi.org/10.3390/en13102608>.
- [127] Ward JC, Fowler MJ, Viselli AM, Goupee AJ, Dagher HJ. Design and validation of a multi-scale model floating offshore test wind turbine. *ASME 2018 1st Int Offshore Wind Tech Conf IOWTC 2018* 2018:1–10. <https://doi.org/10.1115/IOWTC2018-1084>.
- [128] Zhao Y sheng, She X he, He Y ping, Yang J min, Peng T, Kou Y feng. Experimental Study on New Multi-Column Tension-Leg-Type Floating Wind Turbine. *China Ocean Eng* 2018;32:123–31. <https://doi.org/10.1007/s13344-018-0014-0>.
- [129] Azcona J, Bouchotrouch F, González M, Garcíandía J, Munduate X, Kelberlau F, et al. Aerodynamic thrust modelling in wave tank tests of offshore floating wind turbines using a ducted fan. *J Phys Conf Ser* 2014;524. <https://doi.org/10.1088/1742-6596/524/1/012089>.
- [130] Azcona J, Bouchotrouch F, Vittori F. Low-frequency dynamics of a floating wind turbine in wave tank–scaled experiments with SiL hybrid method. *Wind Energy* 2019;22:1402–13. <https://doi.org/10.1002/we.2377>.
- [131] Vittori F, Lemmer F, Bouchotrouch F, Azcona J. Hybrid scaled testing of a 5 MW floating wind turbine using the SIL method compared with numerical models. *Proc. ASME 2018 37th Int. Conf. Ocean. Offshore Arct. Eng. OMAE2018*, 2018, p. 1–8.
- [132] Wright C, O’Sullivan K, Murphy J, Pakrashi V. Experimental comparison of dynamic responses of a tension moored floating wind turbine platform with and without spring dampers. *J Phys Conf Ser* 2015;628. <https://doi.org/10.1088/1742-6596/628/1/012056>.
- [133] Desmond CJ, Hinrichs JC, Murphy J. Uncertainty in the Physical Testing of Floating Wind Energy Platforms’ Accuracy versus Precision. *Energies* 2019;12:1–14. <https://doi.org/10.3390/en12030435>.
- [134] Oguz E, Clelland D, Day AH, Incecik A, López JA, Sánchez G, et al. Experimental and numerical analysis of a TLP floating offshore wind turbine. *Ocean Eng* 2018;147:591–605. <https://doi.org/10.1016/j.oceaneng.2017.10.052>.
- [135] Andersen MT. *Floating Foundations for Offshore Wind Turbines*. Aalborg University, 2016. <https://doi.org/10.5278/vbn.phd.engsci.00175>.
- [136] Matoug C, Augier B, Paillard B, Maurice G, Sicot C, Barre S. An hybrid approach for the comparison of VAWT and HAWT performances for floating offshore wind turbines. *J. Phys. Conf. Ser.*, 2020. <https://doi.org/10.1088/1742-6596/1618/3/032026>.
- [137] Otter A, Murphy J, Desmond CJ. Emulating aerodynamic forces and moments for hybrid testing of floating wind turbine models. *J. Phys. Conf. Ser.*, 2020.

- <https://doi.org/10.1088/1742-6596/1618/3/032022>.
- [138] Meseguer A, Guanche R. Wind turbine aerodynamics scale-modeling for floating offshore wind platform testing. *J Wind Eng Ind Aerodyn* 2019;186:49–57. <https://doi.org/10.1016/j.jweia.2018.12.021>.
- [139] Armesto JA, Jurado A, Guanche R, Counago B, Urbano J, Serna J. Telwind. Numerical analysis of a floating wind turbine supported by a two bodies platform. *Proc Int Conf Offshore Mech Arct Eng - OMAE* 2018;10. <https://doi.org/10.1115/OMAE2018-77587>.
- [140] Pires O, Azcona J, Vittori F, Bayati I, Gueydon S, Fontanella A, et al. Inclusion of rotor moments in scaled wave tank test of a floating wind turbine using SiL hybrid method. *J. Phys. Conf. Ser.*, 2020. <https://doi.org/10.1088/1742-6596/1618/3/032048>.
- [141] Kanner S, Yeung RW, Koukina E. Hybrid testing of model-scale floating wind turbines using autonomous actuation and control. *Ocean 2016 MTS/IEEE Monterey, OCE 2016* 2016:1–6. <https://doi.org/10.1109/OCEANS.2016.7760997>.
- [142] Sauder T, Chabaud V, Thys M, Bachynski EE, Sæther LO. Real-time hybrid model testing of a braceless semi-submersible wind turbine. Part 1: the hybrid approach. *Proc. ASME 2016 35th Int. Conf. Ocean. Offshore Arct. Eng. OMAE2016*, 2016, p. 1–13.
- [143] Bachynski EE, Sauder T, Thys M, Chabaud V, Sæther LO. Real-time hybrid model testing of a braceless semisubmersible wind turbine. Part 2: experimental results. *Proc. ASME 2016 35th Int. Conf. Ocean. Offshore Arct. Eng. OMAE2016 June*, 2016, p. 1–12.
- [144] Berthelsen PA, Bachynski EE, Karimirad M, Thys M. Real-time hybrid model tests of a braceless semisubmersible wind turbine. Part 3: calibration of a numerical model. *Proc. ASME 2016 35th Int. Conf. Ocean. Offshore Arct. Eng. OMAE2016*, 2016, p. 1–13.
- [145] Luan C, Gao Z, Moan T. Design and Analysis of a Braceless Steel 5 MW Semi-Submersible Wind Turbine. *Proc. 35th Int. Conf. Ocean Arct. Eng. OMAE 2016*, 2016, p. 1–12.
- [146] Karimirad M, Bachynski EE, Berthelsen PA, Ormberg H. Comparison of real-time hybrid model testing of a braceless semisubmersible wind turbine and numerical simulations. *Proc. ASME 2017 36th Int. Conf. Ocean. Offshore Arct. Eng. OMAE2017 June*, 2017, p. 1–10.
- [147] Bachynski EE, Chabaud V, Sauder T. Real-time hybrid model testing of floating wind turbines: Sensitivity to limited actuation. vol. 80. Elsevier B.V.; 2015. <https://doi.org/10.1016/j.egypro.2015.11.400>.
- [148] Thys M, Chabaud V, Sæther LO, Magnussen ØB, Eliassen L, Sauder T. Real-time hybrid model testing of a semisubmersible 10MW floating wind turbine and advances in the test method. *Proc. ASME 2018 1st Int. Offshore Wind Tech. Conf. IOWTC2018*, 2018, p. 1–11.
- [149] Madsen FJ, Lemmer F, Müller K, Pegalajar-Jurado A, Faerron-Guzman R, Bredmose H. LIFES50+ D4.6 Model validation against experiments and map of model accuracy across load cases. 2018.
- [150] Chabaud V, Eliassen L, Thys M, Sauder T. Multiple-degree-of-freedom actuation of rotor loads in model testing of floating wind turbines using cable-driven parallel robots. *J Phys Conf Ser* 2018;1104. <https://doi.org/10.1088/1742-6596/1104/1/012021>.
- [151] Hall M, Goupee AJ. Validation of a hybrid modeling approach to floating wind turbine basin testing. *Wind Energy* 2018;21:391–408. <https://doi.org/10.1002/we.2168>.
- [152] Antonutti R, Poirier J-C, Gueydon S. Coupled Testing of Floating Wind Turbines in Waves and Wind Using Winches and Software-in-the-Loop. *Offshore Technol. Conf. 2020, Houston, Texas, USA, Offshore Technology Conference*; 2020. <https://doi.org/10.4043/30555-ms>.
- [153] Schliffke B, Aubrun S, Conan B. Wind Tunnel Study of a “floating” Wind Turbine’s Wake in

- an Atmospheric Boundary Layer with Imposed Characteristic Surge Motion. *J. Phys. Conf. Ser.*, 2020. <https://doi.org/10.1088/1742-6596/1618/6/062015>.
- [154] Rockel S, Camp E, Schmidt J, Peinke J, Cal RB, Hölling M. Experimental study on influence of pitch motion on the wake of a floating wind turbine model. *Energies* 2014. <https://doi.org/10.3390/en7041954>.
- [155] Rockel S, Peinke J, Hölling M, Cal RB. Wake to wake interaction of floating wind turbine models in free pitch motion: An eddy viscosity and mixing length approach. *Renew Energy* 2016. <https://doi.org/10.1016/j.renene.2015.07.012>.
- [156] Bayati I, Belloli M, Bernini L, Zasso A. Wind Tunnel Wake Measurements of Floating Offshore Wind Turbines. *Energy Procedia*, 2017. <https://doi.org/10.1016/j.egypro.2017.10.375>.
- [157] Bayati I, Belloli M, Facchinetti A. Wind tunnel 2-DOF hybrid/HIL tests on the OC5 floating offshore wind turbine. *Proc. Int. Conf. Offshore Mech. Arct. Eng. - OMAE*, 2017. <https://doi.org/10.1115/OMAE2017-61763>.
- [158] Ambrosini S, Bayati I, Facchinetti A, Belloli M. Methodological and technical aspects of a two-degrees-of-freedom hardware-in-the-loop setup for wind tunnel tests of floating systems. *J Dyn Syst Meas Control Trans ASME* 2020. <https://doi.org/10.1115/1.4046155>.
- [159] Bayati I, Belloli M, Ferrari D, Fossati F, Giberti H. Design of a 6-DoF robotic platform for wind tunnel tests of floating wind turbines. *Energy Procedia*, 2014. <https://doi.org/10.1016/j.egypro.2014.07.240>.
- [160] Bayati I, Facchinetti A, Fontanella A, Giberti H, Belloli M. A wind tunnel/HIL setup for integrated tests of Floating Offshore Wind Turbines. *J Phys Conf Ser* 2018;1037. <https://doi.org/10.1088/1742-6596/1037/5/052025>.
- [161] Belloli M, Bayati I, Facchinetti A, Fontanella A, Giberti H, La Mura F, et al. A hybrid methodology for wind tunnel testing of floating offshore wind turbines. *Ocean Eng* 2020;210. <https://doi.org/10.1016/j.oceaneng.2020.107592>.
- [162] Thys M, Fontanella A, Taruffi F, Belloli M, Berthelsen PA. Hybrid model tests for floating offshore wind turbines. *ASME 2019 2nd Int. Offshore Wind Tech. Conf. IOWTC 2019*, 2019. <https://doi.org/10.1115/IOWTC2019-7575>.
- [163] Arnal V, Bonnefoy F, Gilloteaux JC, Aubrun S. Hybrid model testing of floating wind turbines: Test bench for system identification and performance assessment. *Proc. Int. Conf. Offshore Mech. Arct. Eng. - OMAE*, 2019. <https://doi.org/10.1115/OMAE2019-96374>.
- [164] Hall M, Moreno J, Thiagarajan K. PERFORMANCE SPECIFICATIONS FOR REAL-TIME HYBRID TESTING OF 1:50-SCALE FLOATING WIND TURBINE MODELS. *Proc. ASME 2014 33rd Int. Conf. Ocean. Offshore Arct. Eng. OMAE2014*, 2014, p. 1–9.
- [165] Hall M, Goupee A, Jonkman J. Development of performance specifications for hybrid modeling of floating wind turbines in wave basin tests. *J Ocean Eng Mar Energy* 2018;4:1–23. <https://doi.org/10.1007/s40722-017-0089-3>.
- [166] Gueydon S, Lindeboom R, van Kampen W, de Ridder E-J. COMPARISON OF TWO WIND TURBINE LOADING EMULATION TECHNIQUES BASED ON TESTS OF A TLP-FOWT IN COMBINED WIND, WAVES AND CURRENT. *Proc. ASME 2018 1st Int. Offshore Wind Tech. Conf. IOWTC2018*, 2018, p. 1–11.
- [167] Cermelli C, Leroux C, Diaz Dominguez S, Peiffer A. EXPERIMENTAL MEASUREMENTS OF WINDFLOAT 1 PROTOTYPE RESPONSES AND COMPARISON WITH NUMERICAL MODEL. *Proc. ASME 2018 37th Int. Conf. Ocean. Offshore Arct. Eng. OMAE2018*, ASME; 2018, p. 1–10.

- [168] ORE Catapult. Equinor and ORE Catapult collaborating to share Hywind Scotland operational data 2019. <https://ore.catapult.org.uk/press-releases/equinor-and-ore-catapult-collaborating-to-share-hywind-scotland-operational-data/> (accessed January 29, 2021).
- [169] Moan T, Gao Z, Bachynski EE, Nejad AR. Recent Advances in Integrated Response Analysis of Floating Wind Turbines in a Reliability Perspective. *J Offshore Mech Arct Eng* 2020. <https://doi.org/10.1115/1.4046196>.
- [170] Lupton RC, Langley RS. Complex but negligible: Non-linearity of the inertial coupling between the platform and blades of floating wind turbines. *Renew Energy* 2019. <https://doi.org/10.1016/j.renene.2018.11.036>.
- [171] Chen P, Hu Z, Hu C. Software-In-the-Loop Method to Predict the Global Dynamic Responses of Full-scale Floating Wind Turbines by Artificial Neural Network. 11th Int. Work. Sh. Mar. Hydrodyn., Hamburg: 2019.
- [172] Chen L, Basu B. Fatigue load estimation of a spar-type floating offshore wind turbine considering wave-current interactions. *Int J Fatigue* 2018;116:421–8. <https://doi.org/10.1016/j.ijfatigue.2018.06.002>.

Paper B

Emulating aerodynamic forces and moments for hybrid testing of floating wind turbine models

Published in

Journal of Physics: Conference Series, IOP Publishing, 2020, doi:10.1088/1742-6596/1618/3/032022

Authors:

A. Otter¹, J. Murphy¹, C. Desmond²

¹ Marine and Renewable Energy Ireland, University College Cork, P43 C573, Ireland

² Gavin and Doherty Geosolutions Ltd, Dublin 14, D14 X627, Ireland

Abstract.

The use of devices with multiple propellers to simultaneously emulate several aerodynamic loads during hybrid testing of floating wind turbines is the emerging state of the art. In this study a validation methodology and a metric are defined for the standardization of the calibration process for multiple propeller hybrid actuators. A statistical validation between the numerical simulations and experimental results is applied and Power Spectral Density is used to calculate the validation metrics. In this paper, the proposed validation method is applied to a novel design for an actuator, which consists of a custom designed frame with six aerial drone propellers. The actuator is named Multi-Propeller Device (MPD). As a test case for the proposed validation method, the MPD is used in this study to emulate the aerodynamic loads of the NREL 5 MW reference turbine at 1:37 scale. The numerical input is generated with the aero-hydro-elastic solver FAST. The aerodynamic loads and effects investigated are rotor thrust and torque, and gyroscopic moment. The recommended validation metric is the Fraction of Measurements within a user defined Tolerance (FMT), which is 1 for a flawlessly operating device. The MPD performs well at emulating rotor thrust and torque loads, with FMT = 0.97 and 0.98 respectively. However, the MPD underperforms at emulating more complex wind loads, such as gyroscopic moment with FMT = 0.27. The poor results for gyroscopic moment are attributed to the generation of significant amounts of high-frequency vibration when propeller pairs of the MPD are operating intermittently at high rotational speeds.

Introduction

Hybrid testing combines physical and numerical modelling for scale model tests. Some of the environmental loads acting on the physical model are replaced by a numerical model which calculates the resulting forces. These forces are emulated by a mechanical actuator on the physical model. Hybrid testing for floating wind turbine models is used as an alternative to physical generation of either waves, wind or current. It also provides a solution for the scaling mismatch arising from working in two fluid domains; air and water.

The coupled aerodynamics/hydrodynamics of Floating Offshore Wind Turbines (FOWT) present difficulties when attempting scaled physical experiments [1]. Hydrodynamic loading on the floating platform is dominated by gravity-driven surface waves. To correctly scale the gravity and inertial forces acting on the platform Froude scaling is applied. Aerodynamic loading on the turbine is dominated by viscous forces, i.e. the flow of wind around the structure. Correct scaling of the aerofoils of the turbine depends on the Reynolds number. A geometrically scaled rotor using Froude scaling will have a lower Reynolds number at model scale compared to the rotor at prototype scale. As a result, the model scale rotor will have a lower lift coefficient and higher drag coefficient, which will affect the aerodynamic performance of the scale model turbine. This in turn, will cause a misrepresentation of the structural response of the FOWT to wind loading.

During hybrid testing in laboratory basins, waves are modelled physically, and the wind field is introduced numerically. One or more actuators emulate the Froude scaled aerodynamic loads at hub height of the model. Air fans can be used as actuator for hybrid FOWT modelling. Wright et al [2] used a single ducted fan on a 1:50 and a 1:30 scale model of a hexagonal braced TLP platform. Only steady thrust force was emulated in their experiments. Andersen [3] fitted a non-ducted 2-bladed fan on a model of a generic semi-submersible FOWT. The aerodynamic thrust loading was modelled using a turbulent wind time series of the OC4 semi-submersible FOWT, a comparable platform to the platform used in the experiments. Azcona et al [4] installed a single ducted fan at hub height of a 1:40 scale model of the OO Concrete Star Wind

Floater semisubmersible FOWT. In their experiments, motion tracking data of the physical model was used for real-time feedback as input for the numerical simulation. With the real-time feedback method, thrust force is re-calculated for each timestep and adjusted according to the position of the physical model. They named their hybrid test method Software in the Loop (SIL). Oguz et al [5] used the SIL method to test a 1:36 scale model of the Iberdrola TLP with a single ducted fan.

Rotor thrust is the dominant aerodynamic load on the motion response of the platform of floating wind turbines, the choice to use single ducted fans to emulate thrust force therefore seems reasonable. However, it ignores other aerodynamic loadings such as rotor torque and gyroscopic moment [4]. Bachynski et al [6] conducted a sensitivity study for the NOWITECH semisubmersible FOWT and found that all aerodynamic loads except vertical thrust and gyroscopic moment had significant influence on the response of the platform. Hall et al [7] conducted sensitivity studies for three types of FOWT and found that the influence of aerodynamic loads varies significantly depending on the type of platform. While the actual influence of additional aerodynamic loads depends on the type of floating platform, devices with multiple fans for simultaneous emulation of several loads are the emerging state of the art for hybrid testing with FOWTs in wave basins.

In this study a novel methodology is defined for the validation of multiple degree of freedom aerodynamic actuation devices. This validation methodology is applied to a novel actuator design.

Description of the Multi-Propeller Device

The proposed device consists of a custom designed frame with six propellers and is named Multi-Propeller Device (MPD), which is shown in Figure 1.

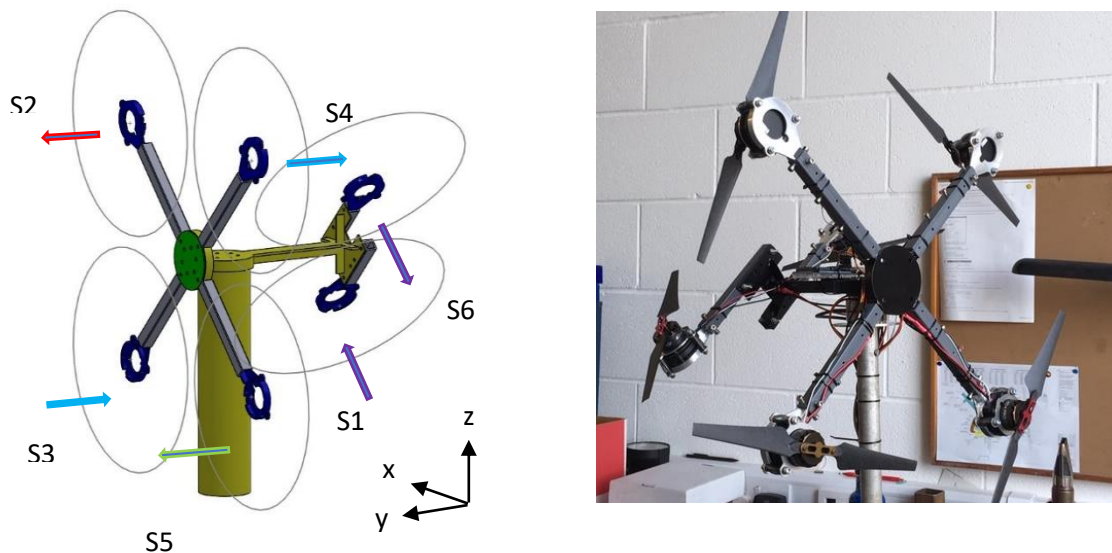


Figure 1. Multi-Propeller Device, the arrows indicate the thrust direction of the propellers

Much of the technology used for the MPD is borrowed from recreational aerial drones. The Electronic Speed Controllers (ESC), electric motors and propeller blades used for the MPD are all the same parts as used in the DJI S800 aerial drone [8]. The frame of the MPD is made of aluminium and its configuration was chosen to suit the unidirectional thrust of the propellers, while keeping the frame as light as possible. In the configuration shown in Figure 1, propellers S3 & S4 emulate aerodynamic thrust, S1 & S6 emulate rotor torque and S2 & S5 in combination with S3 & S4 can be used to emulate wind shear and gyroscopic moment. The minimum length

of each propeller arm is 200 mm from the center of the device. If larger moments are required for pitch, yaw or torque the arms can be extended. The arm extending from the tower to the torque propellers S1 & S6 is 235 mm. The torque propellers are kept away from the other propellers to minimize wake interference while all propellers are in operation. When operating, each propeller will generate its own torque and gyroscopic momentum. To ensure that this effect will not influence the test results, the propellers are installed so that each pair (S3 & S4, S2 & S5 and S1 & S6) has a propeller counter-rotating to the other, cancelling out each other's torque and gyroscopic moment. This technique is also used with aerial drones to ensure torque and gyro effects do not interfere with their flying ability. To control the propellers, the input signal calculated by the numerical simulation is scaled down and sent by the computer to an Arduino Mega 2560 board. The Arduino board translates the input signal into an analog Pulse Width Modulate (PWM) signal and sends it to the ESCs. Each propeller has its own ESC controlling the rotational speed of the DC motor. The motors are powered by a 25V DC power supply, which is connected to an AC power source.

An Interface 6A40-50N/5Nm six-axis load cell is mounted between the top of the tower and the MPD to measure forces and moments in the X-Y-Z reference frame. The load cell is positioned at the center of mass of the rotor-nacelle assembly of the full-scale turbine.

Aerial drone technology was also adopted for the device developed by Meseguer and Guanche [9]. The six propellers on their device were all in the same X-Z plane. Two propellers were used to emulate torque loads and the remaining four propellers were used to emulate thrust loads and pitch moments. None of the propellers on their device were used to create yaw moments.

Researchers from CENER, Spain, have used an MPD with SIL during a hybrid test campaign of an FOWT as part of [10]. Their device used only four propellers, all positioned in the same X-Z plane. The propellers on their device are bi-directional and are used for the emulation of thrust loads, pitch moments and yaw moments but do not include torque loadings.

Methodology

The main objectives were to develop a robust calibration method, and a validation method for use with multi-propeller actuators, such as the MPD, to contribute towards the standardization of the experimental approach used across test facilities. The validation method is based on work done in [11] and applies a statistical comparison between the numerical simulations and experimental results.

The aim of the MPD is to physically emulate the rotor force calculated numerically as accurately as possible, for the NREL 5 MW turbine at 1:37 scale. For simplicity the turbine was modelled on a rigid tower and fixed in the reference frame, i.e. no platform or tower motions were considered. During all physical experiments the MPD was mounted on an aluminium pipe with very high stiffness to replicate the rigid tower.

Two types of propeller blades of different size were used to determine the impact of blade size on the accuracy of the MPD. The first type of blade is the original type used on the S800 drone, and the second type is the blade used on the Mavic drone, with blade lengths of 150 mm and 75 mm respectively.

A test matrix was defined with increasing complexity of the aerodynamic loads. The experiments were designed to test the validation method on the MPD's output and bandwidth, or frequency range. The test matrix is shown in Table 1.

A detailed calibration of the thrust force each propeller can produce was made for both sets of propeller blades. Each propeller was first calibrated individually, then in pairs and finally with the combined propellers operating simultaneously. The difference in the results between individual, paired and combined calibrations gives an estimation of the wake interference between the propellers. The PWM signal range to control the MPD is 320-545 msec. with minimal increments of 5 msec. The propellers were operated for 10 seconds and the measured output was averaged for each PWM step to produce calibration curves. The first two seconds of each record were discarded to exclude the initial vibrations at start-up.

Table 1. Test matrix of experiments performed with the MPD, (TC = Test Case)

	Wind speed			Blades		Thrust	Torque	Gyro
	12 m/s turbulent	25 m/s steady	8 m/s steady	S800 blades	Mavic blades			
TC 1	√	×	×	√	×	√	√	×
TC 2	√	×	×	×	√	√	√	×
TC 3	×	×	√	×	√	√	×	√

Experiments.

The aero-hydro-elastic solver FAST v8 [12] was used as the numerical code for all simulations, and MATLAB was used with the Arduino support package to control the MPD. Except for test case 3, all tower and platform Degrees of Freedom (DOF) were disabled in the FAST simulations. To emulate rotor thrust and torque, a time series of turbulent wind with 12 m/s average wind speed and 14% turbulence intensity was used as input for Test Case 1 & 2. To demonstrate more complex aerodynamic loads, attempts were made to emulate gyroscopic moments, which requires propeller pairs S2 & S4 and S3 & S5 to operate intermittently. For the emulation of gyroscopic moments, a 350 second wind-only time series of the OC4 semisubmersible, at 8 m/s steady wind and platform DOFs enabled, was used as input for Test Case 3. The yaw motion of the platform resulting from the gyroscopic moment was used as input from the FAST simulation. The moment required to replicate this yaw motion was calculated and emulated by the MPD. In this case propeller S2, S3, S4 and S5 were actuating in the direction shown in Figure 1, while S2 & S4 and S3 & S5 were actuating as pairs and were operated intermittently to create the oscillations caused by the gyroscopic moment.

Validation.

To minimize uncertainty of hybrid testing of FOWT models with the MPD, high accuracy and repeatability at replicating demanded forces and moments are essential. The initial step in the validation process is a qualitative comparison consisting of two parts. The first part graphically compares the measured outputs with the numerical inputs. For the second part scatter plots are generated to show the correlation between the measured outputs and numerical inputs, and Power Spectral Density (PSD) is plotted to compare the difference in energy of the quantity of interest between experiment and simulation. The final step is a quantitative comparison. The spectral energy of each time series is used to calculate the quantitative validation metrics. The following validation metrics are used [11]:

Relative Error (RE):

$$RE = 1 - \left(\frac{\overline{E}}{S} \right) \quad (1)$$

Fraction of Measurements within a user defined tolerance (FMT):

$$a < \frac{S}{E} \leq b \quad (2)$$

Where E is the experimental PSD, S is the simulation PSD, a is a lower limit and b is an upper limit. Average values are indicated with an overbar. With a perfect performance RE would be zero, and FMT would be 1, with $a = b = 1$. The direct comparison between simulation and experiment only indicates how well the MPD can replicate the input signal from the FAST simulations and does not give a measure of the ‘accuracy’ of the system, that is, how close the laboratory experiments are to the expected real-world performance. As a performance indicator for the MPD, direct comparison is an interesting metric from an engineering perspective to assist with the set up and calibration of multi degree of freedom actuation devices. However, it does not take the accuracy of the numerical code into account. Work has been done in the Offshore Code Comparison project [13] to assess the accuracy of FAST and other numerical codes, and a methodology to assess uncertainty of FOWT response during wave basin testing has been developed in [14]. However, the work to assign a specific value to the accuracy of numerical and experimental modelling of FOWTs are ongoing. In this work, loads calculated by FAST are assumed to be ‘correct’ and the ability of the MPD to emulate these loads is assessed. A generalized approach is used with RE and FMT for the validation of the MPD. These validation metrics take different sources of error and uncertainty into account and represent bias and scatter of the data. With FMT, a user defined tolerance can be introduced by setting the limits of a and b . This is a clear benefit of FMT over RE as it allows the user to focus analysis on non-trivial or unknown sources of error in the system.

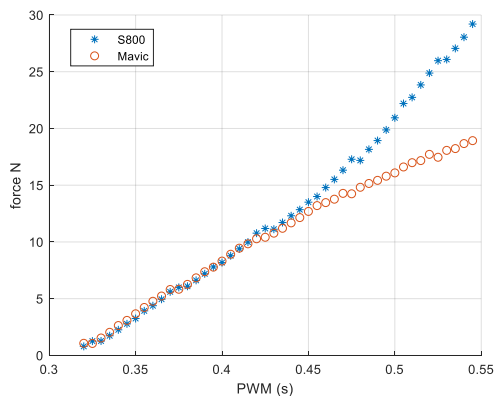


Figure 2. Calibration curves for S3 & S4

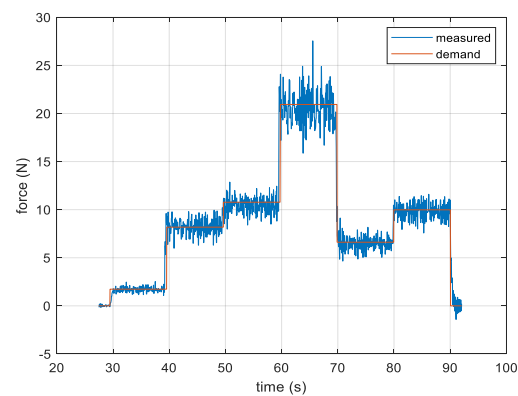


Figure 3. Time series of steady thrust loads by S3 & S4 with S800 blades

Results

A comparison of the calibration curves for aerodynamic thrust with the S800 and Mavic blades is shown in Figure 2. The plots show the combined thrust measured for propellers S3 & S4 for both sets of blades at each PWM step. Note that the thrust at lower rotational speeds is similar for both sets of blades, which is unexpected considering the difference in size.

Maximum delivered thrust per propeller is 15 N and 9 N with the S800 and Mavic blades respectively. The calibration values were tested with a time series of steady loads, shown in Figure 3, which indicates that the MPD generates a considerable amount of high-frequency vibration noise during operation.

The rates of change for thrust and moment by the propellers were also derived from the calibration data. High rates of change are achieved with both S800 blades and Mavic blades. Thrust changes at a rate of 65 N/s and 50 N/s with the S800 and Mavic blades respectively, and moment changes at a rate of 7.5 Nm/s and 5 Nm/s respectively.

Rotor thrust and torque curves of the NREL 5 MW turbine were replicated by emulating thrust and torque at steady wind speeds found with FAST simulations. The propellers were operated for 15 seconds at each wind speed and measured forces and moments were averaged. The results are shown in figure 4 & 5, where the error bars indicate the standard deviation of the measurements.

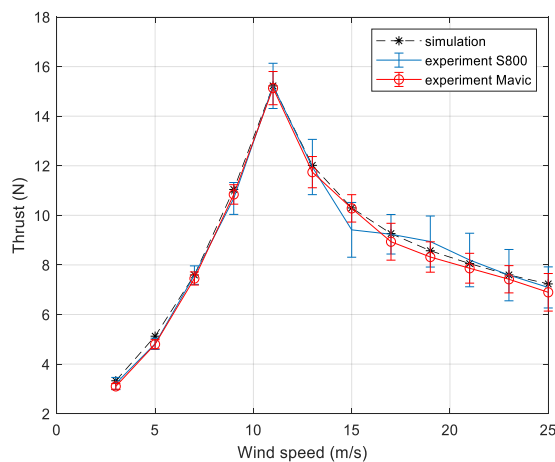


Figure 4. Thrust curve, NREL 5 MW turbine. Thrust values are shown at model scale with corresponding wind speeds at full-scale

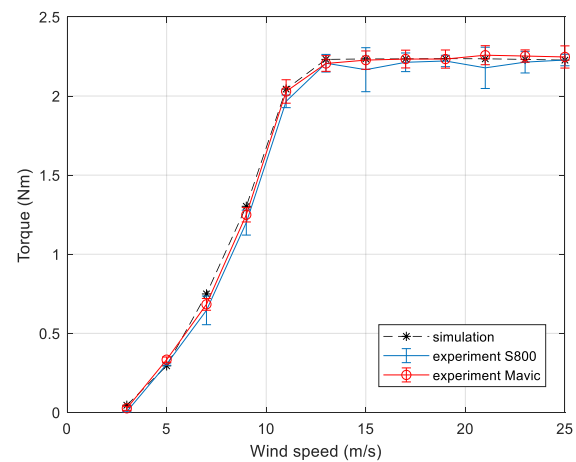


Figure 5. Torque curve, NREL 5 MW turbine. Torque values are shown at model scale with corresponding wind speeds at full-scale

Figure 6 & 7 show Test Case 2 as an example of results for emulating rotor thrust and torque of the NREL 5 MW at 12 m/s turbulent wind with the Mavic blades. All values are shown at scale

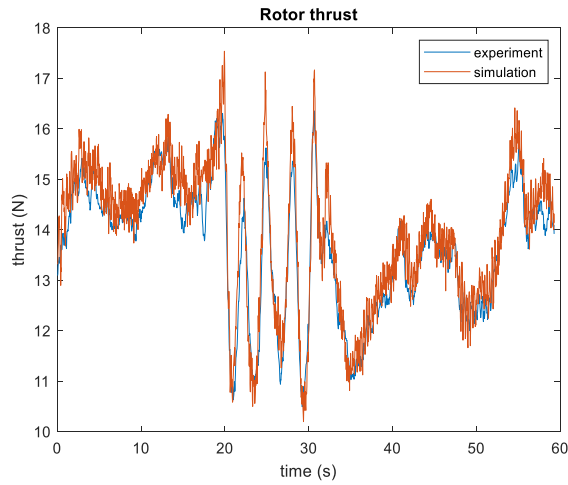


Figure 6. Emulated rotor thrust with Mavic blades

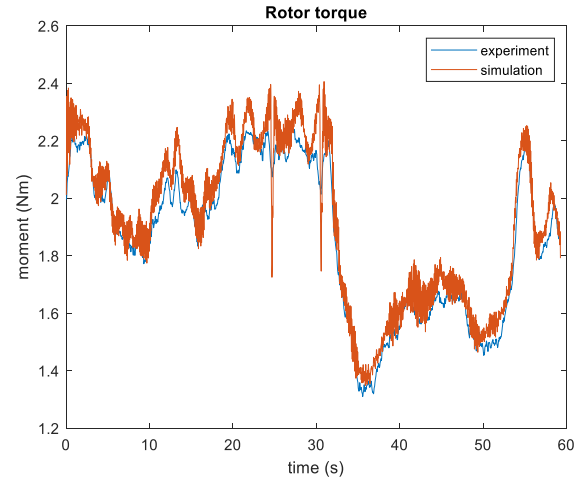


Figure 7. Emulated rotor torque with Mavic blades

This first qualitative comparison indicates that the MPD has the capacity to closely emulate rotor thrust and torque of the turbine. A low-pass filter was applied to the measured data to filter out the high frequency noise.

The next qualitative comparison is shown in Figure 8 & 9.

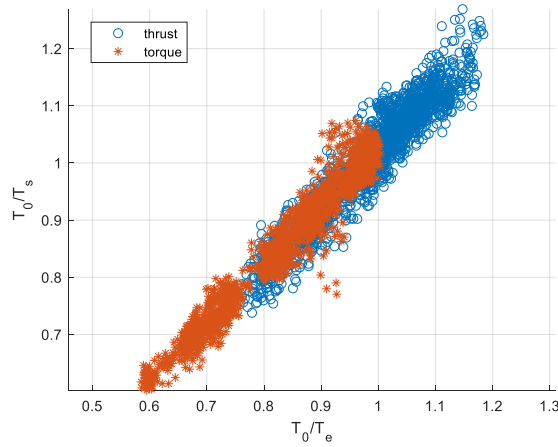


Figure 8. Scatter plot for Test Case 2

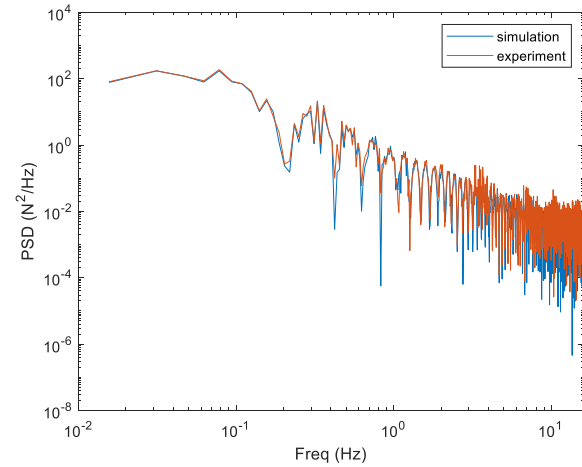


Figure 9. PSD of rotor thrust for Test Case 2

Figure 8 shows a scatter plot for Test case 2 of the normalized noise signal for simulation and experiments, where T_0 is the value at 12 m/s steady wind for the NREL 5 MW turbine, T_s are the values of the turbulent time series from the simulation and T_e are the values of the time series from the experiment. Figure 9 shows a comparison of the PSD of the rotor thrust between simulation and experiment. It shows there is higher energy for the experimental PSD at the high frequencies, attributed to the vibrations measured during the experiments.

While the results shown in Figure 6 through 9 appear encouraging, a non-subjective measure is required. Therefore, the final step in the validation process, the quantitative comparison, is used to calculate a validation metric.

Each Test Case was repeated at least five times and the results of each test have been used for the quantitative comparison. For Test Case 2 RE is -0.03 & -0.04 for thrust and torque respectively. With $a = 0.9$ and $b = 1.05$, for thrust FMT is 0.97 and for torque is 0.98. The quantitative validation metrics for all test cases are shown in table 2.

Table 2. Quantitative validation metrics of the MPD for each Test Case (TC)

	RE	FMT
Thrust S800 (TC1)	0.06	0.61 ; $a=0.9, b=1.05$
Thrust Mavic (TC2)	-0.03	0.97 ; $a=0.9, b=1.05$
Torque S800 (TC1)	0.06	0.74 ; $a=0.9, b=1.05$
Torque Mavic (TC2)	-0.04	0.98 ; $a=0.9, b=1.05$
Yaw moment (TC3)	0.55	0.27 ; $a=0.5, b=2$

The validation process has shown that the MPD is capable of accurately emulating rotor thrust and torque loads with the smaller set of blades, the Mavic blades. However, poor results were achieved for Test Case 3. The emulated yaw moment is shown in Figure 10. A clear time lag is visible, and the experimental curve is far from the smooth curve like that of the simulation. The PSD is shown in Figure 11. The difference in spectral energy is 55% and FMT is 0.27. The propeller pairs S2 & S4 and S3 & S5 acting intermittently at high rotational speeds were exciting a natural frequency of the MPD, with significant vibrations as a result and causing a noticeable displacement of the propeller arms. A slight delay in the start-up of the propellers from zero rpm to the initial spin could explain the time lag.

As the validation metrics clearly show, the emulation of complex aerodynamic loads is very challenging with the MPD in its current configuration.

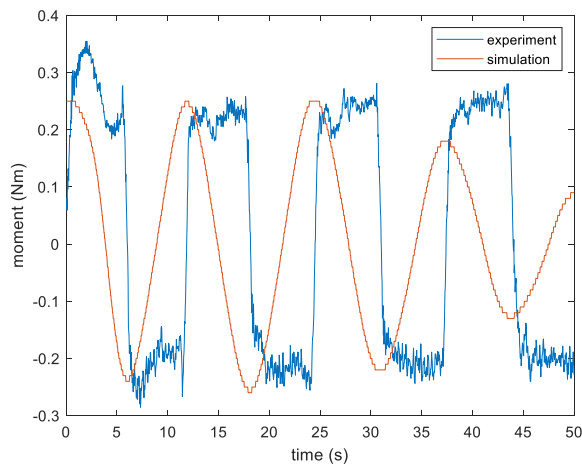


Figure 10. Emulated yaw moment, Test Case 5

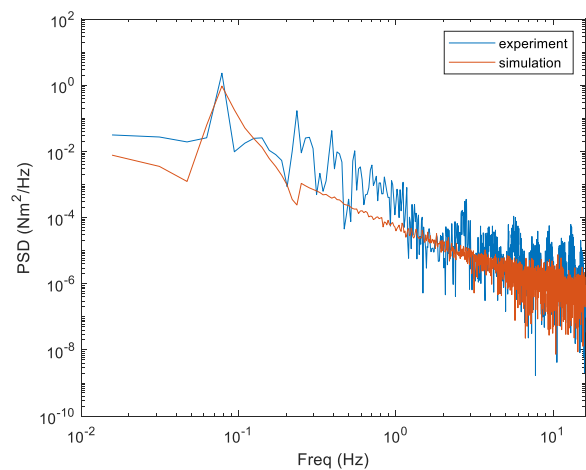


Figure 11. PSD of yaw moment, Test Case 5

Discussion

For the quantitative comparison of the validation process, two validation metrics have been proposed. Of these two metrics, FMT is the preferred metric. Setting the tolerance between limits a and b allows the user to ignore known sources of uncertainty and error such as load cell accuracy and data processing methods. Although still somewhat subjective, as the

tolerance is an estimate, it gives the user control over the level of tolerance. This is not possible with RE; however, it does give a straightforward comparison between simulation and experiment and is therefore useful from an engineering perspective.

Sources of uncertainty and error during this study were: the accuracy of FAST, the accuracy of the 6-axis load cell, the accuracy of the calibration of the propellers, repeatability of actuation, the data processing method and the level of vibrations generated during operation of the MPD. Clearly, a detailed and careful calibration is important to minimize the level of uncertainty. It is also clear that the vibrations of the device have a significant impact on the levels of uncertainty. As the test results showed, the amount of vibrations depend on how the propellers are used. For this reason, the tolerance level has been assessed for each Test Case separately. With the tolerance level set, it is then up to the user to decide what FMT is acceptable for a suitable actuator. For this study, $0.9 \leq \text{FMT} \leq 1$, was considered acceptable.

To calculate the validation metrics PSD was chosen, rather than using the measured and numerical values directly for equations (1) and (2). The high frequency vibrations generated by the MPD are likely to have limited effect on the motion response of the platform of the FOWT model it will be used on. The high frequencies form only a small part of the total spectral energy of the actuator outputs. Therefore, using PSD will give a better representation of how the platform reacts to the MPD and is considered more appropriate to calculate the validation metrics.

The validation process showed that the MPD is a suitable actuator to emulate aerodynamic thrust and torque loads. The rates of change of the propellers are high enough for the MPD to emulate the aerodynamic loads within the required frequency range at model scale.

However, the device underperforms with emulating yaw moments. These poor results are attributed to excessive high-frequency vibrations when the propellers operate at high rotational speeds, made worse when the propeller pairs are operated intermittently to change the direction of the moment acting in the yaw DOF. Structural stiffness of the device and vibration damping will have to be improved to reduce the vibrations, and these issues will need to be addressed in a potential follow-up study. However, the stiffness will be a trade-off between weight and strength; increasing the stiffness will increase the weight of the device, meaning the mass envelope could be exceeded on models with small scales.

Another potential improvement of the device would be the use of bi-directional propellers. Although it would increase the complexity of controlling the MPD, it will also give it more flexibility of actuating in several degrees of freedom.

The number of aerodynamic loads to be emulated simultaneously will depend on the type of FOWT model and its sensitivity to each load. The aim of the design of the MPD was to emulate as many loads as possible and so make it suitable for any type of FOWT. However, for hybrid testing of TLP models, with their strong structural coupling between tower and moorings, the MPD in its current configuration is most likely not the best type of actuator. Semisubmersible FOWTs in contrast, are not as sensitive to tower/mooring coupling, nor is it likely that platform response to aerodynamic yaw will be very high. In that case only thrust and torque would need to be emulated and the MPD would be a very suitable actuator. It is important, however, to investigate the sensitivity of the FOWT to aerodynamic loads numerically prior to each testing campaign to decide on the suitability of the actuator.

6. Conclusion

A proposed validation method of actuators for hybrid testing of floating wind turbine models in wave basins has been outlined in this paper. A validation metric, the Fraction of Measurements within a user defined Tolerance, is recommended and is calculated using the spectral energy of the actuator outputs. With a perfect performance of the actuator, FMT is 1.

The validation method has been applied to the Multi-Propeller Device, a novel type of actuator. Its design, operation and validation are described along with a discussion of the test results. For this study aerodynamic loads of the NREL 5 MW turbine at a scale of 1:37 were emulated in the experiments. The aero-hydro-elastic code FAST v8 was used for the numerical simulations.

The MPD is a suitable actuator for emulating rotor thrust and torque loads. The FMT is 0.97 for thrust loads, 0.98 for torque loads, when using the propeller blades with a length of 75 mm. However, poor results were achieved when trying to emulate the moment required for yaw motion of the platform of a semisubmersible FOWT. These results are highly influenced by high-frequency vibration generated when the propellers are operating at high rotational speeds, and when the propellers are operating intermittently.

The maximum output of each propeller is 15 N, and high rates of change of 65 N/s and 7.5 Nm/s were achieved, when the blades of 150 mm length were used. These high rates give the MPD enough bandwidth to emulate thrust and torque loads from turbulent wind.

Proof of concept is shown for the MPD, however, its suitability as an actuator, in its current configuration, depends on the type of platform and the aerodynamic loads of interest.

Acknowledgements

We would like to acknowledge Oscar Jimenez and José Azcona in CENER for their input on the development of the MPD, and Christian van den Bosch in MaREI for his assistance with the instrumentation.

This work was funded by Science Foundation Ireland under the PhD fellowship programme.

References

- [1] Muller K, Sandner F, Bredmose H, Azcona J, Manjock A and Pereira R 2014 Improved tank test procedures for scaled floating offshore wind turbines *In the proceedings of International Wind Engineering Conference IWECC 2014*
- [2] Wright C, O'Sullivan K, Murphy J and Pakrashi V 2015 Experimental comparison of dynamic responses of a tension moored floating wind turbine platform with and without spring dampers *Journal of Physics: Conference series* **628** (2015) 012056
- [3] Andersen M T 2016 Floating foundations for offshore wind turbines *PhD thesis Aalborg Universitetsforlag. Ph.d.serien for Det Teknisk-Naturvidenskabelige Fakultet, Aalborg Universitet*
- [4] Azcona J, Bouchotrouch F, Gonzalez M, Garcandia J, Munduate X, Kelberlau F and Nygaard T A 2014 Aerodynamic thrust modelling in wave tank tests of offshore floating wind turbines using a ducted fan *Journal of Physics: Conference Series* **524** (2014) 012089
- [5] Oguz E, Clelland D, Day A H, Incecik A, Lopez J A, Sanchez G and Almeria G G 2018 Experimental and numerical analysis of a TLP floating offshore wind turbine *Ocean Engineering* **147** (2018) 591-605
- [6] Bachynski E E, Chabaud V and Sauder T 2015 Real-time hybrid model testing of floating

- wind turbines: sensitivity to limited actuation *Energy Procedia* **80** (2015) 2-12
- [7] Hall M, Goupee A and Jonkman J Development of performance specifications for hybrid modelling of floating wind turbines in wave basin tests *Journal of Ocean Engineering and Marine Energy* **4** (2018) 1-23
- [8] DJI 2012 Spreading wings S800 user manual www.dji-innovations.com
- [9] Meseguer A and Guanche R 2019 Wind turbine aerodynamics scale-modelling for floating offshore wind platform testing *Journal of Wind Engineering & Industrial Aerodynamics* **186** (2019) 49-57
- [10] MARINET 2 <http://www.marinet2.eu/>
- [11] Holmes H A 2011 Quality assurance of wind energy assessment models *WAUDIT Guidance Report – WP6 Deliverable D24*
- [12] Jonkman B and Jonkman J 2016 FAST v8 *National Renewable Energy Laboratory, USA*
- [13] Robertson A, Bachynski E E, Gueydon S, Wendt F and Schunemann P 2020 Total experimental uncertainty in hydrodynamic testing of a semisubmersible wind turbine, considering numerical propagation of systematic uncertainty *Ocean Engineering* **195** (2020) 106605
- [14] Desmond C J, Hinrichs J-C and Murphy J 2019 Uncertainty in the physical testing of floating wind energy platforms' accuracy vs precision *Energies* **12(3)** (2019) 435

Paper C

Current simulation with Software in the Loop for floating offshore wind turbines

Published in

Journal of Physics: Conference Series, IOP Publishing, 2022, doi:10.1088/1742-6596/2265/4/042028

Authors:

A. Otter¹, B. Flannery¹, J. Murphy¹, C. Desmond²

¹ Marine and Renewable Energy Ireland, University College Cork, P43 C573, Ireland

² Gavin and Doherty Geosolutions Ltd, Dublin 14, D14 X627, Ireland

Abstract.

The presence of current is an added source of hydrodynamic loading on the platforms of Floating Offshore Wind Turbines (FOWT). Not only will current add viscous loading on the platform and moorings of FOWTs, but it will also affect wave loadings due to the alteration of wave shapes caused by wave-current interactions. Although the effects of current on platform response, mooring tensions and fatigue life have been numerically investigated, they are mostly neglected during scale model experiments for FOWTs. This paper proposes a novel method to simulate current loading and wave-current interactions during scale model tests by using a dynamic winch which is controlled using a Software in the Loop (SIL) approach. The winch is used in combination with a Multi-Propeller Actuator (MPA), for combined wave/wind/current testing in laboratory basins. The proposed current simulation method has lower costs and is more versatile than traditional physical current generation in a basin, as it allows for a wider range of test conditions and can be applied in any wave basin. A description of the experimental procedure is provided along with numerical validation using both AQWA and FAST. Results show that the winch actuator is capable of reliably emulating the drag force exerted by a current on the platform over a range of test conditions.

Introduction

Typically, the numerical model of a Floating Offshore Wind Turbine (FOWT) design is validated with extensive scale model tests [206] under a range of conditions and environmental loads. Combined wave and wind loading during scale model testing of FOWTs in laboratory wave basins is well documented in the literature. However, although it has been numerically shown [205] that current can have significant impact on platform response, mooring tensions and fatigue life of FOWTs, current loading is largely neglected during physical experiments.

The majority of FOWT experiments found in the literature, which do include current loading, apply physical current in the basin. Utsunomiya et al [207] tested a spar FOWT model with the full physical method, i.e. all environmental loads are applied physically, including current loads. They found that their numerical model underpredicted the current loads found with the experiments when vortex induced motion occurred. The main reason for this underprediction is due to the numerical model not taking vortex induced motions into account. Zhao et al [53] tested a 1/50 scale model of the Windstar Tension Leg Platform (TLP) FOWT, also using the full physical method. They found that under combined wave/wind/current loading, the wind and current loads resulted in damped surge and pitch response of the platform compared to wave-only loading. They also found that wind and current loads governed the low-frequency tension response of the tendons of the TLP. Bachynski et al [68] tested a 1/30 scale model of a semisubmersible FOWT and applied waves and current physically, however, wind loads were applied using the hybrid method, i.e. a combination of numerical modelling and physical testing. They do not elaborate on the effects of current loading on the test results.

Generating high quality laminar current, or a realistic boundary layer in wave basins is difficult to achieve and expensive to operate. As an alternative, Ahn and Shin [50] used a simple hybrid method to simulate current loads. Rather than physical current they used a pulley system with weights to represent a steady current. They tested a 10 MW version of the DeepCwind semisubmersible FOWT and found that the addition of current significantly reduced the surge Response Amplitude Operator (RAO) of the platform. However, their method did not take

wave-current interactions into account, which means it is likely that heave and pitch response of the platform are misrepresented.

This paper proposes a novel method to simulate current using a dynamic winch actuator with Software in the Loop (SIL). This hybrid test method is based on methods to emulate wind loads with dynamic winches and SIL, which has successfully been applied in several test facilities during scaled floating wind experiments, e.g. [68], [76]. The winch will be used in combination with a Multi-Propeller Actuator (MPA) for wind emulation, for combined wave/wind/current hybrid testing in laboratory basins. The new method is tested at the Lir National Ocean Test Facility (NOTF), Cork, Ireland, with a 1/50 scale model of the INNWIND.EU semisubmersible [14] FOWT.

Current emulation system

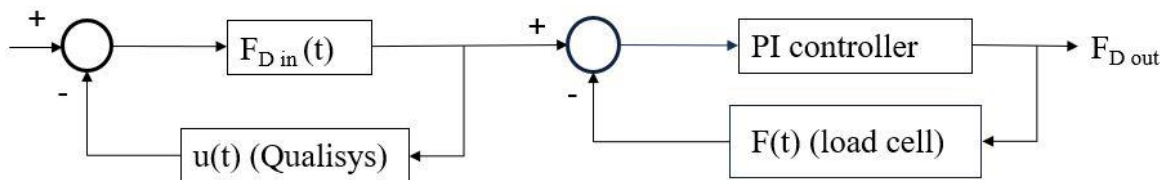
To simulate current, the winch cable is connected to the FOWT model on the downstream side. The tension in the winch cable is altered dynamically to emulate the drag force a current would exert on the platform of the FOWT, depending on the velocity of the current. For floating objects, the relative velocity of the current is found by combining the velocity of the current and the velocity of the floating object. The drag force is calculated with the drag term of the Morison equation:

$$F_D = \frac{1}{2} \rho C_D A |U - u| (U - u) \quad (1)$$

Where F_D is the drag force, ρ is the density of water, C_D is a drag coefficient, A is the wetted cross-sectional area of the platform in still water, U is the velocity of the current, and u is the velocity of the platform.

The winch actuator consists of a Schneider Electric BCH2 servo motor and a custom-made winch drum. The winch motor is operated by a Schneider Electric Lexium 28A servo drive. A dSPACE 1104 real-time controller, which is linked with MATLAB/Simulink for the real-time simulation, controls the servo drive. A simple algorithm in Simulink, based on equation (1), calculates the drag force of the current on the platform for each time step. The demanded force/tension from the motor is determined (at each time step) by the real time simulation and this force is maintained by a Proportion Integration (PI) controller using the measured instantaneous force from a load cell in the winch cable. A Qualisys motion tracking system monitors the velocity of the platform. Real-time data from the motion tracking system is used as feedback to update the relative velocity and drag force of the current for each time step. The control loop of the system is shown in Figure 1, and the hardware layout in Figure 2.

Figure 1. Control loop of the current emulation system.



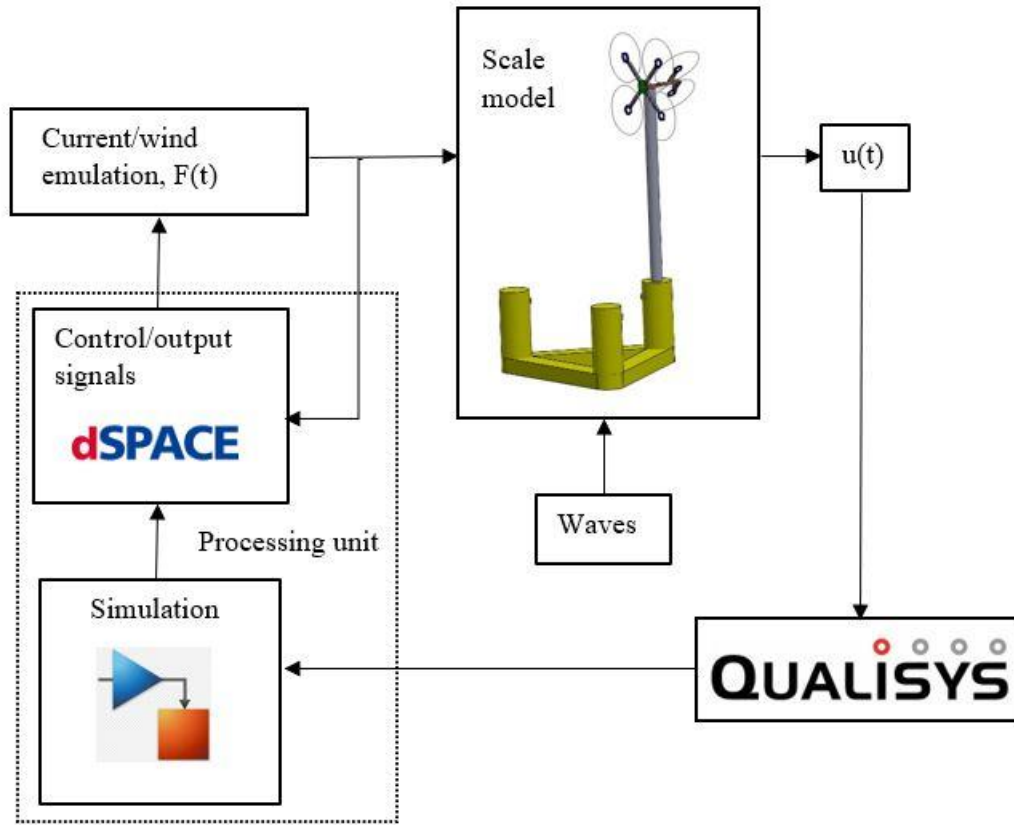


Figure 2. Hardware layout of the system.

Wave-current interactions

Wave-current interaction is a well-known phenomenon, which causes the alteration of wave shapes. When the direction of a sea current opposes the incident wave direction, wave lengths will become shorter and wave heights will increase, resulting in steeper waves. The opposite is true when a current follows the incident wave direction: wave lengths become longer and wave heights will decrease, resulting in shallower waves. It is likely that the heave- and pitch response of FOWTs will change due to wave-current interactions and will therefore have to be considered when performing hybrid tests for current. A brief theoretical overview of wave-current interactions will be given here.

When assuming the current as horizontally- and vertically uniform, and using linear wave theory, a reference frame moving at the current velocity can be defined [31] to simplify the analysis. For waves only, and assuming deep water, the wavelength, L , and wave frequency, ω , are defined as:

$$L = \frac{2\pi}{k}, \quad \omega = \sqrt{gk \tanh kh} \quad (2)$$

Where k is the wave number, g is gravity, and h is the water depth. When a current is present the wavelength and wave frequency are defined as:

$$L_1 = \frac{2\pi}{k_1}, \quad \omega_r = \omega \pm k_1 U = \sqrt{gk_1 \tanh k_1 h} \quad (3)$$

Where U is the velocity of the current, the subscript 1 denotes the conditions with a current, and ω_r is the wave frequency as measured in the reference frame. For a stationary observer ω

will be the same with or without a current present. The altered wave amplitude, A , in the presence of current [32] is defined as:

$$A_1 = A \sqrt{\left(\frac{C_g}{C_{g1} + U} \right) \left(\frac{1}{1 + U / C_{g1}} \right)} \quad (4)$$

Where C_g is the wave group celerity. Similarly, the spectra of irregular waves are altered by the presence of a current. With an opposing current the spectral energy will increase, and for a following current the spectral energy will decrease. The alteration of wave spectra due to the presence of current is defined [33] as:

$$S_1(\omega) = S(\omega) \frac{4}{\left[1 + \sqrt{1 + (4U\omega/g)} \right]^2 \sqrt{1 + (4U\omega/g)}} \quad (5)$$

To simulate wave-current interactions without having physical current in a basin, wave makers can be programmed to generate waves that have been altered as if a current is present. For irregular waves the wave maker can generate an irregular wave spectrum – without the presence of a physical current – which has the same spectral energy as if a current is present. This is done by transforming the wave-only spectrum into a spectrum according to equation (5).

Test setup

Experiments with a 1/50 scale model of the INNWIND.EU semisubmersible were performed in the Ocean Basin at Lir NOTF. The winch wire of the current emulation system is connected, via a pulley system on the instrument bridge, to the turbine column of the platform at $Z = \text{COG}$ in a conventional coordinate system. The connection at $Z = \text{COG}$ was chosen to eliminate unwanted pitch motions of the platform resulting from actuation with the winch. A spring with stiffness coefficient of 265 N/m is fitted between the platform and the load cell in the winch wire to absorb snap loads. Independently from the winch cable, three horizontally mounted mooring cables with springs are attached, above still water level, in a 120-degree spread to the instrument bridge and foot bridge. Although not representative, the horizontal moorings simplify the test set-up and are readily replicated in the numerical model. The moorings provide the restoring force for the wave loading and simulated wind and current loading. An image of the model in the Ocean Basin is shown in Figure 3.

Wind emulation

For wind emulation a MPA is used, which is described in [200]. Rather than the DTU 10 MW turbine, which is featured in the original design of the INNWIND.EU semisubmersible FOWT, the MPA is used to emulate rotor thrust and torque of the NREL 5 MW turbine at hub height. A comparison study between the MPA, simulating the NREL 5 MW, and a physical 1/50 scale model of the NREL 5 MW turbine is planned, which is why this combination of platform and turbine is chosen. To accommodate the NREL 5 MW, the ballast of the platform has been adapted, and only 4 propellers, rather than 6 were used on the MPA to maintain weight similitude of the rotor nacelle assembly. The numerical model has been adapted to reflect the adjusted ballast and different wind turbine model.

Rotor thrust and torque of the NREL 5 MW is calculated with an algorithm in Simulink, based on the method described in [61]. Look-up tables determine the thrust coefficient, which is coupled with the Tip Speed Ratio (TSR), and rotor torque, which is coupled with rotor speed. The dSPACE 1104 controls the rotational speed of the propellers of the MPA.

Methodology

The winch actuator is validated by a series of experiments. First, a demanded tension signal is compared with the emulated tension signal without SIL. A validation metric as described in [200] is applied to the results. Next, the results of experiments with SIL and numerical simulations in Ansys AQWA and FAST for a range of environmental conditions are compared. Again a validation metric is applied to said results.

Besides graphical comparisons of experimental- and numerical results, a quantitative comparison is made to validate the current emulation system. Two metrics, Relative Error (RE) and Fraction of Measurements within a user-defined Tolerance (FMT), are used. Both metrics are defined in [200] and provide a statistical comparison between experimental- and numerical results. For a perfect match between experiment and numerical simulation $RE = 0$, and $FMT = 1$, with a lower tolerance $a = 1$, and upper tolerance $b = 1$. The tolerance between limits a and b can be set by the user to provide an indication of uncertainty and error levels.

The choice of modelling a 5 MW turbine on a platform originally designed for a 10 MW turbine, is perhaps unusual. However, the main objective of this study is not the performance of the platform but the proof of concept of the current simulation method, in combination with wind simulation and physical waves. Proof of concept is assumed to be achieved if the difference between numerical- and experimental results remains under 20%, or when R.E. does not exceed 0.2, and when FMT remains above 0.8 with $a \geq 0$ and $b \leq 5$.

Simplifications and assumptions

To keep the system as robust as possible some simplifications and assumptions have been made. For this study only one direction of the current is considered, which is 180 degrees opposite of the incident wave direction. Vortex shedding around the columns and resulting sway motions of the platform are neglected. AQWA, which uses a combination of the Morison equation and Potential Flow methods, does not capture vortex shedding, so only the drag force in surge direction is modelled with both the numerical model and the winch actuator. The flow of the current is assumed to be steady and uniform. The wetted surface A in equation (1) is assumed to be a constant, although it changes dynamically during testing as the platform moves in heave and pitch. However, this effect is expected to be small and not have a large influence on the results.

Systemic sources of error and uncertainty

Some potential sources of error and uncertainty in the system have been identified. Latency is a problem faced by any SIL application; monitoring, feedback and emulation will all have to be fast enough to fit within the real-time simulation time-step. A suitable frequency for each action is required to keep latency to an acceptable level.

Both the spring in the winch cable and the cable itself are elastic, which helps to prevent damage from large snap loads during testing. However, the spring is likely to cause a phase shift between the demanded signal and measured signal, as can be seen in Figure 4, and is also a potential source of hysteresis effects. The PI controller will mitigate the phase shift and hysteresis effects, but its effectiveness depends in part on the accuracy and noise levels of the sensors used for feedback. Another source of uncertainty is C_D in equation (1), which has been empirically derived from drag tests with the scale model in the Wave Current Flume in Lir

NOTF for a range of velocities. The accuracy of C_D will have significant influence on the demanded drag force, and hence, so will the accuracy of test cases with current. Other sources of uncertainty include facility specific errors such as wave reflection in the basin.

Results

To demonstrate the capabilities of the winch actuator, first a sinusoidal tension signal is emulated with the scale model in still water. For this test case the PI controller received instantaneous tension feedback, however, no motion tracking feedback was used. This test case is therefore regarded as emulating without SIL. The results are shown in Figure 4.

The measured signal is in close agreement with the demanded signal. Furthermore, repeatability is excellent, with a correlation coefficient between the measurements of 0.994. The validation metrics for actuation only, i.e., for the force the actuator is supposed to emulate, of both the winch actuator and MPA are shown in Table 1. Next, the response of the scale model to drag force emulation is compared to numerical simulations with Ansys AQWA and FAST. The test cases are summarized in Table 2. None of the test cases have been repeated with both AQWA and FAST, however, the aim of this study is not a comparison between the two numerical codes but proof of concept of the winch actuator.

Table 1. Validation Metrics for actuation only.

	RE	FMT, $a:0.85, b:1.15$
Winch actuator	0.013	0.95
MPA	0.022	0.95

AQWA can model wave-current interactions, but it cannot model the turbine aerodynamics. On the other hand, FAST can model turbine aerodynamics, but it cannot model wave-current interactions. The two numerical codes are therefore used to complement each other for this study. All the results shown in this paper are at model scale.

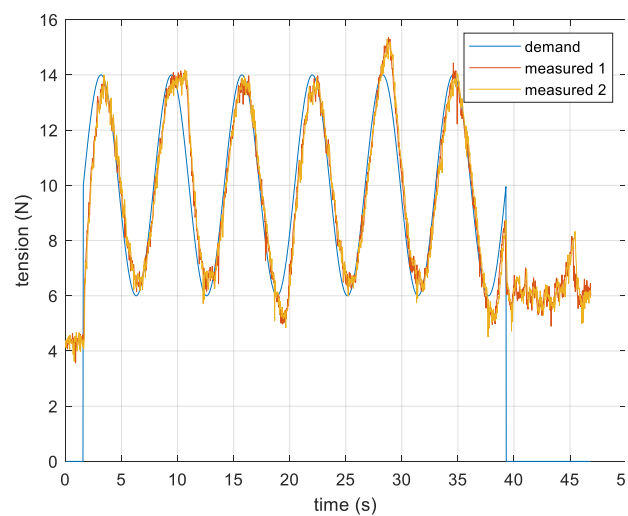
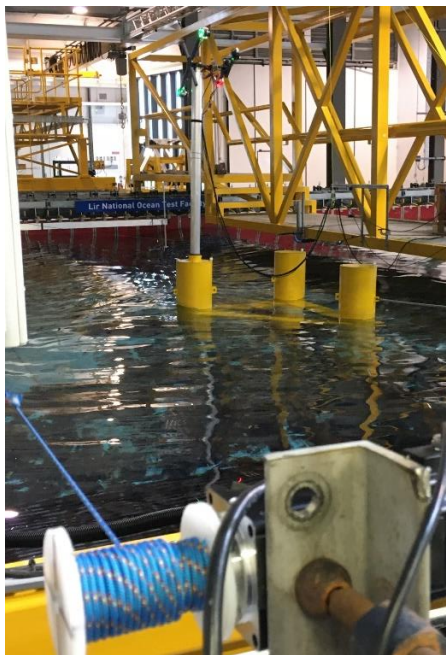


Figure 3. The scale model in the basin in Lir NOTF, with the winch actuator in the foreground.

Figure 4. Demanded and measured tension signal of the winch actuator, while connected to the scale model in the basin.

Table 2. Summary of test cases in the Ocean Basin, TC = Test Case.

Test Case	Conditions	SIL	AQWA	FAST
TC 1	Current only	√	√	x
TC 2	Current only	x	√	x
TC 3	Wind only	√	x	√
TC 4	Current and wind	√	x	√
TC 5	Waves only	x	√	x
TC 6	Waves and current	√	√	x
TC 7	Waves, wind and current	√	x	√

Figures 5 and 6 show the results of response in the surge Degree of Freedom (DOF) to drag force emulation with- and without SIL respectively. Current velocities of 0.11 m/s and 0.14 m/s are simulated, which correspond to 0.75 m/s and 1 m/s respectively at full scale. Greater agreement of results is achieved with SIL. Without SIL, larger- and more oscillations occur before the system settles, and after settling, the surge excursions are smaller than with SIL. A PID controller should be able to damp out oscillations in the no-SIL situation and settle the system quicker. However, the Derivative component requires a clean feedback signal. The tension feedback signal was found to be very noisy, up to 5N without filtration, which was reduced to 0.5N after shielding of all the signal cables. However, adding numerical filters in Simulink, resulted in a broken saw-tooth signal with maximum amplitudes of 2.5N at best. Instead, a PI controller was opted for the current simulation system, which is able to handle the unfiltered noisy signal of 0.5N. Figures 5 and 6 also show there is a slight phase shift between experimental and numerical signals. The numerical signal lags the experimental signal, where the opposite is expected due to the spring in the winch wire.

Lower simulation- and actuation frequencies are used for the current emulation system, compared to frequencies typically used for SIL applications [76]. For this system the motion tracking- and tension feedback frequency is 32 Hz, the actuation frequency is 25 Hz, and the real-time simulation frequency is 22 Hz, giving a simulation time-step of 0.045 seconds. The reason for these lower frequencies is that the dSPACE 1104 is not powerful enough to control both the MPA and winch actuator simultaneously at typical frequencies.

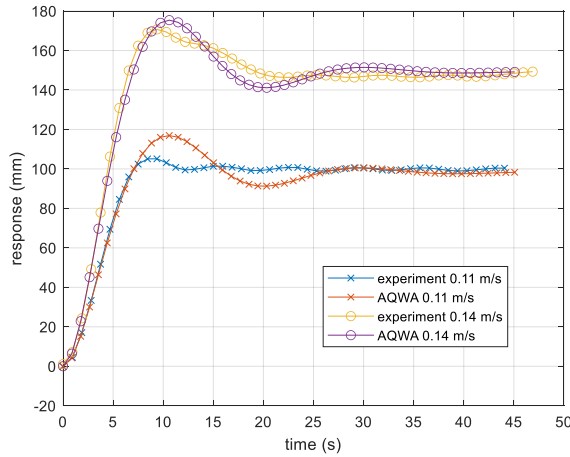


Figure 5. Experiments vs AQWA, surge response to current simulation with SIL, TC 1.

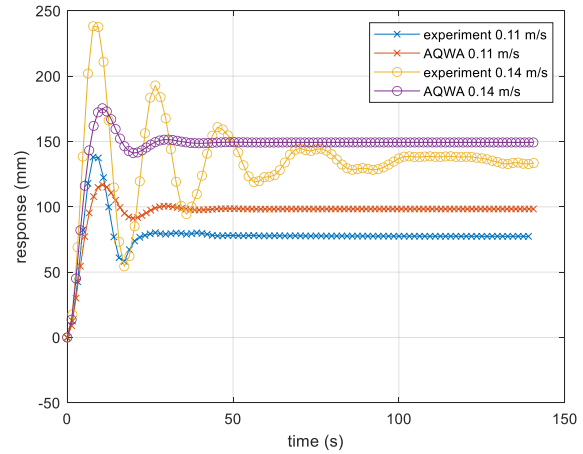


Figure 6. Experiments vs AQWA, surge response to current simulation without SIL, TC 2.

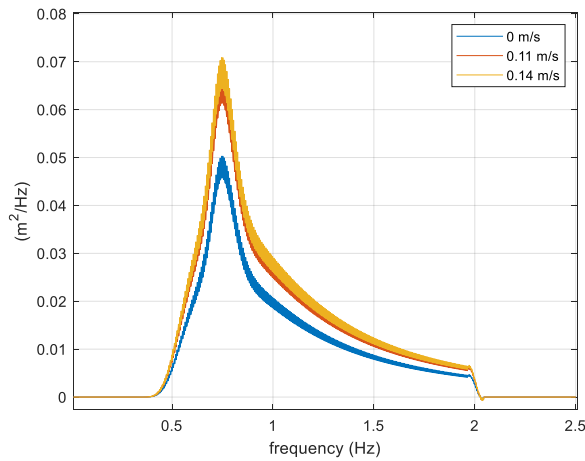


Figure 7. Theoretical wave spectra for wave-only and wave-current test cases.

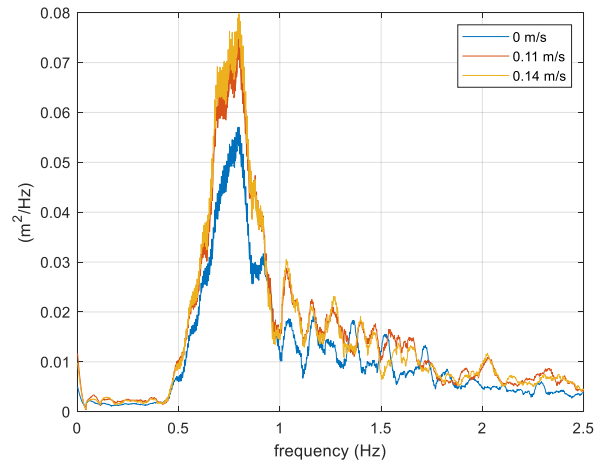


Figure 8. Measured wave spectra for wave-only and wave-current test cases.

Wave-current interactions have been investigated with Test Case 5 and 6. Only irregular waves have been used. For the wave-only cases a JONSWAP spectrum with $T_p = 1.34$ s. and $H_s = 0.1$ m. was used, which corresponds to $T_p = 9.5$ s. and $H_s = 5$ m. at full scale, and which was adjusted for wave-current cases.

Figure 7 and Figure 8 show the theoretical- and measured spectra, which both clearly show a higher peak and increased energy at the higher wave frequencies for the spectra with opposing currents at 0.11 m/s and 0.14 m/s. The difference in spectral energy between theory and measurement is 11.4% for the wave-only cases, 9.9% for waves and current = 0.11 m/s, and 5.8% for waves and current = 0.14 m/s.

The amplitude spectra for the response in the heave DOF of the INNWIND semisubmersible FOWT are shown in Figure 9 and Figure 10. For both the wave-only and wave/current cases the peak is at a lower frequency according to AQWA compared to the experiments, and the experiments show resonance around 0.35 Hz which is not captured by the numerical model.

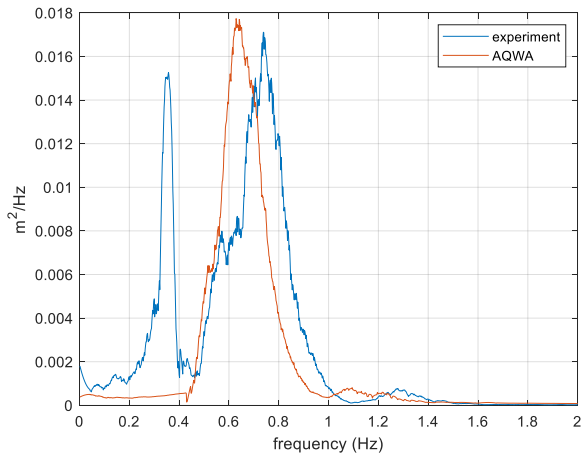


Figure 9. Heave amplitude spectrum of the platform, waves only, TC 5.

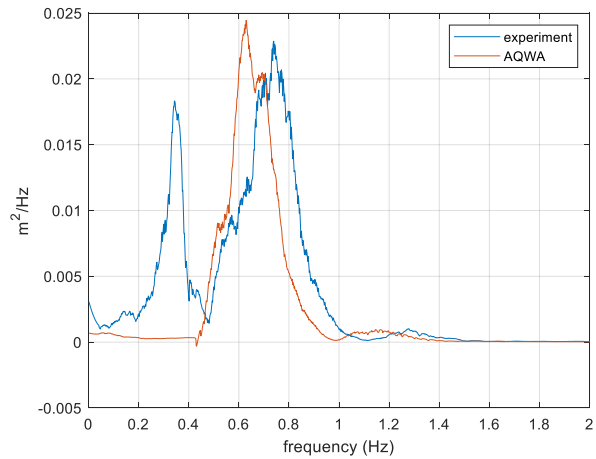


Figure 10. Heave amplitude spectrum of the platform, waves and current = 0.14 m/s, TC 6.

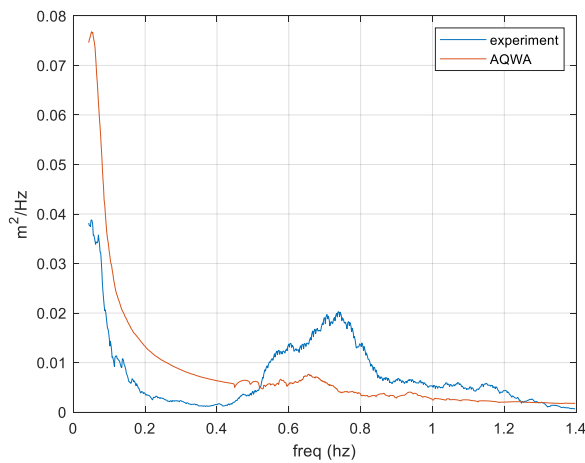


Figure 11. Surge amplitude spectrum of the platform with waves and current = 0.14 m/s, TC 6. Experiments vs AQWA.

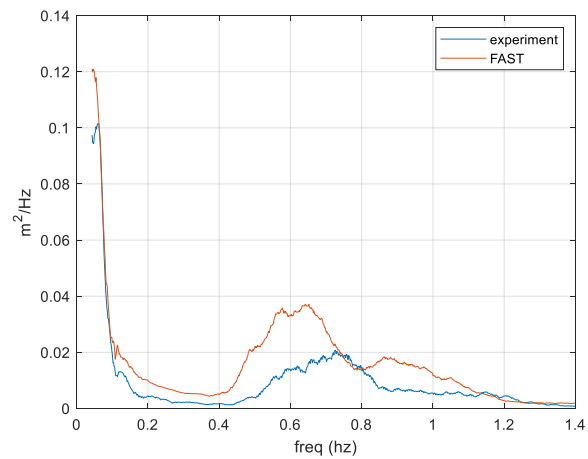


Figure 12. Surge amplitude spectrum of the platform with waves, wind and current = 0.14 m/s, TC 7. Experiments vs FAST.

However, spectral energy around the peak wave frequency is similar for experiments and AQWA, which at least gives some confidence that wave-current interactions are simulated correctly with the current simulation system. Similar results were found for the pitch DOF.

The spectrum for surge response with irregular waves and current is shown in Figure 11, and the spectrum for surge response with irregular waves, current, and turbulent wind around rated speed is shown in Figure 12. Both cases show similar amounts of energy around the wave frequencies during the experiments. However, AQWA underpredicts surge response due to wave excitation, whereas FAST overpredicts surge response due to wave- and wind excitation. This is also illustrated in Table 3, which shows the mean values of surge for the experiments and numerical simulations of TC 6 and TC 7, and the standard deviation of the surge fluctuations.

Table 3. Mean surge values and standard deviations, TC 6, and TC 7.

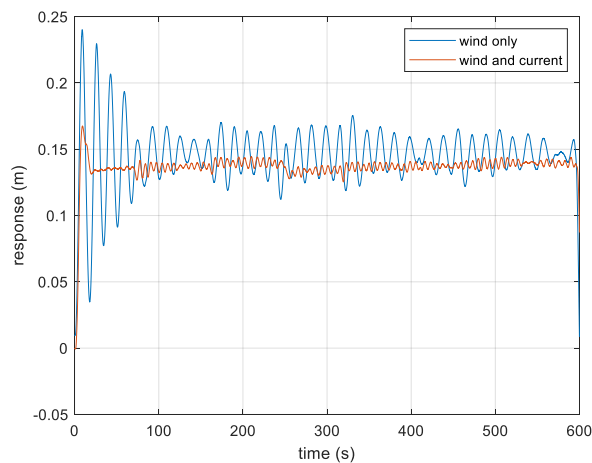
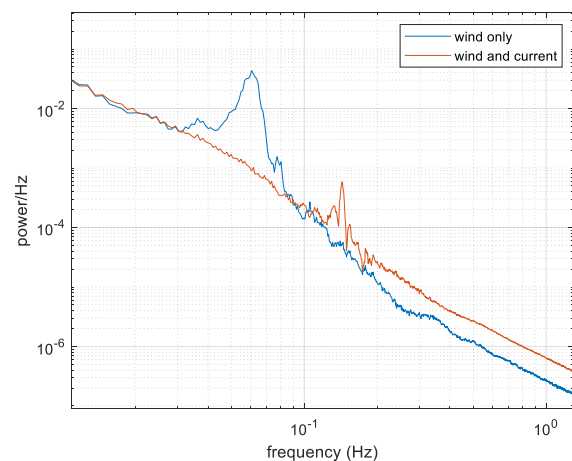
	Experiments		Numerical simulations	
	Mean value surge	Standard deviation	Mean value surge	Standard deviation
TC 6	0.1396 m	0.0105	0.1510 m	0.0032
TC 7	0.1257 m	0.0099	0.1144 m	0.0171

The validation metrics for platform response to environmental loads of the different Test Cases are shown in Table 4.

Table 4. Validation Metrics for platform response to actuation.

	RE			FMT		
	Surge	Heave	Pitch	Surge	Heave	Pitch
TC1	0.02	-	-	$a:0.85,$ $b:1.15$	0.99	-
TC3	-0.03	-	0.03	$a:0.15,$ $b:4.55$	0.87	-
TC4	-0.12	-	0.06	$a:0.15,$ $b:4.55$	0.87	-
TC5	-1.20	-0.36	-	$a:0.15,$ $b:4.55$	0.38	0.34
TC6	0.06	-0.46	-	$a:0.15,$ $b:4.55$	0.92	0.35
TC7	-0.18	-	-	$a:0.15,$ $b:4.55$	0.86	-

Other interesting results found during experiments, show that there is a small amount of damping of the heave motions of the platform due to wind during wave/wind cases compared to wave-only cases, whereas the addition of wind causes a significant increase of pitch response of the platform.

**Figure 13.** Surge response, experimental results of TC 3 vs TC 4**Figure 14.** Surge PSD, experimental results of TC 3 vs TC 4

On the other hand, there is some damping of pitch motions due to current during wind/current cases compared to wind-only cases. Furthermore, there is a significant reduction of wind induced surge motions, and an increase of surge stiffness with the addition of current in wind/current cases compared to wind-only cases, as is shown in Figure 13 and Figure 14. Of course, in real ocean conditions wind and current without waves would be a rare combination. When comparing the wave/wind cases to wave/wind/current cases, there is still some damping of wave/wind induced surge motions with the addition of current, however, surge stiffness remains the same and is dominated by wave excitation.

Discussion

Results and validation metrics show that emulating the current induced drag force with the winch actuator can simulate current with an acceptable degree of accuracy compared to numerical simulations. However, as the number of environmental loads is increased, the level of uncertainty increases, and accuracy drops. Particularly the addition of waves has a detrimental effect on the validation metrics for heave and pitch of the platform. This can be explained by the additional resonance frequency of the platform in heave and pitch which is not captured by the numerical model. The exception is the surge DOF for Test Case 5 and 6, where better results are achieved with the addition of current. This is due to significant underprediction of surge motions by the numerical model in Test Case 5 compared to Test Case 6. This clearly shows that fidelity of the validation metrics used here is dependent on the accuracy of the numerical model.

Where RE is a direct comparison between experiments and numerical models, FMT is more ambiguous. The tolerance in FMT allows the user to estimate errors and uncertainty, and the level of confidence in the numerical model. However, this metric should be used cautiously; a number close to 1 may be achieved but depending on how wide the tolerance is the result may still be unfavourable. Therefore, both the RE and FMT metrics should be used to complement each other, RE for the direct comparison and FMT for uncertainty estimation. If both metrics are favourable, there is high confidence in the accuracy of the results.

As was shown in Figure 4, a phase shift between demanded tension signal and measured tension signal exists due to the presence of a spring in the winch wire. The PI controller mitigates the phase shift, and although it is not able to eliminate it entirely, the phase shift is kept acceptably small. Protecting the winch from snap loads by keeping the spring in the wire was deemed more important than eliminating the phase shift.

Figures 5 & 6 showed that there is a lag in surge between the experimental signals and numerical signals. Unexpectedly, the numerical results are lagging the experimental results. It is possible that, despite the phase shift between demanded tension and measured tension caused by the spring, the PI controller is controlling the winch too aggressively, resulting in higher surge stiffness of the model during experiments. However, it is also possible that surge stiffness is incorrectly applied in the numerical model.

Future work will include a comparison study between the hybrid test method for current and testing with physical current. Such a comparison will be used for further validation of the current simulation system and might reveal its accuracy, and consequently, whether the numerical model needs calibrating, or the PI controller needs tuning. Further future work will include expanding the control algorithm to dynamically alter A in equation (1) during testing and determine its influence on the results. Although the effect is expected to be small, it has

not been quantified during this study. Other future work may include the expansion of the test setup with two or more winches, so that current can be simulated in more than one direction.

Conclusion

A novel hybrid method to simulate current is presented in this paper. This method uses a dynamic winch with SIL to emulate the drag force of a current on a 1/50 scale model of the INNWIND.EU semisubmersible FOWT. The winch actuator is used in combination with a MPA, which emulates aerodynamic loads. The current simulation system is validated by comparing numerical results, found with AQWA and FAST, against experimental results and applying validation metrics to said results. Wave-current interactions are simulated by adjusting a JONSWAP spectrum as if a physical current is present in the wave basin. As more environmental loads are added during tests, more errors are introduced, and the validation metrics become less favourable. However, proof of concept was achieved with the current simulation system for most cases, particularly for platform surge. For the combined wave/wind/current case, RE, the most direct comparison, does not exceed 0.18. However, the correctness of the validation metrics depends on the accuracy of the numerical model, and a comparison with full physical tests for further validation is therefore desirable.

Acknowledgements

The authors would like to acknowledge Christian van den Bosch in Lir NOTF for his assistance with the instrumentation, and the customer service of Schneider Electric for their technical assistance with setting up the winch motor and servo drive.

This work was funded by Science Foundation Ireland under the PhD fellowship programme.

References

- [1] A. Otter, J. Murphy, V. Pakrashi, A. Robertson, and C. Desmond, "A review of modelling techniques for floating offshore wind turbines," *Wind Energy*, 2021, doi: 10.1002/we.2701.
- [2] L. Chen and B. Basu, "Fatigue load estimation of a spar-type floating offshore wind turbine considering wave-current interactions," *Int. J. Fatigue*, vol. 116, no. November 2017, pp. 421–428, 2018, doi: 10.1016/j.ijfatigue.2018.06.002.
- [3] T. Utsunomiya, S. Yoshida, H. Ookubo, I. Sato, and S. Ishida, "Dynamic analysis of a floating offshore wind turbine under extreme environmental conditions," *J. Offshore Mech. Arct. Eng.*, 2014, doi: 10.1115/1.4025872.
- [4] Y. sheng Zhao, X. he She, Y. ping He, J. min Yang, T. Peng, and Y. feng Kou, "Experimental Study on New Multi-Column Tension-Leg-Type Floating Wind Turbine," *China Ocean Eng.*, vol. 32, no. 2, pp. 123–131, 2018, doi: 10.1007/s13344-018-0014-0.
- [5] E. E. Bachynski, T. Sauder, M. Thys, V. Chabaud, and L. O. Sæther, "Real-time hybrid model testing of a braceless semisubmersible wind turbine. Part 2: experimental results," in *Proceedings of the ASME 2016 35th International Conference on Ocean, Offshore and Arctic Engineering OMAE2016 June*, 2016, no. OMAE2016-54437, pp. 1–12.
- [6] H. Ahn and H. Shin, "Experimental and Numerical Analysis of a 10 MW Floating Offshore Wind Turbine in Regular Waves," *Energies*, vol. 13, no. 2608, pp. 1–17, 2020, doi: 10.3390/en13102608.
- [7] M. Hall and A. J. Goupee, "Validation of a hybrid modeling approach to floating wind turbine basin testing," *Wind Energy*, vol. 21, no. 6, pp. 391–408, 2018, doi: 10.1002/we.2168.

- [8] F. Sandner *et al.*, “INNWIND.EU Deliverable D4.3.3 - Innovative Concepts for Floating Structures,” 2015.
- [9] T. S. Hedges, “Some effects of currents on wave spectra,” in *1st Indian Conference on Ocean Engineering, IIT Madras*, 1981.
- [10] S. Draycott *et al.*, “Re-creation of site-specific multi-directional waves with non-collinear current,” *Ocean Eng.*, vol. 152, pp. 391–403, Mar. 2018, doi: 10.1016/J.OCEANENG.2017.10.047.
- [11] N. E. Huang, D. T. Chen, C.-C. Tung, and J. R. Smith, “Interactions between Steady Wav-Uniform Currents and Gravity Waves with Applications for Current Measurements,” *J. Phys. Oceanogr.*, vol. 2, no. 4, pp. 420–431, 1972, doi: 10.1175/1520-0485(1972)002<0420:ibswuc>2.0.co;2.
- [12] A. Otter, J. Murphy, and C. J. Desmond, “Emulating aerodynamic forces and moments for hybrid testing of floating wind turbine models,” in *Journal of Physics: Conference Series*, 2020, doi: 10.1088/1742-6596/1618/3/032022.
- [13] C. Matoug, B. Augier, B. Paillard, G. Maurice, C. Sicot, and S. Barre, “An hybrid approach for the comparison of VAWT and HAWT performances for floating offshore wind turbines,” in *Journal of Physics: Conference Series*, 2020, doi: 10.1088/1742-6596/1618/3/032026.

Paper D

Combined current and wind simulation for floating offshore wind turbines

Accepted for Publication in

Journal of Physics: Conference Series, IOP Publishing, 2022

Authors:

A. Otter¹, C. Desmond², B. Flannery¹, J. Murphy¹

¹ Marine and Renewable Energy Ireland, University College Cork, P43 C573, Ireland

² Gavin and Doherty Geosolutions Ltd, Dublin 14, D14 X627, Ireland

Abstract. This paper describes the validation of a novel method to simulate current loading on a floating offshore wind turbine model. A dynamic winch actuator is used to emulate the drag force of current on the platform of the model with a Software in the Loop application. Current loads are combined with wave- and wind loads. The results of experiments with physical current are validated against the results of experiments with simulated current. A method to simulate wave-current interactions is also described. The results show that the winch actuator can reliably emulate current induced drag forces in comparison with physical current under various combinations of environmental loads. Experimental repeatability of the response of the platform is shown to be superior when using simulated- rather than physical current.

Introduction

Combined wave- and wind loads applied to Floating Offshore Wind Turbine (FOWT) scale models in wave basin experiments [206] is well documented in the literature. Environmental loads are either applied with the full physical method, or with the hybrid method during FOWT experiments. With the latter method some of the environmental loads are not applied physically but calculated in real-time and emulated on the model with a mechanical actuator.

Adding current to waves and wind during FOWT experiments in laboratory basins is an additional step towards creating realistic offshore conditions and providing valuable insight for systems design and numerical tool validation. Current loading, although rarely applied during FOWT experimental campaigns, is typically applied using current generation capabilities.

Bachynski et al [68] applied physical current during their tests with a semisubmersible FOWT model but used a hybrid method for wind loads. Gueydon et al [92] compared experiments with the full physical method and the hybrid method for wind loads on a Tension Leg Platform model but also applied physical current for all tests. Utsunomiya et al [207] tested a spar FOWT model under combined wind/wave/current loads with the full physical method.

Bulky and expensive equipment is required to generate physical current in wave basins and this capability is available in only a limited number of facilities at a scale suitable for the testing of FOWT models. Furthermore, it is challenging in a laboratory environment to generate laminar current flows or turbulent flows which are characteristic of real-world flows over more than a limited range dictated by the facility's operational capabilities and basin lengths. The generation of realistic current flows while also generating realistic waves with low levels of reflection is a further challenge.

In this paper an alternative hybrid method to simulate current loading on a FOWT model is compared to the use of physical current generation. This hybrid method uses a dynamic winch with a Software in the Loop (SIL) application to emulate the resulting drag force from a current on the platform of a FOWT model. The emulation of current induced drag force will be referred to as 'SIL current' in this paper, and physically generated current will simply be referred to as 'physical current'.

The comparison study was conducted in the Wave Current Flume (WCF) at the Lir National Ocean Test Facility (NOTF), Cork, Ireland, with a 1/50 scale model of the INNWIND.EU semisubmersible [14] FOWT. The winch actuator was used in combination with physical waves and a Multi-Propeller Actuator (MPA) for aerodynamic load emulation, which also works with SIL.

Current simulation system

A servo motor and a custom-made winch drum make up the winch actuator. The winch cable is connected to the FOWT model on the downstream side via a pulley system on the instrument bridge. A real-time controller, linked with MATLAB/Simulink for the real-time simulation, controls the winch. The drag force is a function of the velocity of the current, and the winch alters the tension in the cable dynamically to emulate the drag force on the platform of the FOWT. Due to motion of the floating platform the relative velocity of the current is constantly changing. By combining the velocity of the current and the velocity of the floating platform the relative velocity is found. The drag force is calculated with the drag term of the Morison equation:

$$F_D = \frac{1}{2} \rho C_D A |U - u| (U - u) \quad (1)$$

Where F_D is the drag force, ρ is the density of water, C_D is a drag coefficient, A is the wetted cross-sectional area of the platform, U is the velocity of the current, and u is the velocity of the platform.

An algorithm in Simulink, based on equation (1), calculates the drag force of the current on the platform for each time step with steady velocity of the current as input. The demanded force/tension is maintained by a Proportion Integration (PI) controller with feedback from a load cell in the winch cable. Real-time velocity data of the platform is provided by a motion tracking system and used to update the relative velocity and drag force of the current for each time step.

The sampling-rate of the motion tracking system and load cell is 32 Hz, the actuation rate of the winch is 25 Hz, and the real-time simulation rate is 22 Hz, giving a time step of 0.045 seconds. For the experiments, a soft mooring system, i.e., horizontal moorings above still water level, is used for station keeping of the model, with three mooring lines in a 120-degree spread. To eliminate non-representative pitch motion of the model from actuation with the winch, the cable is connected to the turbine column of the model at $Z = \text{Centre of Gravity (COG)}$ in a conventional coordinate system. Although the force centre for current on the wetted area of the platform shifts during pitch and heave, any non-representative pitch is expected to be minimal with the cable at COG. Figure 1 shows the model in the WCF in Lir NOTF, and Figure 2 shows the layout of the winch actuator.

Wind simulation

The MPA, which is described in [200], emulates rotor thrust and rotor torque of the NREL 5MW turbine at hub height on the model. The original design of the INNWIND semisubmersible FOWT is with the DTU 10MW turbine. However, a comparative study between the MPA and a 1/50 physical scale model of the NREL 5MW turbine is planned for a future date and has dictated the use of the 5MW turbine in this study. Although an unusual combination of platform and turbine, the focus of this study is the simulation method of current in combination with wave- and wind loads. The choice of wind turbine is therefore arbitrary.

Rotor thrust and torque are calculated with another algorithm in Simulink, based on the method described in [61]. A single time-series of turbulent wind around 9 m/s at full scale is used as input for the numerical simulation. A lookup table for the thrust coefficient as a function of Tip Speed Ratio (TSR) is used for the calculation of rotor thrust. Another lookup table is used to determine rotor torque as a function of rotor speed. These lookup tables were generated with

offline simulations of the NREL 5MW turbine in FAST. Thrust- and torque loads are scaled down before emulation with the MPA. All wind loads for any test cases with wind were simulated with the MPA. Wind direction was aligned with wave direction for all test cases.

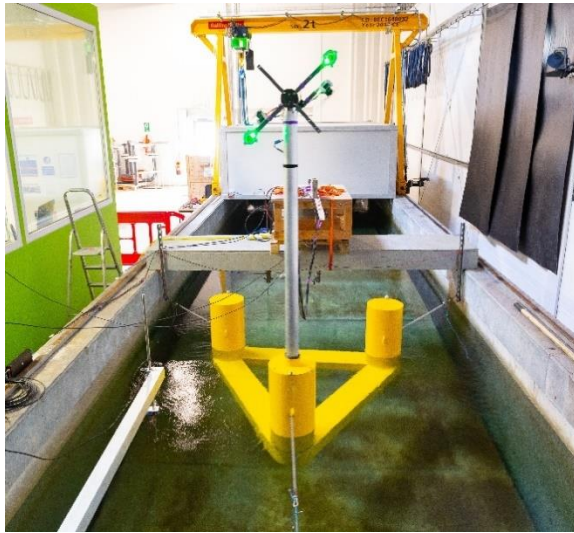


Figure 1. The FOWT model in the WCF at Lir NOTF, with the MPA at the top of the tower. The tower column is downstream of current direction.

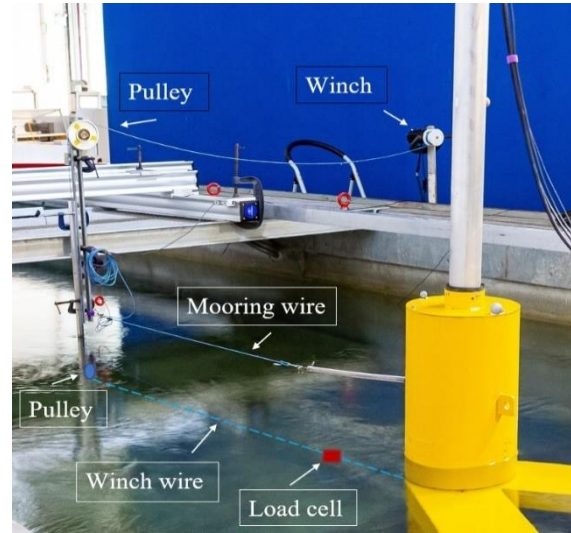


Figure 2. Layout of the winch actuator. The winch is mounted on the basin wall, and the pulley system to the instrument bridge.

Physical current and wave-current interactions

Physical current in the WCF is generated by three thrusters mounted in a circulation gallery beneath the floor of the flume. The flow inlet is near the wave maker and the outlet is at the opposite end of the flume near the wave absorbing ‘beach’. A smoothing screen with porosity of 44% is mounted vertically in front of the flow outlet and beach. The flow in the WCF can be reversed, however, this renders the smoothing screen ineffective. Therefore, only flow directly opposing the wave direction has been used during experiments.

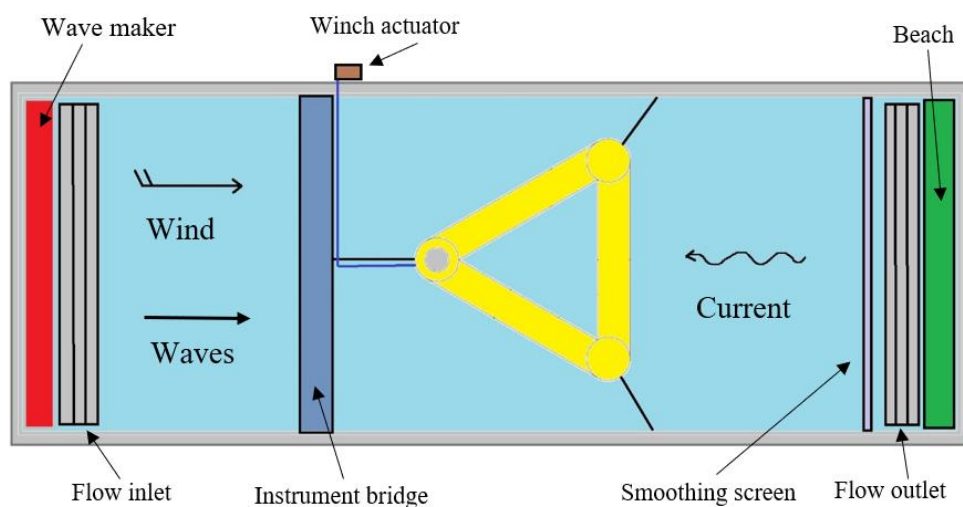


Figure 3. Plan view of the test setup in the WCF. The width/length ratio is exaggerated in this image.

Figure 3 shows a plan view of the model in the WCF, indicating the directions of current, wind, and waves during the experiments. The dimensions of the WCF are somewhat skewed in Figure 3, the actual dimensions of the flume are, Length: 28m, Width: 3m, Depth: 1.2m. The FOWT model is located 17m from the wave maker.

The velocity of the flow was measured on the upstream side of the model at the level of its COG with a Nortek Vectrino acoustic velocimeter, which profiles the water column over a range of 30mm, with a resolution of 1mm. Figure 4 shows the velocity in the X, Y, and Z directions against the percentage of power of the thruster generator, where X is in the longitudinal direction of the flume. The error bars indicate the standard deviation of the measurements. Current velocities used during experiments were 0.11 m/s, 0.14 m/s, and 0.21 m/s, which correspond to 0.75 m/s, 1 m/s, and 1.5 m/s at full scale respectively. The values of C_D in equation (1) were empirically derived for the model over the velocity range shown in Figure 4. The C_D values are shown in Figure 5.

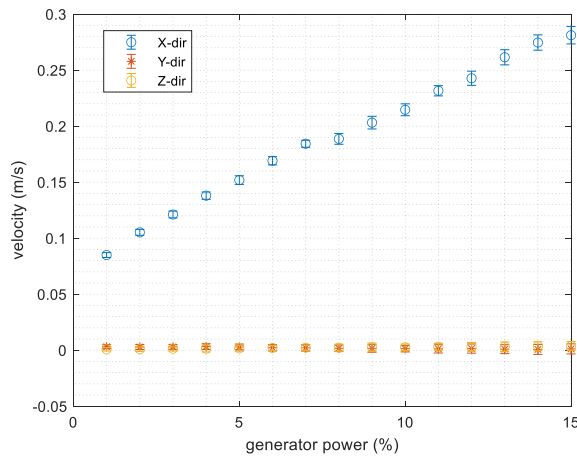


Figure 4. Velocity of the flow in the WCF in X, Y, and Z direction.

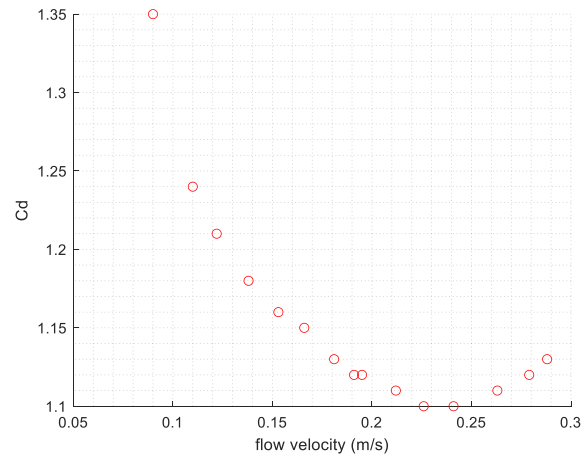


Figure 5. Empirically derived C_D values for the FOWT model.

The well-known phenomena of wave-current interaction is extensively documented in the literature, e.g. Hedges et al [208], and Draycott et al [32]. With an opposing current the spectral energy of an irregular wave time-series will increase. The alteration of wave spectra due to the presence of current is defined by the Huang equation [33]:

$$S_1(\omega) = S(\omega) \frac{4}{\left[1 + \sqrt{1 + (4U\omega/g)}\right]^2 \sqrt{1 + (4U\omega/g)}} \quad (2)$$

Where S_1 is the spectrum with current, S is the spectrum without current, ω is the wave frequency, U is the current velocity, and g is gravitational acceleration.

By altering wave heights and wave steepness, wave-current interaction will influence the response of the platform, particularly in the heave- and pitch Degree of Freedom (DOF). To simulate wave-current interactions with the SIL experiments the wave maker is re-programmed to change the wave heights of an irregular wave spectrum. This results in a wave spectrum with equivalent spectral energy as if a current is present. With physical current only the unaltered, original wave spectrum is used.

Only irregular waves were applied during this study. A wave-only JONSWAP spectrum with $T_p = 1.34$ seconds and $H_s = 0.1$ m at model scale was transformed according to equation (2) for the combined current/wind/wave test cases.

To check the validity of the simulated wave-current interaction, the measured spectra of waves with physical current were compared against measured spectra with SIL current. Initial results showed the energy of the spectra with SIL current was 15% less on average compared to spectra with physical current. A correction coefficient of 1.13 was added to equation (2) to increase spectral energy. Figure 6 shows the difference with- and without correction of the theoretical spectra. After applying the correction coefficient, the difference in spectral energy between waves with physical current and waves with SIL current was 3% on average. Figure 7 shows the measured spectra with current velocity = 0.21 m/s for physical current and SIL current.

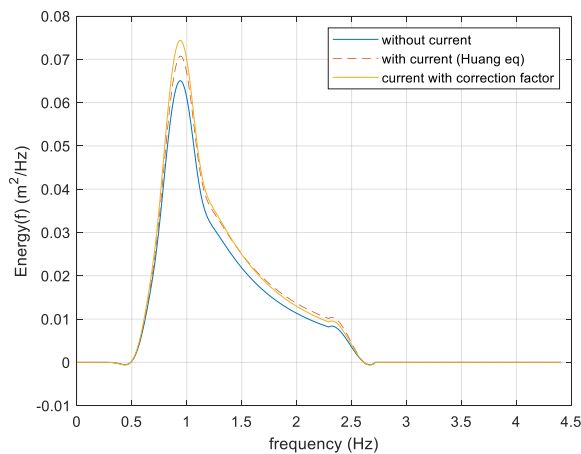


Figure 6. Theoretical wave spectra with- and without current.

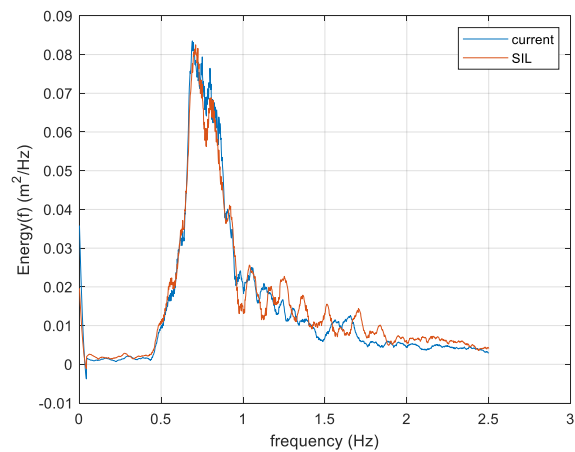


Figure 7. Measured spectra with physical current vs SIL current. Velocity = 0.21 m/s

Validation

Three sets of environmental conditions are repeated with physical current and SIL current: current-only, current/wind, and current/wind/waves. The test matrix is shown in Table 1.

For validation the relative difference between experiments with physical current and SIL current is determined for each test case. The relative difference is found by applying the validation metric Relative Error (RE), which is described in [200] and adapted for this study. Each test case is repeated three times and those repeated measurements are combined into an average record. This is done for all the experiments with physical current and SIL current.

Table 1. All Test Cases (TC), which are repeated with physical current and SIL current.

	Current (model scale)	Wind (full scale)	Waves (model scale)
TC 1	0.11 m/s	-	-
TC 2	0.14 m/s	-	-
TC 3	0.21 m/s	-	-
TC 4	0.11 m/s	9 m/s	-
TC 5	0.14 m/s	9 m/s	-
TC 6	0.21 m/s	9 m/s	-
TC 7	0.11 m/s	9 m/s	T_p 1.34 s, H_s 0.1 m
TC 8	0.14 m/s	9 m/s	T_p 1.34 s, H_s 0.1 m
TC 9	0.21 m/s	9 m/s	T_p 1.34 s, H_s 0.1 m

The spectral energy of platform surge, heave, pitch, and mooring tensions of these average records of test cases with physical current are compared against the equivalent test cases with SIL current to determine RE, which is defined as:

$$RE = 1 - \left(\frac{\overline{E_P}}{\overline{E_S}} \right) \quad (3)$$

Where E_P is the spectral energy of the records with physical current, E_S is the spectral energy of the records with SIL current, and the overbar indicates the average records. A perfect match between the physical- and SIL records would give an RE of zero.

As RE is a direct comparison between experimental results, some potential sources of error and uncertainty may affect the metric. For example, repeatability of the experiments will affect the average records and therefore influence RE. A source of uncertainty is the pulley system of the winch actuator. Low-friction pulleys were used; however, any amount of friction may increase the surge damping of the platform during the SIL current experiments. Another source of uncertainty is C_D in equation (1). The accuracy of C_D will have significant influence on the demanded drag force during SIL current experiments. The blockage by the FOWT model across the width of the WCF is also a source of uncertainty. With a maximum breadth of 1.6m, the FOWT model covers just over half the width of the flume and the blockage may influence the response of the model during physical current experiments. However, during SIL current experiments the boundary layers along the basin walls are ignored.

Results

For the current-only cases the model is pulled against a fixed barrier upstream of the model. While current is running the model is released and the surge motion of the model is allowed to decay and eventually settle at some distance from the start position.

Figure 8 shows the plotted surge motion of the average records with physical current and SIL current for TC 3. Although the decay oscillations are larger with physical current, the model settles at roughly the same surge distance with physical current and SIL current. Similar patterns were achieved with TC1 and TC 2. The period of the oscillations is slightly longer with SIL current; 1.03 times longer compared to physical current. The smaller oscillations show there is indeed surge damping of the model by the pulley system with SIL current, which also leads to a slightly larger natural period of the surge DOF. Figure 8 also shows there are some small random oscillations after settling with physical current. These are caused by vortex shedding around the columns of the model. Vortex shedding is not simulated with SIL current.

Figure 9 shows the demanded tension and the measured tension in the winch wire for TC 3 with SIL current. While the model is held at the start position the measured tension is around 11 N and demanded tension is 0 N. As the model is not moving, no tension is demanded. However, when the model is released and starts moving, demanded tension follows the same pattern as measured tension. There is a small phase shift between demanded- and measured tension caused by the spring in the winch wire. When RE is applied to compare measured- vs demanded tension an average value of 0.015 is found for the current-only test cases, 0.024 for current/wind cases, and 0.074 for current/wind/wave cases.

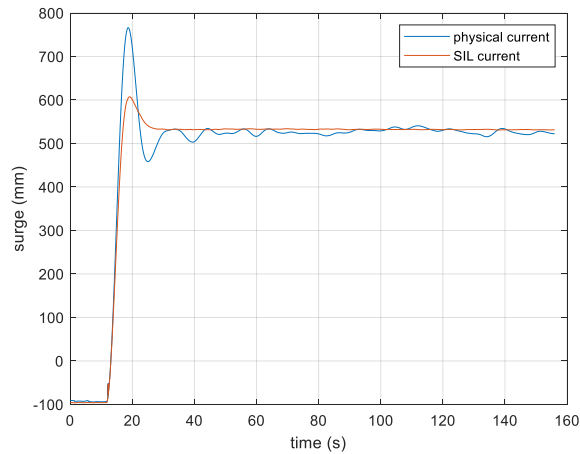


Figure 8. Surge motion of the FOWT model for TC 3 with physical- and SIL current

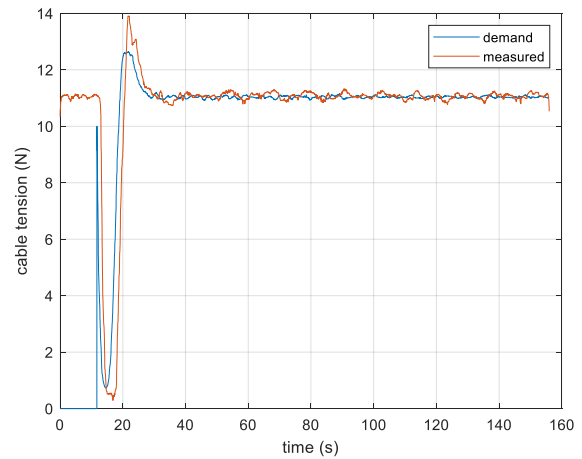


Figure 9. Demanded and measured tension in the winch wire for TC 3 with SIL current.

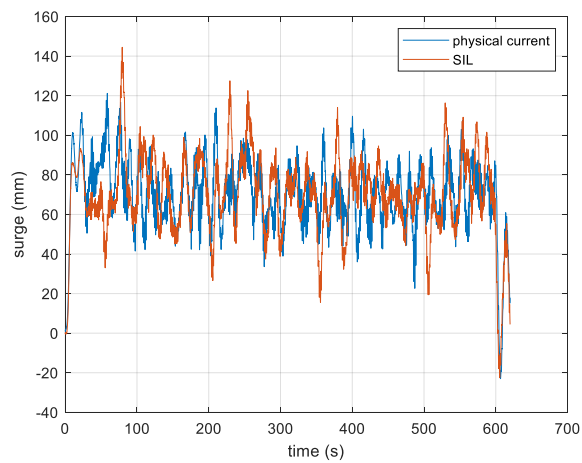


Figure 10. Surge motion for TC 7

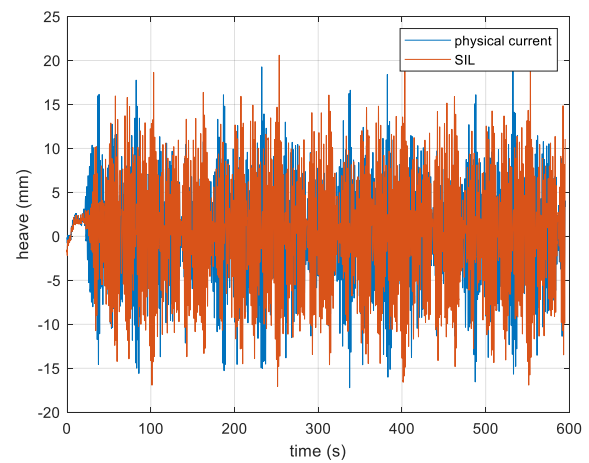


Figure 11. Heave motion for TC 7

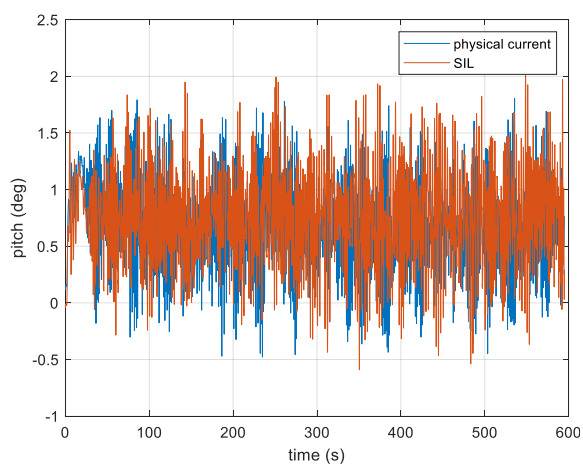


Figure 12. Pitch motion for TC 7

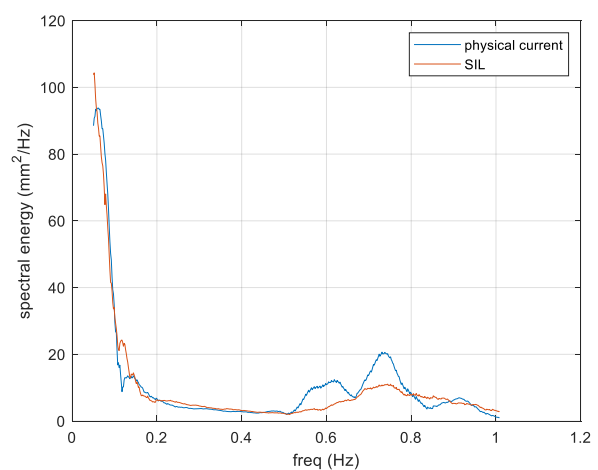


Figure 13. Spectral energy of surge, TC 7

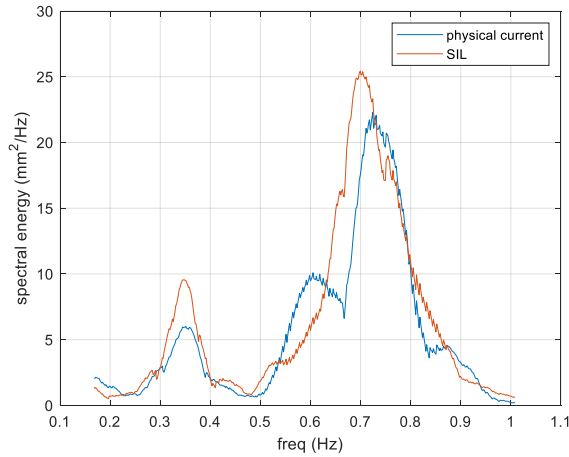


Figure 14. Spectral energy of heave, TC 7

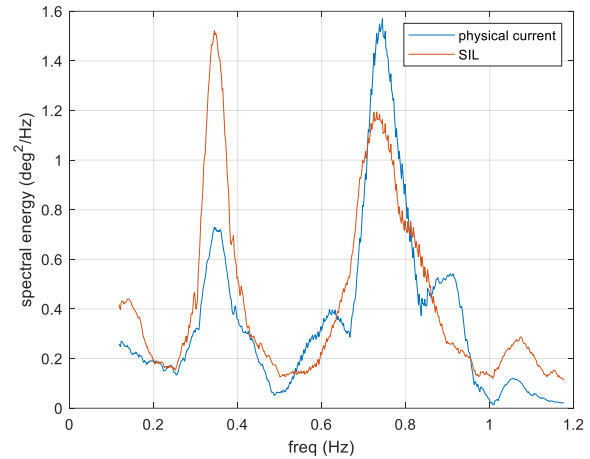


Figure 15. Spectral energy of pitch, TC 7

For TC 4 – 9 current is applied before recording and the start position of the model is the settled surged distance with current. Then, wind and waves are applied according to the test cases. As an example, the results of TC 7 are shown. Figures 10 – 12 show the surge-, heave- and pitch response of the model respectively for TC 7 with physical current and SIL current. Figures 13 – 15 show the spectral energy of the surge-, heave and pitch DOFs of the model for TC 7 with physical current and SIL current. Figure 16 shows the upstream mooring tension for TC 7, and Figure 17 shows the spectral energy of the upstream mooring tension for TC 7. All results shown are at model scale.

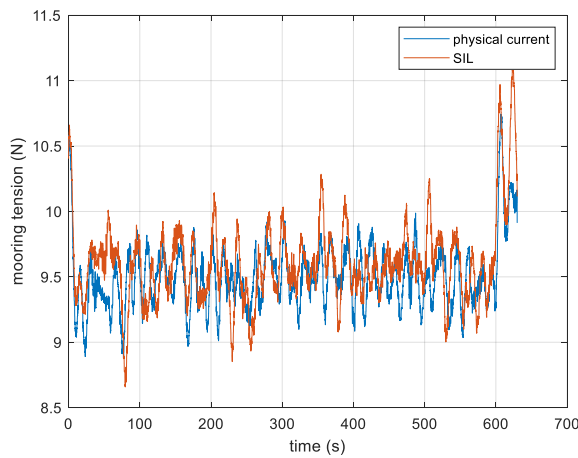


Figure 16. Upstream mooring tension, TC 7

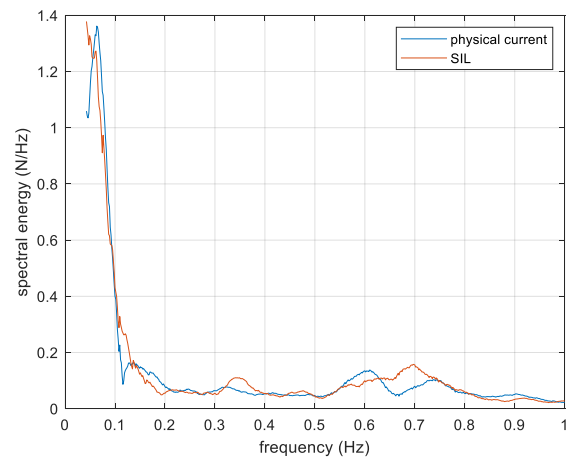


Figure 17. Spectral energy of upstream mooring tension, TC 7

Data from each experiment for TC 4 – 9 between $t = 20$ seconds and $t = 600$ seconds were used for the calculation of RE to make sure current, wind and waves are all acting on the model.

All results for RE of the motion response of the FOWT model and mooring tensions for all test conditions are shown in Table 2. There was no significant pitch- or heave motion during the current-only cases, and no significant heave motion during the current/wind cases. Therefore, only results for surge are given for TC 1 – 3, and results for surge and pitch for TC 4 – 6. Results for surge, heave, and pitch are given for the current/wind/wave cases, TC 7 – 9.

Table 2. RE for surge, heave, and pitch of the platform, and for mooring tensions

	Surge	Pitch	Heave	Mooring tension
TC 1	0.020	-	-	0.017
TC 2	0.023	-	-	0.016
TC 3	0.004	-	-	0.017
TC 4	0.013	0.431	-	0.026
TC 5	0.156	0.142	-	0.068
TC 6	0.087	0.117	-	0.040
TC 7	0.044	0.149	0.189	0.027
TC 8	0.080	0.101	0.162	0.027
TC 9	0.100	0.080	0.072	0.026

Discussion

The results clearly show that the response of the model with simulated current compares well to response of the model with physical current for all test conditions, with RE staying below 0.2 for most cases. The exception is pitch motion with wind, and current of 0.11 m/s (TC4). The pitch natural frequency of the FOWT model is around 0.35 Hz and for all test cases with wind the spectral energy of pitch is higher around this frequency with SIL current compared to physical current, possibly due to the moment created by the connection of the winch cable and the centre of thrust of the MPA during SIL current experiments.

An important reason to simulate current with FOWT experiments is to examine the effect on mooring tensions, which may influence fatigue life and structural integrity of the platform. Good results were achieved for mooring tensions; RE is lower than 0.07 for all test conditions, meaning there is close comparison between physical current and SIL current. Another important reason for current simulation is the alteration of wave shapes due to wave-current interaction and the effect this may have on platform heave and pitch, and hence on accelerations acting on the turbine. Heave- and pitch RE remains below 0.2 for all test cases with waves. This suggests that the method to simulate wave-current interactions with the adjusted wave spectra is adequate.

Good results were achieved for platform surge with SIL current for all test cases, the large blockage ratio of the model in the flume does not affect results, where $RE \leq 0.15$, which suggests that the values of C_D in equation (1) are correct. These validated C_D values can be used for the calibration of numerical models with the INNWIND semisubmersible FOWT.

Table 3. Pearson Correlation Coefficient of surge response for TC 3 and TC 9.

	Experiment 1	Experiment 2	Experiment 3
TC 3 with SIL current	1	1	0.9999
TC 3 with physical current	1	0.9963	0.9940
TC 9 with SIL current	1	0.9848	0.8610
TC 9 with physical current	1	0.8968	0.6487

Repeatability was found to be good with SIL current, although it reduced when all three environmental loads were combined. Repeatability is less favourable with physical current. As an example, the Pearson correlation coefficient for surge response of the FOWT model for the repeated experiments of TC 3 and TC 9 is given in Table 3, where the first experiment is the reference.

Future work will include fine tuning the PI controller for the winch tension. The current-only test cases (TC 1 – 3) show there is higher damping and slightly lower stiffness in the surge DOF of the platform with SIL current compared to physical current. Fine tuning the PI controller of the winch may resolve this.

Further future work will include using the SIL method with catenary moorings on the model rather than the soft mooring system used for this study. The soft mooring system was used to keep the SIL current method as robust and simple as possible. It allows for the current to be assumed as uniform and ignores the vertical shear profile of the water column and hydrodynamic loading on the moorings. With catenary moorings fixed to the bottom of the basin, shear profile and hydrodynamic loading can no longer be ignored and will have to be accounted for in the real-time numerical simulation.

Despite some limitations and uncertainties, the results show that SIL current can reliably emulate current loads on the FOWT model in combination with wind and waves. The advantage of this method is that it can be used in any wave basin without the need for bulky and expensive equipment to generate physical current for a range of test conditions. Furthermore, creating a realistic boundary layer with low turbulent flow, while also limiting wave reflection in the basin when applying physical current, is challenging. A disadvantage of SIL current is that not all response to current loading is captured, such as surge and sway motion of the platform due to vortex shedding.

Conclusion

A novel hybrid method to emulate current induced drag force is compared with physical current in this paper. The SIL current method uses a dynamic winch actuator to emulate the drag force of a current on a 1/50 scale model of the INNWIND.EU semisubmersible FOWT. The winch actuator is used in combination with a MPA, which emulates aerodynamic loads. The SIL current method is validated by comparing experimental results with SIL current against experimental results with physical current. Wave-current interactions are simulated by transforming a JONSWAP spectrum according to the Huang equation and including a correction coefficient. This gives a wave spectrum with equivalent energy as if a physical current is present in the wave basin. A validation metric, RE, is applied to the results for comparison between SIL current and physical current. A perfect match between the two methods will result in $RE = 0$. Results show RE remains below 0.2 for all test conditions, except for pitch motion of the model during the current/wind test case with current velocity of 0.11 m/s. Repeatability of the experiments is better with SIL current compared to experiments with physical current. The real-time numerical simulation does not capture vortex shedding around the columns of the model, which is therefore not simulated during experiments with SIL current. Regardless, the SIL current method can reliably simulate most effects of current loads on the FOWT model in combination with wind and wave loads.

Acknowledgements

The authors would like to acknowledge Christian van den Bosch for his assistance with the instrumentation in Lir NOTF, and the customer service of Schneider Electric for their technical assistance with the servo motor.

This work was funded by Science Foundation Ireland under the PhD fellowship programme.

References

- [1] A. Otter, J. Murphy, V. Pakrashi, A. Robertson, and C. Desmond, “A review of modelling

- techniques for floating offshore wind turbines,” *Wind Energy*, 2021, doi: 10.1002/we.2701.
- [2] E. E. Bachynski, T. Sauder, M. Thys, V. Chabaud, and L. O. Sæther, “Real-time hybrid model testing of a braceless semisubmersible wind turbine. Part 2: experimental results,” in *Proceedings of the ASME 2016 35th International Conference on Ocean, Offshore and Arctic Engineering OMAE2016 June*, 2016, no. OMAE2016-54437, pp. 1–12.
- [3] S. Gueydon, R. Lindeboom, W. van Kampen, and E.-J. de Ridder, “COMPARISON OF TWO WIND TURBINE LOADING EMULATION TECHNIQUES BASED ON TESTS OF A TLP-FOWT IN COMBINED WIND, WAVES AND CURRENT,” in *Proceedings of the ASME 2018 1st International Offshore Wind Technical Conference IOWTC2018*, 2018, pp. 1–11.
- [4] T. Utsunomiya, S. Yoshida, H. Ookubo, I. Sato, and S. Ishida, “Dynamic analysis of a floating offshore wind turbine under extreme environmental conditions,” *J. Offshore Mech. Arct. Eng.*, 2014, doi: 10.1115/1.4025872.
- [5] F. Sandner *et al.*, “INN WIND.EU Deliverable D4.3.3 - Innovative Concepts for Floating Structures,” 2015.
- [6] A. Otter, J. Murphy, and C. J. Desmond, “Emulating aerodynamic forces and moments for hybrid testing of floating wind turbine models,” in *Journal of Physics: Conference Series*, 2020, doi: 10.1088/1742-6596/1618/3/032022.
- [7] C. Matoug, B. Augier, B. Paillard, G. Maurice, C. Sicot, and S. Barre, “An hybrid approach for the comparison of VAWT and HAWT performances for floating offshore wind turbines,” in *Journal of Physics: Conference Series*, 2020, doi: 10.1088/1742-6596/1618/3/032026.
- [8] T. S. Hedges, K. Anastasiou, and D. Gabriel, “Interaction of Random Waves and Currents,” *J. Waterw. Port, Coastal, Ocean Eng.*, vol. 111, no. 2, pp. 275–288, Mar. 1985, doi: 10.1061/(ASCE)0733-950X(1985)111:2(275).
- [9] S. Draycott *et al.*, “Re-creation of site-specific multi-directional waves with non-collinear current,” *Ocean Eng.*, vol. 152, pp. 391–403, Mar. 2018, doi: 10.1016/J.OCEANENG.2017.10.047.
- [10] N. E. Huang, D. T. Chen, C.-C. Tung, and J. R. Smith, “Interactions between Steady Wound Uniform Currents and Gravity Waves with Applications for Current Measurements,” *J. Phys. Oceanogr.*, vol. 2, no. 4, pp. 420–431, 1972, doi: 10.1175/1520-0485(1972)002<0420:ibswuc>2.0.co;2.

MATLAB code for closed-loop control with XIL-API protocols and ds1104

```
%{
Description: This file is based on the ReadWrite sample
file which demonstrates how variables on a dSPACE
platform can be read and written from MATLAB using the
dSPACE XIL API MAPIPort server.
```

The file is adapted to be used for real-time Software in the Loop simulations for wind and current.

Also note in the call to the method Configure of the MAPIPort, the second parameter is set to 'false'. This means that the specified simulation application will not be downloaded unless there is no application loaded on the platform.

If the specified application is already running, no further action will be taken.

If any other application is running on the platform, an exception will be thrown.

Tip/Remarks: Objects of some XIL API types (e.g., MAPIPort, Capture) must be disposed at the end of the function. We strongly recommend using exception handling for this purpose to make sure that Dispose is called even in the case of an error.

```
%}
```

```
NET.addAssembly('ASAM.XIL.Interfaces, Version=2.1.0.0,
Culture=neutral, PublicKeyToken=bf471dff114ae984');
NET.addAssembly('ASAM.XIL.Implementation.TestbenchFactory
, Version=2.1.0.0, Culture=neutral,
PublicKeyToken=fc9d65855b27d387');
```

```
import
ASAM.XIL.Implementation.TestbenchFactory.Testbench.*;
import ASAM.XIL.Interfaces.Testbench.*;
import ASAM.XIL.Interfaces.Testbench.Common.Error.*;
import
ASAM.XIL.Interfaces.Testbench.Common.ValueContainer.*;
import ASAM.XIL.Interfaces.Testbench.MAPIPort.*;
import ASAM.XIL.Interfaces.Testbench.MAPIPort.Enum.*;
```

```
% The following lines must be adapted to the dSPACE
platform used
```

```
%-----
-----
```

```

% Set IsMPApplication to true if you are using a
multiprocessor platform
isMPApplication = false;
% Use an MAPort configuration file that is suitable for
your platform and simulation application
% See the folder Common\PortConfigurations for some
predefined configuration files
maPortConfigFile = 'C:\Users\QTM\Documents\dSPACE\XIL API
.NET\2021-
A\MAPort\Common\PortConfigurations\MAPortConfigDS1104_cur
rent_and_wind.xml';

% Set the name of the task here (specified in the
application's TRC file)
% Note: the default task name is "HostService" for PHS
bus systems, "Periodic Task 1" for VEOS
task = 'HostService';
%-----
-----

masterTaskPrefix = '';
slaveTaskPrefix = '';
masterVariablesPrefix = 'Model Root/';
slaveVariablesPrefix = 'Model Root/';

try
    %-----
    -----
    % Create a TestbenchFactory object; the
TestbenchFactory is needed to
    % create the vendor-specific Testbench
    %-----
    -----
    myTestbenchFactory = TestbenchFactory();

    %-----
    -----
    % Create a dSPACE Testbench object; the Testbench
object is the central object to access
    % factory objects for the creation of all kinds of
Testbench-specific objects
    %-----
    -----
    myTestbench =
myTestbenchFactory.CreateVendorSpecificTestbench('dSPACE
GmbH', 'XIL API', '2021-A');

```



```

%-----
-----
% We need a MAPortFactory to create an MAPort and
also a ValueFactory to create ValueContainer
% objects
%-----
-----

myMAPortFactory = myTestbench.MAPortFactory;
myValueFactory = myTestbench.ValueFactory;

%-----
-----

% For multiprocessor platforms different tasknames
and variable names must be used.
% Some variables are part of the subappliaction
"masterAppl", some belong to the
% subapplication "slaveAppl"
%-----
-----

if (isMPApplication)
    masterTaskPrefix = 'masterAppl/';
    slaveTaskPrefix = 'slaveAppl/';
    masterVariablesPrefix = 'masterappl/Model
Root/master/CentralLightEcu/';
    slaveVariablesPrefix = 'slaveappl/Model
Root/slave/FrontRearLightEcu/';
end

masterTask = [masterTaskPrefix, task];
slaveTask = [slaveTaskPrefix, task];

%-----
-----

% Create and configure a MAPort object and start the
simulation
%-----
-----

fprintf('Creating MAPort...\n');
% Create a MAPort object using the MAPortFactory
demoMAPort =
myMAPortFactory.CreateMAPort('DemoMAPort');
fprintf('...done\n');
% Load the MAPort configuration
maPortConfig =
demoMAPort.LoadConfiguration(maPortConfigFile);
% Apply the MAPort configuration
fprintf('Configuring MAPort...\n');

```

```

demoMAPort.Configure(maPortConfig, false);
fprintf('...done\n');
if (demoMAPort.State ~=
MAPortState.eSIMULATION_RUNNING)
    % Start the simulation
    fprintf('Starting simulation...\n');
    demoMAPort.StartSimulation();
    fprintf('...done\n');
end

% Create variables for the simulation
u = [masterVariablesPrefix, 'u/Value']; % platform
surge
U = [masterVariablesPrefix, 'U/Value']; % current
velocity
pitch = [masterVariablesPrefix, 'pitch/Value']; %
platform pitch
V_wind = [masterVariablesPrefix, 'V_wind/Value']; %
wind speed (fullscale)
load 'windspeed.mat' % Wind speed file
V=V(1:10:end);
load 'current_ts.mat'
n=numel(V);
%     n=4000;

QCM('connect','143.239.222.78','frameinfo','6D') %
QCM is a MATLAB plugin
% for Qualisys Track Manager, it connects to the
Qualisys host computer and
% streams motion tracking data in real-time to MATLAB
the3dlabels=QCM('3dlabels');
the6dlabels=QCM('6doflabels');
[frameinfo, trajectories] = QCM;

X = zeros(1,n);
RY = zeros (1,n);

x_s=trajectories(1,1)/1000;
ry_s=trajectories(1,5);

X(1,1)=x_s;
RY(1,1)=ry_s;
% Loop to update motion tracking for each time-step,
it uses surge motion
% of the tracked object to calculate its velocity
"u", and pitch motion

```

```

    % for angular velocity "ry". "V" is the wind speed at
    hub height of the turbine (at full scale)
    for i=2:n

        [frameinfo, trajectories] = QCM;
    %       v=cs(i) % current velocity from time series
        X(i)=trajectories(1,1)/1000;
        uc=(X(i)-X(i-1))./0.03125 % surge velocity
        RY(i)=trajectories(1,5);
        ry=(RY(i)-RY(i-1))./0.03125 % pitch velocity

        dc1=V(i) % wind speed at hub height
        pause((1/3.5)/sqrt(50))

        %-----
        % Read and Write the value of the variables
        %-----

        demoMAPort.Write(u,
myValueFactory.CreateFloatValue(uc));
    %       demoMAPort.Write(U,
myValueFactory.CreateFloatValue(v));
        demoMAPort.Write(pitch,
myValueFactory.CreateFloatValue(ry));
    %       demoMAPort.Write(V_wind,
myValueFactory.CreateFloatValue(dc1));

    end
    % to stop winch and propellers at end of simulation
    demoMAPort.Write(u,
myValueFactory.CreateFloatValue(0));
    demoMAPort.Write(pitch,
myValueFactory.CreateFloatValue(0));
    demoMAPort.Write(V_wind,
myValueFactory.CreateFloatValue(0));
    %       demoMAPort.Write(U,
myValueFactory.CreateFloatValue(0));

    fprintf('\nDemo successfully finished!\n');

    %-----
    % Attention: make sure to dispose the MAPort object
    in any case to free system resources like

```

```

    % allocated memory and also resources and services on
the platform, and
    % disconnect from QTM to prevent MATLAB from
crashing.
    %-----
-----

    demoMAPort.Dispose();
    QCM('disconnect')
catch e
    if (exist('demoMAPort', 'var'))
        % make sure to dispose the MAPort object in case
of an error
        demoMAPort.Dispose();
    end

    if (isa(e, 'NET.NetException'))
        if (isa(e.ExceptionObject,
'ASAM.XIL.Interfaces.Testbench.Common.Error.TestbenchPort
Exception'))
            %-----
-----

            % Display the XIL API exception information
to get the cause of an error
            %-----
-----

            fprintf('XIL API exception occurred:\n');
            fprintf('Code: %d\n',
e.ExceptionObject.Code);
            fprintf('CodeDescription: %s\n',
char(e.ExceptionObject.CodeDescription));
            fprintf('VendorCode: %d\n',
e.ExceptionObject.VendorCode);
            fprintf('VendorCodeDescription: %s\n',
char(e.ExceptionObject.VendorCodeDescription));
        else
            fprintf('.NET exception occurred:\n');
            fprintf('Message: %s\n', char(e.message));
        end
    end

    rethrow(e);
end

```

MATLAB code for open-loop control with Arduino

```
clc, clear

clear a;
a = arduino('COM3','Mega2560','Libraries','Servo');

s1 = servo(a,'D8','MinPulseDuration',500*10^-6,'MaxPulseDuration',150*10^-5);
s2 = servo(a,'D9','MinPulseDuration',500*10^-6,'MaxPulseDuration',150*10^-5);
s3 = servo(a,'D10','MinPulseDuration',500*10^-6,'MaxPulseDuration',150*10^-5);
s4 = servo(a,'D11','MinPulseDuration',500*10^-6,'MaxPulseDuration',150*10^-5);
s5 = servo(a,'D12','MinPulseDuration',500*10^-6,'MaxPulseDuration',150*10^-5);
s6 = servo(a,'D13','MinPulseDuration',500*10^-6,'MaxPulseDuration',150*10^-5);

writePosition(s1, 0);
writePosition(s2, 0);
writePosition(s3, 0);
writePosition(s4, 0);
writePosition(s5, 0);
writePosition(s6, 0);

% For steady wind:
pause(0.1)
writePosition(s3,0.38),writePosition(s4,0.38);
% ,writePosition(s1,0.385),writePosition(s6,0.385);
pause(10)
writePosition(s3,0),writePosition(s4,0);
% ,writePosition(s1,0),writePosition(s6,0);

% For propeller calibration
pause(5)

for i = 1:40
    writePosition(s1, (0.32+(i.*0.005)))...
    ,writePosition(s2, (0.32+(i.*0.005)))...
    ,writePosition(s3, (0.32+(i.*0.005)))...
    ,writePosition(s4, (0.32+(i.*0.005)))...
    ,writePosition(s5, (0.32+(i.*0.005)))...
    ,writePosition(s6, (0.32+(i.*0.005)));

    pause(10);
    writePosition(s1, 0)...
```

```
,writePosition(s2, 0) ...
,writePosition(s3, 0) ...
,writePosition(s4, 0) ...
,writePosition(s5, 0) ...
,writePosition(s6, 0);
pause(10);
end

writePosition(s1, 0);
writePosition(s2, 0);
writePosition(s3, 0);
writePosition(s4, 0);
writePosition(s5, 0);
writePosition(s6, 0);

% For wind time series:
pause(0.01);

filename = ('turb_11mps_test_filtered_with_gyro.txt');
delimiterIn = '\t';
headerlinesIn = 1;
A = importdata(filename,delimiterIn,headerlinesIn);
SBu = (A.data(:,1));
SBu = SBu(1:12:end,:);
SB1 = (A.data(:,2));
SB1 = SB1(1:12:end,:);
SBs5 = (A.data(:,3));
SBs5 = SBs5(1:12:end,:);
SBs2 = (A.data(:,4));
SBs2 = SBs2(1:12:end,:);

n = numel(SBu);

ts = 0.03125;

filename = 'pwmvalues_mavic_thrust.txt';
delimiterIn = '\t';
headerlinesIn = 1;
thrustvalues =
importdata(filename,delimiterIn,headerlinesIn);
thrustpwm = (thrustvalues.data(:,2));
thrust = (thrustvalues.data(:,3));

filename = 'pwmvalues_mavic_torque.txt';
delimiterIn = '\t';
headerlinesIn = 1;
```

```

torquevalues =
importdata(filename,delimiterIn,headerlinesIn);
torquepwm = (torquevalues.data(:,2));
torque = (torquevalues.data(:,3));

filename = 'pwmvalues_mavic_gyro.txt';
delimiterIn = '\t';
headerlinesIn = 1;
gyrovalues =
importdata(filename,delimiterIn,headerlinesIn);
gyropwm = (gyrovalues.data(:,2));
gyro = (gyrovalues.data(:,3));

SBu(SBu<=thrust(1,1))=thrustpwm(1,1);
SB1(SB1<=torque(1,1))=torquepwm(1,1);
SB1(SB1>=torque(1,1) & SB1<=torque(2,1))=torquepwm(1,1);
SB1(SB1>=torque(2,1)+0.00001 &
SB1<=torque(3,1))=torquepwm(2,1);
SB1(SB1>=torque(3,1)+0.00001 &
SB1<=torque(4,1))=torquepwm(3,1);
SB1(SB1>=torque(4,1)+0.00001 &
SB1<=torque(5,1))=torquepwm(4,1);
SB1(SB1>=torque(5,1)+0.00001 &
SB1<=torque(6,1))=torquepwm(5,1);
SB1(SB1>=torque(6,1)+0.00001 &
SB1<=torque(7,1))=torquepwm(6,1);
SB1(SB1>=torque(7,1)+0.00001 &
SB1<=torque(8,1))=torquepwm(7,1);
SB1(SB1>=torque(8,1)+0.00001 &
SB1<=torque(9,1))=torquepwm(8,1);

for j = 1:35
    SBu(SBu>=thrust(0+j,1)+0.00001 &
SBu<=thrust(j+1,1))=thrustpwm(0+j,1);
end

for h = 1:25
    SB1(SB1>=torque(10+h,1)+0.00001 &
SB1<=torque(h+11,1))=torquepwm(10+h,1);
end

for k = 1:30
    SBs5(SBs5>=gyro(5+k,1)+0.00001 &
SBs5<=gyro(6+k,1))=gyropwm(5+k,1);
end

for l = 1:5

```

```
    SBs5(SBs5>=gyro(0+1,1)+0.00001 &
SBs5<=gyro(1+1,1))=gyropwm(0+1,1);
end

for m = 1:30
    SBs2(SBs2>=gyro(5+m,1)+0.00001 &
SBs2<=gyro(6+m,1))=gyropwm(5+m,1);
end

for o =1:5
    SBs2(SBs2>=gyro(0+o,1)+0.00001 &
SBs2<=gyro(1+o,1))=gyropwm(0+o,1);
end

SBs5(SBs5>0.00001 & SBs5<gyro(1,1))=gyropwm(1,1);
SBs5(SBs5<=0)=0;
SBs2(SBs2>0.00001 & SBs2<gyro(1,1))=gyropwm(1,1);
SBs2(SBs2<=0)=0;
SBu(SBu>=thrust(36,1))=thrustpwm(36,1);
SBl(SBl>=torque(36,1))=torquepwm(36,1);
SBs5(SBs5>=gyro(36,1))=gyropwm(36,1);
SBs2(SBs2>=gyro(36,1))=gyropwm(36,1);

for i = 1:n
writePosition(s3, SBu(i,1));
writePosition(s4, SBu(i,1));
writePosition(s1, SBl(i,1));
writePosition(s6, SBl(i,1));
writePosition(s2, SBs2(i,1));
writePosition(s5, SBs5(i,1));
pause(ts);
end

writePosition(s3, 0)
writePosition(s4, 0)
writePosition(s1, 0)
writePosition(s6, 0)
writePosition(s5, 0)
writePosition(s2, 0)
```


Simulink code (Block diagram) for real-time simulation